

**PROCEEDINGS OF THE  
TENTH ANNUAL  
PACIFIC CLIMATE (PAKLIM) WORKSHOP**

Asilomar, California — April 4-7, 1993

Edited by  
Kelly T. Redmond and Vera L. Tharp

Technical Report 36  
of the  
Interagency Ecological Studies Program  
for the  
Sacramento-San Joaquin Estuary

March 1994

Single copies of this report may be obtained without charge from:

California Department of Water Resources  
P.O. Box 942836  
Sacramento, CA 94236-0001

# PROCEEDINGS OF THE TENTH ANNUAL PACIFIC CLIMATE (PACLIM) WORKSHOP

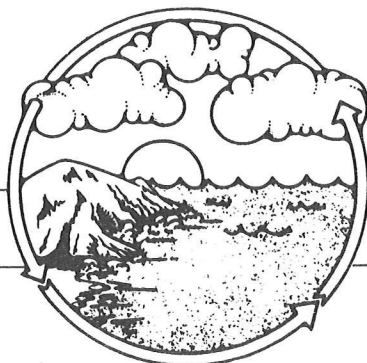
Asilomar, California — April 4-7, 1993

Edited by  
Kelly T. Redmond and Vera L. Tharp

Technical Report 36  
of the  
Interagency Ecological Studies Program  
for the  
Sacramento-San Joaquin Estuary

---

**PACLIM**



**Climate Variability  
of the  
Eastern North Pacific  
and  
Western North America**



## Sponsors

---

The Tenth Annual Pacific Climate Workshop was sponsored by

U.S. GEOLOGICAL SURVEY  
Water Resources Division

U.S. GEOLOGICAL SURVEY  
Geologic Research Division

NATIONAL OCEANIC AND ATMOSPHERIC ADMINISTRATION  
National Geophysical Data Center

U.S. ENVIRONMENTAL PROTECTION AGENCY  
EMAP Program

NATIONAL PARK SERVICE  
Global Change Program

CALIFORNIA DEPARTMENT OF WATER RESOURCES  
Environmental Services Office

NATIONAL OCEANIC AND ATMOSPHERIC ADMINISTRATION  
Western Regional Climate Center

AMERICAN GEOPHYSICAL UNION

SOUTHERN CALIFORNIA EDISON

U.S. FOREST SERVICE  
Global Change Program

NAVAL POSTGRADUATE SCHOOL

NATIONAL OCEANIC AND ATMOSPHERIC ADMINISTRATION  
National Ocean Service

Publication of this proceedings has been sponsored by the

INTERAGENCY ECOLOGICAL STUDIES PROGRAM  
for the

SACRAMENTO-SAN JOAQUIN ESTUARY

A Cooperative Program of:

California Department of Water Resources  
State Water Resources Control Board  
U.S. Bureau of Reclamation  
U.S. Geological Survey

California Department of Fish and Game  
U.S. Fish and Wildlife Service  
U.S. Army Corps of Engineers  
U.S. Environmental Protection Agency

These proceedings were published by the Interagency Ecological Studies Program for the Sacramento-San Joaquin Estuary (Interagency Program) in a cooperative effort with the

Western Regional Climate Center, Desert Research Institute, Reno, Nevada.

Information generated by the PACLIM Workshop provides the Interagency Program with a climatological perspective that cannot be obtained from its own studies.

Views and conclusions contained in this publication do not necessarily reflect the opinions of the Interagency Program or its member agencies.



# Contents

---

Sponsors . . . . .	iii
Authors . . . . .	vii
Acknowledgments . . . . .	ix
Statement of Purpose . . . . .	xi
Introduction . . . . . <i>Kelly T. Redmond</i>	1
ENSO Influences on Atmospheric Circulation and Precipitation in the Western United States . . . . . <i>Daniel R. Cayan and Kelly T. Redmond</i>	5
Semiempirical Down-Scaling of GCM Output to the Local Scale for Temperature, Precipitation, and Runoff . . . . . <i>Frederick Wade Freeman and John A. Dracup</i>	27
Rapid Teleconnections Associated with Individual Tropical Cyclones . . . . . <i>Ronald Gelaro, Tom Murphree, and James Goerss</i>	35
Regional Context of the Climate of H.J. Andrews Experimental Forest, Oregon . . . . . <i>David Greenland</i>	41
Satellite Passive Microwave Observations of the Upper Colorado River Snowpack . . . . . <i>Edward G. Josberger, Per Gloersen, Alfred T.C. Chang, and Albert Rango</i>	59
The California Heat Island: Seasonal Trends in Maximum and Minimum Temperatures . . . . . <i>Lynda M. Klein and Jim Goodridge</i>	67
Seasonal Resolution of Laminated Sediments in Santa Barbara Basin: Its Significance in Paleoclimatic Studies . . . . . <i>Carina B. Lange and Arndt Schimmelmann</i>	83
Near and Distant Connection of Atmospheric Systems to Ocean Temperature Change in the Coastal California Current Region . . . . . <i>Jerrold G. Norton, Daniel R. Cayan, and Douglas R. McLain</i>	93
Modeling the Effect of Snow on Seasonal Runoff within the Truckee River Drainage Basin . . . . . <i>Richard L. Orndorff and Rachael G. Craig</i>	107

Climatological Aspects of the Large-Scale Hydrologic Cycle in the United States . . . . .	117
<i>John Roads, Shyh Chen, Alex Guetter, and Konstantine Georgakakos</i>	
Is the California Drought Over? . . . . .	123
<i>Maurice Roos</i>	
Long-Term and Seasonal Patterns in Coastal Temperature and Salinity along the North American West Coast . . . . .	129
<i>Franklin B. Schwing</i>	

**Appendixes**

---

A	Agenda, Tenth Annual Pacific Climate (PACLIM) Workshop, April 4-7, 1993 . . . . .	145
B	Posters, Tenth Annual Pacific Climate (PACLIM) Workshop, April 4-7, 1993 . . . . .	151
C	Attendees, Tenth Annual Pacific Climate (PACLIM) Workshop, April 4-7, 1993 . . . . .	155

## Authors

---

Daniel R. Cayan  
Climate Research Division  
Scripps Institution of Oceanography and  
U.S. Geological Survey  
University of California, San Diego  
La Jolla, CA 92093-0224

Alfred T.C. Chang  
Hydrological Science Branch  
NASA/Goddard Space Flight Center, Code 624  
Greenbelt, MD 20771

Shyh-Chin Chen  
Climate Research Division  
Scripps Institution of Oceanography  
University of California, San Diego, 0224  
La Jolla, CA 92093-0224

Rachael G. Craig  
Department of Geology  
Kent State University  
Kent, OH 44242

John A Dracup  
Civil Engineering Department  
University of California, Los Angeles  
3066B Engineering I  
Los Angeles, CA 90024-1593

Frederick Wade Freeman  
Civil Engineering Department  
University of California, Los Angeles  
3066 Engineering I  
Los Angeles, CA 90024-1593

Ronald Gelaro  
Naval Research Laboratory  
Monterey, CA 93943-5006

Konstantine Georgakakos  
Iowa Institute of Hydraulic Research  
University of Iowa  
Iowa City, IA 52242-1585

Per Gloersen  
Laboratory for Oceans  
NASA/Goddard Space Flight Center, Code 971  
Greenbelt, MD 20771

James Goerss  
Naval Research Laboratory  
Monterey, CA 93943-5006

Jim Goodridge  
31 Rondo Court  
Chico, CA 95928

David Greenland  
Department of Geography  
University of Oregon  
Eugene, OR 97403-1251

Alex Guetter  
Iowa Institute of Hydraulic Research  
University of Iowa  
Iowa City, IA 52242-1585

Edward G. Josberger  
U.S. Geological Survey  
University of Puget Sound  
Tacoma, WA 98416

Lynda M. Klein  
California State University  
Chico, CA 95929

Carina B. Lange  
Scripps Institution of Oceanography  
Geological Research Division  
University of California, San Diego  
La Jolla, CA 92093-0215

Douglas R. McLain  
National Ocean Service  
Ocean Analysis Branch (NOAA)  
2560 Garden Road, Suite 101  
Monterey, CA 93940

Tom Murphree  
Naval Postgraduate School  
Monterey, CA 93943-5114

Jerrold G. Norton  
Southwest Fisheries Science Center / PFEG  
National Marine Fisheries Service (NOAA)  
P.O. Box 831  
Monterey, CA 93942

Richard L. Orndorff  
Department of Geology  
Kent State University  
Kent, OH 44242

Albert Rango  
Agricultural Research Service  
U.S. Department of Agriculture  
Beltsville, MD 20705

Kelly T. Redmond  
Western Regional Climate Center  
Desert Research Institute  
Reno, Nevada 89506-0220

John Roads  
Scripps Institution of Oceanography  
University of California, San Diego 0224  
La Jolla, CA 92093-0224

Maurice Roos  
California Department of Water Resources  
1416 Ninth Street, 1609-5A  
Sacramento, CA 95814-5515

Arndt Schimmelmann  
Biogeochemical Laboratories, Geology 317  
Department of Geological Sciences  
Indiana University  
Bloomington, IN 47405

Franklin B. Schwing  
Pacific Fisheries Environmental Group  
National Marine Fisheries Service  
P.O. Box 831  
Monterey, CA 93942

## Acknowledgments

---

The PACLIM meetings are kept alive by the voluntary efforts of members of the steering committee, session chairs, and others. A chocolate-covered, gift-wrapped thank you to all who have contributed their time!

The PACLIM meetings are also kept alive by financial contributions from our sponsors, listed elsewhere in this proceedings. Your support is accepted with gratitude. Our goal of obtaining and sharing a better understanding of how our home the Earth functions, and making use of the resulting knowledge is substantially impaired without such assistance.

At the risk of sounding like a broken record, the process of producing a proceedings volume is greatly expedited if at least one of the participants knows what they are doing. Our technical editor, Vera Tharp, has been a pleasure to work with, and is in great measure responsible for the readable quality of the resulting product. She is invariably cheerful and helpful, and her experience and technical competence make my role much easier to accomplish. From all of us, thank you very much, Vera!

Kelly Redmond  
Regional Climatologist  
Western Regional Climate Center  
Reno, Nevada



## **STATEMENT OF PURPOSE**

### **Pacific Climate (PACLIM) Workshops**

---

In 1984, a workshop was held on "Climatic Variability of the Eastern North Pacific and Western North America". From it has emerged an annual series of workshops held at the Asilomar Conference Center, Monterey Peninsula, California. These annual meetings, which involve 80-100 participants, have come to be known as PACLIM (Pacific Climate) Workshops, reflecting broad interests in the climatologies associated with the Pacific Ocean. Participants have included atmospheric scientists, hydrologists, glaciologists, oceanographers, limnologists, and both marine and terrestrial biologists. A major collective goal of PACLIM is to connect their various interests with a common target.

PACLIM arose from broad concern about the impact of possible climate change over the next century. From observed changes in the historical record, it is certain that climate change will have tremendous societal impacts through coincident effects on global ecology, hydrology, geology, and oceanography. It is increasingly clear that our ability to predict climate change is best derived from an understanding of global processes. Human impacts are primarily terrestrial in nature, but the major forcing processes are atmospheric and oceanic in origin and transferred through geologic and biologic conditions. Our understanding of the global climate system and its relationship to ecosystems will arise from a regional study of its components in the Pacific Ocean and the western Americas, where ocean/atmosphere coupling is strongly expressed. With such diverse meteorologic phenomena as the El Niño-Southern Oscillation and shifts in the Aleutian Low and North Pacific High, the Eastern Pacific is a region that has tremendous global influences, and strong effects on North America in particular. This region is rich in climatic records, both instrumental and proxy. Recent research efforts are beginning to focus on better paleoclimatic reconstructions that will put present day climatic variability in context and should allow better anticipation of future changes.

The PACLIM workshops have addressed the problem of defining regional coupling of multifold elements, as organized by phenomena that are global in extent. Because climate expresses itself through the natural system, our activity has been, from the beginning, multidisciplinary in scope and is evolving into a truly interdisciplinary cooperative effort. The specialized knowledge from different disciplines has brought together these characteristic climatic records and process measurements to provide a synthesis of understanding of the complete system.

Our interdisciplinary group uses diverse time series, measured both directly and through proxy indicators, to study past climatic conditions and current processes in this region. Characterizing and linking the geosphere, biosphere, and hydrosphere in this region will provide a scientific analogue and, hence, a basis for understanding similar linkages in other regions, as well as for anticipating the response to future climate variations. Our emphasis in PACLIM is to study the interrelationships among diverse data. The resultant information obtained will be complementary and lead to better synthesis of biological and geophysical variability in the region. By necessity, in order to understand these interactive phenomena, we will incorporate studies that consider a broad range of topics and multiple time scales, from months to millennia.

The benefit of the effort to understand the regulation of ecosystems and their variability is clear. It is critical now, from both a management and scientific point of view, that we develop a more complete understanding of how climatic change affects the structure and function of these systems. The PACLIM venue covers an extraordinary range of ecosystem types and richness. There is empirical evidence that large-scale climatic fluctuations force large-scale ecosystem response in the California current and in a very different system, the North Pacific central gyre. The implications of these observations are highly significant and indicate the need for aggressive pursuit of multidisciplinary studies.

Water supplies in the western Americas exhibit fluctuations over a continuum of scales, with considerable social and economic impact, especially in the Southwest, where demand exceeds supply. The spatial extent and variability of the hydrologic system, such as precipitation deficits and drought, are strongly coupled to climate. For instance, in the western United States where rainfall is primarily a cool-season phenomenon, year-to-year changes in the activity and tracking of North Pacific winter storms have substantial influence on the hydrological balance. In turn, this atmospheric variability is at least weakly coupled to anomalous thermal conditions in the upper ocean. Thus, a primary objective of PACLIM is to better understand the linkage between large-scale atmospheric and hydrologic variabilities, with their complex effects on chemical and biological systems.

Proceedings of the first PACLIM workshops were published as  
AGU Geophysical Monograph 55 (Peterson, ed., 1989).  
Beginning with the Sixth Annual Workshop in 1989, the proceedings have been published by the  
California Department of Water Resources as Technical Reports of the  
Interagency Ecological Studies Program for the Sacramento-San Joaquin Estuary.

Kelly T. Redmond

The PACLIM workshops celebrated their tenth anniversary from April 4 to 7, 1993. The location, as for each of the previous meetings, was the beautiful grounds of the Asilomar Conference Center in Pacific Grove, California. The setting is emblematic of the concerns of those who attend: tucked in amidst the vegetation, a short stroll away from the zone where the land and the ocean and the atmosphere have long continued a meeting of their own, although a meeting with a far more ancient pedigree.

For many of us, the annual visit to this quiet and peaceful place has furnished a needed respite from the hectic daily dose of trips, meetings, proposals, reports, administrators, funding questions, airports, concrete and brick buildings, long office-filled corridors, whirring computer equipment, and the distraction of the moment. In an atmosphere conducive to thought, conversation, and discussion, the opportunity for productive interchange of ideas is improved, and a number of multidisciplinary collaborations have resulted over the years.

In contrast to previous proceedings, the papers in this volume are organized differently — alphabetically by the last name of the first author. This randomizing approach somewhat mimics the workshop itself, one purpose of which is to stir the pot and promote mixing of disciplines.

As with previous volumes, there has been extensive editing in presentation, and minimal editing in content.

In the first paper, Cayan and Redmond extend earlier work on the relationship between ENSO and climate behavior in the western United States. This work began as an outgrowth of the earliest PACLIM workshops, was first reported there, and has benefited greatly from them. The extension is from surface to upper air, and from seasonal to monthly time scales. A discussion is included of the nature of exceptions from the “rule” of atmospheric behavior that has emerged.

In the next paper, Freeman and Dracup present a way to apply the spatially coarse output from general circulation model simulations to the much finer spatial scales (comparable to station spacing) where local information about the effects of potential climate change is greatly desired. Relationships are derived to specify local-scale observed information from large-scale observed information. These relationships are then applied to large-scale model output to estimate local-scale model results.

Galero, Murphree, and Goerss examine an interesting question. How differently would the atmosphere act in remote regions if an observed tropical cyclone were to “unhappen” — if it were to be expunged from the record? They find that removal of a December tropical cyclone near Japan leads to significantly different downstream flow effects over western North America a week to 10 days later.

The 19 sites in the Long Term Ecological Research (LTER) program are intended to represent major biomes in North America and its extension, Antarctica(!). The representativeness of the HJ Andrews Experimental Forest LTER in Oregon is examined by Greenland, who finds that it is quite representative. To understand its present configuration, it is necessary to know its climatic past, and he uses estimation techniques to develop a longer, partially reconstructed record.

For water resource decisions and climate change studies, it is desirable to know the snowpack status throughout the West on a fine scale. No one method of observation suffices. Josberger, Gloersen, Chang, and Rango discuss ways of blending SMMR satellite data with SNOTEL ground truth data in the Upper Colorado Basin. The extremely strong dependence of brightness on snow grain size introduces the necessity for understanding and estimating the temporal evolution of the snowpack microstate.

Is the overall climate changing, or is the observing system changing, or is the climate in the vicinity of the measuring device changing? These are important questions in the ongoing debate about whether global climate change is underway. Klein and Goodridge continue an ongoing examination of California temperatures. They find that minimum temperatures are increasing faster than maximums, and that larger cities (and implied urban warming) account for a large share of this increase.

Lange and Schimmelmänn discuss the prospect of obtaining seasonal information from layered ocean sediments. Their trip down memory lane is extremely brief by ocean paleoclimatic standards, extending only about 165 years into the past. The message that emerges is that resolution to a half-year seems feasible. Their technique will be further tested on a 600-year core.

The relationship of near-shore ocean temperatures in the upper several hundred meters to “regional” (central North Pacific) and “remote” (equatorial Pacific) forcing processes is examined by Norton, Cayan, and McLain. They find influences from both locations on water temperature profiles along the West Coast of the United States.

Using output from a previously produced local climate model, Orndorff and Craig use another (snow) model to apportion precipitation into liquid and solid parts and use this to drive a hydrologic model. In experiments in which snow processes are turned off, they show the necessity of including snow for realistic modeling of seasonality of runoff variables. Their ultimate application is for paleoclimatic studies.

The seasonal cycle of the total and the components of the water budgets of the surface and the atmosphere for the United States are the subject of an article by Roads and Chen. Using a 2.5-degree gridded data set, they discuss the budgets separately and their interactions.

For the first time in 7 years, Roos had to change the title and theme of a PACLIM article from “how much worse is the California drought this year?” to “is it over?” He examines the recent drought from a variety of perspectives, to conclude that it appears indeed to have been a fairly unusual event. He also discusses the different ways of interpreting whether a drought is “over”. Although the conclusion is yes, he intimates that new constraints on system management will create greater susceptibility of water resource availability to annual precipitation variations.

The sole representative of the 19th letter of the alphabet, Schwing discusses the temporal scales of temperature and salinity variations in the coastal ocean along the West Coast of the United States and Canada.



# ENSO Influences on Atmospheric Circulation and Precipitation in the Western United States

Daniel R. Cayan and Kelly T. Redmond

**Abstract:** The influence of ENSO on atmospheric circulation and precipitation over the western United States is presented from two perspectives. First, ENSO-associated circulation patterns over the North Pacific/North America sector were identified using an REOF (*rotated empirical orthogonal function*) analysis of the 700-mb height field and compositing these for extreme phases of the Southern Oscillation Index. Five patterns were identified with associations to extremes of the SOI, similar to results from previous investigations. To determine the precipitation response, composites of precipitation anomalies were taken over cool season months (November through March) using circulation patterns that project onto these REOFs with strongly positive and strongly negative amplitudes. Several of these have strong precipitation expressions over the western United States. Second, we examine the variability of precipitation during the warm and cool phases of ENSO for different locations in the western United States. Choosing sites in the Pacific Northwest and Desert Southwest regions, we diagnose the ENSO response by considering four subsets of the pattern of precipitation and associated atmospheric circulation. The four subsets include wetter- and drier-than-normal months during the warm and the cool ENSO phases. While the Southwest tends toward higher precipitation during the warm phase and lower precipitation during the cool phase, it has both wet and dry months during each phase; analogously, the Northwest tends to be dry during the warm phase and wet during the cool phase but also contains wet and dry months during each phase. Interestingly, circulation patterns and the spatial distribution of precipitation during *a*) the wet cases of the two phases and *b*) the dry cases of the two phases, for each of the two regions, are distinct enough to suggest systematic differences in the winter storm regimes (not just the storm frequency but also the storm pattern) for the two ENSO phases.

## Introduction

One of the few secure predictive links to seasonal anomalous precipitation in the western United States appears to involve the relationship with large-scale disturbed conditions in the tropical Pacific, known as the El Niño/Southern Oscillation phenomenon. In the present study, both the warm and cool phases of the El Niño/Southern Oscillation are considered and are referred to collectively as *ENSO* (eg, Barnett *et al* 1991).

Concerning the linkage between ENSO and the western United States, several previous studies have considered precipitation (Ropelewski and Halpert 1986; Schoner and Nichol森 1989; Andrade and Sellers 1988; Redmond and Koch 1991; Epstein 1992; Redmond and Cayan 1994) and also streamflow and snowpack (Webb and Betancourt 1992; Cayan and Peterson 1989; Redmond and Koch 1991; Cayan and Webb 1991; Kahya and Dracup 1993). Compared to relationships with precipitation in the tropical Pacific (Ropelewski and Halpert 1987), those in North America are relatively weak, and the ones that emerge for the Desert Southwest and Pacific Northwest are unreliable enough that Ropelewski and Halpert (1986) did not include them in their set of ENSO-related study regions across the United States.

In: KT Redmond and VL Tharp, Editors. 1994. Proceedings of the Tenth Annual Pacific Climate (PACLIM) Workshop, April 4-7, 1993. California Department of Water Resources, Interagency Ecological Studies Program, Technical Report 36.

A different methodology reveals, however, that there are statistically significant impacts on the frequency and amount of precipitation during ENSO extremes (both negative and positive phases of the Southern Oscillation Index). This linkage has been detected in precipitation records at stations in each of the two regions (Redmond and Koch 1991; Epstein 1992; Cayan and Webb 1992; Redmond and Cayan 1994).

Some of the pertinent results from previous studies are summarized as follows. Both phases of ENSO exhibit significant anomalous associations with regional precipitation over the western United States. The strongest associations (correlations between SOI and streamflow and between SOI and snowpack) are with precipitation in the Northwest (from Washington to western Montana) and in the Southwest (from southeastern California to New Mexico). The Northwest tends to be dry and the Southwest tends to be wet during the Northern Hemisphere winter of the ENSO mature warm phase. The opposite conditions occur during Northern Hemisphere winters of the ENSO mature cool phase. Similar responses are noted for individual months from about October through May. There also appears to be a several-month lag, such that the SOI leads the circulation and precipitation. The SOI in summer/fall is a reliable precursor to tropical atmospheric behavior during the following winter. In turn, the summer/fall SOI is also related (although not as strongly) to winter extratropical Pacific climate including precipitation in the regions noted above (Redmond and Cayan 1994).

The present study builds on the previous body of results by scrutinizing the links to various atmospheric circulation patterns and by focusing on monthly, as opposed to seasonal, variations. Both negative and positive phases of the SOI are considered in relating ENSO to monthly atmospheric circulation over the North Pacific and western North America sector and to the pattern of regional precipitation over the western United States.

## Data

---

Monthly total precipitation was used from 94 climate divisions over the western conterminous United States west of 102°W. Precipitation values are averages over several stations within a climate division, as defined by the National Climate Data Center (Karl and Knight 1985). The divisional data series employed covers 1895 through 1991. Since divisional data were not reported before 1931, they were retrospectively estimated by NCDC from statewide average values of nearby states using a multiple regression scheme (Karl and Knight 1985). Specific regions were constructed by averaging the anomalies of monthly precipitation over 11 divisions in the Pacific Northwest (*PNW*) and 10 divisions in the desert Southwest (*DSW*). A third region, the northern Rocky Mountains, was also examined, but associated circulation and precipitation patterns were similar to those for PNW, so they are not shown here. These regions are shown in Figure 1, and associated circulation and precipitation

patterns are delineated later in this paper, under "Extreme Precipitation During Warm and Cool Phases of ENSO". Precipitation considered in this study is for November through March (NDJFM), when the ENSO influence on climate fluctuations over the western United States is likely to be strongest (Redmond and Cayan 1994).

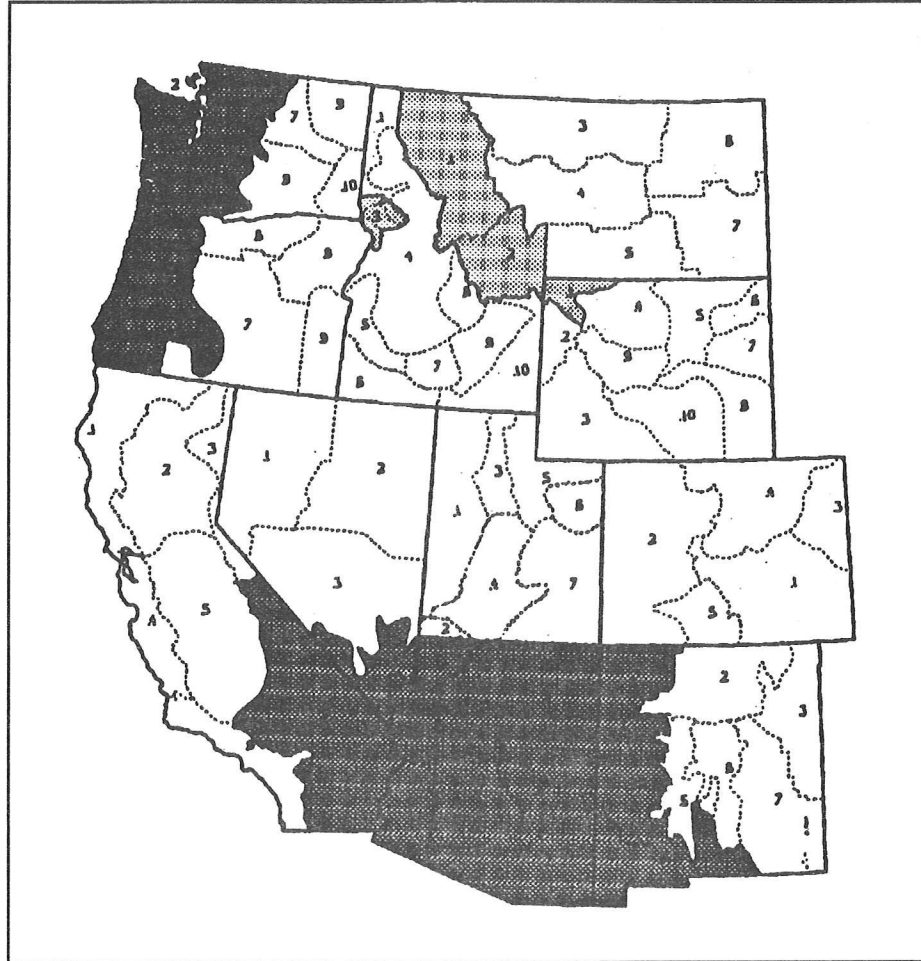


Figure 1. Climate divisions employed in the Pacific Northwest and Desert Southwest regions used in the regional precipitation analyses. The northern Rocky Mountain region in Idaho, Montana, and Wyoming was also considered, but results are not shown here.

Atmospheric circulation measures are obtained from monthly 700-mb height on a 5° latitude by 10° longitude Northern Hemisphere staggered grid, provided by the NOAA Climate Analysis Center. The 700-mb height data are for the NDJFM cool season from 1947-48 through 1990-91.

The Southern Oscillation Index, a normalized difference in monthly anomalies of surface pressure between Tahiti and Darwin (Ropelewski and Jones 1987), was employed for 1895 through 1991. The June-November average of the monthly values, denoted *JJASON*, was constructed as an index of the summer/fall SOI. To investigate linkages to the tropical Pacific, the *JJASON* SOI index was related to the atmospheric circulation and precipitation anomalies over the western United States. In all cases, the analyses compare *JJASON* SOI and the overlapping/subsequent fall-spring NDJFM monthly atmospheric circulation and precipitation. When the SOI is negative, the tropical Pacific is usually in

its warm state; when the SOI is positive, the tropical Pacific is usually in its cool state. In this study, a negative JJASON average normalized SOI anomaly  $\leq -0.5$  is used to designate the warm phase of ENSO, called *El Niño*, and a positive SOI  $\geq +0.5$  designates the cool phase, called *La Niña*.

### **700-mb Height REOFs: Their Relationship to the SOI and Precipitation**

Our first approach was to isolate atmospheric circulation patterns associated with ENSO and then to determine how each of these affected precipitation over the western United States. The atmospheric circulation patterns were determined using an REOF (*rotated empirical orthogonal function*) analysis (Barnston and Livezey 1987) of the monthly 700-mb height anomaly field. The NDJFM cool season months were employed to investigate the winter-like response. The anomaly fields were constructed by removing the individual monthly long-term means (1947-1972 base period). All five months were pooled together. Since the focus is on the western United States, we only considered the sector of the 700-mb height from 110°E to 65°W longitude and from 20°N to 70°N latitude. Given the REOFs, their relationship to the two phases of the SOI and their relationship to the geographic distribution of precipitation over the western United States were investigated.

#### **700-mb Height REOFs: Their Relationship to the SOI**

A traditional empirical orthogonal function analysis (Davis 1976) was employed to isolate a limited number of spatial modes (spatially uncorrelated), along with their associated time-varying coefficients (temporally uncorrelated). The monthly 700-mb height anomaly data analyzed were multiplied by  $[\cos(\text{latitude})]^{0.5}$  to provide equal weighting of the variance over each grid in the domain. The first eight EOFs, ordered by variance, were retained and rotated using the IMSL library "varimax" rotation. This rotation preserves temporal orthogonality, but the resulting spatial patterns are no longer constrained to be uncorrelated. The resulting REOFs still contain the same amount of variance (in this case the sum of the variance is 73%), but the variance is more evenly distributed over the eight REOFs than it was for the original EOF analysis, whose variance is dominated by the first few components (Table 1).

	1	2	3	4	5	6	7	8
	WPO	PNA1	PNA2		EP	TNH		
Explained Variance (%)	14.8	11.4	11.4	8.0	7.8	6.8	6.8	5.6

The REOF patterns were then evaluated for ENSO influences, as gaged by their correspondence with the SOI. First, strong positive and negative REOF cases were identified, based on the amplitude of the time coeffi-

clients of the REOFs. A threshold was chosen such that each case contained between 30 and 44 months; together the positive and negative extremes of each REOF represent about one-third of the 225 total over the data set. This threshold, amplitudes  $\geq 1$ , is at a level of one standard deviation of each of the REOF time series. Hereafter, the extreme cases selected under this criterion are called "strong positive" and "strong negative" extremes of the REOFs.

Table 2 is a set of contingencies, providing the number of months with strong positive or negative expressions of each of the eight REOFs for El Niño, La Niña, and for all conditions regardless of ENSO state.

Another measure is in Table 3, which gives the average value of each of the REOF amplitudes during the NDJFM months (each month individually and the 5-month average) for El Niño, La Niña, and for all conditions regardless of ENSO state.

Table 2  
NUMBER OF CASES OF EACH REOF EXCEEDING POSITIVE/NEGATIVE THRESHOLD  
FOR EL NIÑO, LA NIÑA, AND ALL CASES, BY MONTH, 1947-48 THROUGH 1990-91

	Strong Positive REOF						Strong Negative REOF					
	N	D	J	F	M	All	N	D	J	F	M	All
REOF 1 (WPO)												
El Niño	0	0	0	0	1	1	2	3	1	2	3	11
La Niña	3	3	2	4	5	17	0	0	1	1	0	2
All	5	5	9	10	6	35	3	4	6	9	9	31
REOF 2 (PNA1)												
El Niño	1	2	2	0	2	7	3	1	4	5	3	16
La Niña	4	4	3	4	3	18	1	3	0	0	1	5
All	8	8	7	8	9	40	5	7	6	7	10	35
REOF 3 (PNA2)												
El Niño	2	1	2	0	1	6	2	3	3	4	2	14
La Niña	1	3	3	3	1	11	1	1	2	0	0	4
All	6	8	7	5	6	32	5	8	6	8	5	32
REOF 4												
El Niño	0	3	4	2	2	11	1	2	2	2	4	11
La Niña	1	0	2	0	2	5	1	2	1	2	1	7
All	6	8	7	5	7	33	5	9	6	8	9	37
REOF 5 (EP)												
El Niño	1	2	1	5	3	12	0	1	1	1	3	6
La Niña	2	1	1	1	1	6	2	3	2	4	1	12
All	5	9	7	11	8	40	4	7	5	8	6	30
REOF 6 (TNH)												
El Niño	2	4	1	2	3	12	3	2	2	4	3	14
La Niña	1	1	3	3	2	10	0	1	1	0	1	3
All	7	8	8	7	7	37	6	8	7	8	7	36
REOF 7												
El Niño	3	3	0	3	4	13	1	3	1	0	6	11
La Niña	2	2	2	0	3	9	4	2	0	1	3	10
All	10	13	6	5	10	44	8	10	6	5	10	39
REOF 8												
El Niño	0	2	2	1	0	5	1	2	1	2	3	9
La Niña	2	2	1	1	3	9	3	3	1	2	1	10
All	6	9	7	4	7	33	9	9	6	5	6	35

A  $\chi^2$  test on the contingencies in Table 2 and a *t*-test of the REOF amplitudes in Table 3 indicate that REOFs 1 and 2 are strongly differentiated according to the positive and negative phases of the SOI. Considering the sample set where all five months are pooled together, the two significance tests allow rejection of the null hypothesis that the REOFs are undifferentiated during El Niño vs. La Niña at greater than the 99% level of confidence. Three other REOFs (3, 5, 6) appear to be differentiated, but not as strongly; for these cases, the null hypothesis may be rejected at a level of confidence ranging from 85% to more than 99%.

These five REOFs (1, 2, 3, 5, 6) are mapped on Figures 2-6, along with the precipitation anomaly pattern that occurs when a particular REOF is in its strong positive or strong negative extreme. Three other REOFs, which did not exhibit significant associations with ENSO, are not shown, but they represent circulations that also produce important precipitation anomalies. The values depicted by these REOF maps are correlations

Table 3  
COMPOSITE OF REOFs FOR LA NIÑA AND EL NIÑO  
BY MONTH AND FOR ALL MONTHS (NOVEMBER-MARCH), 1947-48 THROUGH 1990-91

	La Niña						El Niño					
	N	D	J	F	M	All	N	D	J	F	M	All
REOF 1 (WPO)												
n	11	11	11	11	11	11	12	12	12	12	12	12
Mean	0.70	0.44	0.19	0.41	0.79	0.51	-0.33	-0.72	-0.49	-0.54	-0.07	-0.43
Standard Deviation	1.09	0.91	1.17	0.89	0.93	0.46	0.83	0.75	0.82	0.78	0.84	0.43
REOF 2 (PNA1)												
n	11	11	11	11	11	11	12	12	12	12	12	12
Mean	0.46	0.13	0.68	0.61	0.38	0.45	-0.32	0.02	-0.31	-0.63	-0.28	-0.30
Standard Deviation	1.15	1.15	0.99	0.75	0.96	0.64	0.92	0.87	0.89	0.94	1.04	0.52
REOF 3 (PNA2)												
n	11	11	11	11	11	11	12	12	12	12	12	12
Mean	-0.18	0.22	0.25	0.49	0.05	0.17	-0.02	-0.22	-0.49	-0.54	-0.35	-0.33
Standard Deviation	0.68	0.93	1.15	0.97	0.75	0.49	0.99	0.95	1.22	1.10	1.04	0.72
REOF 4												
n	11	11	11	11	11	11	12	12	12	12	12	12
Mean	-0.19	-0.33	0.25	-0.16	0.16	-0.05	-0.11	0.15	0.31	-0.06	-0.20	0.02
Standard Deviation	0.83	0.78	0.90	0.59	1.04	0.42	0.69	1.03	1.22	0.87	1.30	0.72
REOF 5 (EP)												
n	11	11	11	11	11	11	12	12	12	12	12	12
Mean	-0.02	-0.39	-0.41	-0.41	-0.03	-0.25	0.11	0.06	0.14	0.24	-0.23	0.06
Standard Deviation	1.24	0.91	1.01	1.30	0.75	0.46	1.09	0.91	0.99	1.01	1.42	0.45
REOF 6 (TNH)												
n	11	11	11	11	11	11	12	12	12	12	12	12
Mean	0.01	-0.21	0.39	0.52	0.27	0.20	-0.13	0.18	-0.45	-0.12	-0.10	-0.12
Standard Deviation	0.70	0.67	1.22	0.71	0.88	0.29	1.28	1.06	0.99	1.29	1.15	0.80
REOF 7												
n	11	11	11	11	11	11	12	12	12	12	12	12
Mean	-0.42	-0.05	0.16	-0.14	-0.04	-0.10	0.11	-0.08	-0.17	0.22	-0.40	-0.06
Standard Deviation	1.47	0.89	0.71	0.70	1.01	0.53	0.90	0.90	0.55	1.00	1.39	0.53
REOF 8												
n	11	11	11	11	11	11	12	12	12	12	12	12
Mean	0.04	0.00	-0.04	-0.05	0.15	0.02	-0.01	0.14	0.24	-0.10	-0.29	0.00
Standard Deviation	1.48	1.17	0.70	1.06	1.06	0.86	0.68	1.02	1.06	1.00	1.11	0.66

between the REOF amplitude time series and the corresponding 700-mb height anomaly time series at each grid point. To identify these patterns, we follow Barnston and Livezey's (1987; denoted *BL*) classification of Northern Hemisphere anomalous circulation patterns.

The first REOF (14% of the variance) is the West Pacific Oscillation, with a north-south dipole of out-of-phase anomaly features. These anomalies are centered at about 55°N, just north of Kamchatka, and over a broader region at about 30°N, southeast of Japan. Tables 2 and 3 indicate the El Niño phase of ENSO favors the WPO phase with negative anomalies over Kamchatka and positive anomalies at lower latitudes of the western

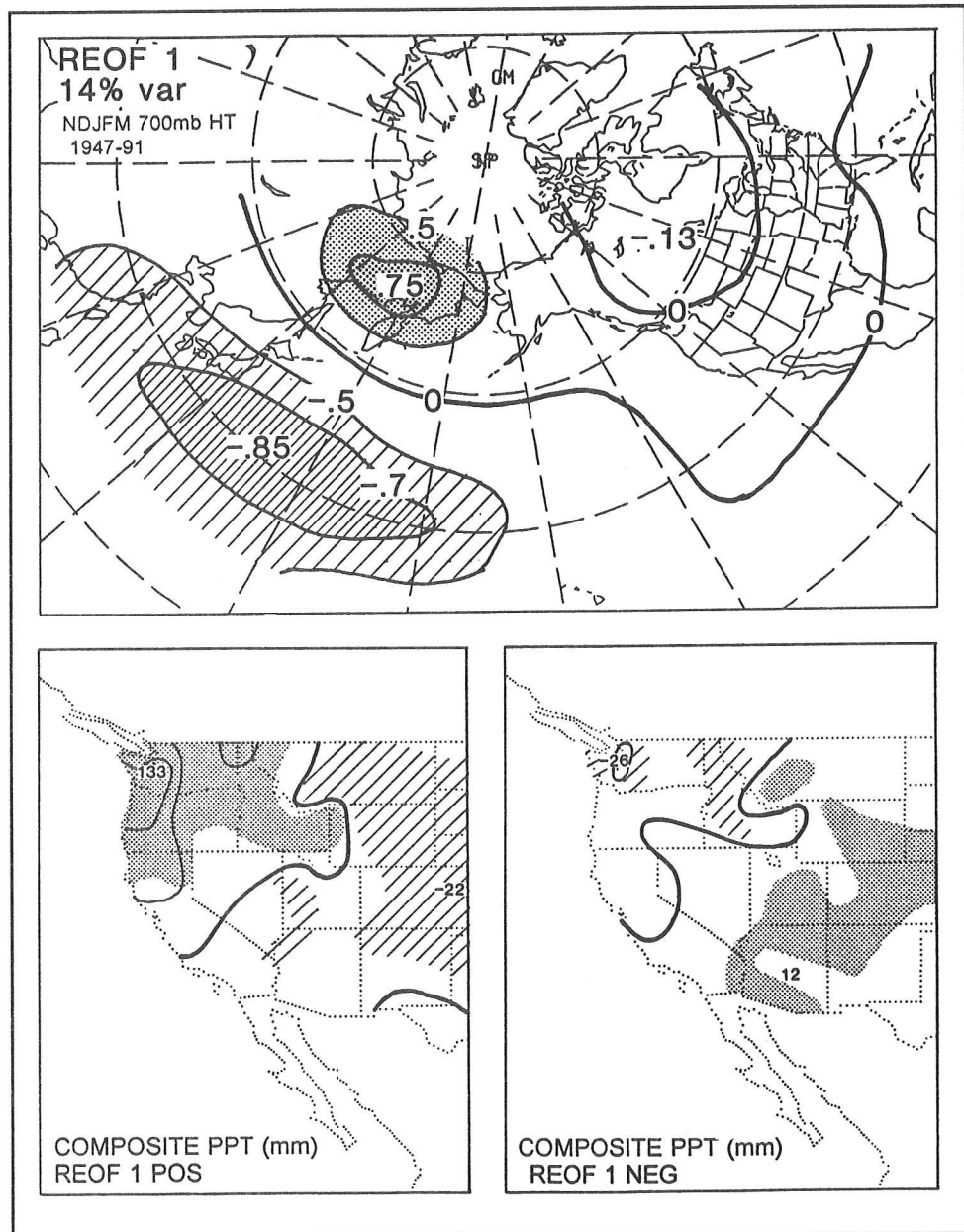


Figure 2. REOF 1 of Monthly NDJFM 700-mb Height Anomalies, 1947-48 through 1990-91, and Associated Precipitation Anomaly Patterns over the Western United States. Precipitation anomalies are shown as composites of positive (left) and negative (right) extremes of each mode. REOF values are correlations, with shading on magnitudes exceeding 0.5. Shading (stippled/hatched) indicates (positive/negative) precipitation anomalies exceeding the 90% significance level, using a 2-tailed *F*-test. Amount of total anomaly variance accounted for is indicated for each mode.

North Pacific; the La Niña phase of ENSO favors the opposite — a blocking positive pressure anomaly over Kamchatka and an activated storm track to the south. The WPO link to ENSO was quite strong. During El Niño the WPO pattern was in its strengthened Kamchatka Low state in 11 months and in its weakened Kamchatka Low state in only 2 months; during La Niña the WPO pattern was in its weakened Kamchatka Low state in 17 months and in its strengthened Kamchatka Low state in only one month.

REOFs 2 and 3 (each accounts for about 11% of the variance) appear to be hybrids of the Pacific/North America pattern and are called PNA1 and PNA2 for the present study. REOF 2 is mainly a central North Pacific feature

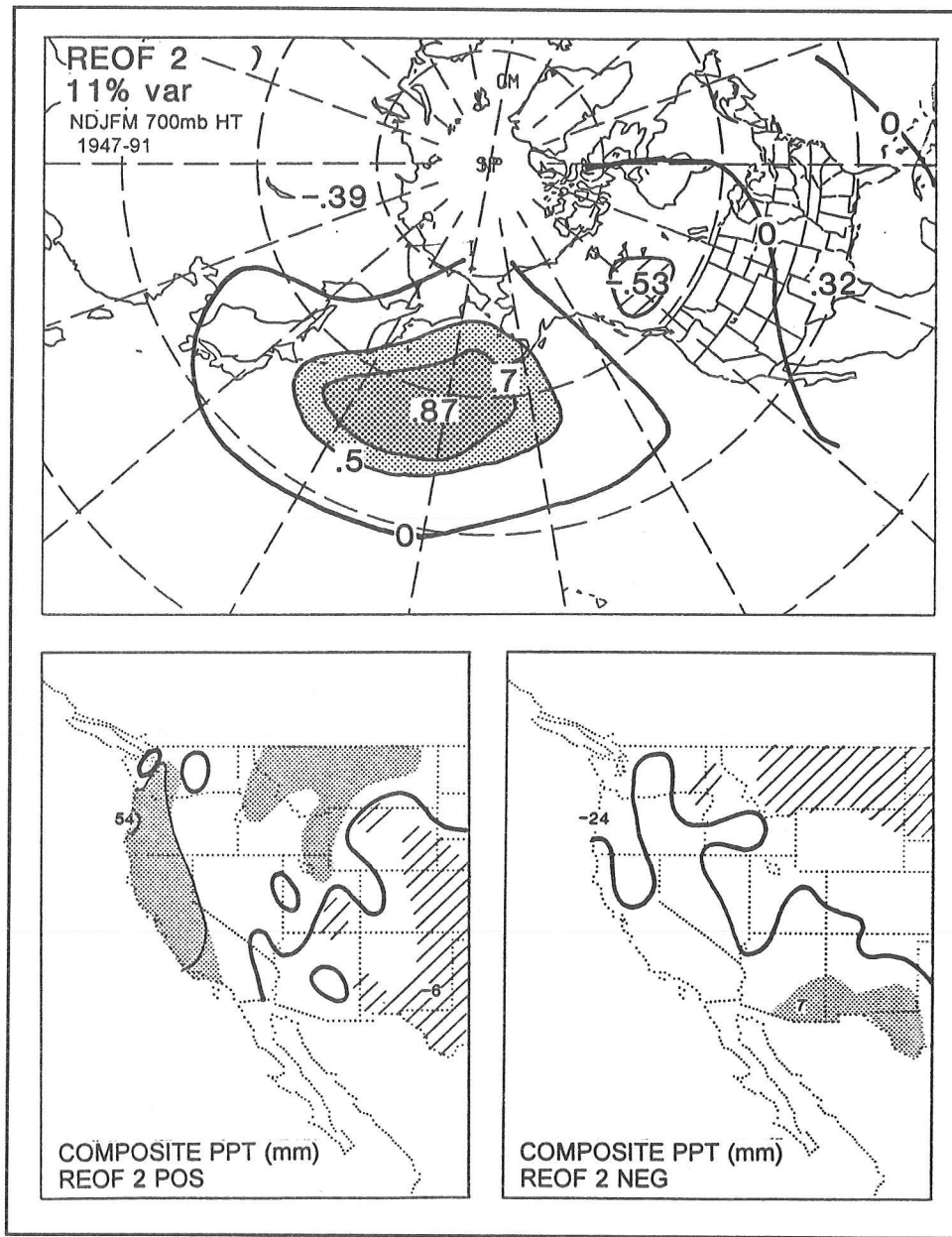


Figure 3. REOF 2 of Monthly NDJFM 700-mb Height Anomalies, 1947-48 through 1990-91, and Associated Precipitation Anomaly Patterns over the Western United States. Precipitation anomalies are shown as composites of positive (left) and negative (right) extremes of each mode. REOF values are correlations, with shading on magnitudes exceeding 0.5. Shading (stippled/hatched) indicates (positive/negative) precipitation anomalies exceeding the 90% significance level, using a 2-tailed t-test. Amount of total anomaly variance accounted for is indicated for each mode.

centered at about 45°N 175°E but also contains a secondary center over western Canada at about 55°N 120°W. REOF 3 contains a modest center at about 50°N 150°W, in the western Gulf of Alaska; another center at about 60°N 90°W, over central Canada; and a strong, large center at about 30°N 80°W, over the southeastern United States. Hence, REOF 2 contains more of the central North Pacific portion of the PNA pattern, while REOF 3 contains more of the eastern extension of the PNA over North America. Tables 2 and 3 indicate the El Niño phase of ENSO favors the states of REOF 2 and 3 with deepened Aleutian or Gulf of Alaska Lows; in contrast, the La Niña phase of ENSO favors the circulation with

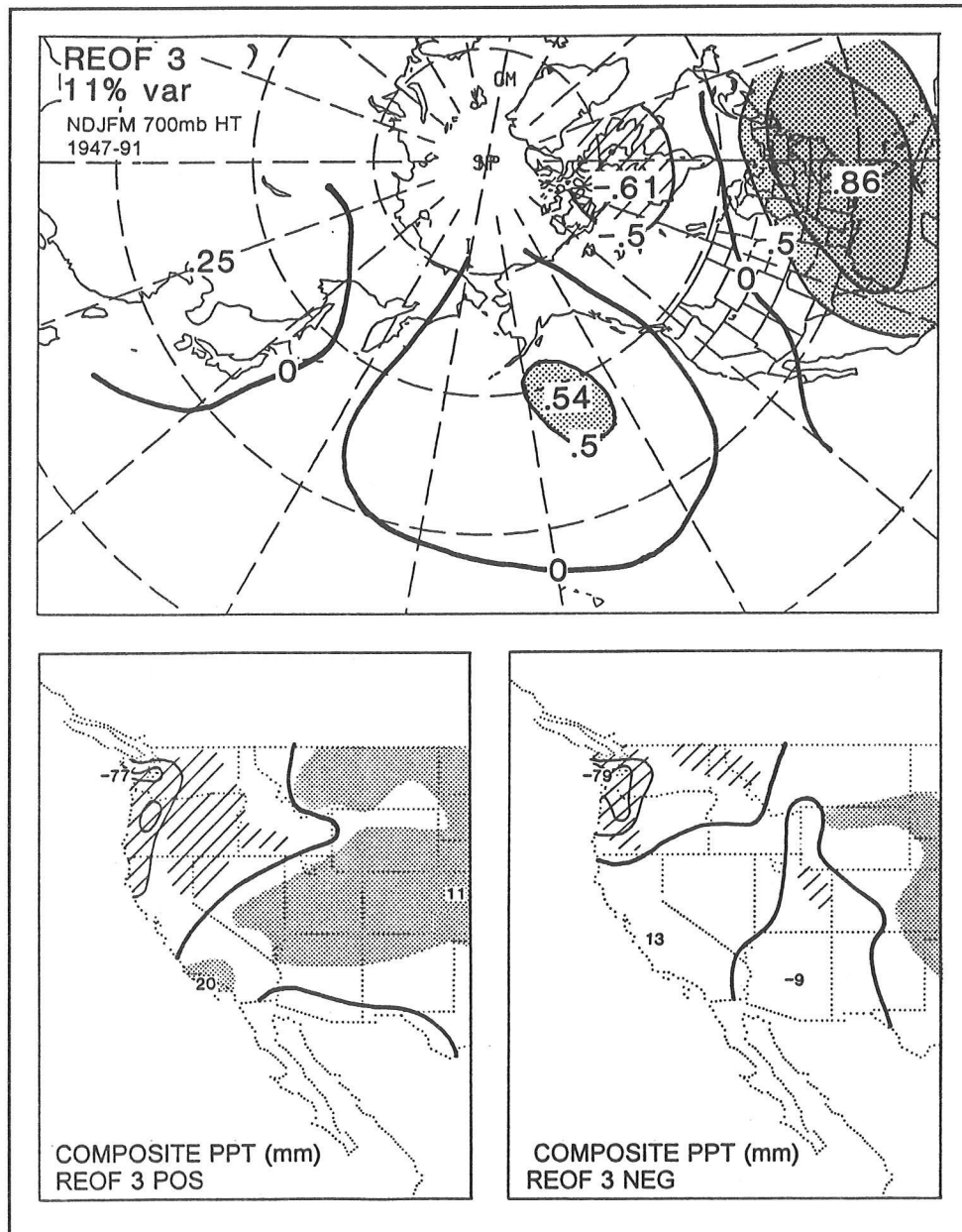


Figure 4. REOF 3 of Monthly NDJFM 700-mb Height Anomalies, 1947-48 through 1990-91, and Associated Precipitation Anomaly Patterns over the Western United States. Precipitation anomalies are shown as composites of positive (left) and negative (right) extremes of each mode. REOF values are correlations, with shading on magnitudes exceeding 0.5. Shading (stippled/hatched) indicates (positive/negative) precipitation anomalies exceeding the 90% significance level, using a 2-tailed t-test. Amount of total anomaly variance accounted for is indicated for each mode.

positive anomalies south of the Aleutians or in the Gulf of Alaska, symptomatic of a less active storm track across the central North Pacific.

REOF 5 strongly resembles the Eastern Pacific (EP) pattern, with a dipole of out-of-phase north-south centers at about 60°N, over Alaska, and a broader center at about 30°N, north of the Hawaiian Islands. Tables 2 and 3 indicate the El Niño phase of ENSO favors the EP phase with positive anomalies over Alaska and negative anomalies to the south, over the eastern North Pacific; the La Niña phase of ENSO favors the opposite anomaly pattern, with negative anomalies to the north and positive

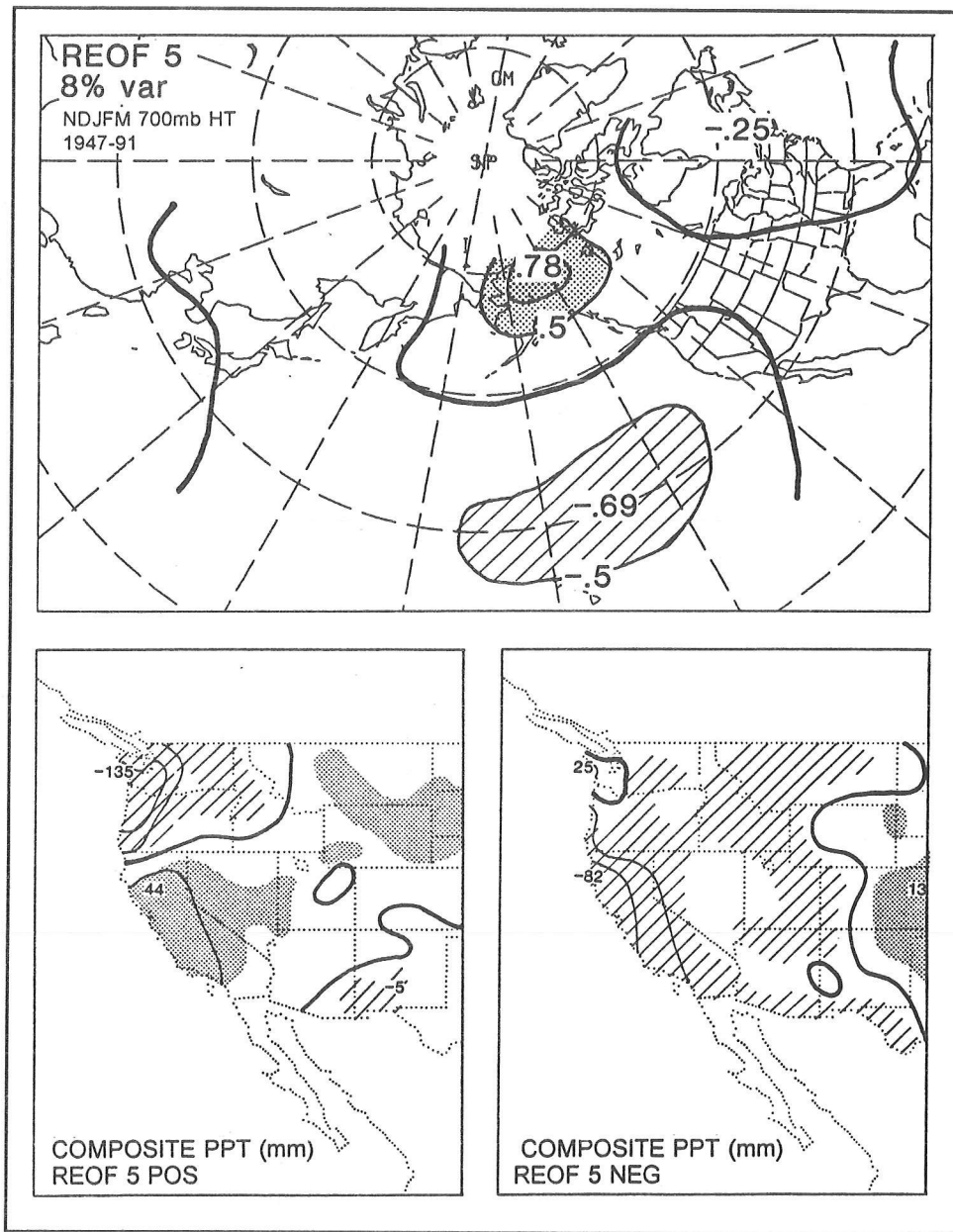


Figure 5. REOF 5 of Monthly NDJFM 700-mb Height Anomalies, 1947-48 through 1990-91, and Associated Precipitation Anomaly Patterns over the Western United States. Precipitation anomalies are shown as composites of positive (left) and negative (right) extremes of each mode. REOF values are correlations, with shading on magnitudes exceeding 0.5. Shading (stippled/hatched) indicates (positive/negative) precipitation anomalies exceeding the 90% significance level, using a 2-tailed *F*-test. Amount of total anomaly variance accounted for is indicated for each mode.

anomalies to the south, symptomatic of a less active storm track across middle latitudes of the eastern North Pacific.

REOF 6 appears to be the Tropical/Northern Hemisphere pattern, with west-east out-of-phase centers at about 40°N 130°W, in the eastern North Pacific, and at 50°N 90°W, over Ontario, just north of the Great Lakes. Tables 2 and 3 indicate the El Niño phase of ENSO favors the TNH phase with negative anomalies off the west coast of the United States and positive anomalies upstream, over the Great Lakes. The La Niña state of ENSO is about equally split between both phases of TNH.

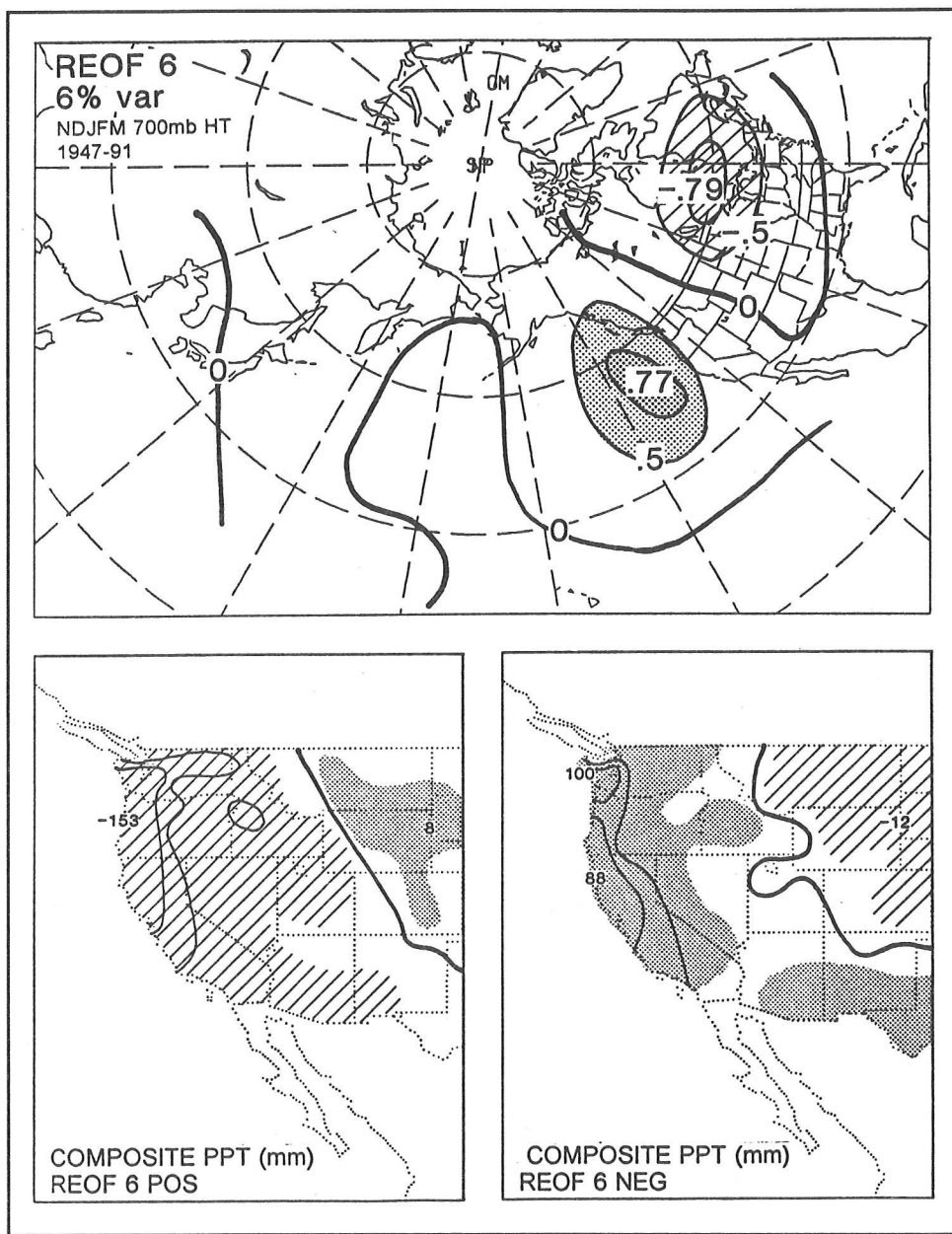


Figure 6. REOF 6 of Monthly NDJFM 700-mb Height Anomalies, 1947-48 through 1990-91, and Associated Precipitation Anomaly Patterns over the Western United States. Precipitation anomalies are shown as composites of positive (left) and negative (right) extremes of each mode. REOF values are correlations, with shading on magnitudes exceeding 0.5. Shading (stippled/hatched) indicates (positive/negative) precipitation anomalies exceeding the 90% significance level, using a 2-tailed t-test. Amount of total anomaly variance accounted for is indicated for each mode.

Note that the present analysis differs from BL because this one included the more limited domain of the Pacific-North America half of the Northern Hemisphere, and because five months (NDJFM) were pooled in forming the EOFs and REOFs. BL performed separate analyses for each month, with the result that some of the modes exhibited considerable differences from one month to the next. Presumably these differ because of sampling variations (BL used the Northern Hemisphere 700-mb height archive from 1950 to 1984) and because the physical characteristics of the circulation change greatly over the annual cycle. On the latter, the BL PNA pattern (see BL, Figure 3, pp. 1092-1093) undergoes a dramatic expansion of its zonal wavelength from a minimum in September to a maximum in February, when zonal winds are maximum across the North Pacific, and then recedes to a minimum in April, when the westerlies have waned. The spatial configuration of REOF 2 more closely resembles the winter-month, longer-wavelength BL PNA pattern; REOF 3 is closer to the earlier-fall, later-spring, shorter-wavelength BL PNA patterns. This seasonal modulation of the PNA may be one reason the present NDJFM analysis has produced two PNA-like hybrids.

#### **700-mb Height REOFs:**

#### **Their Relationship to Precipitation Over the Western United States**

To investigate the effect of the ENSO-related circulation patterns on precipitation, the distribution of precipitation over the western United States was examined during months with extreme patterns (positive or negative) of the five REOFs. Composites of precipitation anomalies were taken over NDJFM months with circulation patterns that project onto these REOFs with strongly positive and strongly negative amplitudes. Note that although this categorization was based exclusively on the amplitudes of the REOFs, the influence of tropical Pacific is implicit in the resulting relationships because these five REOFs are biased toward one of their extremes or the other (strong positive or strong negative) in association with the La Niña or El Niño state of the SOI. These composites are an average of positive anomalies over at least 30 months (the range was 30 to 44 months) in each of the extreme negative or extreme positive cases.

Several of the REOF-based precipitation composites have strong expressions over the western United States. Regarding REOF 1, the WPO, a relatively strong precipitation pattern appears over the western United States. The degree of this relationship is somewhat surprising in view of the western North Pacific location of its major centers. The positive anomaly over Kamchatka (blocking) phase of REOF 1 is wet over the Northwest from Northern California, Oregon, and Washington to Idaho, while parts of the Southwest through the central and northern Great Plains are dry. Several climate divisions in the Northwest exhibit composite precipitation anomalies exceeding 50 mm/month. Above-normal precipitation in the Northwest during positive REOF 1 months is consistent with the La Niña phase of ENSO tendency for wet conditions in this region, as the La Niña state favors this positive extreme of REOF 1

(Tables 2 and 3). The negative anomaly over the Kamchatka phase (strong, high-latitude westerlies in the western North Pacific) of REOF 1 has a precipitation pattern nearly opposite of that of the positive phase but not as strong. It is dry over the Northwest and wet from parts of the Southwest through the central Great Plains. This pattern is consistent with the tendency for negative REOF 1 to occur during the El Niño phase of ENSO, as indicated in Tables 2 and 3.

The weakened Aleutian Low phase of REOF 2 is associated with heavy precipitation over most of the West Coast and in the northern Rocky Mountain states; dry conditions appear in New Mexico, Texas, Colorado, and Wyoming. For the deep Aleutian Low phase of REOF 2, the precipitation pattern is nearly opposite, with a strip of positive precipitation anomalies in the Southwest and negative anomalies in the Northwest. Like REOF 1, these patterns are consistent with the precipitation tendencies for the La Niña and El Niño phases of ENSO, which favor positive and negative extremes of REOF 2, respectively.

The weakened Gulf of Alaska Low phase of REOF 3 is associated with lighter-than-normal precipitation over most of the Northwest and heavier-than-normal precipitation from the Southwest through the Great Plains. Surprisingly, the precipitation pattern for the strengthened Gulf of Alaska Low phase of REOF 3 is also light in the Pacific Northwest and rather weak over the rest of the region.

The phase of REOF 5 (the EP pattern) with positive 700-mb height anomalies over Alaska is associated with lighter-than-normal precipitation over the Northwest and heavier-than-normal precipitation over California and Nevada. This dry western pattern during a positive anomaly EP episode tends to occur during the El Niño phase of ENSO. The REOF 5 phase with negative 700-mb height anomalies over Alaska has lighter-than-normal precipitation over most of the western United States, but the largest anomalies are in central and northern California.

The phase of REOF 6 (the TNH pattern) with positive anomalies over the eastern North Pacific is associated with lighter-than-normal precipitation over the western United States, with strongest deficits over the coastal region from northern California to Washington. For the REOF 6 phase with negative anomalies over the eastern North Pacific, the precipitation pattern is nearly opposite, with heavier-than-normal precipitation over the western United States. This negative anomaly extreme of TNH is favored by the El Niño phase of ENSO.

### **Extreme Precipitation During Warm and Cool Phases of ENSO**

The above analysis reveals the inclination toward a set of preferred modes of the monthly average circulation over the North Pacific-North America sector during the La Niña and El Niño states of the SOI. Along with this, there are distinct precipitation anomaly patterns over the western United

States. Despite the inclination toward anomalous regional precipitation of one sign or the other, the historical record shows that both extremes of precipitation do occur during La Niña and during El Niño. A follow-on issue, then, is whether the pattern of atmospheric circulation that produces precipitation and whether the associated geographic distribution of precipitation are changed from La Niña to El Niño, even though each may have anomalously heavy or light regional precipitation.

Thus, the second approach to examining the atmospheric circulation and precipitation behavior during ENSO extremes was to target particular regions, with conditioning on the state of ENSO and the state of precipitation. We examined two regions: the Pacific Northwest (PNW) and the Desert Southwest (DSW). Both of these exhibit El Niño and La Niña responses (eg, Redmond and Cayan 1994), with significant precipitation anomalies over the fall-winter-spring period following the La Niña or El Niño state of the SOI in JJASON. The PNW and DSW regions were prominent locales in the overall precipitation patterns associated with several of the REOF circulation anomalies discussed above.

Despite their long-term anomaly differences during the two extremes of ENSO, both positive and negative precipitation anomalies occur in individual months and seasons. To augment the analyses that have determined ENSO relationships to the amount of precipitation, this investigation attempts to determine how the causal atmospheric circulation and the associated spatial distribution of precipitation change in response to ENSO. (Hypothetically, it could be that for a given region all storms are identical, regardless of ENSO state, but that the storm frequency changes, so the total amount changes.) To examine this, composites were constructed of the 700-mb height anomaly during four groups: when ENSO is in its El Niño state and regional precipitation is either heavy or light, and when ENSO is in its La Niña state and regional precipitation is either heavy or light.

The extreme ENSO cases are based on the SOI values of the JJASON preceding the NDJFM months. Heavy/light precipitation is defined as a month when the magnitude of the regional precipitation anomaly exceeds 0.5 standard deviations. To test the consistency of the precipitation patterns, two periods were considered for each case: 1895-1930 and 1931-1991. This delineation was chosen because before 1931 divisional precipitation values were estimated from statewide averages, and after 1931 divisional values were constructed from stations within each division. No such long series is available for the 700-mb height, so only one map was constructed for its anomalies, using data from 1947 to present. The number of months used to form the average anomalies shown in the composites ranged from 5 to more than 30; in all but one case, 12 or more months were included.

Before describing precipitation patterns for each of the composites, some overall observations are pertinent. In general, the pair of precipitation maps (1895-1930 and 1931-1991) are quite consistent, with a surprising degree of agreement over the western United States sector. Downstream (east of

about 100°W), the degree of correspondence is degraded, but we have not shown this area, because the intent is to study the western United States. This discussion does not describe the two individual maps for each case, but rather provides a view from the consensus of major features of each.

**Extreme Precipitation Patterns in the PNW Region**

The first set of circulation and precipitation composites is for the PNW. SOI negative (Figure 7) and positive (Figure 8) are divided into the PNW wet (left) and the PNW dry (right) cases. The SOI negative wet case has heavy precipitation extending from northern California through the Pacific Northwest. Monthly anomalies in the PNW region exceed 100 mm. The 700-mb height anomaly pattern features a broad, negative anomaly centered at about 45°N 160°W and extending from the Aleutian Islands to the North American coast. To the south are strong positive anomalies throughout most of the subtropical North Pacific, and downstream there is a negative anomaly center over the southeastern United States. This pattern is a symptom of active storms tracking zonally across from the

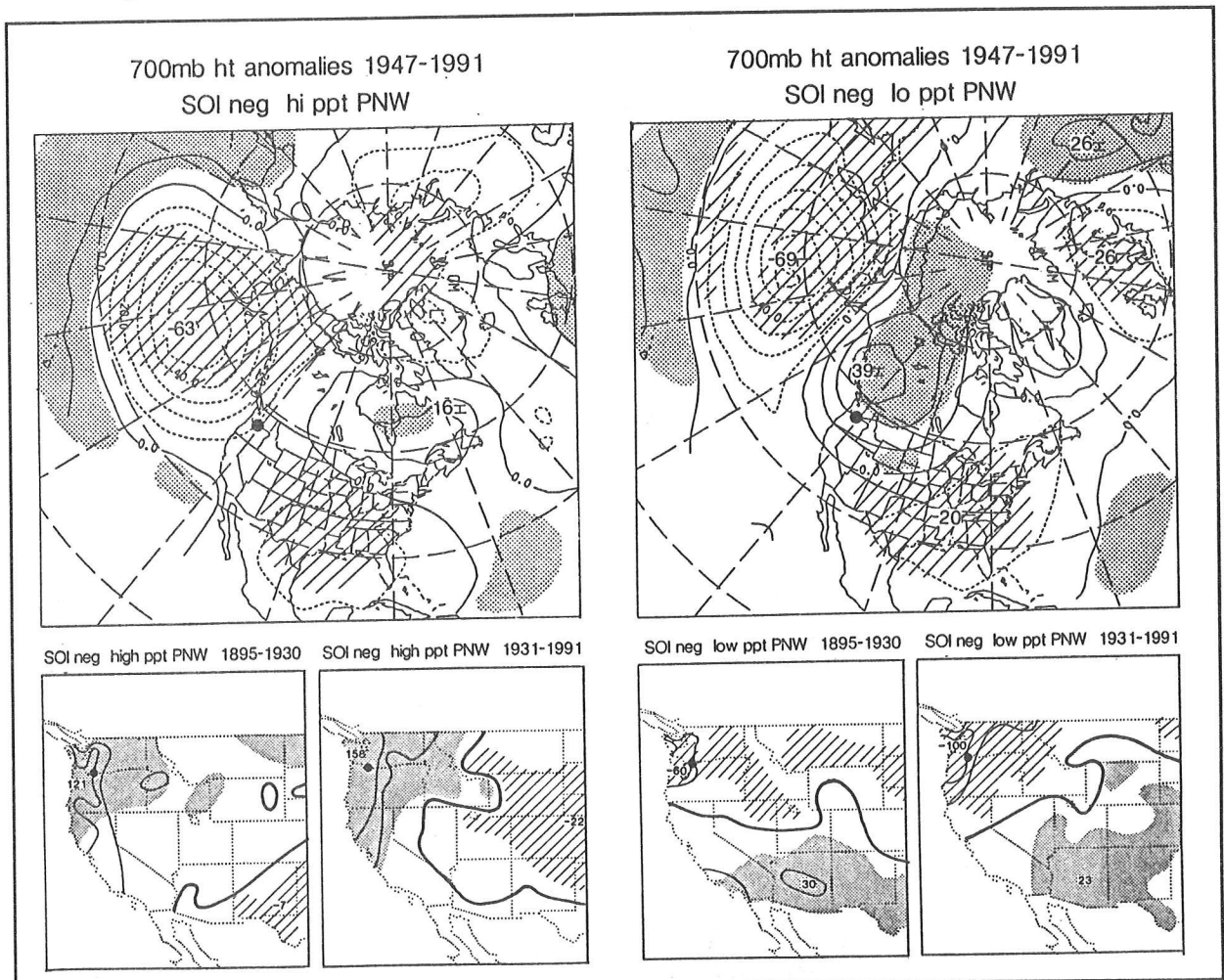


Figure 7. Composite 700-mb Height Anomaly Pattern and Precipitation Distribution over the Western United States for Negative SOI — Pacific Northwest.

Classes are divided into months when PNW region (indicated by dot; but see Figure 1) was wet (left) and dry (right). Anomalies exceeding the 90% significance level, using a 2-tailed *F*-test, are shaded (stippled/hatched, designating wet/dry). 700-mb height anomalies contoured at 10-m intervals, precipitation anomalies contoured at 0, 25, and 50 mm.

central North Pacific into the Pacific Northwest. The SOI negative dry case has light precipitation throughout the Northwest, with maximum negative anomaly values in excess of 75 mm. To the south, there is heavy precipitation over the Southwest. The 700-mb height anomaly pattern is quite similar to that for the SOI negative wet PNW case, but the North Pacific negative anomaly center is stationed farther west at about 170°W, and there is a strong positive anomaly seated over western Canada. With the strong positive anomalies over the subtropical North Pacific and the negative anomalies over the southeastern United States, this is strong expression of the PNA pattern (Barnston and Livezey 1987).

In contrast to the atmospheric circulations that prevail during the negative SOI precipitation patterns, those for the positive SOI (Figure 8) do not have very strong anomalies over the North Pacific, and largest anomaly centers are more constricted to higher latitudes. The SOI positive wet PNW composite has heavy precipitation extending from Oregon and Washington through Idaho. To the south, precipitation is light over the southwestern United States, consistent with the positive 700-mb height

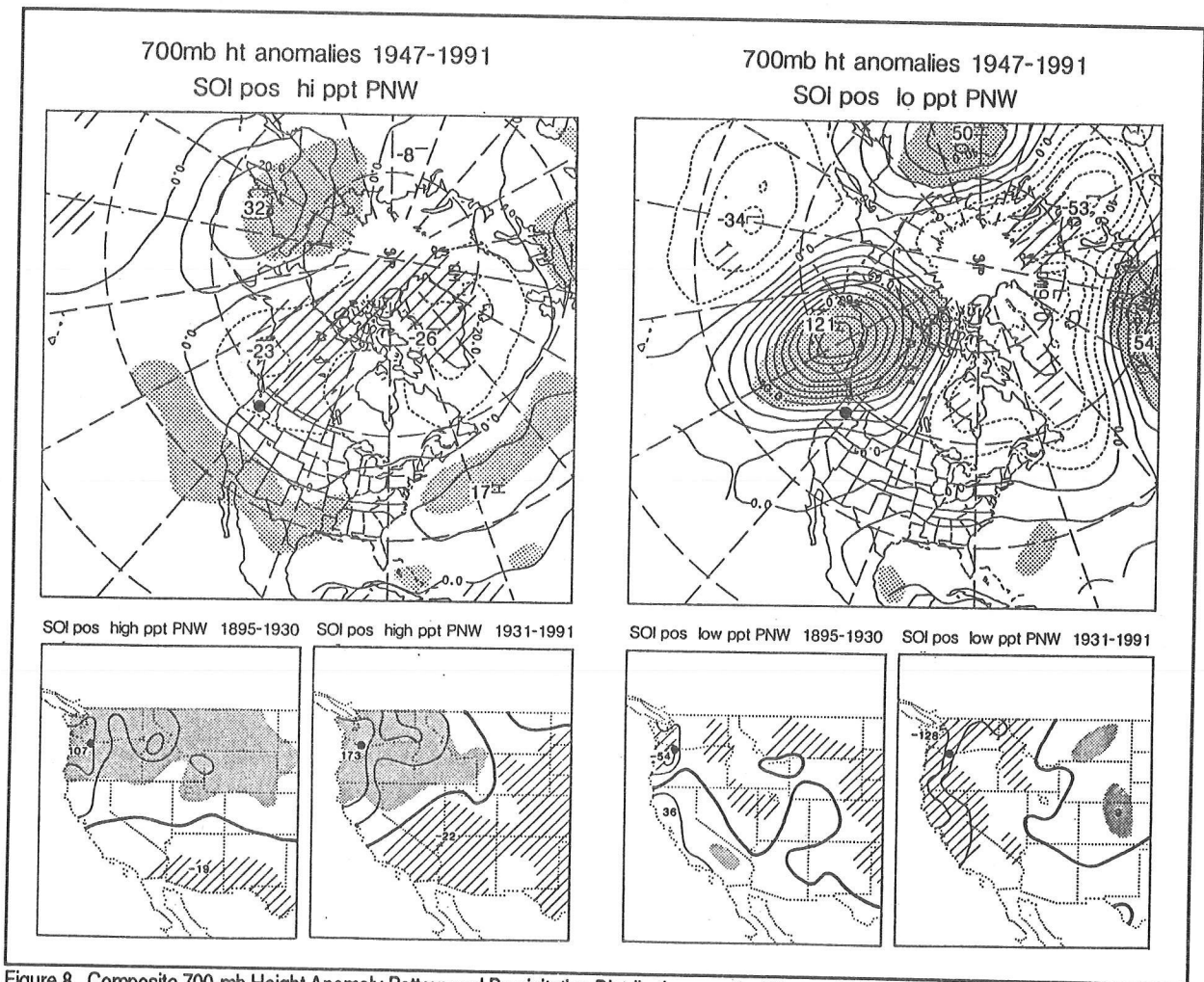


Figure 8. Composite 700-mb Height Anomaly Pattern and Precipitation Distribution over the Western United States for Positive SOI — Pacific Northwest.

Classes are divided into months when PNW region (indicated by dot; but see Figure 1) was wet (left) and dry (right). Anomalies exceeding the 90% significance level, using a 2-tailed t-test, are shaded (stippled/hatched, designating wet/dry). 700-mb height anomalies contoured at 0, 25, and 50 mm.

anomalies overlying this region. The SOI positive dry PNW pattern is dry over much of the western United States, although somewhat patchy. The 700-mb height anomaly pattern has a strong positive anomaly straddling the Gulf of Alaska and the Alaska/British Columbia region. This pattern lacks a strong teleconnection to the west, indicating the behavior over the central and western North Pacific during SOI positive dry PNW months is not very similar from one event to the next.

**Extreme Precipitation Patterns in the DSW Region**

The second set of circulation and precipitation composites is for the DSW precipitation extremes during SOI negative (Figure 9) and positive (Figure 10). Wet and dry cases are mapped on the left and right panels, respectively. The SOI negative wet DSW case has heavy precipitation extending from California through New Mexico and northward to the central Rocky Mountain states. Precipitation is light over the Northwest, showing a north-south out-of-phase pattern similar to some of those seen in Figures 7 and 8 associated with the PNW wet/dry composites. The

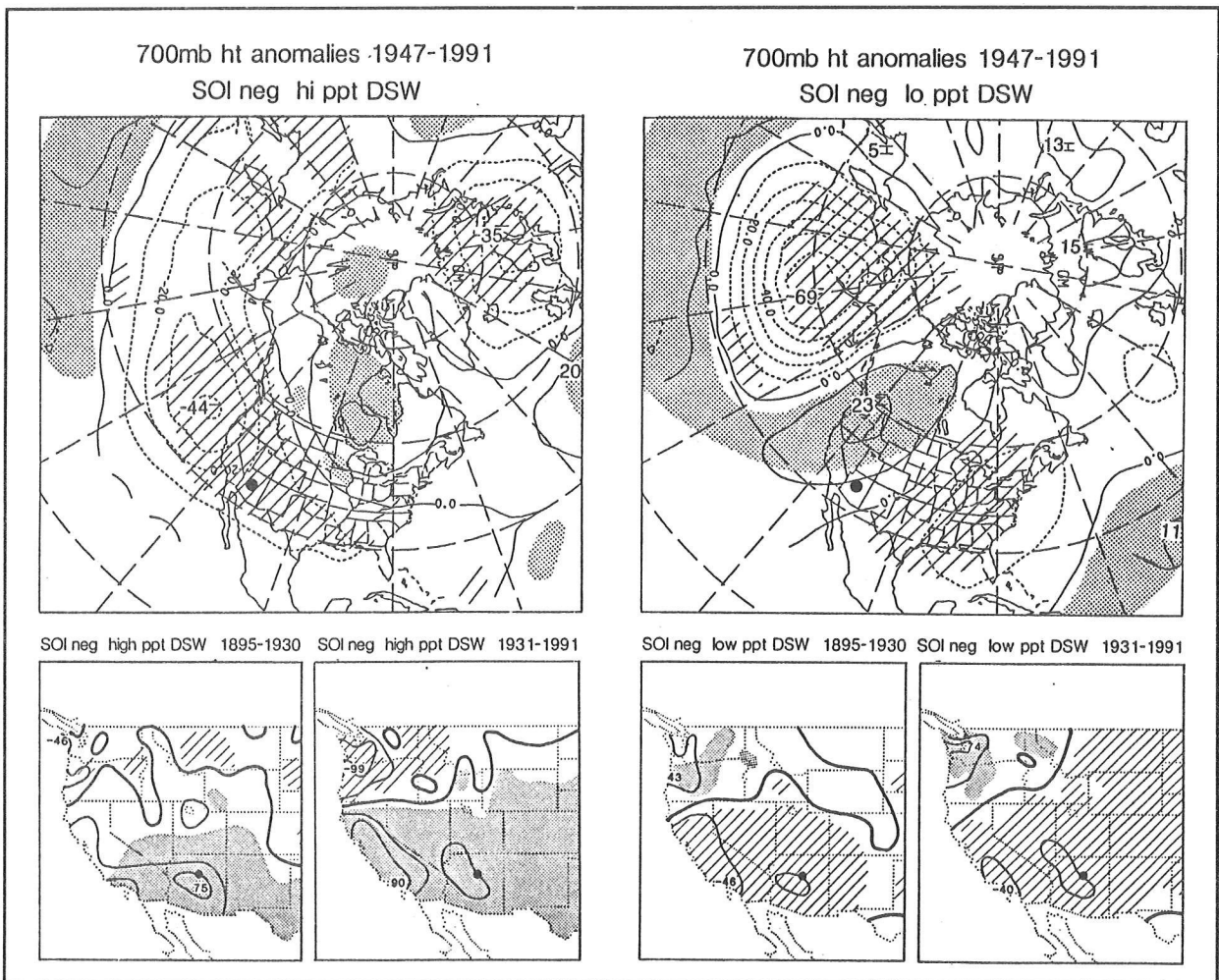


Figure 9. Composite 700-mb Height Anomaly Pattern and Precipitation Distribution over the Western United States for Negative SOI — Desert Southwest.

Classes are divided into months when DSW region (indicated by dot; but see Figure 1) was wet (left) and dry (right). Anomalies exceeding the 90% significance level, using a 2-tailed t-test, are shaded (stippled/hatched, designating wet/dry). 700-mb height anomalies contoured at 10-m intervals, precipitation anomalies contoured at 0, 25, and 50 mm.

700-mb height anomalies feature negative anomalies in low-middle latitudes (about 30-40°N) from 150°W across the entire western half of the United States. This zonal swath is consistent with active storms and broad heavy precipitation across the southern United States shown by the precipitation maps. Like the SOI negative PNW patterns, there are positive anomalies across the subtropical western North Pacific. The SOI negative dry DSW composite is nearly opposite from the SOI negative wet DSW case, with light precipitation extending from California through New Mexico and northward to the Rocky Mountain states. Also, precipitation is out of phase in the Pacific Northwest, with patches of heavy precipitation there. The SOI negative dry DSW 700-mb anomaly pattern is similar to the one for SOI negative dry PNW, with a strong negative anomaly south of the Aleutian Islands. However, the positive anomaly enveloping the West Coast for the dry DSW case is extended farther south than that of the PNW case, and actually joins the positive anomalies that cover the subtropical North Pacific. With the negative anomaly center stationed downstream over the southeastern United States, this is another strong example of the PNA pattern.

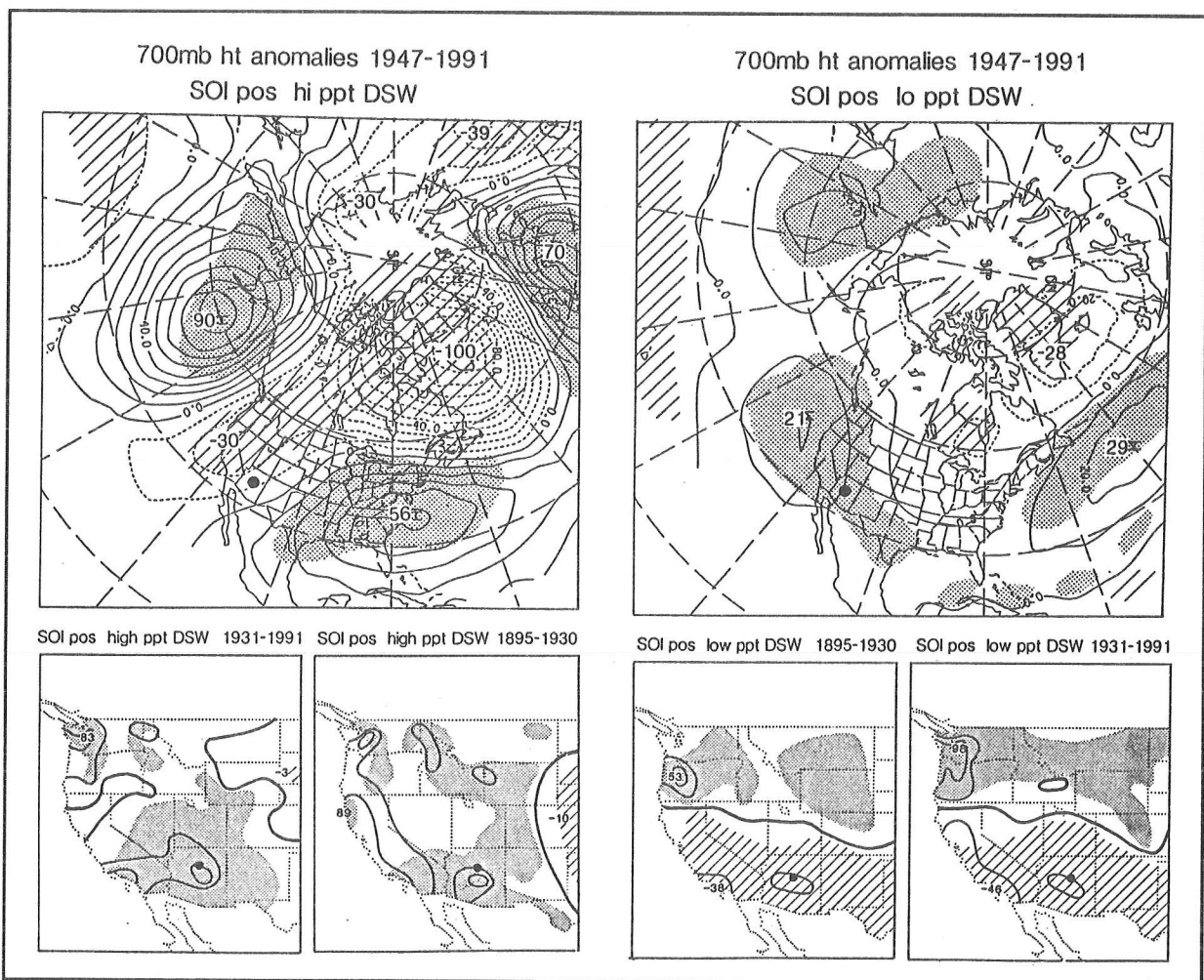


Figure 10. Composite 700-mb Height Anomaly Pattern and Precipitation Distribution over the Western United States for Positive SOI — Desert Southwest.

Classes are divided into months when DSW region (indicated by dot; but see Figure 1) was wet (left) and dry (right). Anomalies exceeding the 90% significance level, using a 2-tailed t-test, are shaded (stippled/hatched, designating wet/dry). 700-mb height anomalies contoured at 10-m intervals, precipitation anomalies contoured at 0, 25, and 50 mm.

As in the PNW composites, the positive SOI patterns for DSW wet and dry cases (Figure 10) are very different from their negative SOI counterparts. The SOI positive wet DSW composite has heavy precipitation covering much of the western United States, including most of the Southwest and parts of the Rocky Mountains and the Northwest. In contrast to the extensive zonally-oriented pattern of the SOI negative wet DSW case, the SOI positive wet DSW circulation is a tight, high amplitude wave pattern with positive 700-mb height anomalies to the west centered at about 50°N 150°W, negative anomalies over the West Coast, and positive anomalies downstream over the southeastern United States. The negative anomalies over the West Coast are actually a southward-extending tongue of a circumpolar patch that also covers most of Canada, the Arctic, and the far North Atlantic. (Note that the SOI negative wet DSW case had positive 700-mb height anomalies over much of this region.) Finally, the SOI positive dry DSW composite has light precipitation over a band from California to Texas. A marked feature of the precipitation pattern is the out-of-phase heavy precipitation over the Northwest from Oregon and Washington to Wyoming and Montana. The circulation is again very distinct from that of the negative SOI counterpart, with positive 700-mb height anomalies over the eastern North Pacific just off the West Coast through the DSW region. Interestingly, these are associated with negative anomalies in the subtropics of the western North Pacific.

## Summary and Conclusions

---

Two approaches were taken to decipher the response to the El Niño/Southern Oscillation by atmospheric circulation over the North Pacific/North America and by precipitation over the western conterminous United States.

First, using rotated empirical orthogonal functions of the 700-mb height, prominent monthly anomalous atmospheric circulation patterns were identified over the November-March cool "season" from a data set covering 1947 to 1991. By compositing the amplitudes of each REOF, those REOFs that are significantly related to positive and negative phases of the SOI were determined.

Second, an analysis was conducted based on extreme regional western United States precipitation during each of the two ENSO states. Precipitation averaged over the Pacific Northwest and the Desert Southwest was targeted. This second part was aimed at:

- Determining differences in the atmospheric circulation responsible for the precipitation anomalies between the two ENSO states, and
- Determining the extent and configuration of the spatial precipitation anomalies associated with the PNW and DSW regional extremes and how they vary from the El Niño to the La Niña states.

Concerning the response of individual circulation modes to ENSO, five modes exhibited preferences of either their positive or negative extremes during the NDJFM cool season that overlaps with a JJASON whose average normalized SOI anomaly magnitude exceeded 0.5. The REOFs were associated with the patterns determined by Barnston and Livezey (1987) in their study of the anomalous monthly atmospheric circulation over the Northern Hemisphere. Four of the five — identified as the Western Pacific Oscillation, two hybrids of the Pacific/North American pattern, and the East Pacific pattern — had a symmetric response, with opposite biases for the El Niño and La Niña phases of ENSO. The fifth mode, the Tropical/Northern Hemisphere pattern, exhibited biases during El Niño episodes but not during La Niña. Virtually all of the five REOFs have significant anomaly expressions over the North Pacific sector. Some contained extremely strong ENSO relationships. For example, during El Niño the WPO pattern was in its strengthened Kamchatka Low state in 11 months and in its weakened Kamchatka Low state in only 2 months. In contrast, during La Niña the WPO pattern was in its weakened Kamchatka Low state in 17 months and in its strengthened Kamchatka Low state in only 1 month. Using composites, it is clear that most of these modes produce statistically significant, regional-scale precipitation anomaly patterns over the western United States. Even the WPO, with its western-centered anomaly features, has a strong precipitation anomaly association over the western United States. During El Niño, these modes tend to reinforce the tendency for the northwestern United States to be dry and the southwestern United States to be wet during El Niño, and for the opposite conditions to occur during La Niña.

From the analyses based on the PNW and DSW regional precipitation, it was determined that precipitation anomalies cover broad regional scales, but with quite different geographic distributions during El Niño *vs.* La Niña. In turn, these precipitation distributions and their differences are driven by the large-scale atmospheric circulation, which differs greatly during El Niño *vs.* La Niña. Consistent with results of the analysis of the NDJFM circulation modes in the first part of this study, the El Niño circulation patterns tended to have strong negative 700-mb height anomalies and attendant strengthened westerly winds over middle latitudes of the central-to-eastern North Pacific sector. In the subtropics west of the international date line, the height anomalies were positive during El Niño, both for heavy and light regional precipitation. In cases where the westerlies break through to the West Coast, precipitation is heavy, but in cases where the westerlies are confined to the central North Pacific with a ridge of high pressure to their east (over the West Coast), precipitation is light.

Both positive and negative precipitation anomalies arising during La Niña cases were quite different from those during El Niño. The La Niña circulation patterns tended to have a weak anomaly structure over much of the North Pacific, with strongest anomaly centers over high latitudes

and over the North American sector. The La Niña circulation patterns associated with regional precipitation anomalies featured rather strong meridional flow anomalies, as opposed to those for El Niño, which displayed zonal flow anomalies.

Concerning the geographic distribution of precipitation anomalies associated with PNW and DSW conditions, there were broad regional scales of precipitation anomalies. Consistent with the differences between the atmospheric circulations of the two ENSO states, the geographic distribution of precipitation differed from El Niño to La Niña. The reliability of this result was indicated by the consistency of the patterns derived for each subset from two separate periods: 1895-1930 and 1931-1991.

## References

- Andrade, ER, and WD Sellers. 1988. El Niño and its effect on precipitation in Arizona and western New Mexico. *Journal of Climate* 8:403-410.
- Barnett, TP, M Latif, E Kirk, E. Roeckner. 1991. On ENSO Physics. *Journal of Climate* 4:487-515.
- Barnston, AG, and RE Livezey. 1987. Classification, seasonality and persistence of low-frequency atmospheric circulation patterns. *Monthly Weather Review* 225:1083-1126.
- Cayan, DR, and DH Peterson. 1989. The influence of North Pacific atmospheric circulation on streamflow in the west. Pages 337-397 in *Aspects of Climate Variability in the Pacific and the Western Americas*. DH Peterson, editor. Geophysical Monograph 55, Washington, DC, American Geophysical Union.
- Cayan, DR, and RH Webb. 1992. El Niño/Southern Oscillation and streamflow in the western United States. Pages 29-68 in *Historical and Paleoclimatic Aspects of the Southern Oscillation*. HF Diaz and V Markgraf, editors. Cambridge University Press.
- Douglas, AV, and PJ Englehart. 1981. On a statistical relationship between rainfall in the central equatorial Pacific and subsequent winter precipitation in Florida. *Monthly Weather Review* 114:1716-1738.
- Kahya, E, and JA Dracup. 1993. U.S. Streamflow patterns in relation to the El Niño/Southern Oscillation. *Water Resources Research* 29:2491-2503.
- Kiladis, GN, and HF Diaz. 1989. Global climatic anomalies associated with extremes in the Southern Oscillation. *Journal of Climate* 2(9):1069-1090.
- Koch, RW, CF Buzzard, DM Johnson. 1991. Variation of snow water equivalent and streamflow in relation to the El Niño/Southern Oscillation. Pages 37-48 in *Proceedings, 1991 Western Snow Conference, Juneau, Alaska*.
- Livezey, RE, and KC Mo. 1987. Tropicaextratropical teleconnections during the Northern Hemisphere winter, Part II: Relationships between monthly mean Northern Hemisphere circulation patterns and proxies for tropical convection. *Monthly Weather Review* 115:3115-3132.
- Molles, MC, and CN Dahm. 1990. A perspective on El Niño and La Niña: Global implications for stream ecology. *Journal of North American Benthological Society* 9:68-76.
- Redmond, KT, and DR Cayan. 1994. El Niño/Southern Oscillation and western climate variability. AMS Annual Meeting. Nashville, TN. Preprints.
- Redmond, KT, and RW Koch. 1991. Surface climate and streamflow variability in the western United States and their relationship to large scale circulation indices. *Water Resources Research* 27:2381-2399.

- Ropelewski, CF, and MS Halpert. 1986. North American precipitation and temperature patterns associated with the El Niño/Southern Oscillation (ENSO). *Monthly Weather Review* 114:2352-2362.
- Schonher, T, and SE Nicholson. 1989. The relationship between California rainfall and ENSO events. *Journal of Climate* 2:1258-1269.
- Webb, RH, and JL Betancourt. 1990. *Climatic Variability and Flood Frequency of the Santa Cruz River, Pima County, Arizona*. U.S. Geological Survey, Open-File Report 90-553, 69 pp.
- Woolhiser, DA, TO Keefer, KT Redmond. 1993. Southern Oscillation effects on daily precipitation in the Southwestern United States. *Water Resources Research* 29:1287-1295.
- Yarnal, B. 1985. Extratropical teleconnections with El Niño/Southern Oscillation (ENSO) events. *Prog Phys Geogr* 9:315-352.
- Yarnal, B, and H F Diaz. 1986. Relationship between extremes of the Southern Oscillation and the winter climate of the Angloamerican Pacific coast. *Journal of Climatology* 6:197-219.

# Semiempirical Down-Scaling of GCM Output to the Local Scale for Temperature, Precipitation, and Runoff

Frederick Wade Freeman and John A. Dracup

**ABSTRACT:** An empirically derived multiple linear regression model is used to relate a local-scale dependent variable (either temperature, precipitation, or surface runoff) measured at individual gauging stations to six large-scale independent variables (temperature, precipitation, surface runoff, height to the 500-mbar pressure surface, and the zonal and meridional gradient across this surface). Regression equations are calibrated and verified for each dependent variable, for each station, and for each calendar month. The regression equations are then inverted and operated in a semiempirical mode by substituting in GCM produced large-scale output from a CO<sub>2</sub> doubled simulation for the independent variables. The resulting equations are used to predict local values for the three dependent variables; this is the down-scaling process. Down-scaled values for each dependent variable are plotted and contoured to reveal local-scale features. Model performance statistics (the R<sup>2</sup> and F test statistics) are plotted to indicate the spatial variability of the model's performance.

The area investigated is the western United States. The variance explained by the regression model, as indicated by the R<sup>2</sup> test statistic, displays spatial and temporal differences. The explained variance for domains centered over the Sacramento River Basin, in northern California, are 72 to 90 percent for temperature, 42 to 78 percent for precipitation, and 60 to 87 percent for runoff. Results for the area around the Upper Colorado River Basin are slightly lower. The calibration data set is from 1948 through 1988 and includes data from 268 joint temperature and precipitation stations, 152 streamflow stations (which are converted to runoff data), and 24 gridded 500-mbar pressure height nodes.

This study focuses on changes in the temporal and spatial pattern of the local-scale climate and hydrology in the western United States as characterized by altered temperature, precipitation, and surface runoff values for a simulated global climate with a doubled concentration of atmospheric CO<sub>2</sub>, a common "greenhouse" gas. Detailed attention is given to the response of two river systems important to the economies of the western United States: the Sacramento (in northern California) and the Upper Colorado (split mainly between Utah and Colorado). Runoff values were determined from streamflow volumes and drainage basin size data for unimpaired basins only.

This research augments in a unique way the existing set of investigations into the effect of climate change on these two basins and on the western United States in general by using a new climatic and hydrologic data set (Wallis *et al* 1991) with an investigative technique new to the field of hydrology: the semiempirical down-scaling regression model. The specific question addressed is how to increase the resolution of large-scale climatic and hydrologic data generated from climate-simulating computer models. The answer we present is a regression model that correlates

local-scale values of temperature, precipitation, and runoff to large-scale averages of the same three variables plus three atmospheric pressure terms (refer to equations 1.1 through 1.3).

## Methodology

---

Our methodology is derived from the well-documented semiempirical modeling approach first employed by Kim *et al* (1984) and later expanded on by Wilks (1989), Wigley *et al* (1990), Karl *et al* (1990), and Storch *et al* (1993). This modeling approach uses an empirically derived multiple linear regression model in conjunction with computer simulated data to translate large-scale, coarse-resolution information into more useful local-scale, high-resolution information. This union between empirical relations and computer simulations inspires the term “semiempirical”.

Semiempirical techniques have been employed to model the climatic variables of surface air temperature and precipitation. In this research effort we investigate, along with these two climatic variables, the applicability of this modeling technique to a third parameter: the hydrologic variable of surface runoff.

Model development and use follow the two-step process of:

- Calibration and validation with observed data as the independent and dependent variables, and then
- Down-scaling with computer-simulated data for a changed climate scenario in place of the observed independent variables.

The first step, called the “calibration step”, is as follows. Observed data from an individual hydrometeorological station — either temperature, precipitation, or runoff — are used to describe the local-scale characteristics and serve as the dependent variable, which are regressed on a set of five or six independent variables. The independent variables are large-scale values determined by averaging together observed data from all stations located within a specified large-scale domain, which includes the single station used as the dependent variable. It is convenient to set the large-scale domains equal to the established grid elements of a well-tested GCM (general circulation model). We have chosen to use the Goddard Institute for Space Studies (GISS) GCM, which is described by Hansen *et al* (1983) and Hansen *et al* (1988). GISS grid domains are shown in Figure 1.

The six large-scale area average values are: temperature, precipitation, and runoff plus the three atmospheric variables of height to the 500-millibar pressure surface, and the zonal (east-west) and meridional (north-south) 500-millibar pressure gradients. Inclusion of atmospheric pressure data has been shown to increase model performance (*eg*, Wigley *et al* (1990) use three pressure terms; Karl *et al* (1990) use six pressure terms). Calibration equations are established for each calendar month and for

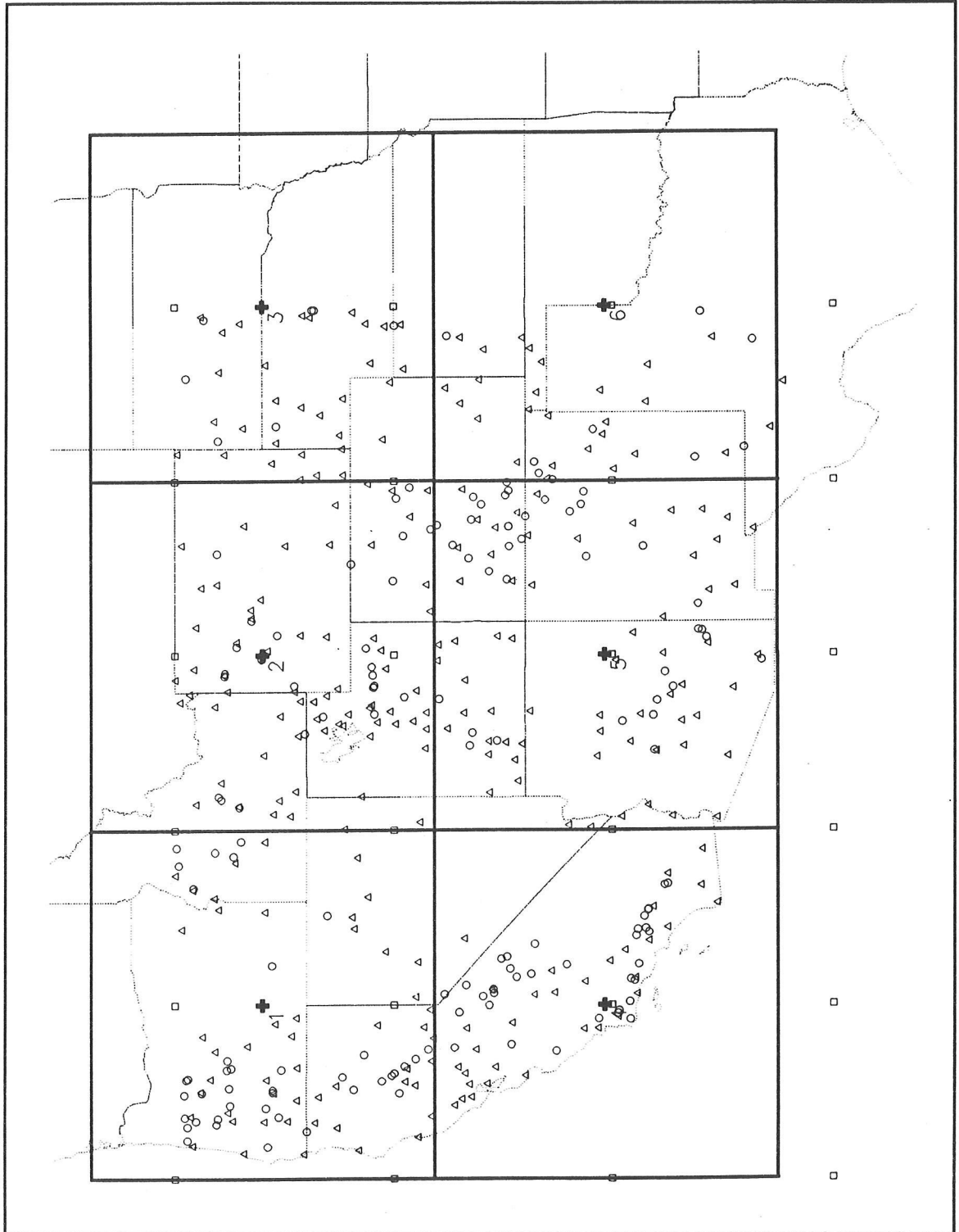


Figure 1. Location of Grid Elements and Node Points for the GISS GCM Model with the Combined Temperature and Precipitation Stations (triangles), Runoff Stations (circles), and Pressure Stations (squares). The map is shown on a latitude by longitude coordinate system.

each individual temperature, precipitation, and runoff station from 41 years of observed data (1948 through 1988).

The calibration equations take one of the three following forms:

$$\begin{aligned} TEMP_{myi} = & \beta_{0mi} + \beta_{1mi}\overline{TEMP}_{my} + \beta_{2mi}\overline{PRCP}_{my} + \\ & \beta_{3mi}\overline{PRESSZ}_{my} + \beta_{4mi}\overline{PRESSU}_{my} + \beta_{5mi}\overline{PRESSV}_{my} + \epsilon_{mi} \end{aligned} \quad (1.1)$$

$$\begin{aligned} PRCP_{myi} = & \beta_{0mi} + \beta_{1mi}\overline{TEMP}_{my} + \beta_{2mi}\overline{PRCP}_{my} + \\ & \beta_{3mi}\overline{PRESSZ}_{my} + \beta_{4mi}\overline{PRESSU}_{my} + \beta_{5mi}\overline{PRESSV}_{my} + \epsilon_{mi} \end{aligned} \quad (1.2)$$

$$\begin{aligned} FLOW_{myi} = & \beta_{0mi} + \beta_{1mi}\overline{FLOW}_{my} + \beta_{2mi}\overline{TEMP}_{my} + \beta_{3mi}\overline{PRCP}_{my} \\ & + \beta_{4mi}\overline{PRESSZ}_{my} + \beta_{5mi}\overline{PRESSU}_{my} + \beta_{6mi}\overline{PRESSV}_{my} + \epsilon_{mi} \end{aligned} \quad (1.3)$$

where *TEMP*, *PRCP*, and *FLOW* are observed local-scale dependent variables for temperature, precipitation, and runoff;  $\overline{TEMP}$ ,  $\overline{PRCP}$ , and  $\overline{FLOW}$  are observed large-scale area average independent variables for these same three quantities;  $\overline{PRESSZ}$ ,  $\overline{PRESSU}$ , and  $\overline{PRESSV}$  are observed large-scale area average independent variables for the three pressure terms: *Z* is for the 500-millibar surface height, *U* is for the zonal gradient across this surface, and *V* is for the meridional gradient across this surface; the  $\beta$ s are regression coefficients; the  $\epsilon$ s are the error terms; and *m*, *y*, and *i* are the calendar months, the specific year from the time series, and a specific gauging station, respectively (*m* = 1, 2, ... 12; *y* = 1, 2, ... 41; and *i* = 1, 2, ... 268 for temperature and precipitation, and *i* = 1, 2, ... 152 for runoff). *FLOW* is not included among the independent variables when regressing for *TEMP* or *PRCP* because there is no clear physical linkage in this direction. During the calibration step, the equations are solved to determine the value of the  $\beta$ s.

The second step of the modeling process begins once the regression relationships are calibrated and the regression coefficients, the  $\beta$ s, are known. In this step, the observed large-scale data originally used as the independent variables are directly replaced with large-scale data simulated by the GISS GCM operated under the climate-changed scenario of a doubled concentration of atmospheric CO<sub>2</sub>. With the GCM data in place and the  $\beta$ s known, the regression equations are said to be “inverted” and are now operated to generate local-scale values at individual observation stations for the climate condition employed by the GCM. This application of the model is termed the “down-scaling step”. Observed values for the three pressure terms were used in the down-scaling step (as well as in the calibration step) because GCM-simulated values were not available.

The modeling procedure is complete after regressions are first calibrated and then down-scaled for each individual observation station, for each of the three dependent variables, and for each month of the year. The modeling philosophy is summarized by Giorgi and Mearns (1991) as follows: The strategy is to treat large-scale forcings explicitly through the use of GCMs, and account for local-scale forcings in an empirical fashion.

When we view the process of down-scaling coarse-resolution data to the local scale, or sub-grid scale, as depicted schematically by Gates (1985) in Figure 2, we see that the semiempirical model presented here allows for the computation of step number two labeled “local climate change”. The other steps can be easily accomplished with existing models and statistical procedures. The result is a complete methodology to determine the local-scale effect of climate change on temperature, precipitation, and runoff — which is labeled as step four “local impact”. An outcome of having adapted a known meteorological regression technique to basin-scale streamflow and runoff is that a new avenue now exists for the investigation of hydrologic drought resulting from a changed climate. As a result, drought statistics can be generated on a local scale from GCM-simulated data for a CO<sub>2</sub> doubled environment.

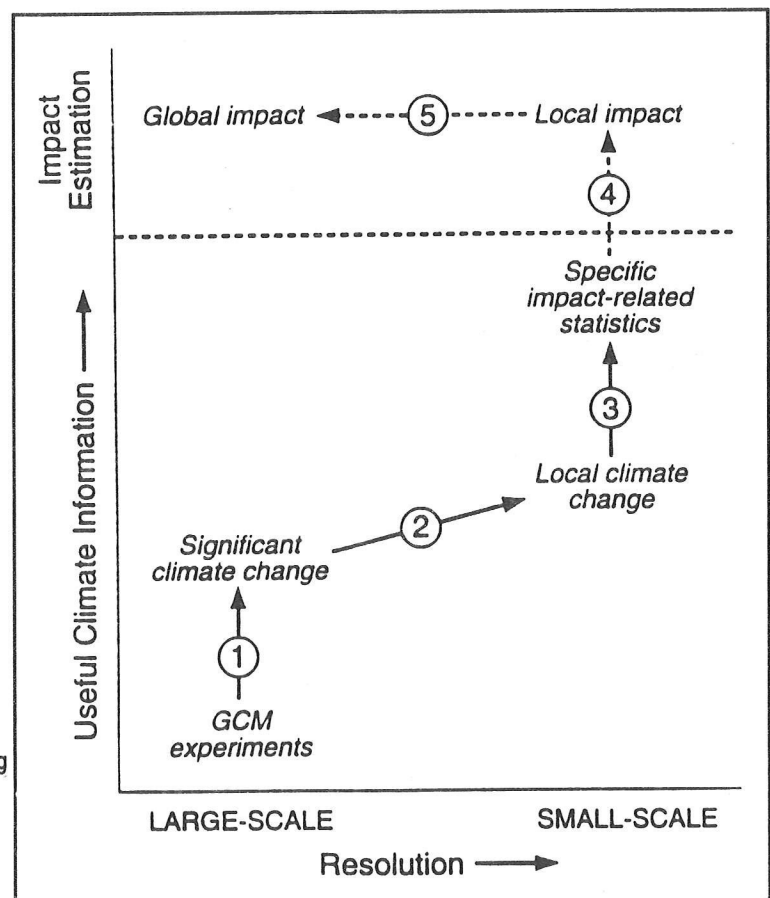


Figure 2. Schematic of the Processes of a Strategy for Down-Scaling to the Local (or Small) Scale the Results from a GCM Experiment Simulating Climate Change (From Gates 1991)

The output from the regression model serves two significant purposes.

- Down-scaled values can easily be used to construct contour maps, with local-scale resolution, that display monthly values for temperature, precipitation, and runoff for an environment with a doubled CO<sub>2</sub> concentration. Two statistical parameters are also plotted along with the down-scaled values. The first is the goodness of fit statistic  $R^2$ , which measures the proportion of variance in the dependent variable that is explained by the model. The second is the F statistic, a significance test of the model as a whole.

- The output can also be used as a comparison data set for similar quantities produced from GCMs. Comparisons of output from the regression model and GCMs can serve to validate GCM simulations and to help modify the underlying parameterizations used in the hydrologic processor internal to several GCMs (Giorgi and Mearns 1991).

Only the first purpose is explored here.

## **Analysis**

---

Presented next are the down-scaled results for the western United States for temperature, precipitation, and runoff based on a CO<sub>2</sub> doubled climate simulated by the GISS GCM. Results are determined as differences (CO<sub>2</sub>x2-CO<sub>2</sub>x1) for temperature and as ratios (CO<sub>2</sub>x2/CO<sub>2</sub>x1) for precipitation and runoff. Figure 3 shows contoured January output for temperature, and Figure 4 is a contour map of the model performance statistic R<sup>2</sup>. Figures 5 and 6 show the same information for precipitation. These maps reveal the local-scale variation of the down-scaled values. Values for the F statistics are not shown. Down-scaled runoff values for July and the corresponding R<sup>2</sup> values are plotted on Figures 7 and 8. Similar plots for the remaining months have been generated but are not included here.

A high degree of spatial variability for the change in down-scaled runoff is observed over regions encompassing the Sacramento and Upper Colorado River Basins, with only limited variability elsewhere. This is most pronounced during winter months for the Sacramento Basin and during summer months for the Upper Colorado Basin. Down-scaled temperature change displays a fairly even amount of variability throughout the year, although the model output does show a gentle preference for greatest variability over the Upper Colorado Basin during winter and over the Sacramento Basin and the southern Sierra Nevada during summer. Down-scaled change in precipitation is more similar to down-scaled runoff than temperature, with greater variability occurring over western Oregon and northern California during winter and spring, and over the Rocky Mountains and the western Great Plains during summer.

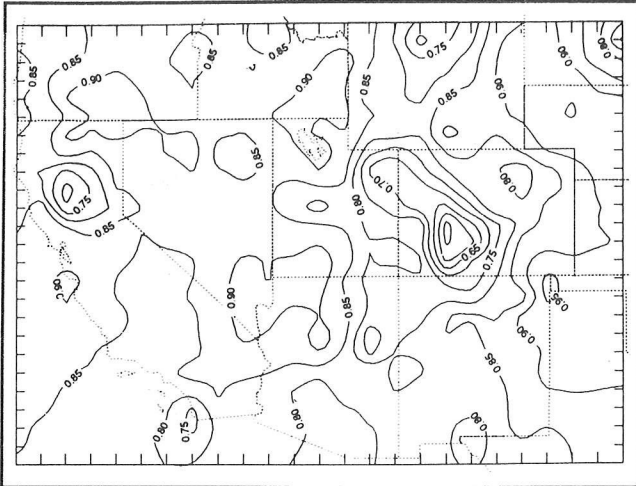


Figure 3. Contours of the SCI Model Performance Statistic  $R^2$  for January for the Down-Scaling of Temperature

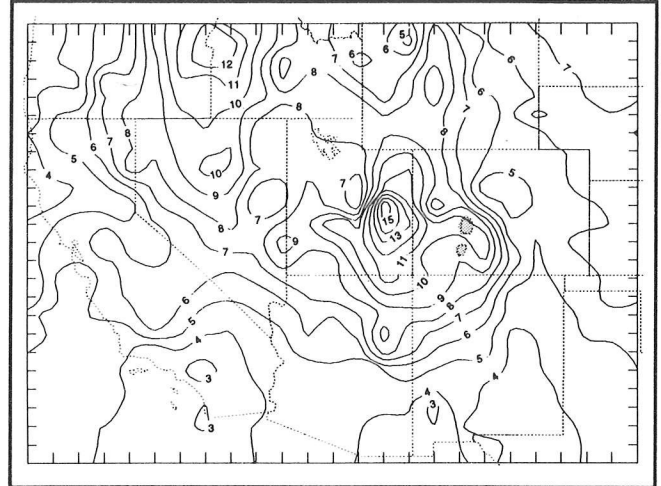


Figure 4. Down-Scaled Change in Temperature, as  $CO_2x2-CO_2x1$  and Measured in  $^{\circ}C$ , for January Using GISS GCM Output Data. Shaded areas indicate regions where the  $R^2$  value is below 0.5.

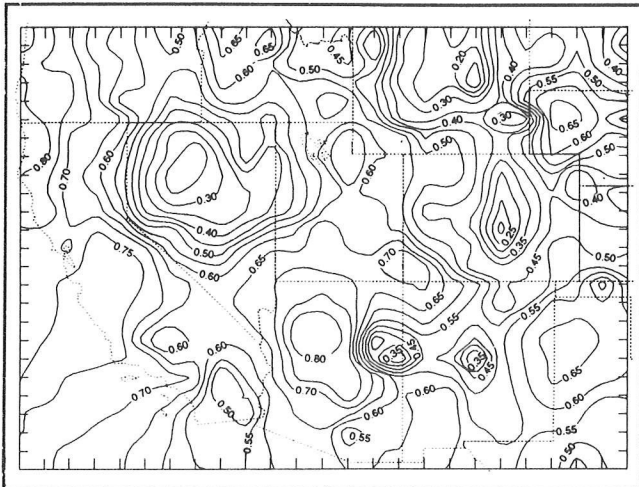


Figure 5. Contours of the SCI Model Performance Statistic  $R^2$  for January for the Down-Scaling of Precipitation

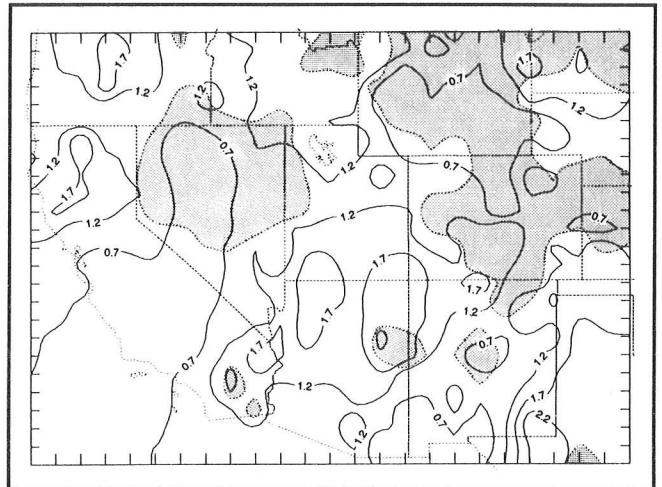


Figure 6. Down-Scaled Change in Precipitation, as a Percent of  $CO_2x1$  Precipitation and Measured in Millimeters/Day, for January Using GISS GCM Output Data. Shaded areas indicate regions where the  $R^2$  value is below 0.5.

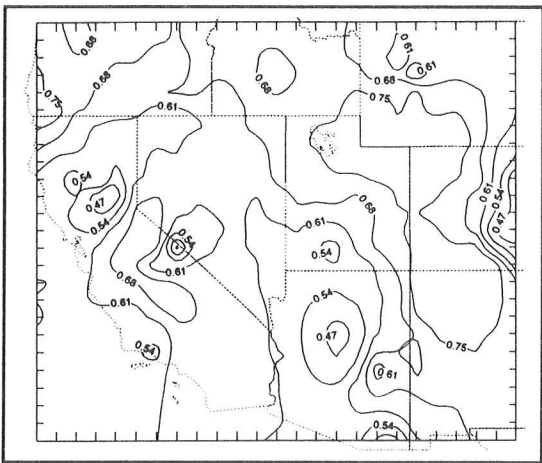


Figure 7. Contours of the SCI Model Performance Statistic  $R^2$  for July for the Down-Scaling of Runoff

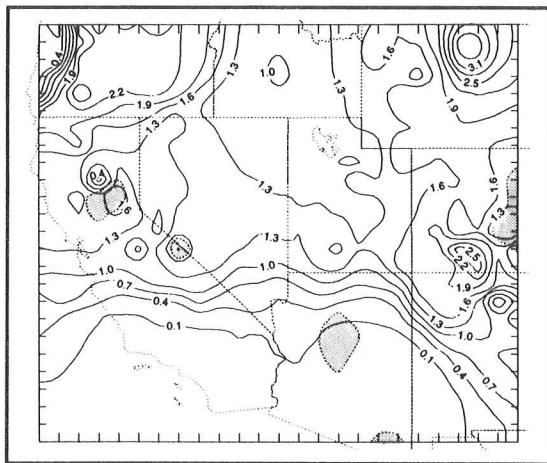


Figure 8. Down-Scaled Change in Runoff, as a Percent of  $CO_2x1$  Runoff and Measured in Millimeters/Day, for July Using GISS GCM Output Data. Shaded areas indicate regions where the  $R^2$  value is below 0.5.

## **References**

---

- Gates, WL. 1985. The Use of General Circulation Models in the Analysis of the Ecosystem Impacts of Climate Change. *Climatic Change*. 7:267-284.
- Giorgi, F, and LO Mearns. 1991. Approaches to the Simulation of Regional Climate Change: A Review. *Reviews of Geophysics*. 29:191-216.
- Hansen, J, G Russell, D Rind, P Stone, A Lacis, S Lebedeff, R Ruedy, L Travis. 1983. Efficient Three-Dimensional Global Models for Climate Studies: Models I and II. *Monthly Weather Review*. 3:609-662.
- Hansen, J, I Fung, A Lacis, D Rind, S Lebedeff, R Ruedy, G Russell, P Stone. 1988. Global Climate Changes as Forecast by Goddard Institute for Space Studies Three-Dimensional Model. *Journal of Geophysical Research*. 93(D8):9341-9364.
- Karl, TR, W-C Wang, ME Schlesinger, RW Knight, D Portman. 1990. A Method of Relating General Circulation Model Simulated Climate to the Observed Local Climate, Part I, Seasonal Statistics. *Journal of Climate*. 3:1053-1079.
- Kim, J-W, J-T Chang, NL Baker, DS Wilks, WL Gates. 1984. The Statistical Problem of Climate Inversion: Determination of the Relationship between Local and Large-Scale Climate. *Monthly Weather Review*. 112:2069-2077.
- Storch, HV, E Zorita, U Cubasch. 1993. Downscaling of Global Climate Change Estimates to Regional Scales: An Application to Iberian Rainfall in Wintertime. *Journal of Climate*. 6:1161-1171.
- Wallis, JR, DP Lettenmaier, EF Wood. 1991. A Daily Hydroclimatological Data Set for the Continental United States. *Water Resources Research*. 27:1657-1663.
- Wigley, TML, PD Jones, KR Briffa, G Smith. 1990. Obtaining Sub-Grid-Scale Information from Coarse-Resolution General Circulation Model Output. *Journal of Geophysical Research*. 95:1,943-1,953.
- Wilks, DS. 1989. Statistical Specification of Local Surface Weather Elements from Large-Scale Information. *Theoretical and Applied Climatology*. 40:119-134.

# Rapid Teleconnections Associated with Individual Tropical Cyclones

Ronald Gelaro, Tom Murphree, and James Goerss

Several studies have shown that tropical heating variations at intra-seasonal to interannual time scales may be associated with global climate anomalies. During the past decade, relatively high frequency (daily to weekly) variations in tropical convective activity have also been found to produce significant midlatitude responses within days to weeks (*eg*, Nitta 1987; Hurrell and Vincent 1990, 1991; Gelaro 1992). In this study, we investigate the processes by which individual tropical cyclones affect midlatitude weather and climate.

To identify these processes, we performed a series of experimental forecasts using the Navy's global operational data assimilation system and numerical weather prediction model. In these experiments, the strength and position of individual typhoons in the forecast initial conditions were systematically modified over several days of data assimilation. These modifications were done using a tropical cyclone bogus procedure to strengthen, weaken, or eliminate individual storms in the initial conditions, with little or no impact on the initial conditions outside the immediate vicinity of the storm. Comparisons of the forecasts from these different initial conditions were used to assess the global impacts of individual typhoons.

## Results

We present here the results from forecasts performed for typhoon Yuri, which occurred in the western north Pacific from November 23 to December 2, 1991. Yuri recurved on November 29 and became an extratropical storm on December 2. Figure 1 shows a forecast sequence of stream function and total vertically integrated heating based on initial conditions produced by the operational bogus procedure (referred to as a *positive* bogus forecast). This procedure gives the most realistic representation of Yuri in the initial conditions. Yuri is initially located in the area of high heating east of the Philippines (Figure 1a). Subsequently, Yuri recurves and moves within the high heating area that stretches northeastward from the subtropical western Pacific (Figure 1b), and then becomes an extratropical storm (Figure 1c).

Figure 2 shows a corresponding forecast sequence based on initial conditions in which Yuri was strongly suppressed (referred to as a *negative* bogus forecast). Note that throughout this sequence, the heating associated with Yuri is strongly reduced, while the heating elsewhere is very similar to that in Figure 1.

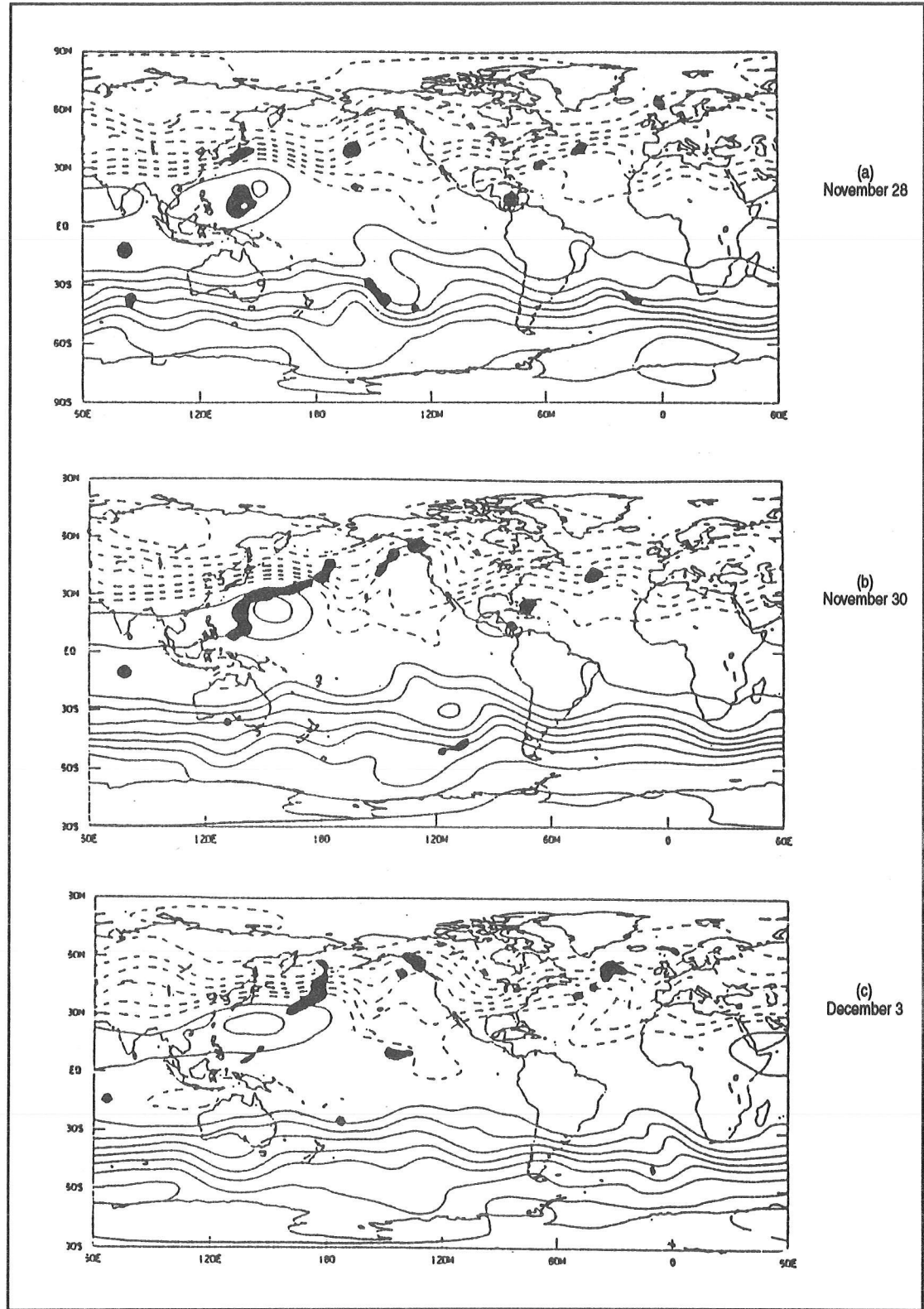


Figure 1. Forecasts of 200-millibar Stream Function (contoured) and Vertically Integrated Heating (shaded) at OOUTC of the Positive Bogus Run Initialized at OOUTC on November 26. Negative stream function values are dashed, and only heating rates greater than 5°C d<sup>-1</sup> are shown.

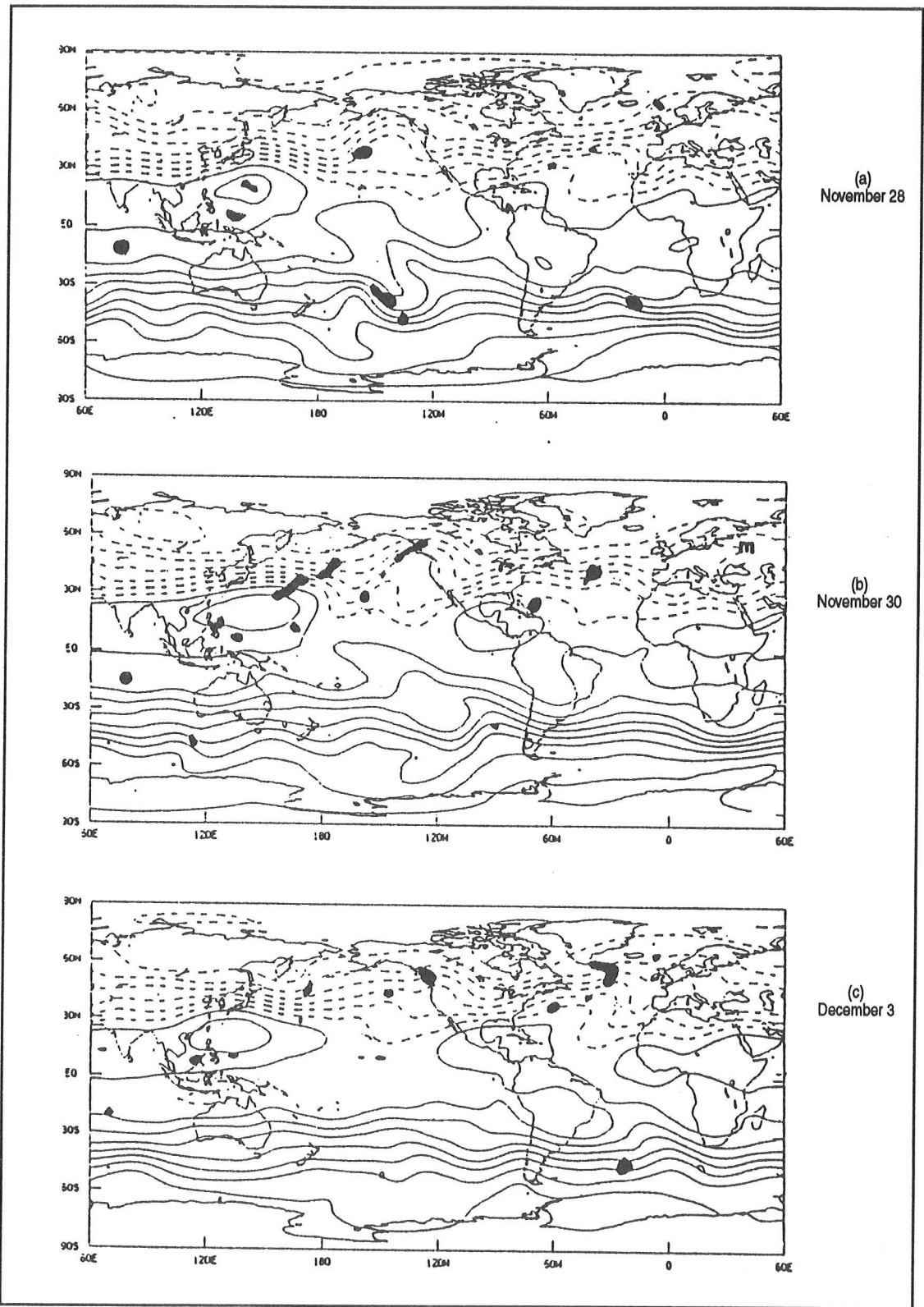


Figure 2. Forecasts of 200-millibar Stream Function (contoured) and Vertically Integrated Heating (shaded) at OOUTC of the Negative Bogus Run Initialized at OOUTC on November 26. Negative stream function values are dashed, and only heating rates greater than  $5^{\circ}\text{C d}^{-1}$  are shown.

The global impacts of Yuri are shown by the differences between the positive and negative bogus forecasts (Figure 3). The first persistent difference is an anticyclonic anomaly in the north Pacific near a strong heating difference (Figure 3a). This anticyclonic anomaly first developed as Yuri approached the midlatitudes. Later in the sequence, the heating differences diminish, but the storm's impacts on flow over the North Pacific and North America continue to evolve (Figure 3b,c). This evolution leads to a quasi-stationary wavetrain over the northeast Pacific and North America (Figure 3d).

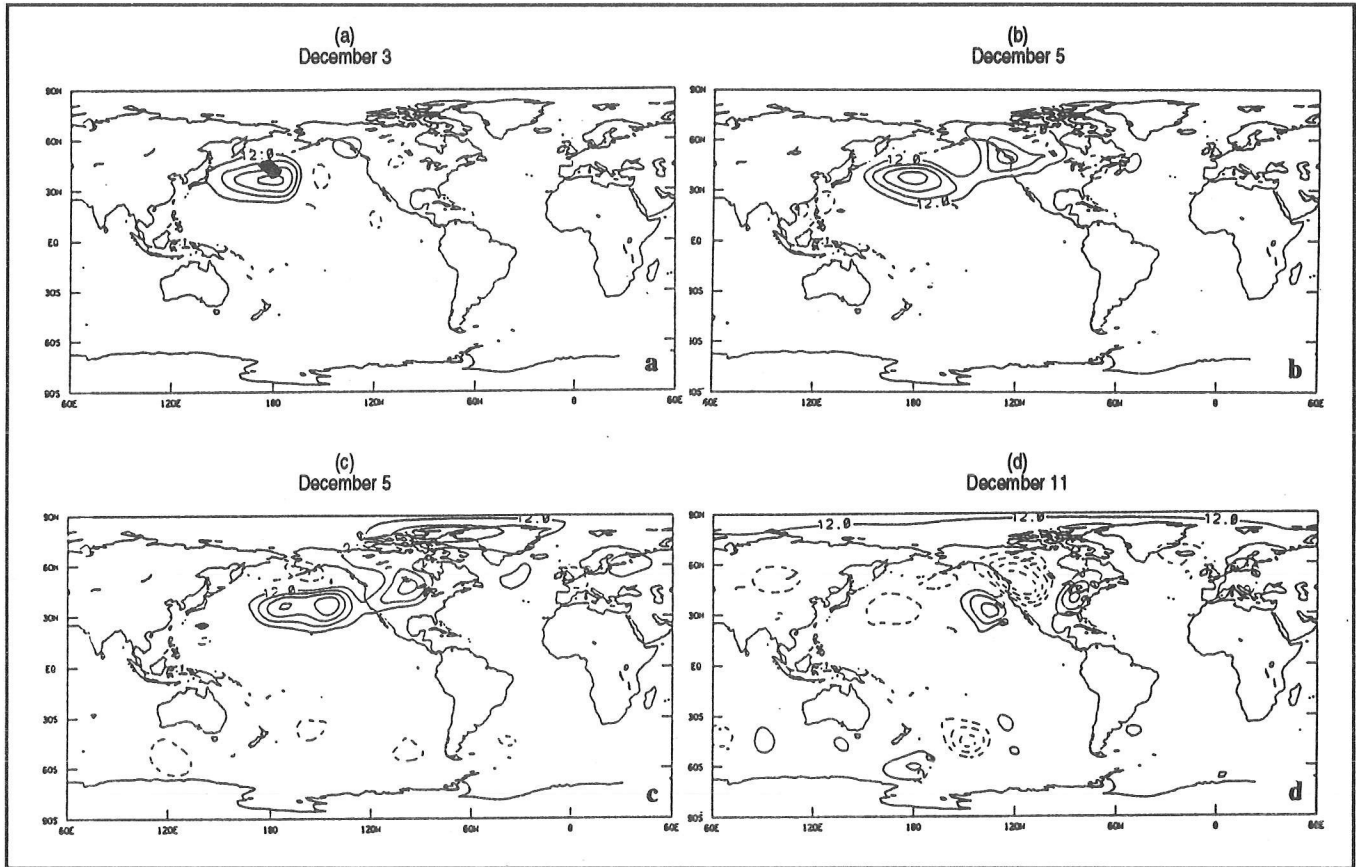


Figure 3. Differences of 200-Millibar Stream Function (contoured) and Vertically Integrated Heating (shaded) between the Positive and Negative Bogus Forecasts at OOUTC. Negative stream function differences are dashed, and only heating rates greater than  $5^{\circ}\text{C d}^{-1}$  are shown.

## Conclusions

---

Further analyses of these and other forecast experiments show that individual typhoons in the western Pacific can produce distinct global circulation anomalies, especially over the north Pacific and North America. These anomalies result from poleward and eastward energy propagation in association with an enhanced midlatitude jet and increased barotropic instability over the North Pacific. The resulting anomalies over the north Pacific/North American region remain as coherent patterns long after the storm's demise. These anomalies are similar to those that occur in response to much lower frequency tropical phenomena, such as the El Niño-Southern Oscillation. These results indicate that small-scale, short-term tropical forcing may play a significant role in the development of global intraseasonal climate anomalies.

## References

---

- Gelaro, R. 1992. A Normal Mode Analysis of Rapid Teleconnections in a Numerical Weather Prediction Model. Part I: Global Aspects. *Mon. Wea. Rev.* 120:2897-2913.
- Hurrell, JW, and DG Vincent. 1991. On the Maintenance of Short-Term Subtropical Wind Maxima in the Southern Hemisphere During SOP-1, FGGE. *J. Climate.* 4:1009-1021.
- Nitta, T. 1987. Convective Activities in the Tropical Western Pacific and Their Impact on the Northern Hemisphere Summer Circulation. *J. Meteor. Soc. Japan.* 65:373-390.



# Regional Context of the Climate of H.J. Andrews Experimental Forest, Oregon

---

David Greenland

H.J. Andrews Experimental Forest is a 6400 ha forest of Douglas fir, western hemlock, and Pacific silver fir located in, and typical of, the central portion of the western slope of the Cascade mountain range of Oregon. The forest is one of 19 sites in the Long-Term Ecological Research (LTER) program sponsored by the National Science Foundation (Franklin *et al* 1990). During the 1970s it was a representative site in the Coniferous Forest Biome Project of the U.S. International Biological Program. It was originally established in 1948 as an Experimental Forest of the U.S. Forest Service. An immense legacy of research has resulted from the participation of Andrews Forest in these programs (McKee *et al* 1987, Blinn *et al* 1988). Future participation in LTER ensures the continuing scientific importance of the site.

Climatological information has been collected at Andrews Forest since 1951, with a continuous, electronically-sensed record since May 1972. The observing system is composed of a primary meteorological station and a network of satellite temperature and precipitation recording stations. Because of the scientific significance of Andrews Forest, it is important to investigate the temporal variability of annual and seasonal temperature and precipitation values at the site and identify past times of anomalous climatic conditions. It is also important to establish quantitatively the relationships between the climate of Andrews Forest and that of its surrounding area and, hence, place the climate of Andrews Forest into its regional context.

## Climate of Andrews Forest

---

The primary meteorological station of Andrews Forest is at an elevation of 426 meters (1397 feet) at latitude 44° 15' N and longitude 122° 10' W. Andrews Forest occupies the Lookout Creek watershed, which ranges from 420 to 1630 meters (1378 to 5346 feet) and drains into Blue River. Below 1050 meters (3444 feet) is the Western Hemlock zone, characterized by western hemlock and Douglas fir. Above 1050 meters (3444 feet), the Pacific Silver Fir zone is established (Bierlmaier and McKee 1989).

Bierlmaier and McKee (1989) have described Andrews Forest climate as wet and fairly mild in winter and warm and dry in summer. They emphasize the role of the polar front jet stream in funneling into the area

one low pressure zone and frontal storm after another during winter. Precipitation comes mainly from cold or occluded fronts. The storms are slowed by the Coast and Cascade ranges and are, consequently, of long duration and low intensity. The summer season is dominated by establishment of a ridge of high pressure along the coast and the eastern Pacific. Consequently this season is characterized by highly stable air and low amounts of precipitation. During 1973 to 1984, the average annual temperature was 8.5°C (47.3°F). Monthly temperatures ranged from 0.6°C (33.1°F) in January to 17.8°C (64.0°F) in July. Annual average precipitation was 2302 millimeters (90.6 inches), 71 percent of which fell from November through March. At 1203 meters (3946 feet) annual precipitation rises to 2785 mm (109.7 in). Above 1050 meters (3444 feet) a persistent snowpack up to 4 meters (13 feet) deep may form and last into June (Bierlmaier and McKee 1989). Further details of the climatology of Andrews Forest may be found in Emmingham and Lundburg (1977, quoted by Bierlmaier and McKee 1989), Waring *et al* (1978), and McKee and Bierlmaier (1987).

### **Regional Climate of Oregon and the Pacific Northwest and Importance of the Pacific Ocean**

---

Regional climatologies of Oregon and the Pacific Northwest have been given by Phillips (1960), Sternes (1960), Pacific Northwest River Basins Commission (1969), and Loy *et al* (1976). No understanding of this climate would be complete without reference to the seminal role of interactions between the ocean and the atmosphere in the area of the northern Pacific Ocean and, to some degree, the tropical and southern parts of the Pacific as well. Namias pioneered this concept in a series of important papers (1959, 1968, 1969, 1971, 1972, 1978, 1979, 1981). More recently, the ocean/atmosphere interconnections have been treated in synoptic climatology through the use of PCA (*principal component analysis*) (Walsh and Richman 1981) and teleconnections and in dynamic climatology increasingly by the use of GCMs (*General Circulation Models*) of the atmosphere and ocean.

The GCMs, by definition, deal with the atmosphere at the global scale. PCA and teleconnective studies, on the other hand, can be designed to investigate particular parts of the world and those studies relevant for the Pacific Northwest are based on the Southern Oscillation Index, the Pacific-North American Index, and the Central North Pacific Index. These three indices exhibit a certain degree of intercorrelation (Cayan and Peterson 1989).

The strength of teleconnective patterns is not necessarily stable over time. Ropelewski and Halpert (1986) have shown that, depending on the data used, the Pacific Northwest is either in or on the southern edge of an area having lower rainfall when El Niños are in progress and in many of the months following the El Niño maximum.

Wallace and Gutzler (1981) were the first to introduce the PNA (*Pacific-North American*) index. However, the PNA index designed by Leathers *et al* (1991) following Yarnal and Diaz (1986) is the one used in this study. The PNA index describes the amplitude of the 700-mb flow pattern over the United States, which has a basic pattern of low pressure troughs in the eastern Pacific and eastern United States, and a high pressure ridge over the Rocky Mountain cordillera. The meridional extreme of the pattern produces positive PNA values (and potentially more southwest-erly winds over Andrews Forest), while the zonal extreme produces negative PNA values (and potentially more westerly winds over Andrews Forest). Yarnal and Diaz (1986) demonstrated how strongly positive PNA and negative (reverse) PNA patterns are associated, respectively, with warm and cold ENSO (*El Niño Southern Oscillation*) events and, in turn, with precipitation and temperature anomalies on the west coast of North America.

Cayan and Peterson (1989) defined the CNP (*Central North Pacific*) index as the MSLP over the region 35-55°N and 170°E to 150°W. They show that streamflow in the West has correlations in the range 0.3 to 0.6 SLP with anomalies in the North Pacific. During times of a weak CNP index, streamflows are high in Washington and Oregon. During times of a strong CNP index, the polar front jet stream flows north of the Pacific Northwest, and below-average streamflow is observed. Often, this is also the case during El Niño events (see Cayan and Peterson 1989, Figure 9).

All of the synoptic studies indicate quite clearly the linkages between SSTs and particular pressure and teleconnective patterns in the Pacific Ocean and various aspects of climate on the West Coast and in the Pacific Northwest.

## Data Processing and Analysis

---

Data were screened for temporal continuity of the observing station and preprocessed to make them available for analysis. Stations deemed most likely to provide pertinent information were Corvallis, Cottage Grove, Eugene, Leaburg, McKenzie Bridge, and Cascadia. The history of each station was scrutinized for continuity using station histories for Oregon from Redmond (1985). After analysis of pre- and post-move observations for Eugene, that record was dropped. Data from Andrews Forest were provided from the Long-Term Ecological Research section of the Forest Science Data Bank in the Forest Sciences Laboratory at Corvallis. Precipitation data for the primary meteorological site for 1973 through 1978 were taken from Bierlmaier and McKee (1989). The Oregon Climate Service provided data for the NWS stations, the Willamette Valley and Northern Cascade climate divisions of Oregon, and most SOI values. Supplementary SOI values were provided by Dr. R. Cerveny of the Department of Geography at Arizona State University. PNA values were provided by Dr. D. Leathers of the Department of Geography at the University of Delaware.

**Regression Analysis**

Multiple regression analysis was used to find the monthly values of mean temperature and total precipitation at Andrews Forest from values at the selected stations. The same multiple regression function was used to produce all correlation coefficients in this paper, and correlation coefficient values are reported as positive irrespective of whether they are positive or negative.

**Precipitation Data**

The multiple regression analysis identified good correlation in monthly and annual precipitation values between the five stations. All regression equations were significant at the 99 percent level, as assessed by their F values. Regression equations were computed for different sets of stations for three time periods determined by the length of station records. The time periods were 1936 to 1972, 1919 to 1935, and 1910 to 1918. Table 1 shows the monthly range of  $r^2$  and standard error of estimate values for these periods. The sum of the 12 monthly totals is used for the annual total value.

Table 1 STATIONS USED, RANGE OF REGRESSION COEFFICIENTS, AND STANDARD ERROR OF ESTIMATES FOR MULTIPLE REGRESSION EQUATIONS USED TO OBTAIN MONTHLY TOTAL PRECIPITATION AT H. J. ANDREWS EXPERIMENTAL FOREST		
<i>Water Year = October to September (Johnson &amp; Dart, 82)</i>		
<i>All <math>r^2</math> values significant at 99% level</i>		
	$r^2$	Standard Error of Estimates (inches)
1936 - 1972		
Corvallis, Leaburg, McKenzie Bridge, Cascadia, Cottage Grove		
Monthly	0.89 to 0.98	0.30 to 1.81
Annual	0.93	4.91
Water Year	0.98	3.22
1919 - 1935		
Corvallis, Cascadia, Cottage Grove		
Monthly	0.83 to 0.94	0.33 to 2.12
Annual	0.91	5.28
Water Year	0.96	3.76
1910 - 1918		
Corvallis		
Monthly	0.47 to 0.86	0.43 to 3.44
Annual	0.61	10.05
Water Year	0.77	8.43

A similar analysis was performed for water year periods. Following Johnson and Dart (1982) the water year is defined as October 1 to the next September 30 and is numbered for the year in which it ends. The

analysis was also performed for the winter part of the water year (October to April). This selection of seasons follows the approach of Johnson and Dart (1982) and has obvious practical and hydrological advantages. The water year and winter water year correlations carry a higher degree of accuracy than those for the calendar year. The values found in this report are of the same order and consistent with the findings of Dart and Johnston (1982, pages 104-111), who worked on the whole state of Oregon.

### Temperature Data

The same five predictor stations were scrutinized for efficiency in simulating temperature, using their average annual data from 1973 to 1991. Correlation coefficient, standard error of estimates, and significance values between the five stations and the Andrews Forest data indicated data from Cascadia impaired the strength of the regression equations. Cascadia was, therefore, omitted for the rest of the analysis. The range of individual monthly regressions (Table 2) displays slightly lower correlations than for precipitation, but still shows strong values.

	$r^2$	Standard Error of Estimates ('F)
1936 - 1972 Corvallis, Leaburg, McKenzie Bridge, Cottage Grove		
Monthly	0.69 to 0.92	0.84 to 1.83
Annual	0.50 (95.0%)	1.02
1917 - 1935 Corvallis, Cottage Grove		
Monthly	0.57 to 0.84	0.73 to 1.80
Annual	0.49	0.96
1890 - 1916 Corvallis		
Monthly	0.56 to 0.84	1.06 to 1.97
Annual	0.49	0.93

### Analysis of the Synthetic and Observed Record

Simulated monthly mean temperature and total precipitation data verified quite well against an observed independent dataset from Watershed 2 in Andrews Forest. The simulated temperature and precipitation series were determined to have an accuracy level that justifies further temporal and spatial analysis of the data.

### **Precipitation**

The regression analysis described above was used to produce a set of observed and synthetic monthly and annual precipitation values for Andrews Forest for 1910 to 1991 (continuous from 1913). The total annual water year precipitation record from 1911 to 1991 displayed considerable interannual variability.

Trends represented by the 5-year running mean of the same data plainly showed the prolonged and severe drought of the 1930s and the wetter years of the late 1940s and the 1950s. The record exhibits greater variability in more recent years, with two peaks of precipitation centered on 1973 and 1984 and droughts centered on the late 1970s and one that persisted at least through 1991. Both droughts, as judged by the value of water year precipitation, were as severe as the drought of the 1930s, but at least the 1970s drought did not last as long.

The variations of precipitation at Andrews Forest found here match quite well the trends in the Willamette Valley described by Johnson and Dart (1982), who also note high interannual variability and, correspondingly, relatively few groupings of wet or dry years for western Oregon.

### **Temperature**

The observed and synthetic annual mean temperature record for Andrews Forest from 1890 to 1991 also showed considerable interannual variability. Analysis in terms of 5-year running means displayed a warming trend between the beginning of the record and the early 1940s, punctuated by two cool periods in the early 1910s and the early 1920s. Another cool period is seen from the late 1940s to the mid-1970s, with the exception of one warm year (1958). A warming trend is seen from the mid-1970s to the present. The magnitude of this trend, at least up to 1991, is similar to that of the warming trend at the beginning of the century.

Bradley (1982) notes that 1921 to 1935 stand out over the western United States as anomalously warm in the context of the last 100 years. The Andrews Forest data do show high temperatures during this time. At Andrews Forest, 8 of these 15 years have above mean (1890-1991) temperatures, and 3 of the years exceed the mean by 1 standard deviation. Comparison of individual years of high and low temperatures for Oregon as a whole identified by Bradley is not easily possible in the absence of Bradley's data in tabular form. Comparison of low- and high-temperature winters for selected West Coast stations (Roden 1989) shows that, more often than not, Andrews Forest values parallel the coastal values.

### **Recent Warming**

Since there is considerable evidence of a trend of increasing minimum temperatures over the last two to three decades (Karl *et al* 1988), the Andrews Forest record was examined to see if it contained this signal. Maximum, minimum, mean seasonal, and mean annual temperatures were regressed against year number for 1973 through 1991. At Andrews Forest, this period had not only increasing minimum temperatures but increasing maximum and mean temperatures as well. Of ecological importance is the fact that the greatest increases occurred in spring (March, April, May), possibly affecting growth rates. The warming is also seen at Corvallis and Cottage Grove, although not quite as intense and not during winter. Again, the magnitude of this recent warming trend is similar to one that took place at Andrews Forest at the beginning of the century.

### **Step Functions**

Several investigators have identified step functions in certain of the meteorological time series during the period of modern record. Ebbesmeyer *et al* (1991) have investigated a step function in biogeophysical time series of the Pacific Northwest and the Pacific in 1976. Leathers and Palecki (1992) have identified a step function in the value of the PNA index during the late 1950s and centered on about 1957. The 1957 step was also noticed in records of the mean height of sea level along the West Coast (Namias 1972). An analysis was performed to investigate whether such steps exist in the climatic data for Andrews Forest.

First, the difference of the means before and after the steps were tested using a 2-tailed t test. Using the means of the 8 years before and after the 1976 step, there was a significant difference (99% level) in Andrews Forest annual mean temperatures. A significant difference (99% level) was also displayed in annual mean temperatures when 15-year means either side of 1976 were taken. No significant difference was seen in the winter water year precipitation values at Andrews Forest when 8-year means were taken either side of 1976, but a significant difference (95% level) was found in these values when a 15-year mean either side of 1976 was selected.

No significant differences were found in Andrews Forest annual mean temperatures or winter water year precipitation between 18-year means or 8-year means either side of 1957. At first this result seems hard to explain, since there is a weak relationship between the PNA values and Andrews Forest precipitation and temperature values (Table 3). However, this relationship is seen more in winter values than in annual values. Perhaps more important is the fact that Leathers and Palecki (1992) show that the 1957 PNA step is seen most clearly in the southeastern United States center of action of the PNA index rather than either of the two centers closer to the Pacific Northwest.

Table 3  
CORRELATION COEFFICIENT VALUES BETWEEN  
ANNUAL, JANUARY, AND JULY MEAN TEMPERATURE AND PRECIPITATION TOTALS  
AT H.J. ANDREWS EXPERIMENTAL FOREST AND SELECTED GENERAL CIRCULATION INDICES,  
1948 TO 1987

Variable Regressed Against	Precipitation					
	Annual or Winter Water Year		January		July	
	r <sup>2</sup>	Significance Level (%)	r <sup>2</sup>	Significance Level (%)	r <sup>2</sup>	Significance Level (%)
PNA Annual	0.08	<95				
PNA Winter Water Year	0.25	99				
PNA			0.16	95	0.00	<95
CNP Annual	0.04	<95				
CNP Winter Water Year	0.17	99				
CNP			0.10	95	0.06	<95
CNP Annual (1914-1990)	0.03	<95				
CNP Winter Water Year (1914-1990)	0.21	99				
CNP (1914-1990)			0.11	99	0.03	<95
Variable Regressed Against	Temperature					
	Annual or Winter Water Year		January		July	
	r <sup>2</sup>	Significance Level (%)	r <sup>2</sup>	Significance Level (%)	r <sup>2</sup>	Significance Level (%)
PNA	0.12	95	0.40	99	0.11	95
CNP	0.45	99	0.40	99	0.04	<95
CNP (1910-1990)	0.44	99	0.31	99	0.05	95

There is evidence in Andrews Forest record for the 1976 step but not for the PNA-related 1957 step. However we interpret the Andrews record in terms of pre- and post-1976 values, it is clear that 1976 was a marked turning point at Andrews Forest for both temperature and precipitation. For about 15 years before 1976, the annual temperature trend had been downward. Since 1976, the trend has been upward. In absolute terms, the 1977 water year (which includes the winter of 1976-77) had the lowest precipitation values in the entire record, with generally higher values both before and after 1977. The 5-year running mean of these data places the turning point two years later. Clearly the atmosphere changed to a different mode of operation in the mid-1970s, and this change is well represented in Andrews Forest data as well as in data for many other parts of the Pacific Northwest.

### **The Tree Ring Record**

The general temporal variation that Graumlich (1987) reports in a study of tree ring width data for the present century in her defined Western Lowlands and Columbia Basin (but not the Southern Valleys) divisions is similar to the Andrews Forest precipitation record. Data from Andrews are generally consistent with those of Graumlich and tend to suggest that her findings for earlier years, back to 1640, would also apply to Andrews Forest.

More confidence should be attributed to runs of dry (and presumably wet) years rather than to individual years. One reason for this is the masking of extreme values in the simulated Andrews Forest data, related to the least squares analysis methodology. Graumlich finds marked droughts in the Columbia Basin around 1680, in the 1750s, 1780s, 1790s, 1840s, 1865 to 1895, and in the 1920s and 1930s. Wet periods occurred from 1695 to 1715, 1740 to 1760, and 1810 to 1835. The wet and dry periods were similar in the Western Lowlands, except that the duration of droughts was less. Hatton (1989) found similar results from a tree ring record at Lost Forest, in the eastern end of the Fort Rock Basin in Lake County in central Oregon.

Graumlich and Brubaker (1986) analyzed a tree ring record for Longmire, Washington, and commented that temperatures between 1900 and 1940 were higher than any other 40-year period. Andrews Forest temperature data for the present century also display high temperatures during this time and, thus, imply that earlier "warm" periods in the Washington record also occur at Andrews Forest. These warm periods were 1655-1670, 1690-1695, and 1825-1830. "Cool" periods in the Longmire record were 1610-1630, 1640-1650, 1695-1760, 1800-1808, 1840-1850, and 1875-1895.

### **The Regional Context**

Synthetic and observed precipitation data for Andrews Forest for 1915 to 1991 were compared by correlation techniques on a month-by-month and an annual basis with precipitation data from the Willamette Valley (OR2) and the Northern Cascades (OR4) Oregon Climate Divisions. There is a slight degree of autocorrelation, because data from some stations in the divisions were used to simulate part of the Andrews Forest dataset. The autocorrelation is very small; Cascadia, Corvallis, Cottage Grove, and Leaburg are just 4 of the 33 stations in the Willamette Valley Division, and McKenzie Bridge is just one of eight stations in the Northern Cascades Division. Consequently it is reasonable to assume that the small amount of autocorrelation does not markedly affect the results from this analysis.

For precipitation, the relevant  $r^2$  values indicate a strong relationship between Andrews Forest data and both the Willamette Valley and Northern Cascades divisional data. Monthly correlation coefficient values range from 0.60 to 0.92. It is remarkable that high values are found even for summer months. On the basis of these values precipitation at Andrews Forest is slightly more related to the Northern Cascades division (in which it is located), but the high  $r^2$  values indicate it is representative of the area covered by both divisions. Monthly correlation coefficients between temperature values of the climatic divisions and Andrews Forest are slightly lower than those for precipitation and range from 0.59 to 0.87. The Willamette Valley division has the higher correlation values in most cases. This may be due to the high degree of variation of temperature values in complex terrain associated with the wide variety of different microclimates.

### General Circulation Indices

The observed and synthetic Andrews Forest data were compared with general circulation indices designed to relate to the Pacific Northwest region following an approach of Wigley *et al* (1990) and Jones (1991), who were interested in how to estimate regional values of projected climate change from the projected values at grid points on the coarse network used by current general circulation models. The indices were constructed for use with a dataset of reconstructed monthly MSLP developed by Jones *et al* (1987).

Data for North America are on a 5° latitude by 10° longitude grid. Following the approach by Jones (1991), three general circulation indices were developed. The first was simply a pressure index (SLP) at 45°N 120°W, a location in the center of Oregon not far from Andrews Forest. The second was a zonal index comprised of the difference in SLP between 40°N 120°W and 50°N 120°W. Positive values of this index indicate the general strength of westerly winds. The third index was a meridional index comprised of the difference in SLP between 45°N 120°W and 45°N 130°W. Positive values of this index indicate the general strength of southerly winds. These points differ somewhat from those employed in Jones' original study. To clarify the regression analysis, the value of the first index was modified by subtracting 1014 mb from each value.

The correlation coefficients for the temporally aggregated data (Table 4) indicate a slight correlation between the Central Oregon SLP and winter water year precipitation and between the meridional index and annual mean temperature, where southerly winds are expectedly associated with higher temperatures, but no other relationships are apparent. On the monthly time scale there is greater correlation of Andrews Forest temperature and precipitation values and the circulation indices in January but no correlation in July (Table 5). This is to be expected, given the more vigorous general circulation in the Northern Hemisphere winter and the low absolute amount of precipitation at Andrews Forest in summer.

Table 4  
CORRELATION COEFFICIENT VALUES BETWEEN  
ANNUAL MEAN TEMPERATURE AND WINTER WATER YEAR PRECIPITATION TOTALS  
AT H.J. ANDREWS EXPERIMENTAL FOREST AND  
SELECTED GENERAL CIRCULATION INDICES

Winter Water Year Precipitation, 1914-1980.		
Variable Regressed Against	r <sup>2</sup>	Significance Level (%)
Central Oregon Pressure	0.24	99
Zonal Index	0.15	99
Meridional Index	0.03	<95
Annual Mean Temperature, 1890-1980		
Variable Regressed Against	r <sup>2</sup>	Significance Level (%)
Central Oregon Pressure	0.01	<95
Zonal Index	0.01	<95
Meridional Index	0.36	99

Table 5  
CORRELATION COEFFICIENT VALUES BETWEEN  
JANUARY AND JULY MEAN TEMPERATURE AND PRECIPITATION TOTALS  
AT H.J. ANDREWS EXPERIMENTAL FOREST AND  
SELECTED GENERAL CIRCULATION INDICES, 1914-1980

Variable Regressed Against	Precipitation			
	January		July	
	r <sup>2</sup>	Significance Level (%)	r <sup>2</sup>	Significance Level (%)
Central Oregon Pressure	0.29	99	0.03	<95
Zonal Index	0.22	99	0.04	<95
Meridional Index	0.07	95	0.04	<95
All Three Indices	0.52	99	0.19	99
Variable Regressed Against	Temperature			
	January		July	
	r <sup>2</sup>	Significance Level (%)	r <sup>2</sup>	Significance Level (%)
Central Oregon Pressure	0.32	95	0.00	<95
Zonal Index	0.32	99	0.04	<95
Meridional Index	0.28	99	0.00	<95
All Three Indices	0.56	99	0.04	<95

To be more consistent with Jones' analysis, all three circulation indicators were used together in a multiple regression for January and July. This analysis yielded correlation coefficients of 0.56 (January temperature) and 0.52 (January precipitation), which is comparable to Jones' findings, and 0.04 (July temperature) and 0.19 (July precipitation), which

is much lower than Jones found for the general location of Andrews Forest. In summary the relationships in winter are much stronger than those in summer. The implication of these results is that output values predicted by general circulation models for the general area of the Pacific Northwest may be applied to Andrews Forest with more confidence in winter season than in summer.

### **Pacific-North American and Central North Pacific Indices**

Correlations were also made between Andrews Forest data and the PNA and the CNP indices for 1948 to 1987. The results (Table 3), in the context of this kind of synoptic climatological analysis, indicate quite marked correlations between Andrews Forest winter water year precipitation and both the PNA index and the CNP index. Precipitation at Andrews Forest for January, representing winter months, also displays a weak but significant correlation with both indices. No relationships are seen for July, representing summer months, or for the calendar year precipitation totals. Annual and January mean values of temperature exhibit a strong correlation with the CNP index. The relationship of January mean temperatures to the PNA index is also strong, but relationships for the year and for July, although significant, are not so strong. Redmond and Koch (1991) also found significant relationships between concurrent precipitation and temperature values in the Pacific Northwest and PNA values, with temperature having the strongest relationship.

Physically, when the PNA index is positive and high, a meridional circulation in the westerlies with a ridge of high pressure shunts storms to the north of Oregon (and Andrews Forest), giving rise to relatively dry weather. This situation also brings in warm air with relatively high temperatures from the southwest. When the PNA index is negative, the zonal circulation in the westerlies brings in storms from the Pacific Ocean, giving rise to wetter weather and somewhat lower air temperatures. These interpretations are also consistent with the CNP values, which when low indicate a well-developed Aleutian low pressure zone will guide storms northward to British Columbia but when high allow storms to travel more directly eastward into Washington and Oregon.

The advantage of using the CNP is that it has a long record dating back to 1899. Comparison of relationships between Andrews Forest data and the CNP index for the longer periods of 1910 or 1914 to 1990 (Table 3) indicates little difference in the correlation coefficients found for the shorter 1948-1990 period. This is encouraging, because it suggests the relationships are fairly stable over time and the time series are somewhat stationary.

### **Southern Oscillation Index**

Direct comparison of winter water year Andrews Forest values and SOI values suggests a relationship in which low SOI values (warm event, El

Niño years) tend to be associated with low precipitation values at Andrews Forest and high SOI values (cold event, La Niña years) tend to be associated with high precipitation values at Andrews Forest. The relationship is clear, although it is not strong statistically ( $r^2=0.14$ , significant at 99%). The 1983 year, which had an extraordinarily strong low SOI value is a noteworthy outlier on the scattergram. Without the 1983 value, the relationship is stronger ( $r^2=0.23$ , significant at 99%). A similar, though stronger and reverse, relationship exists on an annual time scale between the SOI values and the annual mean temperature at Andrews Forest (with inclusion of the 1983 data point  $r^2=0.24$ , significant at 99%).

Further light is given to this issue by examining Andrews Forest climate values for extreme SOI years. Two sets of extreme SOI years have been provided by Yarnal and Diaz (1986) and Halpert and Ropelewski (1992). Yarnal and Diaz identified a number of warm (El Niño) and cold (La Niña) event winters (December, January, February). During warm event winters, Andrews Forest precipitation is near average, at 0.03 standard deviation of the long term (1914-1991) mean and the temperature is well above (0.77 SD) the long-term (1890 to 1991) mean. During cold event winters, Andrews Forest precipitation is well above (0.69 SD) the long-term mean and temperature is below it (-0.33 SD).

Halpert and Ropelewski defined warm event years as those in which the SOI index value remained in the lower 25 percent of the distribution for five months or longer and similarly defined cold event years by using the upper 25 percent of the distribution. By these definitions, at Andrews Forest during warm event years, the annual precipitation is near the long-term mean (-0.02 SD), the winter water year precipitation is slightly above the long-term mean (0.15 SD), but the following winter water year is markedly below the long-term mean (-0.32 SD). Also during warm event years, Andrews Forest temperatures are well above the long-term mean (0.45 SD). During cold event years, Andrews Forest annual precipitation is well above the long-term mean (0.48 SD), although the winter water year precipitation is near the long-term mean (-0.05 SD). Most striking, however, is that during cold event years, the following winter water year is 0.88 standard deviation above the long-term mean. Also, during the cold event years the annual mean temperature is notably below (-0.37 SD) the long-term mean.

Thus, it seems there are definite relationships such that during many warm events (El Niño years) the winter water year precipitation at Andrews Forest is relatively low and annual mean temperatures are relatively high. During cold events (La Niña years) winter water year precipitation at Andrews Forest is relatively high, especially in the water year following a calendar year with a cold event, and annual mean temperatures are relatively low.

These findings are consistent with those of Yarnal and Diaz (1986) and Redmond and Koch (1991). The latter noted that, for the Pacific Northwest as a whole, precipitation is low and temperature is high during low

SOI values with the opposite also being true. Interestingly, they found the relationship tended to be strongest in the mountainous climate divisions. They point out that a combination of low precipitation and high temperature values implies a smaller than average snowpack during El Niño years.

With one exception, there were no significant correlations in either precipitation or temperature when the data were lagged at monthly intervals. The exception was a weak relationship between Andrews Forest January precipitation and the SOI value of the previous March ( $r^2=0.10$ , significant at 95%). The relationship is interesting enough to pursue later, using seasonal rather than monthly data.

## Conclusions

---

Researchers at most LTER sites would benefit by having a climate record at their sites extended back into the last century. The foregoing discussion provides a model methodology for local climate analysis and synthesis at LTER sites. While synthesis by regression analysis is not new, placing the site into its regional context by using relationships with Climatic Division data and local and hemispheric general circulation indices does provide a new method of viewing the local climatic environment. This methodology will become increasingly important as LTER sites begin to scale up to landscape and regional levels.

It cannot be assumed *a priori* that any single LTER site will relate well to the larger regional climatic environment. This has been demonstrated, for example, in the case of the Niwot Ridge, Colorado, LTER site (Greenland and Swift 1991).

Comparisons of Andrews Forest climate with values from nearby Climatic Divisions, and local and hemispheric general circulation indices all suggest the climate of Andrews Forest is well representative of the climate of the northern Cascades and their foothills in particular and of the Pacific Northwest in general. The only exception is that as one moves to the larger, geographic-scale indices, the relationships become weaker and even non-existent in summer months. The reason is that during summer Andrews Forest is usually dominated by a ridge of high pressure and the processes of microclimatology tend to dominate those of larger scales. In contrast, in winter with the expansion of the high energy circumpolar vortex into mid-latitudes, and with our growing awareness of the linkages between tropical and extra-tropical circulation, it is not surprising that Andrews Forest is well coupled with these hemispheric-scale events. This coupling has important implications for the climate of Andrews Forest one, two, or possibly more seasons ahead, thus allowing a new dimension in planning ecological experiments.

## Acknowledgments

This study has been greatly benefited by the help and encouragement of Dr. Fred Swanson. Funding was provided in part by the USDA, Forest Service, Pacific Northwest Research Station, Cooperative Agreement No. Pacific Northwest 92-0221. Datasets for H. J. Andrews Forest were provided by the Forest Science Data Bank, a partnership between the Department of Forest Science, Oregon State University, and the U.S. Forest Service Pacific Northwest Research Station, Corvallis, Oregon. Funding for these data was provided by the Long-Term Ecological Research (LTER) program and other National Science Foundation programs, Oregon State University, and U.S. Forest Service Pacific Northwest Research Station. NSF grants: DEB-7611978, BSR-9011663. The aid of Mr. Don Henshaw is appreciated in provision of these datasets. Datasets for National Weather Service stations in Oregon were provided by the Oregon Climate Service through the courtesy of State Climatologist Mr. George Taylor. Assistance or data were also provided by Dr. D. Leathers, Dr. R. Cervený, and Mr. J. B. Fisher.

## References

- Blinn, T, FJ Swanson, A McKee. 1988. *Research Publications of the H.J. Andrews Experimental Forest, Cascade Range, Oregon, 1988 Supplement*. General Technical Report PNW-GWT-223. U.S. Department of Agriculture, Forest Service, Pacific Northwest Research Station. Portland, OR. 26 pp.
- Bierlmaier, FA, and A McKee. 1989. *Climatic Summaries and Documentation for the Primary Meteorological Station, H.J. Andrews Experimental Forest, 1972-1984*. General Technical Report PNW-GTR-223. USDA Forest Service, Pacific Northwest Research Station. Portland, OR. 26 pp.
- Bradley, RS. 1982. Climatic Fluctuations of the Western United States During the Period of Instrumental Records. Pages 1-76 in *Climatic Fluctuations of the Western United States During the Period of Instrumental Records*. RS Bradley, RG Barry, and G Kiladis, authors. Contribution No. 42. Department of Geology and Geography, University of Massachusetts. Amherst. 01003-0026. 169 pp.
- Cayan, DR, and DH Peterson. 1989. The Influence of North Pacific Circulation on Streamflow in the West. Pages 375-397 in *Aspects of Climate Variability in the Pacific and Western Americas*. DH Peterson, editor. American Geophysical Union. 445 pp.
- Ebbesmeyer, CC, DR Cayan, DR McLain, FH Nichols, DH Peterson, KT Redmond. 1991. 1976 Step in the Pacific Climate: Forty Environmental Changes between 1968-1975 and 1977-1984. Pages 115-126 in *Proceedings of the Seventh Annual Pacific Climate (PACCLIM) Workshop, April 1990*. JL Betancourt and VL Tharp, editors. California Department of Water Resources, Interagency Ecological Studies Program Technical Report 26.
- Franklin, JF, CS Bledsoe, JT Callahan. 1990. Contributions of the Long-Term Ecological Research Program. *Bioscience*. 40(7):509-523.
- Graumlich, LJ. 1987. Precipitation Variation in the Pacific Northwest (1675-1975) as Reconstructed from Tree Rings. *Annals of the Association of American Geographers*. 77(1):19-29.
- Graumlich, LJ, and L Brubaker. 1986. Reconstruction of Annual Temperature (1590-1979) for Longmire, Washington, Derived from Tree Rings. *Quaternary Research*. 25:223-234.

- Greenland, D, and LW Swift Jr. 1991. Climate Variability and Ecosystem Response: Opportunities for the LTER Network. *Bulletin of the Ecological Society of America*. 72(2):118-126.
- Halpert, MS, and CF Ropelewski. 1992. Surface Temperature Patterns Associated with the Southern Oscillation. *Journal of Climate*. 5:577-593.
- Hatton, RR. 1989. Climatic Variations and Agricultural Settlement in Southeastern Oregon. Ph.D. Dissertation. Department of Geography. University of Oregon. 1989. 262 pp.
- Johnson, DM, and JO Dart. 1982. *Variability of Precipitation in the Pacific Northwest: Spatial and Temporal Characteristics*. Water Resources Research Institute, Oregon State University. Corvallis. WRRI-77. 181 pp.
- Jones, PD. 1991. How Much of the Local Climate Variability Can Be Explained by Large-Scale Changes? Pages J7-J14 in *Proceedings of the 20th Conference on Agricultural and Forest Meteorology, Sept 10-13, 1991, Salt Lake City, Utah*. American Meteorological Society. Boston.
- Jones, PD, TML Wigley, KR Briffa. 1987. *Monthly Mean Pressure Reconstructions for Europe (Back to 1780) and North America (to 1858)*. US Department of Energy. Report DOE/ER/60397-H1. 99pp.
- Karl, TR, RG Baldwin, MG Burgin. 1988. *Historical Climatology Series*. 4-5. National Climatic Data Center. 107 pp.
- Leathers, DJ, B Yarnal, MA Palecki. 1991. The Pacific/North American Teleconnection Pattern and United States Climate. Part I: Regional Temperature and Precipitation Associations. *Journal of Climate*. 4(5):517-528.
- Leathers, DJ, and MA Palecki. 1992. The Pacific/North American Teleconnection Pattern and the United States Climate. Part II: Temporal Characteristics and Index Specification. *Journal of Climate*. 5:707-716.
- Loy, WG, S Allan, CP Patton. 1976. *Atlas of Oregon*. University of Oregon Press: Eugene. 215 pp.
- McKee, A, and F Bierlmaier. 1987. H.J. Andrews Experimental Forest, Oregon. Pages 11-17 in *The Climates of the Long-Term Ecological Research Sites*. D Greenland, editor. Institute of Arctic and Alpine Research, University of Colorado. Occasional Paper 44.
- McKee, A, GM Stonedahl, JF Franklin, J Swanson. 1987. *Research Publications of the H.J. Andrews Experimental Forest, Cascade Range, Oregon, 1948 to 1986*. General Technical Report PNW-GWT-201. US Department of Agriculture, Forest Service, Pacific Northwest Research Station. Portland, OR. 74 pp.
- Namias, J. 1959. Recent Seasonal Interactions between North Pacific Waters and the Overlying Atmospheric Circulation. *Journal of Geophysical Research*. 64(6):631-646.
- 1968. The Labile Gulf of Alaska Cyclone — Key to Large Scale Weather Modification Elsewhere. Pages 735-746 in *Proceedings of the International Conference on Cloud Physics, August 26-30, 1968*. Toronto.
- 1969. Seasonal Interactions between the North Pacific Oceans and the Atmosphere during the 1960s. *Monthly Weather Review* 97(3):173-192.
- 1971. The 1968-69 Winter as an Outgrowth of Sea and Air Coupling during Antecedent Seasons. *Journal of Physical Oceanography*. 1(2):65-81.
- 1972. Experiments in Objectively Predicting Some Atmospheric and Oceanic Variables for the Winter 1971-72. *Journal of Applied Meteorology*. 11(8):1164-1174.
- 1978. Multiple Causes of the North American Abnormal Winter 1976-77. *Monthly Weather Review*. 106(3):279-295.
- 1979. Premonitory Signs of the 1978 Break in the West Coast Drought. *Monthly Weather Review*. 107(12):1676-1681.

- 1981. The Heavy California Winter Rains of 1979-80 as a Manifestation of Macroscale Air/Sea Coupling. *Proceedings of the Fifth Annual Diagnostics Workshop, Joint Institute for the Study of Atmosphere and Ocean, University of Washington, Oct 22-24, 1980*. US Department of Commerce, National Oceanographic and Atmospheric Administration.
- Pacific Northwest Rivers Commission. 1969. *Climatological Handbook of the Columbia Basin States*. 3 volumes. Private publication by the PNW Rivers Commission.
- Phillips, EL. 1960. Climates of the States No. 60-45: Washington. Pages 1042-1049 in *Climates of the States. Volume 2*. Gale Research Company. Detroit.
- Redmond, KT. 1985. *An Inventory of Climate Data for the State of Oregon*. Report SCP-3. Office of the State Climatologist. Climatic Research Institute. Oregon State University. Corvallis. 160 pp.
- Redmond, KT, and RW Koch. 1991. Climate and Streamflow Variability in the Western United States and Their Relationship to Large-Scale Circulation Indices. *Water Resources Research*. 27(9):2381-2399.
- Roden, GI. 1989. Analysis and Interpretation of Long-Term Climate Variability along the West Coast of North America. Pages 93-111 in *Aspects of Climate Variability in the Pacific and Western Americas*. DH Peterson, editor. American Geophysical Union. 445 pp.
- Ropelewski, CF, and MS Halpert. 1986. North American Precipitation and Temperature Patterns Associated with the El Niño/Southern Oscillation (ENSO). *Monthly Weather Review*. 114:2352-2362.
- Sternes, GL. 1960. Climates of the States No. 60-35: Oregon. Pages 806-811 in *Climates of the States. Volume 2*. Gale Research Company. Detroit.
- Wallace, JM, and DS Gutzler. 1981. Teleconnections in the Geopotential Height Field during the Northern Hemisphere Winter. *Monthly Weather Review*. 109:784-812.
- Walsh, JE, and MB Richman. 1981. Seasonality in the Associations between Surface Temperatures over the United States and the North Pacific Ocean. *Monthly Weather Review*. 109:767-783.
- Waring, RH, HR Holbo, RP Bueb, RL Fredriksen. 1978. Documentation of Meteorological Data from the Coniferous Forest Biome Primary Station in Oregon. General Technical Report PNW-73. US Department of Agriculture, Forest Service, Pacific Northwest Research Station. Portland, OR. 23 pp.
- Wigley, TML, PD Jones, KR Biffra, G Smith. 1990. Obtaining Sub-Grid Scale Information from Coarse-Resolution General Circulation Model Output. *Journal of Geophysical Research*. 95(D2):1943-1953.
- Yarnal, B, and HF Diaz. 1986. Relationships between Extremes of the Southern Oscillation and the Winter Climate of the Anglo-American Pacific Coast. *Journal of Climatology*. 6:197-219.



# Satellite Passive Microwave Observations of the Upper Colorado River Snowpack

Edward G. Josberger, Per Gloersen, Alfred T.C. Chang, and Albert Rango

Seasonal snow cover in the mountains of the Upper Colorado River Basin is a major source of water for a large portion of the southwestern United States. The extent and amount of this snowpack not only reflects changes in weather patterns and climate but also influences the general circulation through modification of the energy exchange between land and atmosphere. Traditional surface-based snowpack observations consist of point measurements at a relatively limited number of sites when compared to the extent and variability of the snowpack. These point measurements may not be representative of the water storage of the snowpack at the meso- and regional scales. Airborne measurements (Carroll 1992) use the attenuation of terrestrial gamma radiation by the snowpack to determine average snowpack water equivalent over flight lines as long as 8 kilometers. However, neither observational technique is capable of providing the synoptic observations over the large scales necessary to determine the role of seasonal snow cover in the general atmospheric circulation.

Satellite observations and remote sensing techniques can enhance the standard snowpack observations to provide the temporal and spatial measurements required for understanding the role of snow in the surface energy balance and improving the management of water resources. The most extensively used satellite observations are those in the visible and near infrared bands, and they are used only to determine snow extent. The NOAA National Operational Hydrologic Remote Sensing Center (NOHRSC) uses the Advanced Very High Resolution Radiometer (AVHRR) data to map the snow extent in 4,000 basins in the United States and Canada, at a resolution of 1 kilometer (Carroll 1992). However, satellite observations in the visible and near infrared bands are limited by cloud cover and solar illumination and do not provide any information on the snowpack water equivalent. Rango (1993) reviews the use of remote sensing in studying snow hydrology processes.

The Nimbus-7 Scanning Multichannel Microwave Radiometer (SMMR) provided passive microwave observations of this snowpack from 1979 through 1987. Gloersen *et al* (1984) give a complete description of the SMMR; its capabilities, frequencies, wavelengths and footprint sizes. The SMMR instrument makes observations in 10 channels, and Chang *et al* (1976) show that the 18- and 37-GHz frequencies are best suited for snowpack remote sensing. The sensor footprints for these channels are 50 km and 25 km, respectively. The Special Sensor Microwave Imager

---

In: KT Redmond and VL Tharp, Editors. 1994. Proceedings of the Tenth Annual Pacific Climate (PACLIM) Workshop, April 4-7, 1993. California Department of Water Resources, Interagency Ecological Studies Program, Technical Report 36.

(SSM/I), which is part of the Defense Meteorological Satellite Program, provides continuing global passive microwave coverage from 1987 to present. When these latter data become readily available, the resulting continuous 15-year record will provide new insights on snowpack properties for the Upper Colorado River Basin and the entire globe.

Microwave radiation from a snowpack, as observed by a satellite sensor, consists of the emission by the snow and the emission from the underlying ground, with a small atmospheric effect. Chang *et al* (1976) and Stiles and Ulaby (1980a,b) describe the scattering process and have determined the dependence of the brightness temperature of various frequencies on snowpack water equivalent and grain size. The microwave emission of a snowpack provides information on the water equivalent and other internal snowpack properties because the emitted radiation results from the combination of the substrate emission, as attenuated by the snow, and that emitted by the snowpack itself. The result is a microwave emitter with an emissivity of less than one, and the reduction of emitted radiation is a measure of the snowpack mass or water equivalent.

Chang *et al* (1976) show the dependence of the 37-GHz brightness temperature on both the snowpack water equivalent and the grain size, for grains up to 0.5 millimeter radius. Sensitivity to grain size is strong. For example, an increase in radius from 0.3 to 0.5 millimeter for a snowpack with a water equivalent of 0.5 meter, reduces the 37-GHz brightness temperature by about 50 Kelvin. These studies were carried out assuming snow grains were spherical and uniformly distributed within the snowpack, conditions seldom found in natural snowpacks. Hence, development of accurate algorithms to extract snowpack properties from satellite passive microwave observations requires knowledge of not only the water equivalent but also the internal snowpack structure, particularly the grain size distribution.

In addition to water equivalent, passive microwave observations can be used to determine other snowpack parameters of hydrologic importance. First, time series of differences between day and night observations indicate the presence of liquid water in the snowpack. Early in the season, the difference is small, indicating the absence of liquid water. As spring approaches the difference grows, indicating the daytime presence of liquid water that refreezes at night. When the liquid water does not refreeze at night, the difference becomes small and the "ripe" snowpack will start melting.

A second parameter is the snow extent. Passive microwave observations can augment observations in the visible and near infrared bands and are particularly useful during long periods of cloudiness. Josberger and Beauvillain (1989) developed a criteria for determining the snow extent of the Upper Colorado River Basin from passive microwave observations. Finally, Josberger *et al* (1993) found a strong relationship between the discharge of the Upper Colorado River and an index derived by spatially integrating the SMMR observations from the entire basin.

## SMMR/SNOTEL Correlations

For this study, we mapped the 9 years of SMMR observations into  $\frac{1}{4}$ -degree latitude by  $\frac{1}{4}$ -degree longitude pixels for the region bounded by  $36^{\circ}\text{N}$  to  $44^{\circ}\text{N}$  and  $105^{\circ}\text{W}$  to  $113^{\circ}\text{W}$ , which contains the Upper Colorado River Basin. Figure 1 shows the study area and the mountains of the region as delineated by the 7,000-foot elevation contour. This mapping yielded a complete night map of the region every 6 days. The 6-day interval resulted from the SMMR swath width, orbital parameters and a 1-day-on/1-day-off duty cycle that was a consequence of power availability on the Nimbus-7 satellite. We also produced the corresponding day maps to investigate day/night differences.

Despite the complex snowpack structure and snowpack variations within the mesoscale footprint, the satellite observations show strong correlation with point snow observations

by the USDA Soil Conservation Service SNOTEL program (snow telemetry). The SNOTEL observations consist of daily observations of water equivalent made by a snow pillow as well as minimum and maximum temperatures. Figure 1 shows the location of all the SNOTELs used in this study, and Table 1 gives the number of SNOTELs in 1979 to 1987, for each of the three mountainous areas, called Colorado, Wyoming, and Utah. For the satellite observations, we defined a parameter called the negative gradient ratio (NGR), which is  $-1,000$  times the difference between the 37- and 18-GHz vertically-polarized channels divided by the sum of the two channels. Taking the difference removes, to first order, surface temperature effects. This variable is a non-dimensional positive integer quantity.

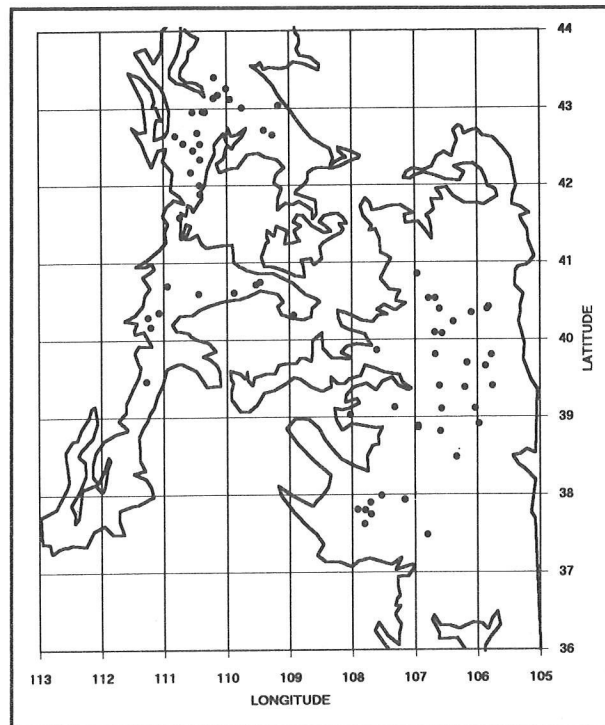


Figure 1. Location of Snow Pits within the SMMR Study Region and the 7,000-foot Contour Line

Table 1  
NUMBER OF SNOTEL SITES IN EACH REGION

Year	Colorado	Utah	Wyoming	Year	Colorado	Utah	Wyoming
1979	11	8	3	1984	34	20	8
1980	14	8	3	1985	35	22	8
1981	30	15	3	1986	42	26	15
1982	32	19	3	1987	39	26	16
1983	25	18	3				

We obtained the average correlation for each of the nine years from the individual correlations that result from comparing the NGR values from a pixel to the SNOTEL observations in the pixel. The time series is generated by calculating the correlation with the first 60 days of the water year (about 10 pairs of data points), and then adding a new observation every 6 days and recalculating the correlation. Figure 2 shows the time series of average correlation between the NGR and the SNOTEL water equivalent observations for the three regions. Because 1979, 1981, and 1986 exhibit special characteristics (described later), these three years are denoted by separate symbols. The other six years show similar behavior and are all plotted with the same symbol.

The general behavior of the time series is the same for all regions. Initially, the correlations range from 0.3 to 0.8 and then rise to a broad plateau that typically begins near water-year day (WYD) 100 (January 8). The increase in correlation results from the snowpack completely covering the pixel. Maximum correlations are as high as 0.95. The correlations decrease around WYD 175 (March 26), as the snowpack warms and begins to melt but the liquid water does not refreeze at night. For clarity, the standard deviations for each correlation point are not shown, but they are typically less than 0.1. These standard deviations decrease as the water year progresses and then increase when the correlations drop.

The Wyoming region initially has the highest correlations and also shows the greatest correlations with the least amount of spread. The Utah and Colorado regions each begin with lower correlations that increase as the water year increases, but these regions never attain the correlations found in the Wyoming region. This behavior may result from several reasons. The Wyoming SNOTELs may be more representative of snow conditions in their respective pixels. The snowpack may have more consistent grain size and structure from year to year. The temperatures in the Wyoming region may be colder which would result in drier snow over the entire elevation range, from valleys to mountain tops. Finally, as Table 1 shows, there are fewer SNOTELs in Wyoming which would tend to make correlation coefficients higher.

The interesting behavior in 1979, 1981, and 1986, is worth a few comments. For 1979, the satellite began acquiring data on WYD 82, hence the data set is much shorter than that from the other years. As a result, these correlations represent the lower bound of almost all the correlations for all years; however, they still attained values of 0.75. The very low-snow year, 1981, had the greatest effect on correlations from the Utah region. These are the lowest correlations found for any of the regions, ranging between 0.5 and 0.7. Correlations from the Colorado and Wyoming regions for this year show no abnormal behavior, and it is not obvious why the Utah region should exhibit such behavior. Finally, as shown by Josberger *et al* (1990), a strong basin-wide warming in 1986 produced a sudden drop in correlation at about WYD 150, much earlier than normal, which can be as late as WYD 200.

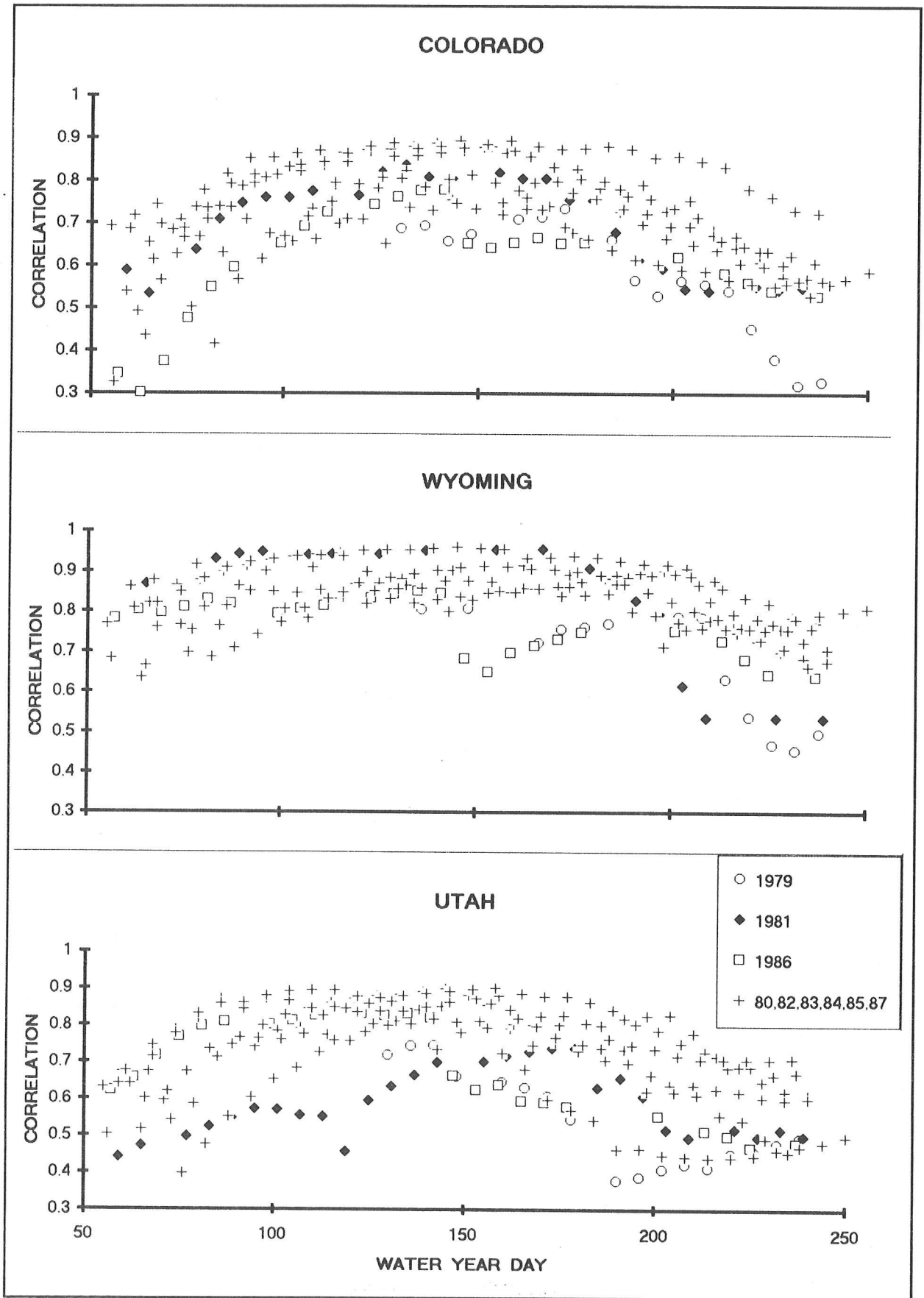


Figure 2. Time Series Correlations from the Three Regions for 1979 through 1987

## Effects of Snowpack Grain Size

The interannual variations in these correlations result primarily from differences in water equivalent and in the grain size of the snowpacks. Because systematic observations of snowpack grain size, density, and structure were not available, we began a sampling program in 1984 to obtain these data from representative sites within the entire Upper Colorado River Basin. At about the time of maximum snowpack at the end of March, field teams visited as many as 30 SNOTEL sites, dug a snow pit, and measured vertical profiles of grain size, density, temperature, and stratigraphy. This field program has continued since 1984 and has collected a unique dataset of snowpack properties specifically for passive microwave studies.

Table 2 gives the vertically-averaged grain size of the snow pit observations from each region for 1984 through 1987, which are the years when the SMMR instrument operated and for which we have grain size measurements. The table also gives the average water equivalent from all of the SNOTELs in each region at the time of maximum water equivalent.

Year	Wyoming			Colorado and Utah		
	SWE (mm)	Grain Size (mm)	NGR	SWE (mm)	Grain Size (mm)	NGR
1984	428	2.10	82	413	1.00	48
1985	290	1.50	64	351	1.50	31
1986	347	1.40	85	330	1.20	22
1987	235	2.70	30	208	1.50	17

A multiple regression analysis of the average grain sizes, the water equivalent, and the satellite observations gives:

$$NGR = 0.153 SWE + 3.31 \text{ Grainsize} - 6.87 \quad R = 0.76,$$

where both water equivalent and grain size are measured in millimeters. The fact that the grain size coefficient is 20 times larger than the water equivalent coefficient clearly shows the strong dependence of NGR on the snowpack grain size.

The snowpack in the Upper Colorado River Basin is a continental type that consists of a bottom layer of large depth hoar crystals (up to 5 mm) and an upper layer of fine- to medium-grained new and old snow with grain sizes up to 2 millimeters. Variations in the depth hoar layer strongly affect the averages in Table 2 and, hence, the satellite signatures. Characteristics of the depth hoar layer are determined early in the accumulation season, which allows us to compare the average grain size measurements with the water equivalent values even though these data are usually from different times of the snow year.

## Conclusions

---

The 9-year SMMR passive microwave record of the Upper Colorado River Basin shows strong correlations with the snowpack water equivalent as measured by the SNOTEL system. These correlations can reach values of 0.9 or greater and, hence, provide synoptic large-scale observations of this important snowpack. The utility of these observations for global change and water resource investigations will greatly increase when the datasets become longer and when more accurate algorithms are developed for mountainous snowpacks through improved spatial resolution and a greater understanding of snow deposition in mountainous terrain. The Special Sensor Microwave Imager (SSM/I) observations, when available, will yield a 15-year dataset that continues to grow.

## References

---

- Carroll, TR. 1992. *Airborne Operational Snow Survey Program and Satellite Hydrology Program, User's Guide Version 4.0*. National Operational Hydrologic Remote Sensing Center, Office of Hydrology, NOAA.
- Gloersen, P, DJ Cavalieri, ATC Chang, TT Wilheit, WJ Campbell, OM Johannessen, K Katsaros, KF Kunzi, D Ross, D Staelin, EPL Windsor, FT Barath, P Gudmansen, E Langham, RO Ramseier. 1984. A Summary of Results from the First Nimbus-7 SMMR Observations. *Journal of Geophysical Research*, 89(D4):5335-5344.
- Chang, ATC, P Gloersen, T Schmugge, T Wilheit, HJ Zwally, 1976. Microwave Emission from Snow and Glacier Ice. *Journal of Glaciology*, 16(74):23-39.
- Stiles, WH, and FT Ulaby. 1980a. The Active and Passive Microwave Response to Snow Parameters, 1. Wetness. *Journal of Geophysical Research*, 85(C2):1037-1044.
- \_\_\_\_\_. 1980b. The Active and Passive Microwave Response to Snow Parameters, 2. WaterEquivalent of Dry Snow. *Journal of Geophysical Research*, 85(C2):1045-1049.
- Josberger, EG, and EB Beauvillain. 1989. Snow Cover of the Upper Colorado River Basin from Satellite Passive Microwave and Visual Imagery. *Nordic Hydrology*, 20(2):73-84.
- Josberger, EG, WJ Campbell, P Gloersen, ATC Chang, A Rango, 1993. Snow Conditions and Hydrology of the Upper Colorado River Basin from Satellite Passive Microwave Observations. *Annals of Glaciology*, 17:322-326.
- Josberger, EG, C Ling, WJ Campbell, P Gloersen, ATC Chang, A Rango. 1990. Correlations of Scanning Multichannel Microwave Radiometer (SMMR) Observations with Snowpack Properties of the Upper Colorado River basin for Water Year 1986. *IGARRS '90 Proceedings*, 3:1317-1320.
- Rango, A. 1993. Snow Hydrology Processes and Remote Sensing. *Hydrological Process*, 7:121-138.



# The California Heat Island: Seasonal Trends in Maximum and Minimum Temperatures

Lynda M. Klein and Jim Goodridge

This paper summarizes progress in an ongoing study of California's temperature trends. It supplements studies reported at PACLIM in 1984, 1986, and 1987. Prior studies based on mean annual temperature, reported that air temperature at coastal stations in California is highly correlated with sea surface temperature and that "global heating", as reported by Hanson (1987) and Jones *et al* (1986), is an urban phenomenon in California.

Other studies have also found no general warming trend. Kahl *et al* (1993), using Russian Arctic radiosonde data for 1954 to 1990, found no long-term warming trend. Christy (1993) has found no global warming trend using satellite-borne microwave radiometers to measure atmospheric temperature for 14 years ending in February 1993.

Balling, Idso, and Hughes (1991) found no warming trend in 43 rural Australian temperature stations for 1911 to 1990. Their study did find an increase in minimum temperatures similar to those in this study.

Urban heat islands have been studied extensively by Landsberg (1981) and others, but have failed to attract the attention given to global heating. This may be because the temperature records have been digitized extensively (Quayle 1989) and are readily available to those whose major interests and skills appear to be manipulating computerized datasets rather than looking for the physical processes taking place at the temperature measuring stations.

## Objectives

Objectives of this study are twofold: to examine and map the trends in maximum and minimum temperatures for the warm and cool seasons separately, and to examine regional differences in maximum and minimum temperature trends in California.

The long-term maximum and minimum temperature trends were considered without strict regard to the length of record. Trends are fairly consistent, and we thought it better to have more records in the analysis than to eliminate shorter datasets. The starting year for records used ranged from 1897 to about 1930; the ending year was 1991 for all 136 stations. The average period of record was 81 years. More than 8 million daily temperature observations were represented.

The second part of this study is a time series analysis of annual temperature data. This is a subset of the main data file, with a consistent length of record for inter-regional comparison.

## **Data**

---

Study data consist of mean monthly maximum and minimum temperatures calculated by averaging all of the daily maximum and minimum temperatures reported during each month. The data were collected by the National Weather Service and published by the National Climatic Data Center in Ashville, NC. Most of the records for July 1948 to 1991 were obtained from the Western Regional Climate Center, Desert Research Institute, University of Nevada, in Reno. Records for January 1897 to June 1948 were from several sources. Records for station names beginning with A through L were from observers' original records on microfiche from NCDC. Records for station names beginning with L through Z were summarized by the Weather Bureau State Climate Office. When this office was disbanded in 1973, the climatological records were scattered, so the entire dataset was not available. A few station records for recent years, such as Barrett Dam and Claremont Pomona College, were obtained from cooperative observers, since these stations were dropped from the NWS network.

Of the 136 stations, only 25 percent of the records began in 1897; 61 percent began by 1906, and 94 percent began by 1920. (In 1906, California's weather record archive was lost in a fire.) A subset of the 136-station network consists of 90 records that are complete for the 80 years from 1912 to 1991. This subset was used for the regional comparisons.

We intended to develop a complete dataset that would resemble the records of observers, with no corrections or adjustments for time of observation, equipment changes, or changes in station location. There were estimates for some missing records, but the assembled dataset was better than 95 percent complete. Missing records for a station were estimated by multiplying the mean maximum (or minimum) temperature recorded at a nearby station by the ratio of the monthly averages for the same two stations.

The database of this study is available to other researchers on a data-exchange basis. It is about 12 megabytes and is recorded in Macintosh Excel 4 format.

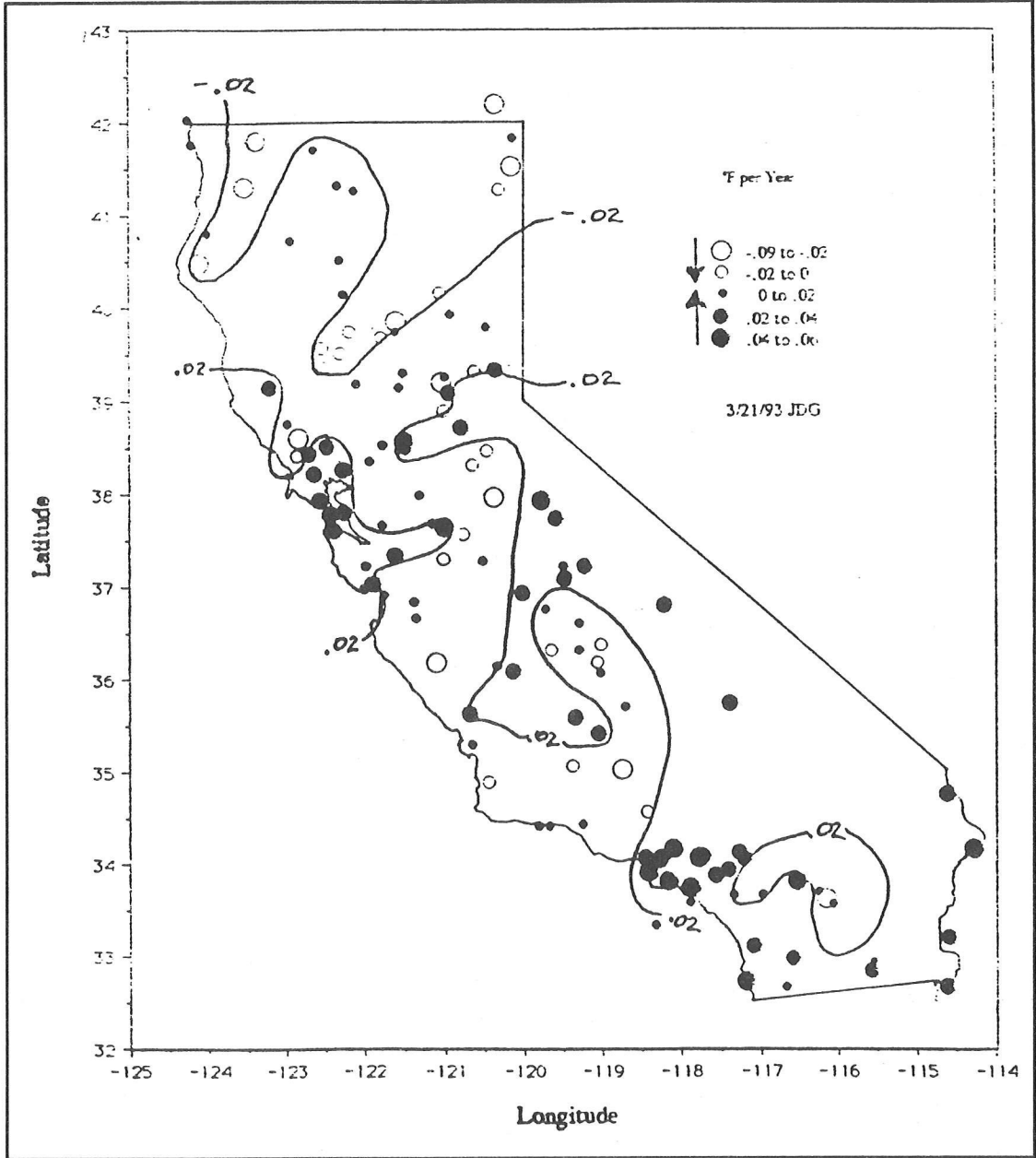
## **Analysis, Part 1**

---

Part 1 of this study is of trends in maximum and minimum temperatures for 136 stations. These trends are summarized on Maps 1 through 7 and discussed in the following sections.

**Trend in Mean Annual Temperature**

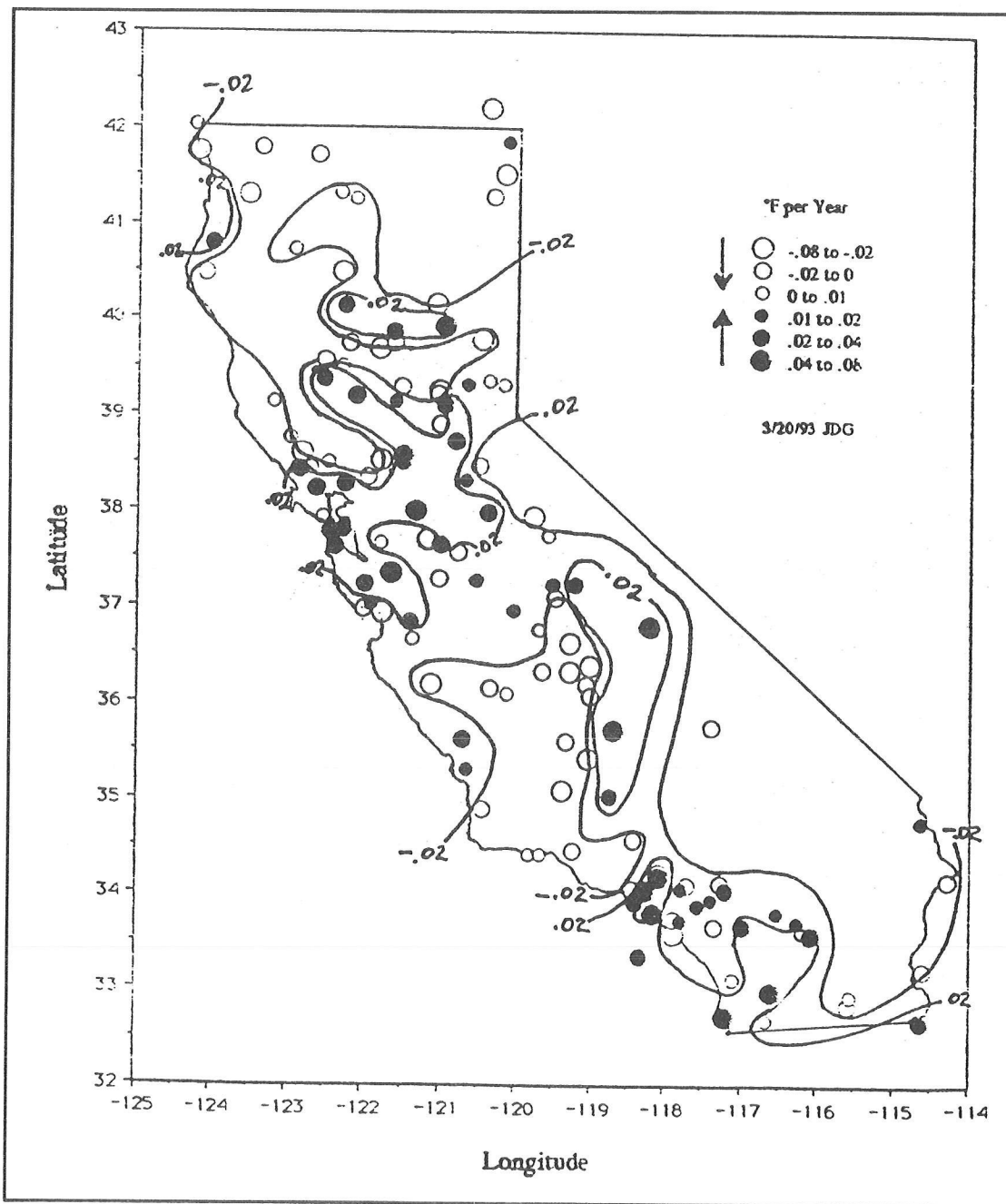
Map 1 clearly shows the warming trend of the urban areas. The San Diego/Los Angeles and San Francisco/Sacramento areas are clearly regions of extensive warming. Another zone of stations with a pronounced warming trend ranges from about Santa Maria, on the central coast, northeastward to Owens Valley and the lower desert area.



Map 1. Trend in Mean Annual Temperature

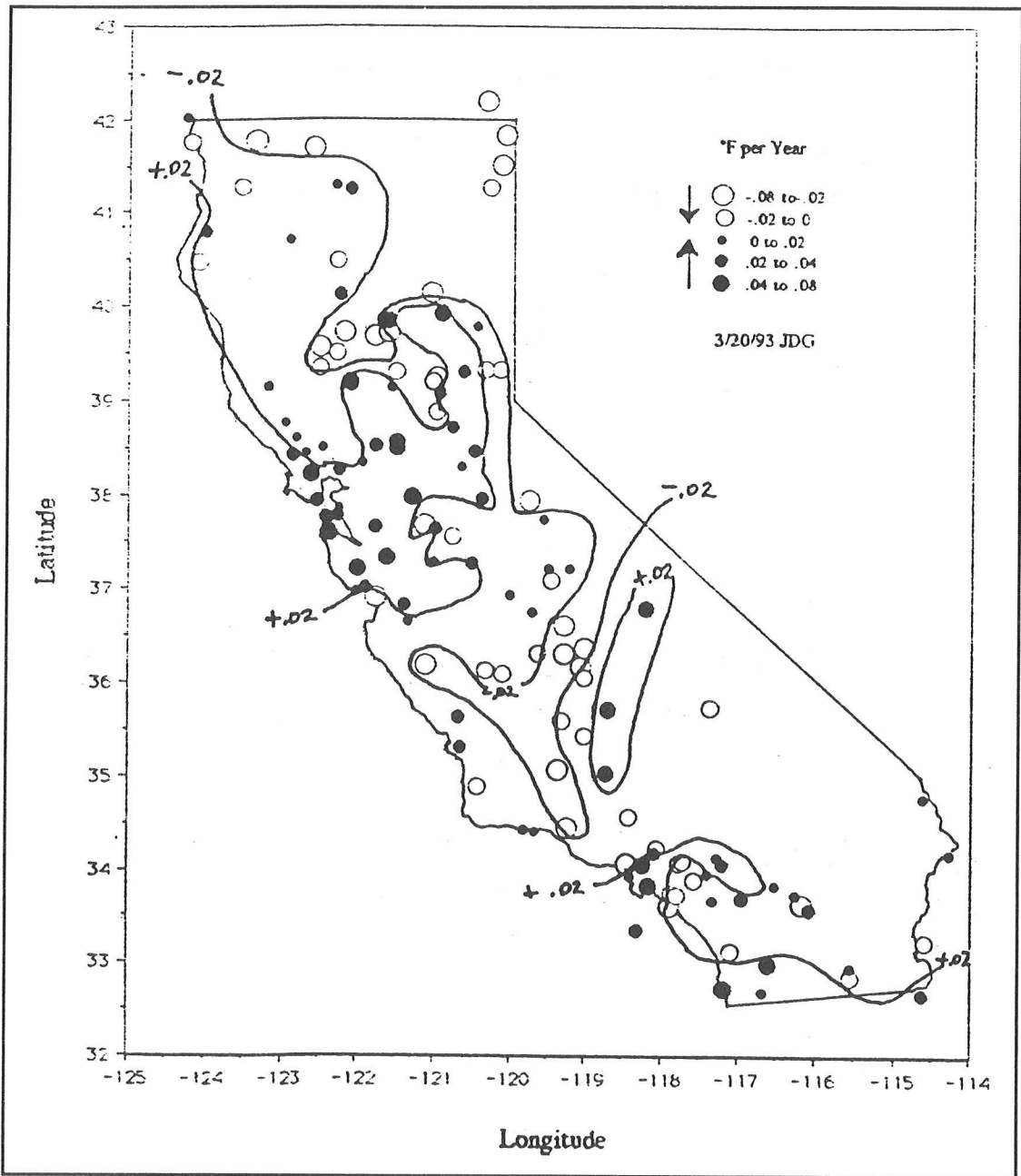
### Trend in Maximum Temperature

Map 2 shows the upward trend of average maximum temperature in the urban centers. The most impressive feature of Map 2 is the broad zone of a declining trend in the San Joaquin Valley from about Fresno and extending south to Santa Barbara and Ventura counties, on the coast. The other notable area of a downward temperature trend is in the northern part of the state, from about Redding north.



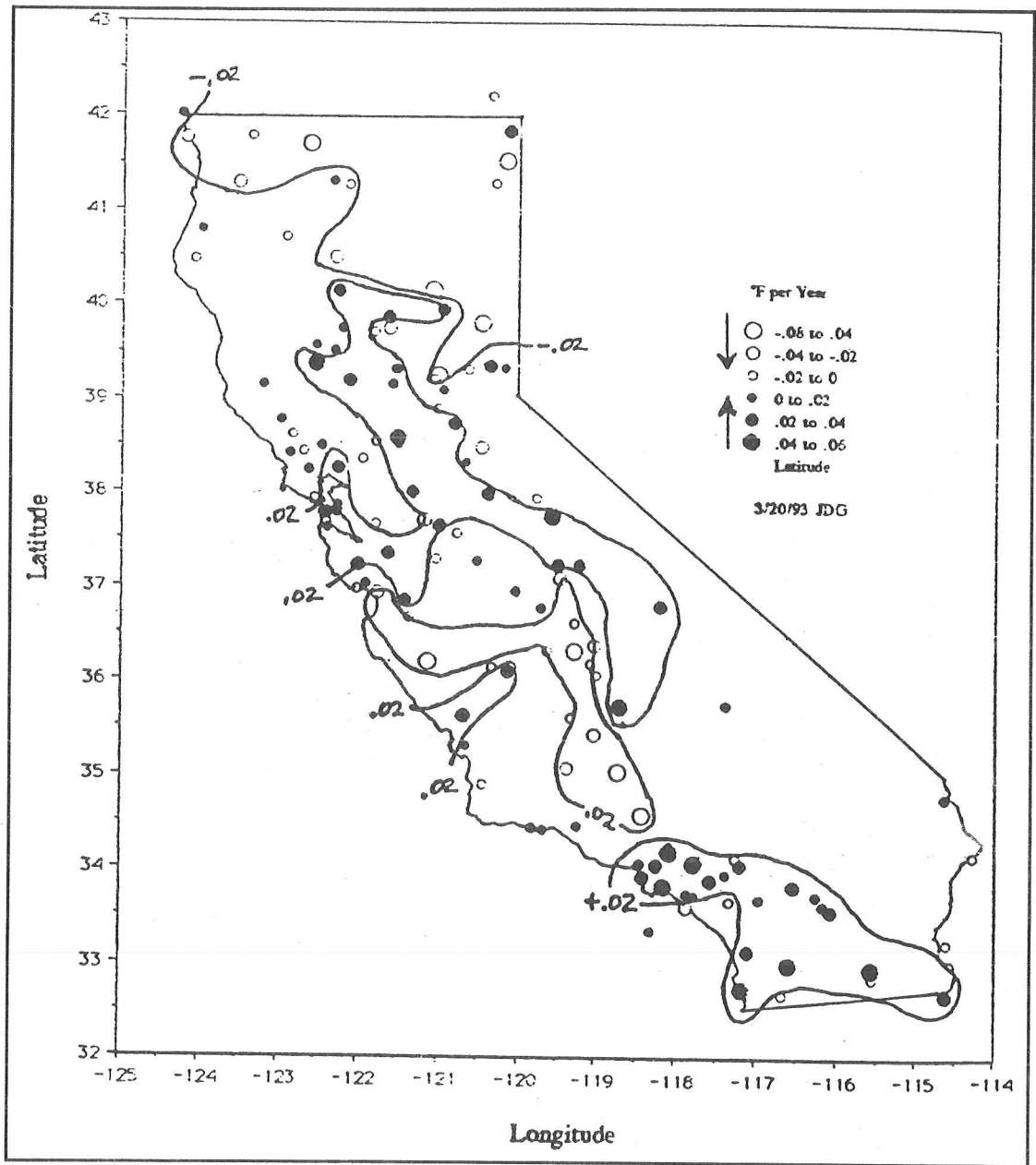
Map 2. Trend in Average Maximum Temperature

The trend in maximum temperatures was further examined for regional characteristics in the warm and cool seasons. For this study, the warm season is defined as May through October and the cool season as November through April. Map 3 shows a warming trend during the warm season in the major urban areas. Notable exceptions are the southern half of the San Joaquin Valley and the sparsely-populated Siskiyou, Modoc, and Glenn counties.



Map 3. Trend in Warm Season Maximum Temperature

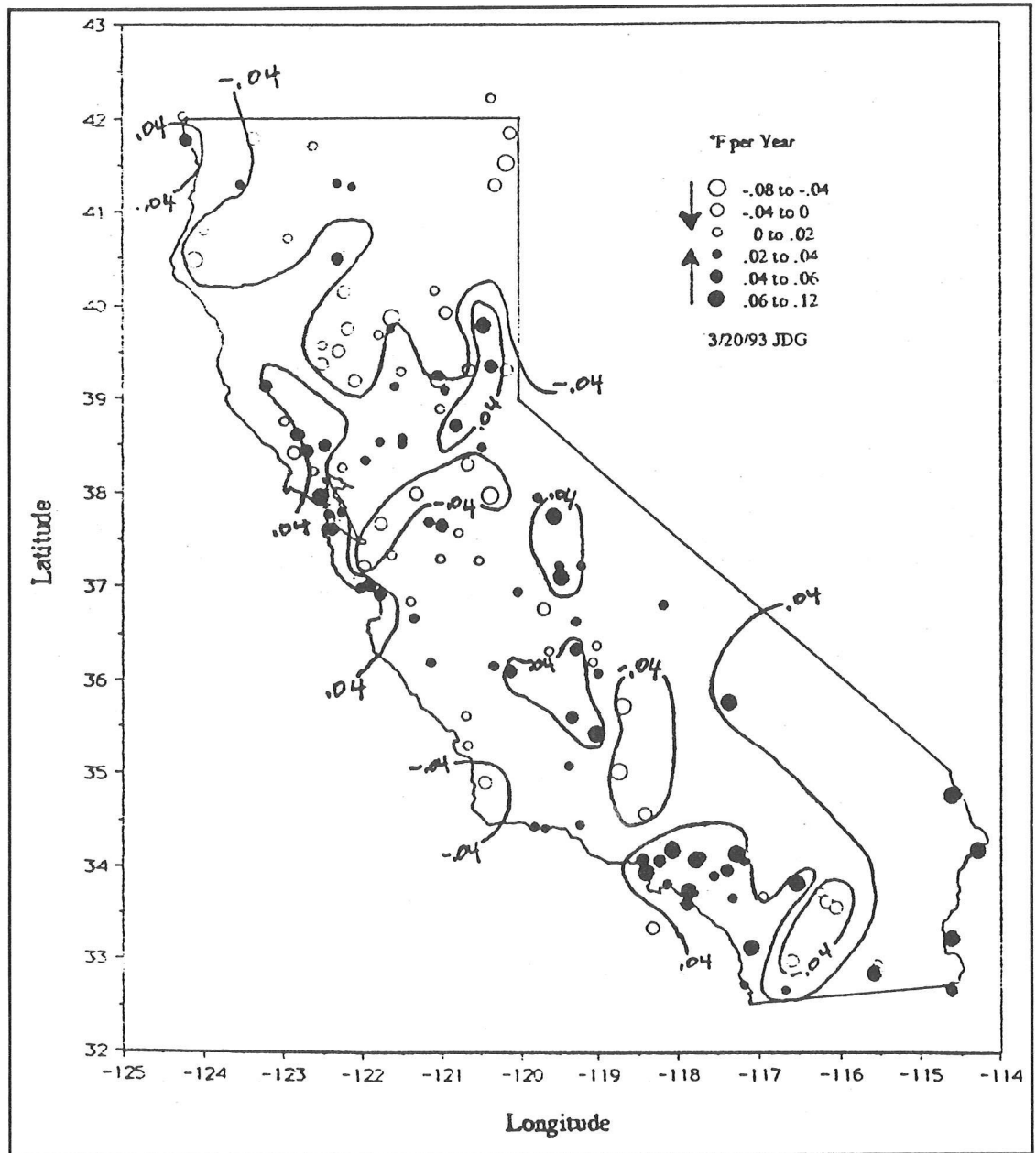
Map 4 shows the San Diego/Los Angeles area with an extensive warming trend during the cool season. The map shows a similar cool season warming trend in the southern Sierra Nevada and in the Sacramento Valley. The San Joaquin Valley is clearly an area of cooling, as is the extreme northern part of the state. An exception to the lower cool season maximum temperatures is the Fort Bidwell station. That station is near a heated house where, in 1991, the temperature shelter and the house were sheltered jointly by the canopy of some large trees.



Map 4. Trend in Cool Season Maximum Temperature

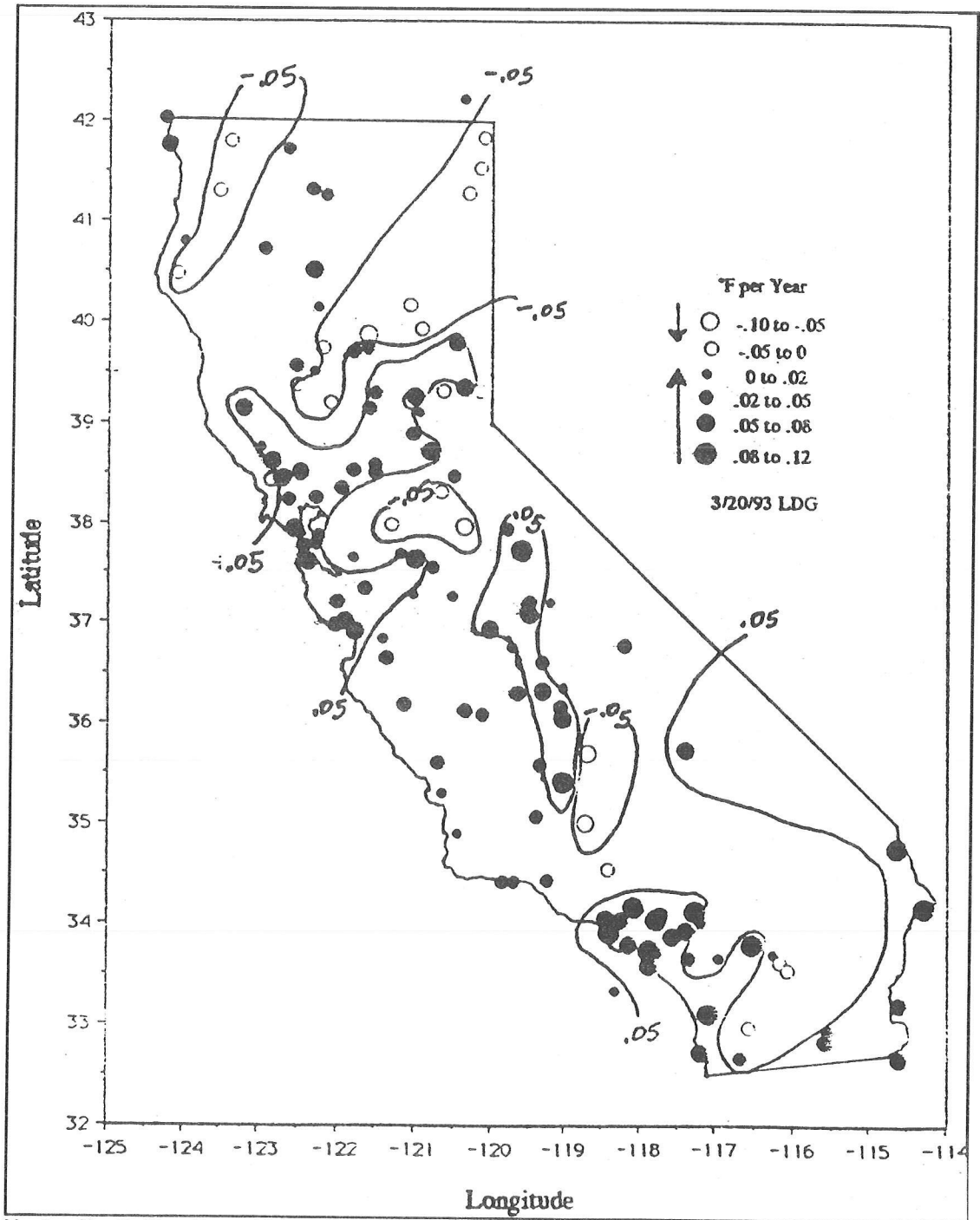
**Trend in Minimum Temperature**

Map 5 shows a complex pattern in the trend in average minimum temperature. In general, urban areas show a warming trend. The area between Glenn and Modoc counties shows a definite decreasing temperature trend.

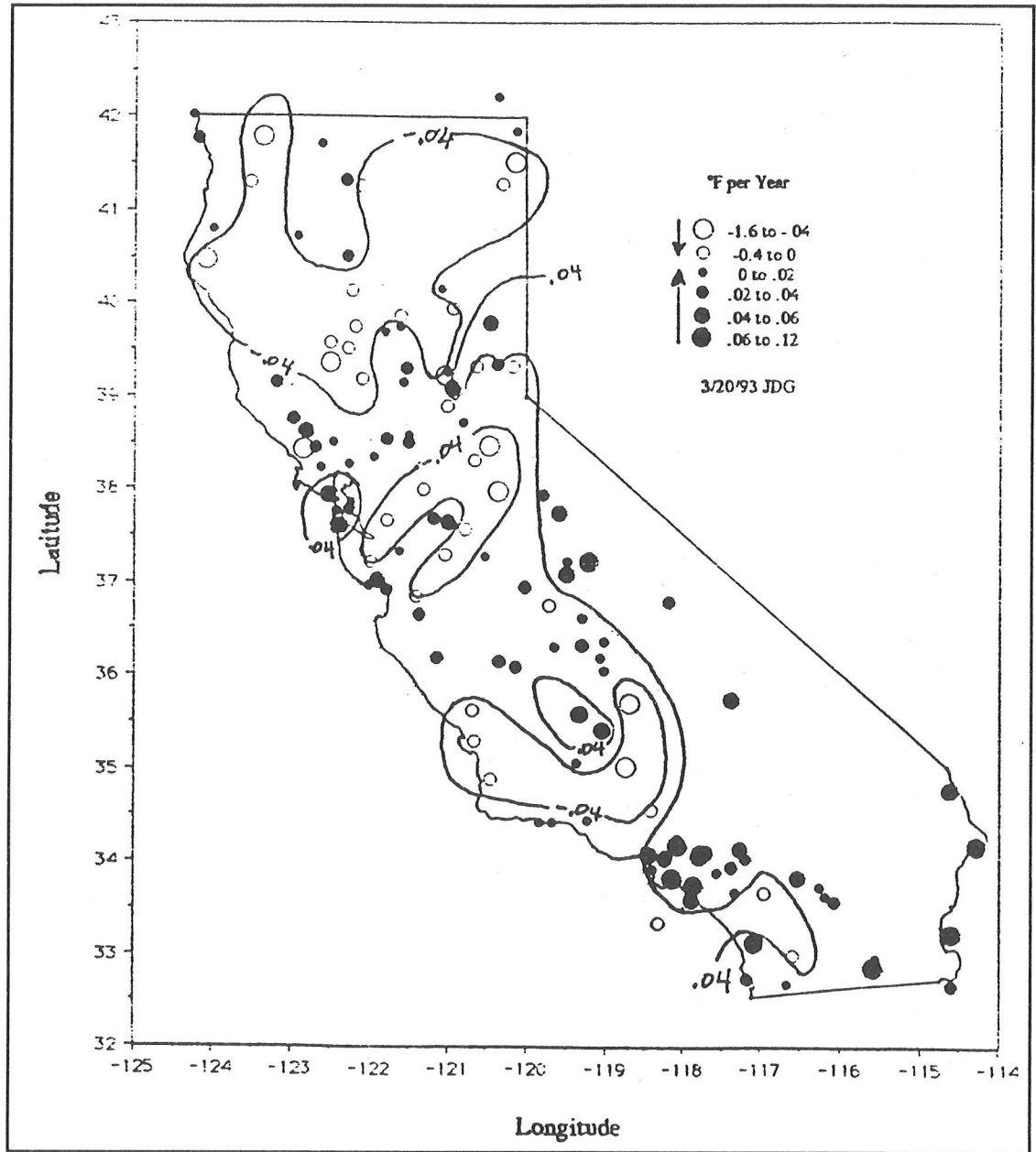


Map 5. Trend in Average Minimum Temperature

Map 6 shows a trend of higher warm season minimum temperatures in most of California, especially in urban areas. A notable exception is a cooling trend in a narrow band from the sparsely populated area extending from Glenn County to Modoc County. Of the 136 records, 25 still show a declining warm season minimum temperature. These are remote stations in rural areas. They include Fairmont Reservoir in northern Los Angeles County and Cuyamaca in the mountains of San Diego County.



For cool season minimum temperatures, Map 7 shows a trend of warming in the urban areas and cooling in some rural areas. The Glenn County area is a center of a zone with a cooling trend, as is the southern San Joaquin Valley.



Map 7. Trend in Cool Season Minimum Temperature

## Analysis, Part 2

In the second part of this study, we compare the average trends in climatic divisions used in Climatological Data for California. All 90 stations used in this comparison have an 80-year record covering 1912 to 1991. Regional trends are summarized in Table 1.

Climatic Division	Trend per Year (in °F)		Number of Stations
	Maximum	Minimum	
1 North Coast	0.00525	0.02835	9
2 Sacramento Valley	0.00156	0.01192	22
3 Northeast Interior	0.00196	0.02072	3
4 Central Coast	0.01242	0.02045	13
5 San Joaquin Valley	0.00077	0.00756	22
6 South Coast	0.01393	0.03969	15
7 Southeast Desert	0.01589	0.04548	6
Statewide	0.00634	0.02069	90

Regions of greatest upward temperature trend are clearly the Desert and the South Coast. Regions of least trend are the San Joaquin and Sacramento valleys.

The Climatic Division temperature trends suggest urban/rural temperature differences, as was the case in prior studies of the mean temperature (Goodridge 1992). To check this, the records were sorted into three classes according to county population. Small counties had 8,000 to 88,000 people at the 1990 census; mid-sized counties had 101,000 to 667,000 people; large counties had 669,000 to 8,863,000 people.

Figure 1 shows that the large counties have an increasing trend of 0.019°F per year for the maximum temperature and 0.031°F per year for the minimum temperature; the small counties have an increase of -0.0009°F in the maximum and 0.0081°F in the minimum. Differences in maximum and minimum temperatures at large and small counties is 0.023°F per year for the maximum and 0.020°F per year for the minimum, as shown in Figure 2.

In summary, the overall mean temperature trend in California is +0.0135°F per year. The trend for all 90 of the stations is 0.0063 for maximum temperatures and 0.0207 for minimum temperatures, as shown in Figure 3. The same 80-year trends are broken down into warm and cool season trends and shown in Figure 4. Warm season minimum temperatures have the greatest warming trend, with an increase of 0.027°F per year over the 80-year period.

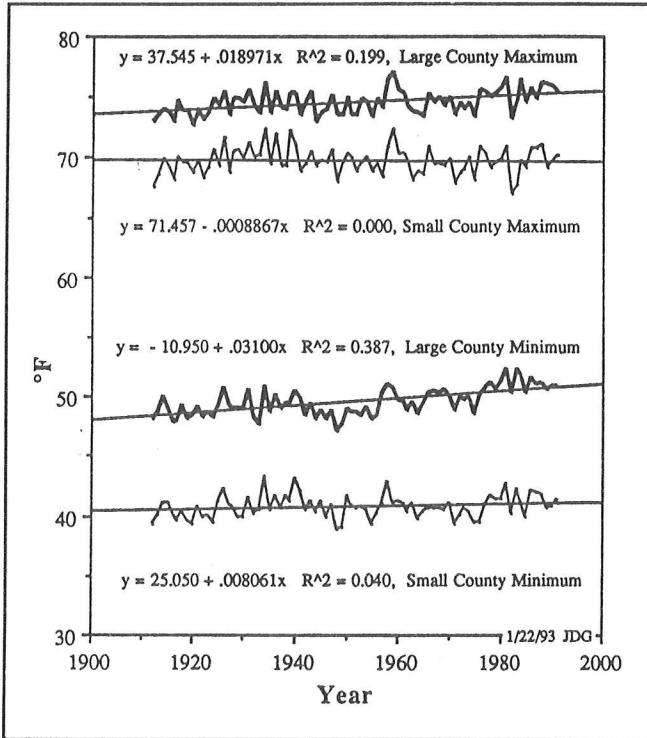


Figure 1. Temperature Trends for Large and Small California Counties  
Based on 24 stations in counties with 8,000 to 88,000 people and 27 counties with 669,000 to 8,863,000 people in 1990.

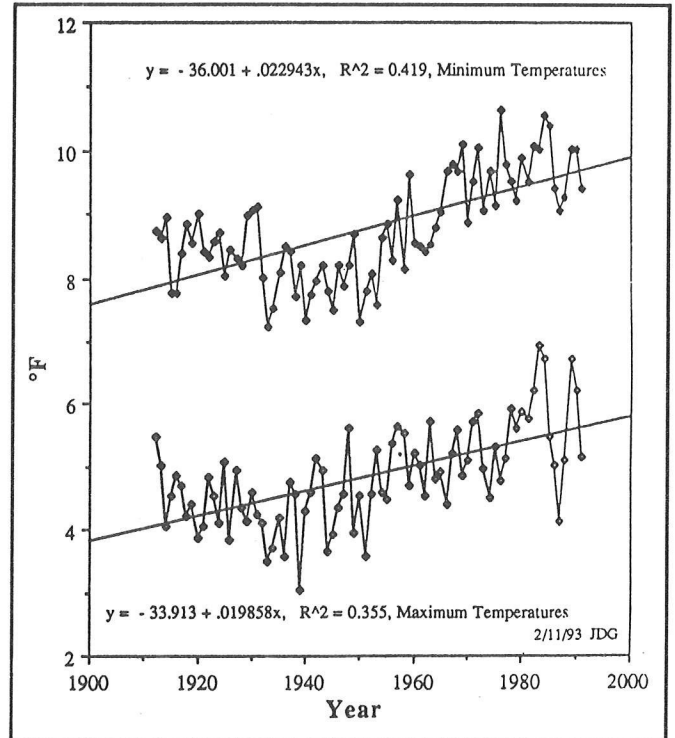


Figure 2. Urban/Rural Temperature Differences in California  
Based on 24 stations in counties with 8,000 to 88,000 people and 27 counties with 669,000 to 8,863,000 people in 1990.

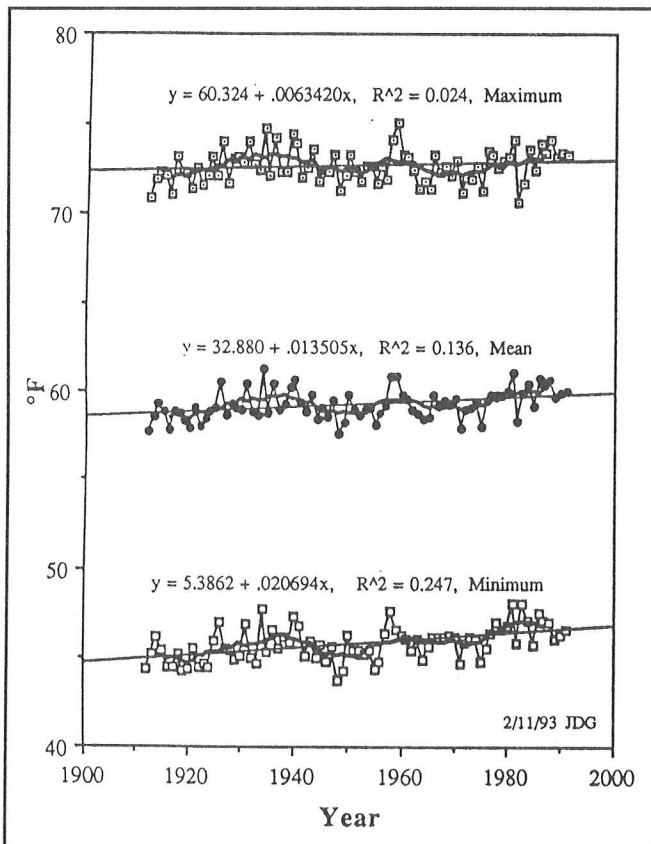


Figure 3. Average Temperature for California  
Based on 80 records for 1912 to 1991.

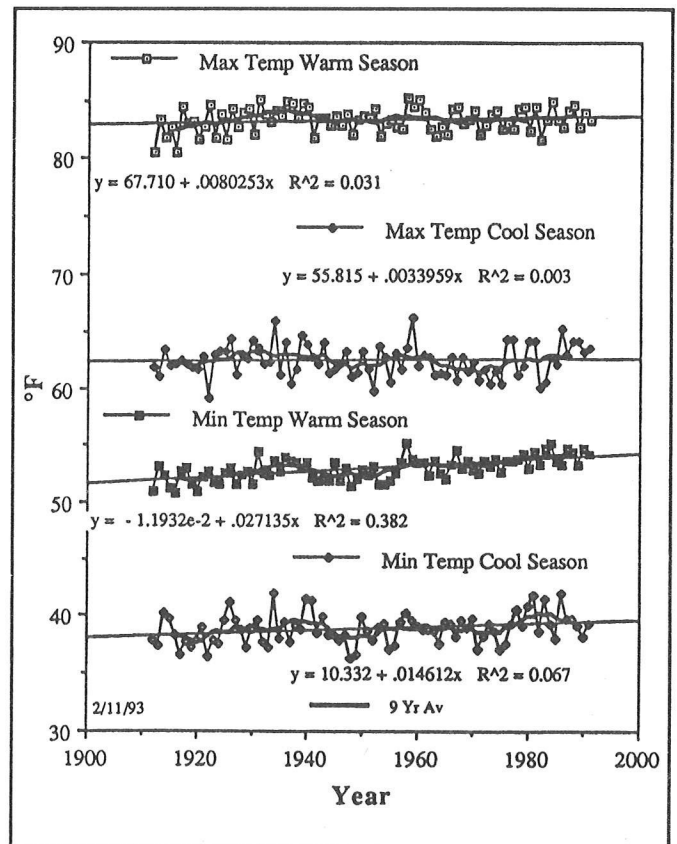


Figure 4. Annual Temperature Trends for 90 California Stations

Trends in warm season minimum temperatures were further classified by 1990 county population, and the large, urban counties were found to have an 80-year warming trend of 0.38°F per year, compared to 0.013°F per year in the smaller and rural counties, as shown in Figure 5.

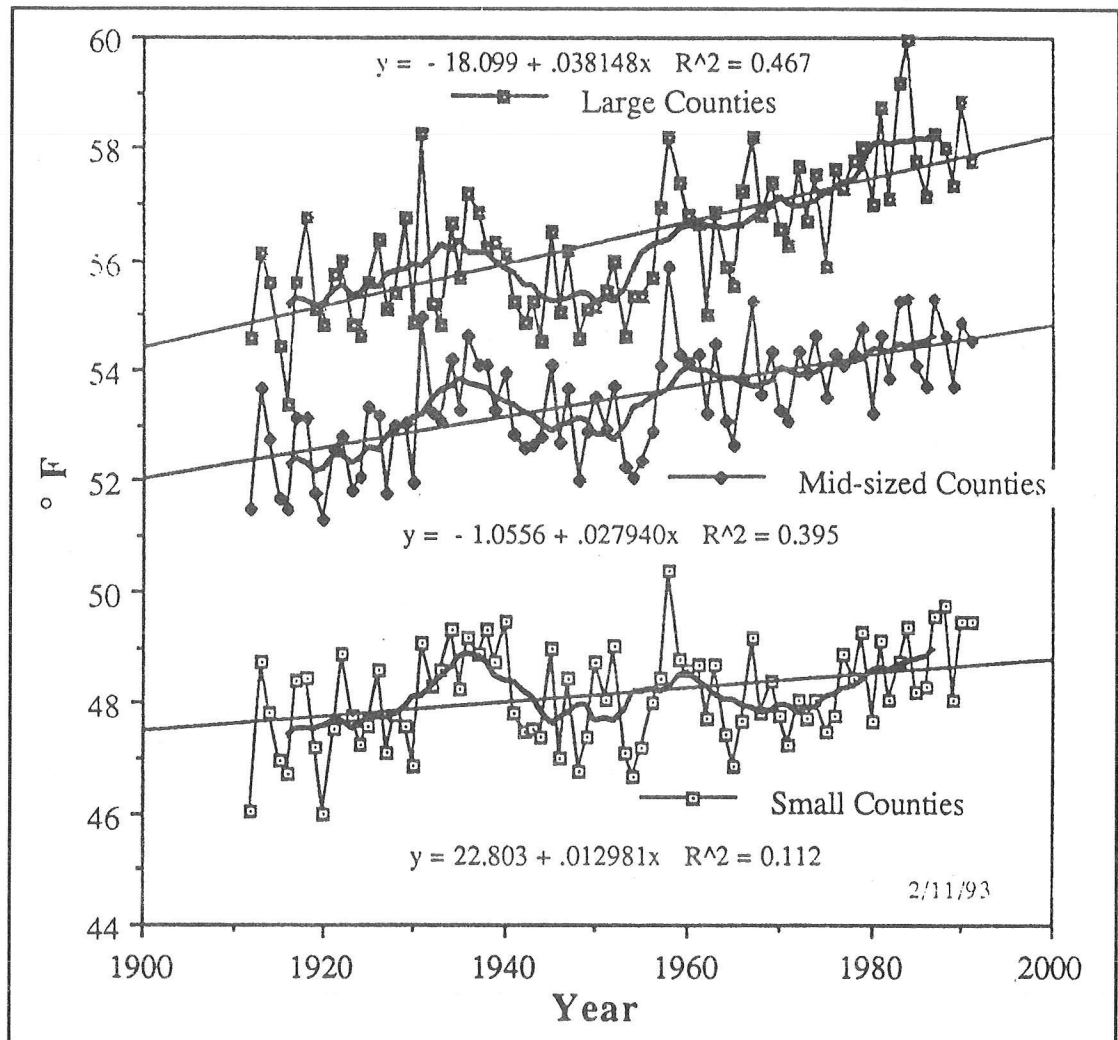


Figure 5. Trends in Warm Season Minimum Temperatures

The 1912-to-1991 trend in mean annual temperature at 36 stations in counties with less than 88,000 people is +0.036°F per year. This increase is a function of the selection of the 80-year base period. With a base period of only 70 years, the trend for 1922 to 1991 is -0.0034°F per year, as shown in Figure 6. It seemed unreasonable to make a statement about the sign of the California long-term temperature trend with only 80 years of reliable record, when an arbitrary starting date has a large influence on the indicated trend.

The trend in mean annual temperature at 42 stations in counties with more than 669,000 people is an increase of 0.024°F per year, as shown in Figure 7. This large warming trend is believed to be a function of the urban heat island effect from waste heat, vegetation stripping, or other forms of urban thermal pollution. The positive warming trend of thermally polluted records was little affected by selection of a base period for the study.

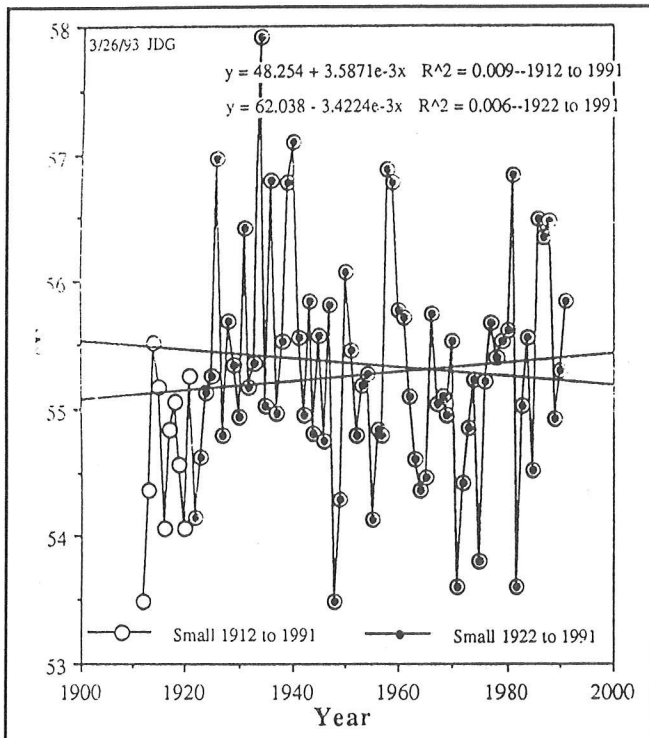


Figure 6. Trend in Mean Annual Temperature at 36 Stations in Counties with Less Than 88,000 People  
 Note that the long-term trend is dependent on the starting year.

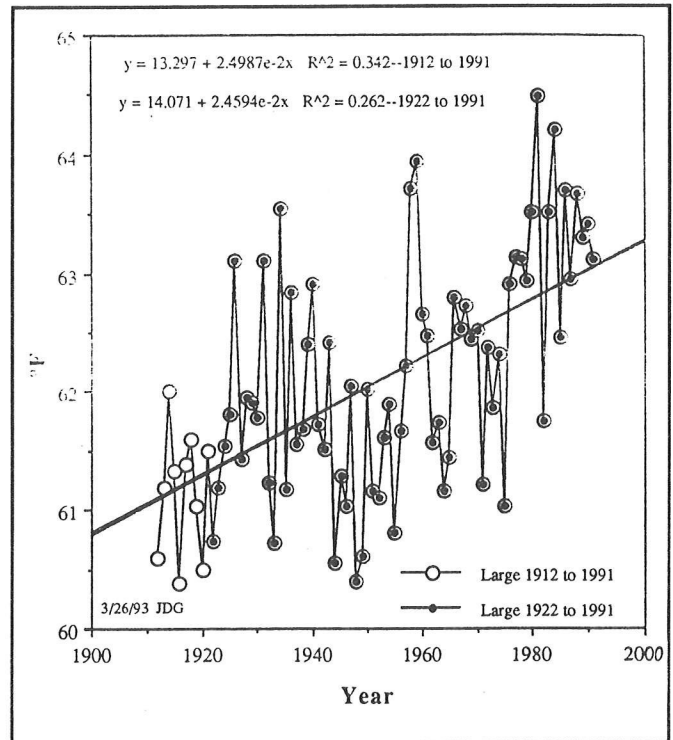


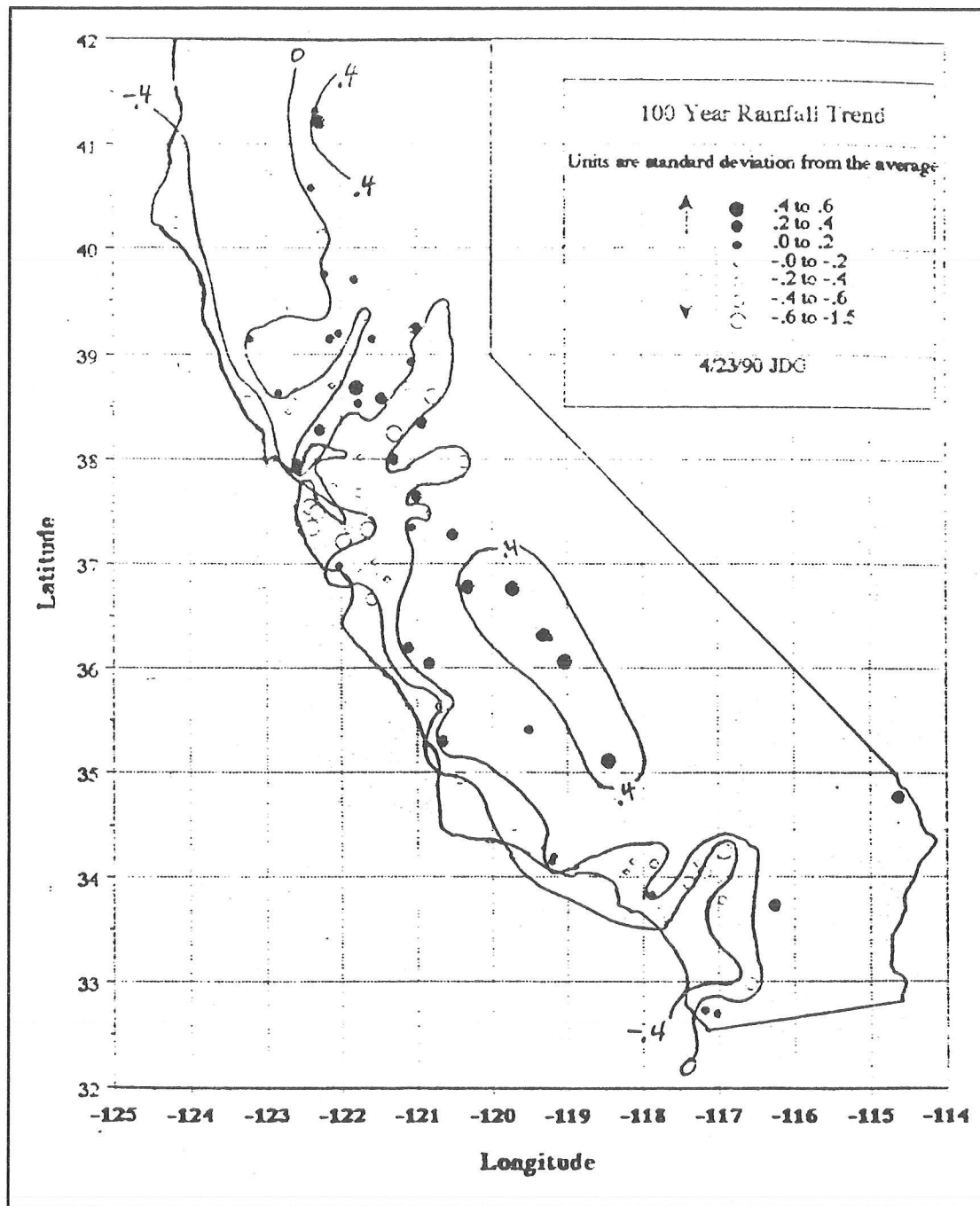
Figure 7. Trend in Mean Annual Temperature at 42 Stations in Counties with More Than 669,000 People  
 Note that the long-term trend is not dependent on the starting year. The trend is probably related to urban thermal pollution.

It is possible waste radiant heat in the view shed of a thermometer shelter is being measured. The most sensitive areas seem to be the deserts, which lack vegetation to further shield the thermometers or moisture to buffer the measurements.

Another possibility is that extensive irrigation in the San Joaquin Valley could increase atmospheric humidity. This could account for some of the long-term minimum temperature increases in parts of the valley.

There are broad regions of similarity in long-term temperature trends shown on Maps 1 to 7, and only a few examples of outliers that could represent unique problem temperature records. Since good records are highly correlated, we believe there are a large number of very good records in the basic data of this study.

Several forces seem to be affecting temperature trends in California. One is the effect of urban waste heat and increased relative humidity. Another is climatic variation. The high correlation of temperature trend and county population is an index of the thermal pollution of the urban areas. The extent of climatic variation is unclear in the case of temperature, but it is quite evident for precipitation. The rain records of the coastal areas indicate a declining trend over the last 100 years, and interior regions have an increasing trend, as shown on Map 8. This suggests a future project of separating the climate variation signal from the variation due to thermal pollution.



Map 8. 100 Years of California Rainfall Trends  
Based on 96 records from stations with data from 1890 to 1989.

## Acknowledgments

---

We gratefully acknowledge the assistance of Jim Ashby and Kelly Redmond of the Western Regional Climate Center in supplying data, of Day Cayan for sea surface temperature data, and of Larry Riddle for help in mapping.

## Bibliography

---

- Balling, RC, SB Idso, WS Hughes. 1992. Long-Term and Recent Anomalous Temperature Changes in Australia. *Geophysical Research Letters*. 19(23):2317-2320.
- Christy, JR. 1993. Personal communication in March 1993.
- Goodridge, JD. 1992. Urban Bias Influences on Long-Term California Air Temperature Trends. *Atmospheric Environment*. 26B(1):1-7.
- Hanson, J, and S Lebedeff. 1988. *Global Surface Air Temperatures: Update 1987*. American Geophysical Union.
- Jones, PD, SCB Raper, RS Bradley, HF Diaz, PM Kelley, TML Wigley. 1986. Northern Hemisphere Surface Temperature Variations: 1851-1984. *J. Climate Appl. Meteor.* 25(2).
- Kahl, JD, DJ Charleviox, NA Zaitseva, RC Schnell, MC Serreze. 1993. Absence of Evidence for Greenhouse Warming Over the Arctic Ocean in the Past 40 Years. *Nature*. Vol. 361.
- Landsberg, HE. 1981. *The Urban Climate*. Academic Press.
- National Climatic Data Center. *Climatological Data*. Published Monthly since 1897 for Each State. NCDC, Federal Building, Ashville, NC 28801.
- Owenby, JR, and DS Ezell. 1992. Monthly Station Normals of Temperature, Precipitation, and Heating and Cooling Degree Days 1961-1990. *Climatology of the United States*. No. 81. National Climatic Data Center, Ashville, NC 28801.
- Quayle, RG. 1989. *The Wolbach Dataset for Climate Monitoring — Philanthropy and Climatology*. Bulletin of the American Meteorological Society. 70(12).
- Quinlan, FT, TR Karl, CN Williams Jr. 1987. *United States Historical Climatological Network (HNC) Serial Temperature and Precipitation Data: CDIAC Numeric Data Collection, NDP-019*. Carbon Dioxide Information Analysis Center, Oak Ridge, TN.



# Seasonal Resolution of Laminated Sediments in Santa Barbara Basin: Its Significance in Paleoclimatic Studies

Carina B. Lange and Arndt Schimmelmann

Sediments in Santa Barbara Basin contain microfossil and sedimentological information that allows reconstruction of major features of the California Current such as water temperature, strength of upwelling, and productivity. Changes in the California Current are correlated with the climatic pattern in the North Pacific, and with rainfall in Southern California (Namias 1975). The Santa Barbara Basin underlies a very productive coastal ocean and is characterized by high sedimentation rates (>2 mm per year). Oxygen depletion in the near-bottom waters inhibits bioturbation by macrobenthos and allows for preservation of discrete laminae. The varves (light/dark lamina pairs) originate from seasonal variations in the composition of particles supplied to the basin floor and from change in bottom water conditions associated with seasonal flow in the California Current (Soutar and Crill 1977; Reimers *et al* 1990). Episodic events within seasons (*eg*, diatom spring blooms) are preserved as distinctive microlaminations within seasonal laminae. Several microfossil paleoclimatic indicators (diatoms, forams, radiolarians) have been used by our group at the Scripps Institution of Oceanography and by colleagues at other institutions to reconstruct decadal variability in the California Current system (see review in Fisher 1990, and Lange *et al* in press).

Until now, investigations of Santa Barbara Basin sediments have utilized analytical techniques that could not resolve seasonal laminae, permitting annual resolution of variations in sediment composition and structure only. With the exception of a study in 1988, no seasonal resolution of the sedimentary record has been attempted. The 1988 data on biogenic and detrital components indicate that seasonality is strong in the Santa Barbara Basin, with episodic events of the order of days to weeks (Reimers *et al* 1990).

Based on a successful technique for preparation of epoxy-embedded and highly polished thin-sections (Spurr 1969; Kemp 1990; Grimm 1992a) that permit economical optical and electron microscope evaluation of laminated sequences, it is our long-term goal to reconstruct, with unprecedented detail, the history of sedimentation processes in the Santa Barbara Basin by developing ultra-high-resolution time series of biotic and detrital proxies.

## Material and Methods

This pilot study focuses on a sediment interval from about 1825 to 1849, including the *Macoma* shell layer, for which we have detailed information from an earlier study (Schimmelmann *et al* 1992). Subsequent to X-radiography of the original sediment slab to be studied (Figure 1), sectioning of it into rectangular “blocks” of about 4x3x1 centimeters was necessary for sizing of thin sections. Saline pore water was removed in a sequence of baths, first with 50:50 acetone/water, then acetone, and finally with a 4-component epoxy-resin (Spurr low-viscosity embedding media, Polysciences, Inc.; Spurr 1969). The resulting epoxy-embedded “blocks” were cured for 2 weeks at 50° to 70°C. Finally, thin sections were made at the Scripps Analytical Facility, including polishing the epoxy block with 1 µm diamond grit and then mounting it onto a 7x5-cm glass slide. The block is cut (perpendicular to bedding) to about 200-µm thickness, then ground to 45-µm thickness in a lapping and optical polishing machine (Logi-Tech LP 30), using a 600-µm silicon carbide grit and water slurry, and followed by polishing steps with 6-µm and 3-µm diamond, and 0.05-µm alumina in ethylene glycol to 35 µm final thickness.

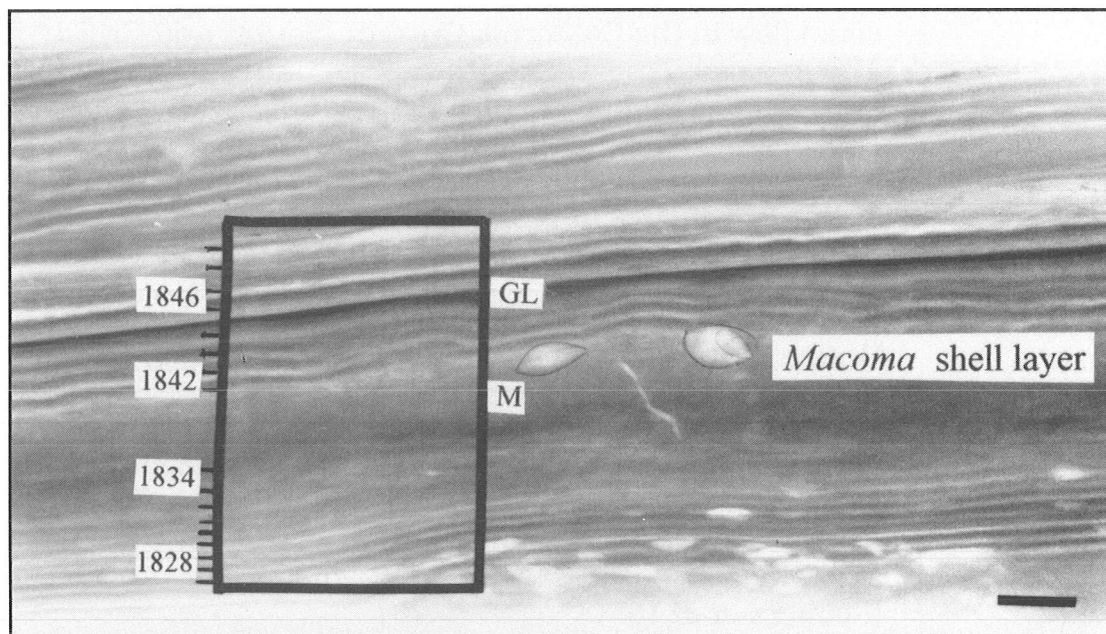


Figure 1. Contact Print of X-Radiograph of the Area Across the *Macoma* Shell Layer, AD 1825-1849, Showing the Sector Used for Preparation of Thin Sections.

A few dates are added as guidelines.

M = *Macoma* shell layer; GL = gray layer of 1845. Scale at bottom right is 1 cm.

Thin sections were first examined with light microscopy with bright field illumination. For electron microscopy analysis, they were mounted on conductive stubs and carbon coated in vacuum. We used a Cambridge 360 electron microscope equipped with an X-ray detector and associated energy-dispersive analytical system (EDS) for chemical analysis of the composition of selected samples.

Each thin section encompasses about 20 to 25 years of record (Figure 2). The thin sections are easily and unambiguously correlated stratigraphically with our existing sediment X-radiography varve record (continuous from about AD 900 to 1988).

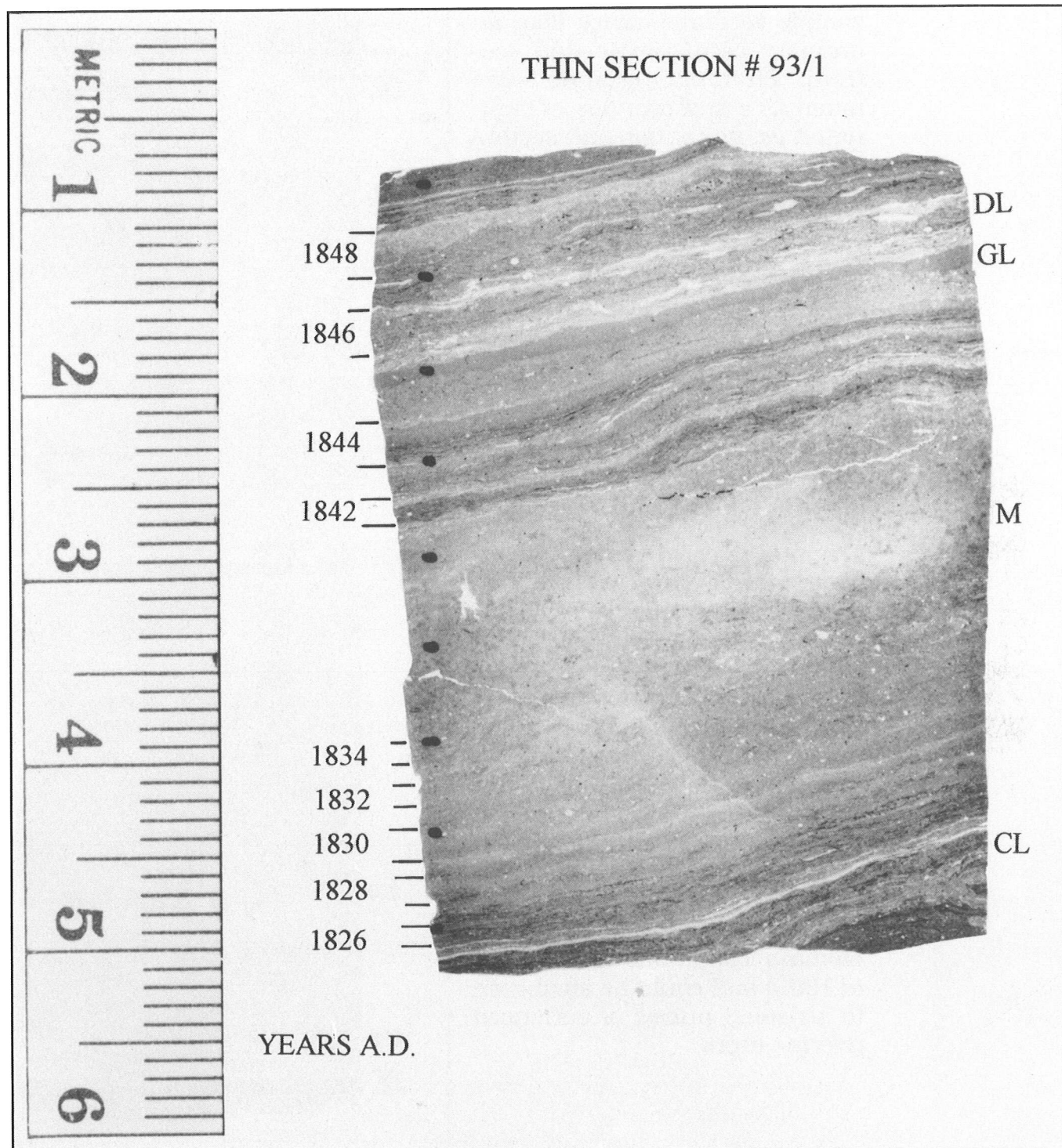


Figure 2. Photograph of Thin Section #93/1.

Varve chronology is marked on left, AD 1825-1849.

Layers: CL = *Chaetoceros*, DL = diatom-rich (abundant *Coscinodiscus*), GL = gray, M = *Macoma*; details of CL and GL are shown in Figures 4 and 5.

Scale in centimeters.

## Results and Discussion

Observation of thin sections with light microscopy provided for sample reconnaissance (like an ordinary petrographic thin section). Photomicrographs were taken as a first overview of laminated *vs.* non-laminated sectors within the selected interval to study (Figure 3).

High-resolution analysis of laminae was achieved with an electron microscope in the back-scattered electron mode (Kemp 1990; Grimm 1992a). Grain types in this mode can be differentiated by their morphology and brightness characteristics (Pye and Krinsley 1984; Krinsley and Manley 1989).

The images permit detailed compositional assessment of discrete laminae. Intra-annual/intra-seasonal events can be evaluated, and the nature and origins of the laminae can be determined. For example, laminations rich in diatom spores of the genus *Chaetoceros* are produced by spring blooms. Fine-grained laminae (clay-rich) that contain sparse biogenic grains alternate with biosiliceous-rich ones. The former emerge from winter, low-biomass conditions (Reimers *et al* 1990) and could be attributed to seasonal pulses of enhanced riverine input.

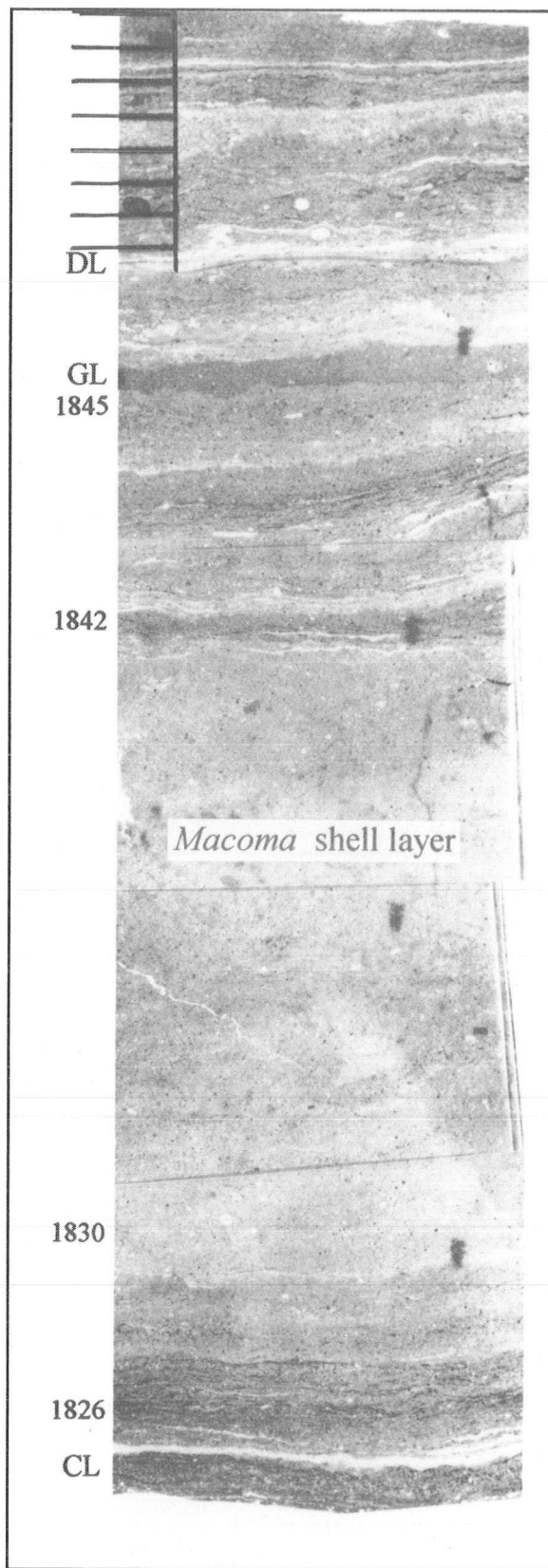


Figure 3. Photomicrograph Composite of the Left Half of Thin Section Shown in Figure 2 Viewed with Bright Field Illumination.

A few dates are added as guidelines.

Abbreviations as in Figure 2.

Scale in upper left corner: the space between tickmarks is 1 mm.

Figure 4 shows a sub-millimeter (typically 100 to 200 micrometers thick) lamination composed of *Chaetoceros* resting spores, mainly *C. debilis*. *Chaetoceros* resting spore laminae are a distinctive lamination type. We interpret them as a single episode of mass flux at the termination of a local phytoplankton bloom. Diatom resting spore flux events are common at the end of an upwelling pulse, when standing stocks are high and availability of dissolved limiting nutrients is low (Smetacek 1985). Spore formation and consequent mass sinking is regarded as an optimal reproductive strategy favoring survival of phytoplankton populations (Smetacek 1985; Garrison 1981; Pitcher 1990).

In addition to the rhythmic alternations of clay-rich and microfossil-rich laminae, discrete laminations of gray silty clay to clayey silt named "gray layers" because of their color (Munsell chart 5Y 5/1), are scattered throughout the laminated sections in the Santa Barbara Basin. They range from millimeters to decimeters in thickness, typically between 1 millimeter and 5 centimeters. Gray layers may result from rapid redeposition of sediment from the upper slope triggered by factors internal to the fan system or to its riverine sources (Thornton 1986). They can be considered instantaneous depositional events whose frequency and local thickness are chiefly controlled by internal mechanisms, with climate playing only a minimal role. Identification of thin, "varve-like" gray layers is necessary to avoid erroneous varve-counts. A 1-mm-thick gray layer was recognized within the 1845 varve; BSEM photographs are shown in Figures 5 and 6. X-ray microanalysis showed richness in aluminum (Figure 7) in addition to the very strong peak in Si, which is a common feature of every lamina (Figure 8).

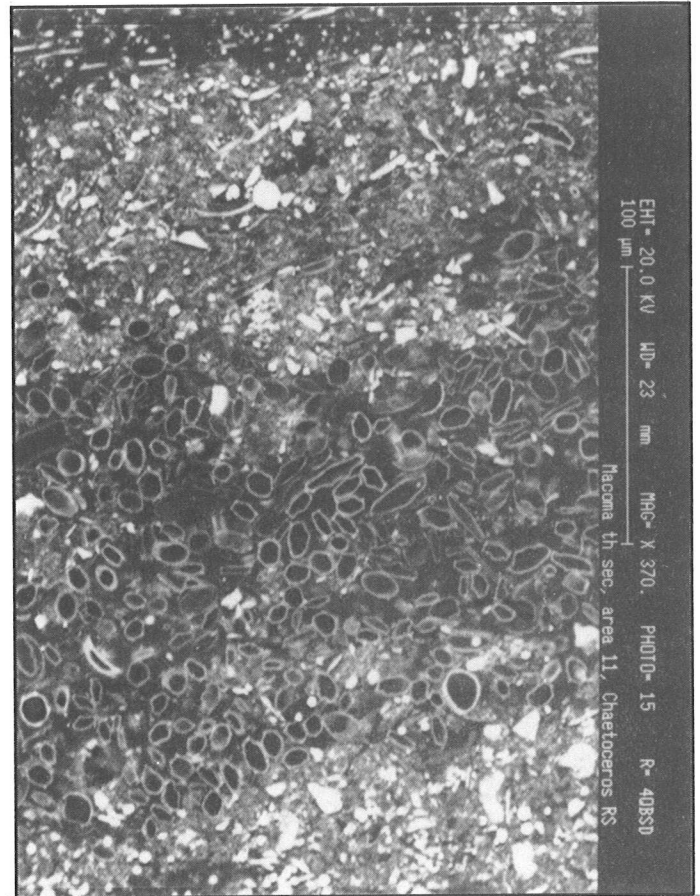


Figure 4. Back-Scattered Electron Image of a Polished Section of Epoxy-Embedded Sediment Showing a Distinct Microlamina Composed of *Chaetoceros* Resting Spores. The individual spores are between 8 and 25  $\mu\text{m}$  in diameter. Scale is 100  $\mu\text{m}$  (vertical bar on right side of picture).

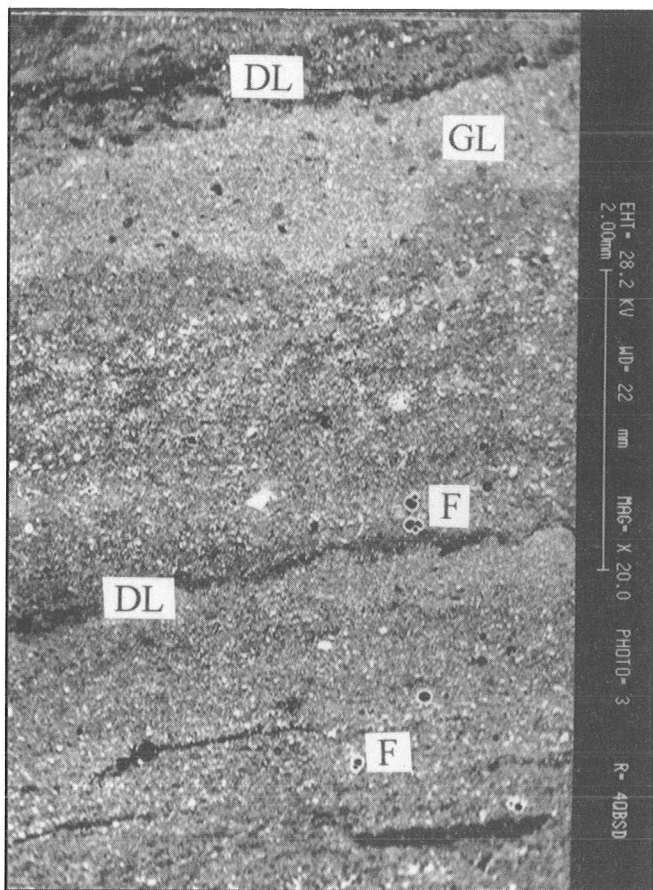


Figure 5. Back-Scattered Electron Image of a Polished Section of Epoxy-Embedded Sediment Showing Fine Detail of Laminations Defined by Differences in Composition.

The impregnating resin shows up black. The pale layer at top is a gray layer (GL) about 1 mm thick. The darkest laminations over the gray layer and at about 2 mm below it are diatom-rich, with *Chaetoceros* and *Coscinodiscus* representatives (DL). The medium dark laminations beneath the gray layer include a mixture of diatoms, coccoliths, silicoflagellates, radiolaria and foraminifers. The small black objects with a white outline are planktonic and benthic foraminifers (F).

Scale is 2 mm (vertical bar on right side of picture).

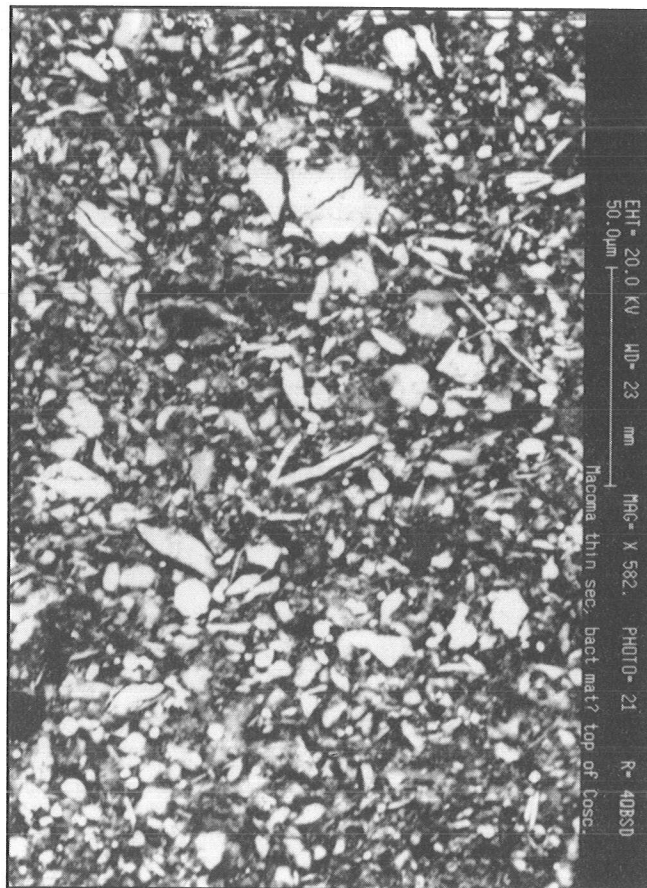


Figure 6. Detail of Gray Layer Showing the Fine-Grained Mineral Composition. Note the absence of microorganisms.

Scale is 50  $\mu\text{m}$  (vertical bar on right side of picture).

## Conclusion

Visual analysis of epoxy-impregnated and highly-polished samples is a fairly new methodological approach for hemipelagic sediments (Kemp 1990; Grimm 1992a, b; Kemp and Baldauf 1993). Applying this methodology to 19th century Santa Barbara Basin laminated sediments permitted detailed compositional assessment of individual lamina to deduce the mechanisms of its formation. It also permitted greatly improved accuracy of dating of 19th century varves, to within 0.5 year. This approach is significantly faster and offers higher resolution than techniques involving wet chemistry and handling of manually-sectioned sediment intervals that have provided us with our 600-year "background record" of previous investigations. Both approaches, used together, will permit attainment of seasonal resolution time series on a level of detail never attempted before and will provide crucial evidence of intra-annual and inter-annual sedimentation fluctuations in the Santa Barbara Basin.

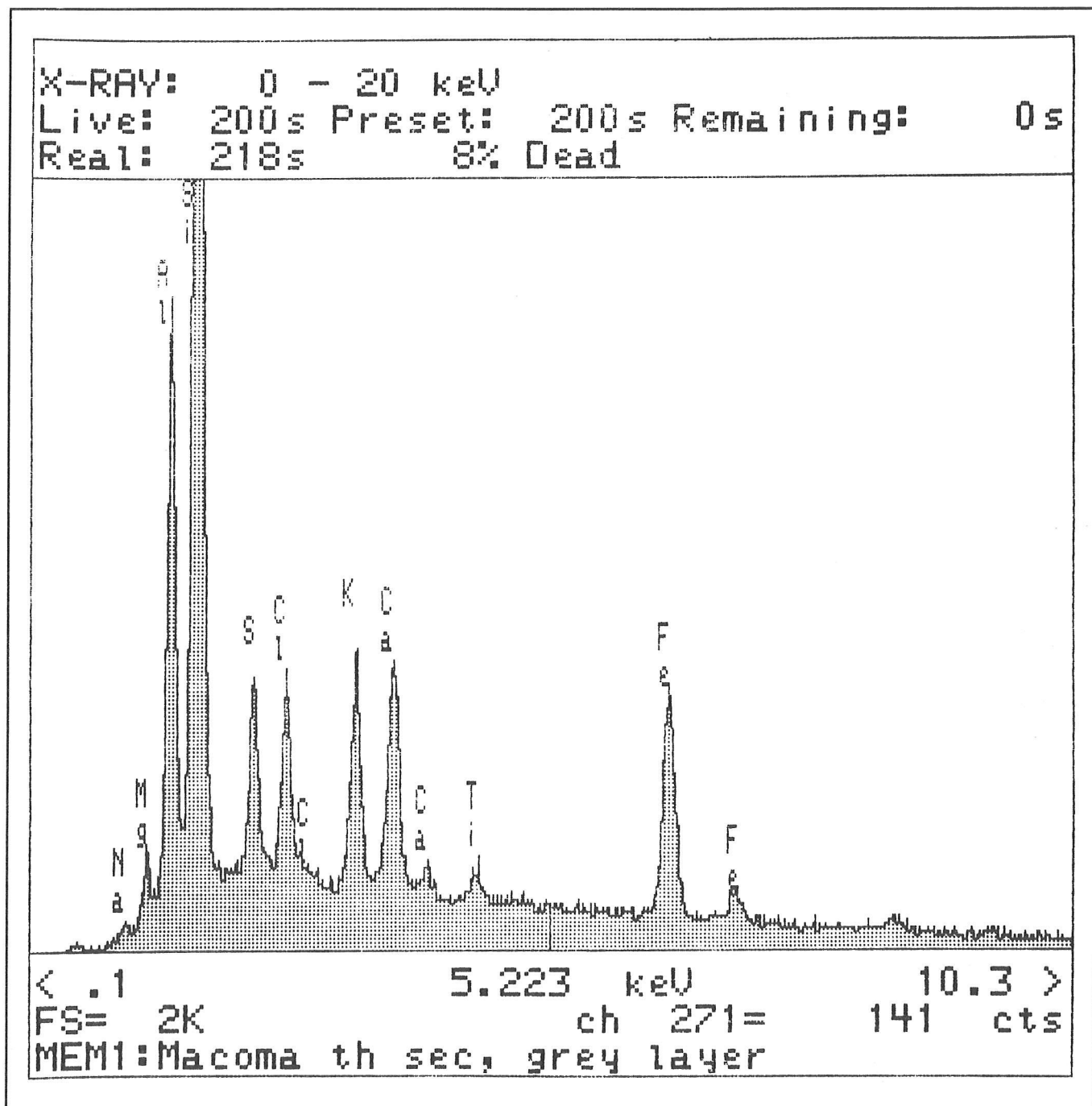


Figure 7. Example of X-Ray Spectra for the 1845 Gray Layer.

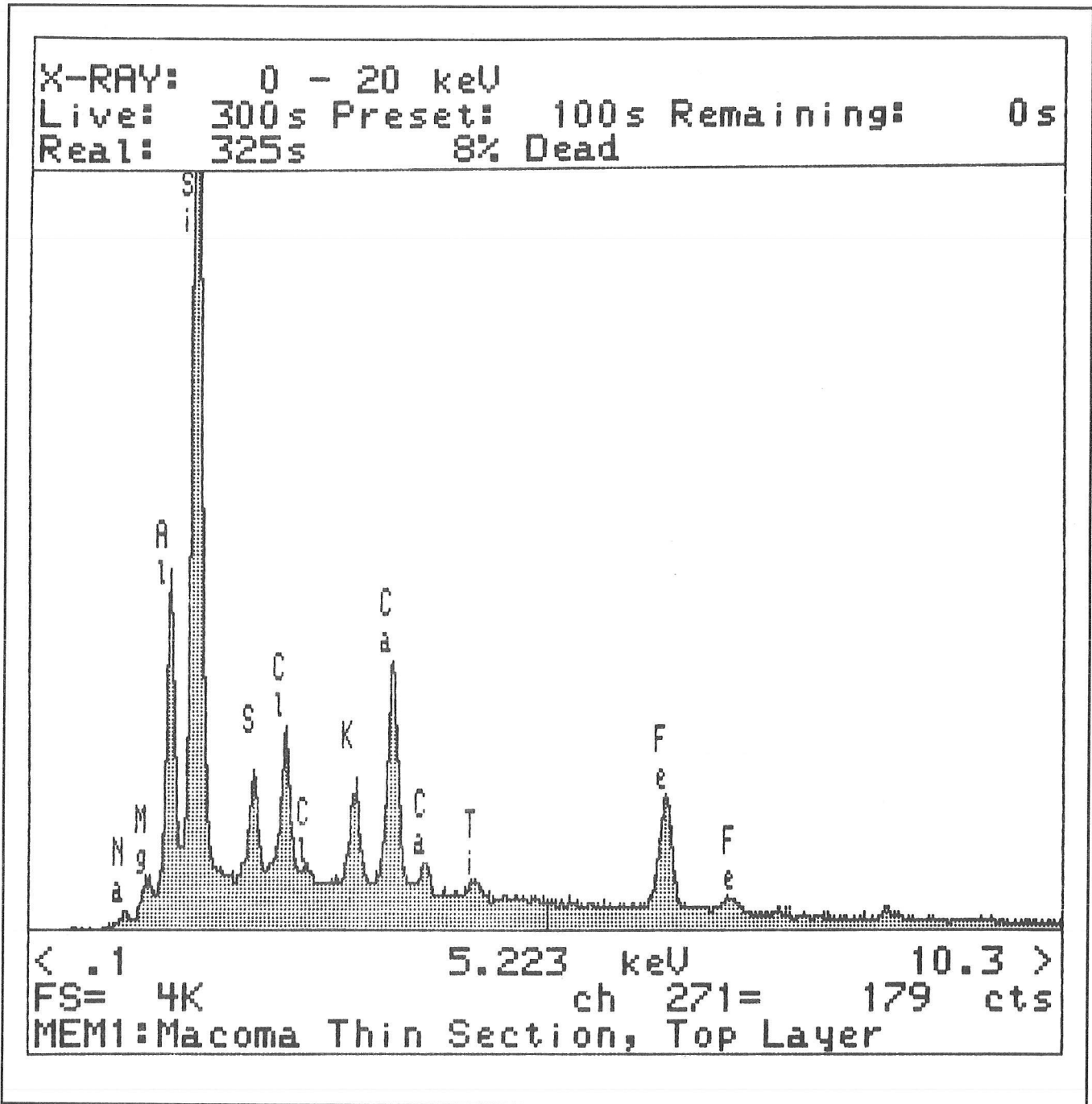


Figure 8. Example of X-Ray Spectra for the Light Lamina of the Year 1848.

## Acknowledgments

We thank Richard Myers of Scripps Institution of Oceanography for preparation of thin sections and Charles Graham at the Scripps Scanning Electron Microscope Facility for technical assistance. Discussions with Kurt Grimm (UBC) and Alan Kemp (University of Southampton) are greatly appreciated. This research was supported in part by National Oceanographic and Atmospheric Administration grants NA16RC0083-01 and NA27GPO455.

## References

- Fisher, CG. 1990. *Bibliography and Inventory of Holocene Varved and Laminated Marine Sediments*. NOAA Paleoclimate Publications Series, Report 1, pp.1-107.
- Garrison, DL. 1981. Monterey Bay Phytoplankton. II. Resting Spore Cycles in Coastal Diatom Populations. *Journal of Plankton Research*. 3:137-156.
- Grimm, KA. 1992a. Preparation of Weakly Consolidated, Laminated Hemipelagic Sediment for High-Resolution Visual Microanalysis: An Analytical Method. Pages 57-62 in *Proceedings Ocean Drilling Program, Scientific Results 127/128*. KA Pisciotto, JC Ingle Jr, MT von Breyman, J Barron, *et al*, editors.
- . 1992b. High-Resolution Imaging of Laminated Biosiliceous Sediments and Their Paleooceanographic Significance (Quaternary, Site 798, Oki Ridge, Japan Sea). Pages 547-557 in *Proceedings Ocean Drilling Program, Scientific Results 127/128*. KA Pisciotto, JC Ingle Jr, MT von Breyman, J Barron, *et al*, editors.
- Kemp, AES. 1990. Sedimentary Fabrics and Variation in Lamination Style in Peru Continental Margin Upwelling Sediments. Pages 43-58 in *Proceedings Ocean Drilling Program, Scientific Results 112*. E Suess, R von Huene, *et al*, editors.
- Kemp, AES, and JG Baldauf. 1993. Vast Neogene Laminated Diatom Mat Deposits from the Eastern Equatorial Pacific Ocean. *Nature*. 362:141-143.
- Krinsley, DH, and CR Manley. 1989. Backscattered Electron Microscopy as an Advanced Technique in Petrography. *Journal of Geological Education*. 37:202-209.
- Lange, CB, A Schimmelmann, MK Yasuda, WH Berger. In press. Paleoclimatic Significance of Marine Varves Off Southern California. In *Southern California Climate: Trends and Extremes of the Past 2000 Years*. P Wigand and M Rose, editors. Desert Research Institute, Reno, Nevada.
- Namias, J. 1975. Short Period Climatic Variations. Pages 1-905 in *Collected Works of J. Namias 1934 through 1974*. University of California, San Diego, Graphics & Reproduction Services.
- Pitcher, GC. 1990. Phytoplankton Seed Populations of the Cape Peninsula Upwelling Plume, with Particular Reference to Resting Spores of *Chaetoceros* (Bacillariophyceae) and Their Role in Seeding Upwelling Waters. *Estuarine, Coastal and Shelf Science*. 31:283-301.
- Pye, K, and DH Krinsley. 1984. Petrographic Examination of Sedimentary Rocks in the SEM Using Backscattered Electron Detectors. *Journal of Sedimentary Petrology*. 54:877-888.
- Reimers, CE, CB Lange, M Tabak, JM Bernhard. 1990. Seasonal Spillover and Varve Formation in the Santa Barbara Basin, California. *Limnology and Oceanography*. 35:1577-1585.
- Schimmelmann, A, CB Lange, WH Berger, A Simon, SK Burke, RB Dunbar. 1992. Extreme Climatic Conditions Recorded in Santa Barbara Basin Laminated Sediments: The 1835-1840 *Macoma* Event. *Marine Geology*. 106:279-299.

- Smetacek, VS. 1985. Role of Sinking in Diatom Life-History Cycles: Ecological, Evolutionary and Geological Significance. *Marine Biology*. 84:239-251.
- Soutar, A, and PA Crill. 1977. Sedimentation and Climatic Patterns in the Santa Barbara Basin During the 19th and 20th Centuries. *Geological Society of America Bulletin*. 88:1161-1172.
- Spurr, AR. 1969. A Low-Viscosity Epoxy-Resin Embedding Medium for Electron Microscopy. *Journal of Ultrastructure Research*. 26:31-43.
- Thornton, SE. 1986. Origin and Mass Flow Sedimentary Structures in Hemipelagic Basin Sediments: Santa Barbara Basin, California Borderland. *Geo-Marine Letters*. 6:15-19.

# Near and Distant Connection of Atmospheric Systems to Ocean Temperature Change in the Coastal California Current Region

Jerrold G. Norton, Daniel R. Cayan, and Douglas R. McLain

In studying hydrosphere, atmosphere, and biosphere interactions, it is useful to focus on specific subsystem processes and energy exchanges (forcing). Since subsystem scales range over ten orders of magnitude, it may be difficult to focus research on scales that will yield useful results in terms of establishing casual and predictive connections between more easily and less easily observed subsystems. In an effort to find pertinent scales, we have begun empirical investigations into relationships between atmospheric, oceanic, and biological systems having spatial scales exceeding  $10^3$  kilometers and temporal scales of six months or more. Reasons for this scale selection include:

- Significant changes at these scales (interannual events) can be detected and analyzed using established and actively updated data sets.
- Combining observations for interannual analysis allows sufficient numbers of observations to be grouped so that investigation results have reasonable statistical reliability.

Previous studies established connections between interannual fall-winter temperature changes in the coastal California Current region (Figure 1) and two widely separated locales of atmospheric forcing: remote atmospheric forcing from the Equatorial Pacific, and regional atmospheric forcing from the Northeastern Pacific (Norton and McLain 1993). Previous studies are reviewed and extended from the fall-winter period to a complete annual analysis. In addition, 700mb height anomaly fields are used to show relationships between atmospheric forcing over the North Pacific and ocean temperature change in the study region.

## Data Series and Fields

A brief outline of data series development follows. Norton and McLain (1993) have previously provided a detailed description. For the ocean temperature series,  $1.9 \times 10^4$  ocean temperature profiles were extracted from the U.S. Navy's Master Oceanographic Observations Data Set (McLain *et al* 1985) for the study region and sorted into six areas (Figure 1). Monthly mean anomaly values for 34 years (1953-1986) were computed at five depths from the profile information and divided by the standard deviation of the monthly means at each depth and for each of

In: KT Redmond and VL Tharp, Editors. 1994. Proceedings of the Tenth Annual Pacific Climate (PACCLIM) Workshop, April 4-7, 1993. California Department of Water Resources, Interagency Ecological Studies Program, Technical Report 36.

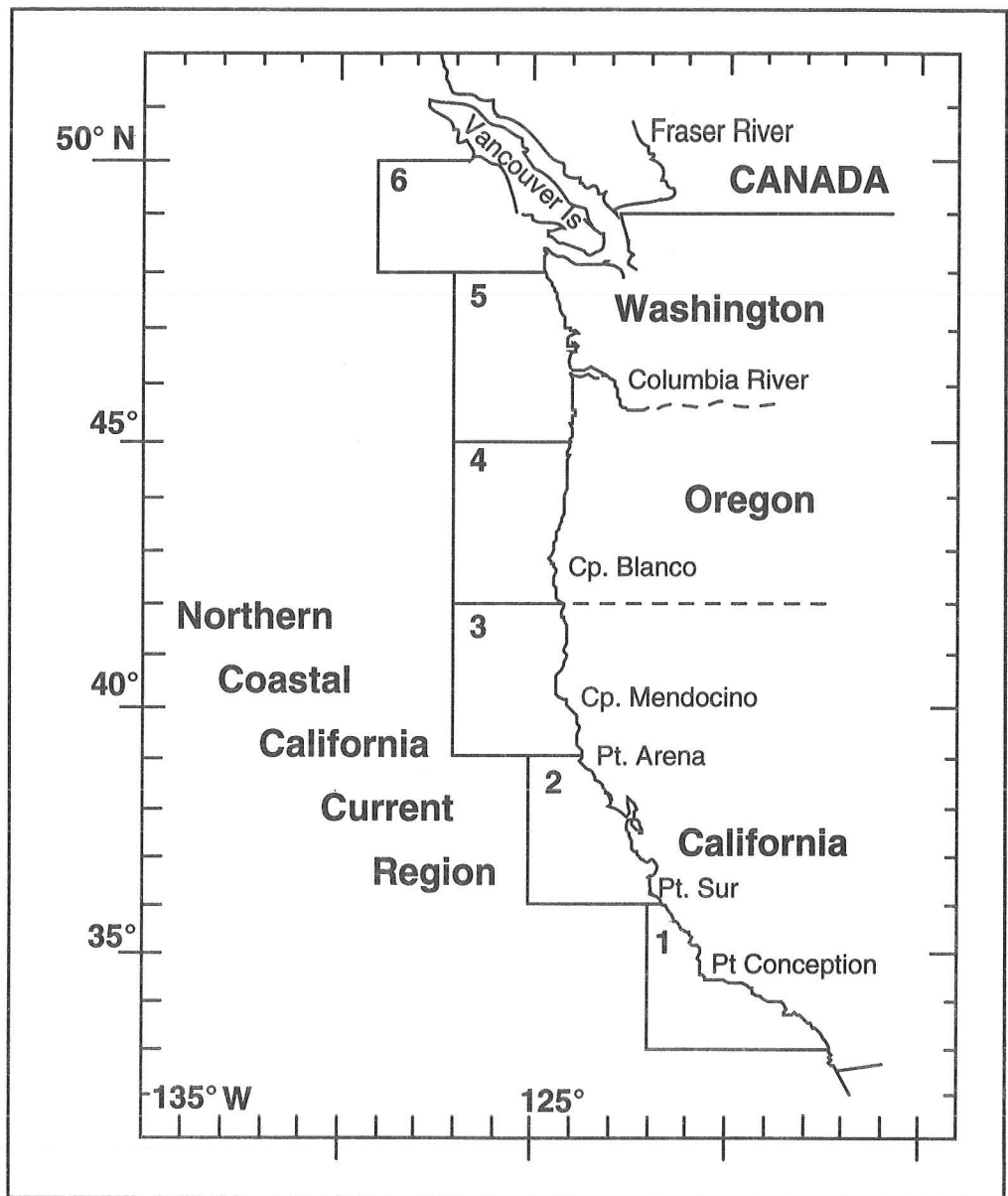


Figure 1. The northern coastal California Current region used in this study is a composite of the six subareas shown. Standardized monthly temperature anomaly values were obtained for each of the six subareas, then combined to give overall values representative of the entire area.

the six areas. This standardization allows intercomparison of depths and equal weighting between areas. Average unit magnitude in standardized anomaly is about 1.0°C above 50 meters, 0.6° at 100 meters, and 0.5°C below 150 meters.

For each depth, standardized anomaly values for the six subareas were averaged to give monthly anomaly values representative of the entire northern coastal California Current region. These monthly anomalies were then time-averaged over six months at each depth to give a single standardized anomaly value representing the entire 6-subarea region for fall-winter (September-February) and spring/summer (March-August).

Two monthly mean series of atmospheric sea level pressure (SLP) representing remote (Indonesian Low in the Equatorial Pacific at 12.4°S×130.9°W near Darwin, Australia) and regional (Aleutian Low in the North Pacific at 45°N×165°W) were used as forcing indicators. These single-point series were smoothed with a 6-month running mean as a preliminary processing step.

Quarterly (3-month average) 700mb height anomaly fields were used to study spatial variation of correlation coefficients ( $r$ ) over the Pacific. The height anomalies were computed for the extra-tropical Northern Hemisphere as monthly means for 2°×2° areas, then averaged by month to give spring, summer, fall, and winter fields.

Interannual change values of ocean temperature, remote atmospheric forcing, and regional atmospheric forcing are used in all the following single atmospheric point analyses. For the current year, the interannual change value is found by subtracting the parameter value for the previous year ( $yr-1$ ); *eg*, for a particular seasonal value of ocean temperature change,  $D_{z,yr}$ ,

$$D_{z,yr} = A_{z,yr} - A_{z,yr-1},$$

where  $A$  is the combined standardized anomaly value for a given year,  $yr$ , at depth,  $z$ . Interannual change values are also referred to below as "interannual differences".

Vertical Empirical Orthogonal Functions (EOFs) were derived from the 4×33 matrix having 0, 100, 200, and 300 meters as rows and 33 years of interannual differences at these depths as columns. Series of time varying coefficients (DEOFs) were computed from the input matrix and EOFs. Studies outlined in the next section deal only with EOFs for fall-winter.

In some years an atmospheric teleconnection may link changes in Equatorial Pacific sea surface temperature to SLP over the North Pacific (Rasmusson and Wallace 1983). This physical relationship causes North Pacific and Equatorial Pacific interannual difference series to have common variability, especially in winter. Correlation between the remote and regional atmospheric indicator series is easily demonstrated (Wallace and Gutzler 1981; McLain and Norton 1993). However, the present objective is to show discrete effects of North Pacific and Equatorial Pacific atmospheric forcing in regional ocean temperature change. To correct for the atmospheric teleconnection, each atmospheric series was linearly regressed on the other, and the residual series was used in place of the original series. These residual index series were used in Table 1.

Correlation of interannual temperature differences at 0m and 200m and 1st and 2nd EOFs to Atmospheric Forcing Indices.				
Atm. Index	Correlation (r) and atm. leads/lags (+/-) in months			
	0m	200m	EOF1	EOF2
Eq. Pac. (12.4°S x 130.9°E)	.65, +6	.72, +6 .71, n.r.	.74, +5	.33, +7 .34, -5
No. Pac. (45°N x 165°W)	-.61, n.r.	-.20, n.r.	-.31, n.r.	-.66, n.r.
n.r. - lead/lag not resolved by present technique				

Table 1. Correlation between atmospheric forcing indices and interannual ocean temperature change values for the fall-winter period. Values are correlation coefficients (r). Coefficients in the top row are positive, showing positive SLP anomaly at 12.4°S×130.9°E (Indonesian Low, remote forcing) to be correlated with positive temperature anomaly in the ocean study area. The bottom row has negative coefficients showing a reverse relationship between the ocean study area and SLP anomalies at 45°N×165°W (Aleutian Low, local forcing). For  $|r| \geq 0.4$ , significance levels are greater than 0.05 (Norton and McLain 1993).

## Previous Studies

This section summarizes previous work by Norton and McLain (1993).

During fall-winter, remote forcing from the Equatorial Pacific atmosphere-ocean system and regional forcing from the North Pacific lead to interannual ocean temperature change along the west coast of the United States (Figure 1). Correlations between the subsurface temperature and the atmospheric index time series indicate that coherent ocean temperature changes extending from the surface to 300 meters depth indicate remote forcing from the equatorial atmosphere through the ocean. Correlations between time series of interannual ocean temperature change and series of equatorial interannual sea level pressure change at 12.4°S×130.9°E were as large ( $r > 0.6$ ) below 100 meters as at the surface. From 1954 through 1986, vertically coherent warming events occurred only during moderate to strong El Niño years as shown by Quinn *et al* (1987). The inference is that changes in the Equatorial Pacific atmosphere excite oceanic Kelvin waves, which travel to the eastern Pacific border and then poleward to higher latitudes where this influx of energy favors downwelling and warming. Ocean events associated with North Pacific SLP change at 45°N×165°W and direct atmospheric forcing have correlations that are greatest in the upper 50 meters. In general, changes in regional temperature below 100 meters depth are not significantly correlated with changes in North Pacific SLP indices. These results are illustrated in Table 1, which shows that correlation of temperature change in the study area with the equatorial atmosphere is greater at 200 meters than at the surface. At 200 meters and below, an additional oceanic response

appears in phase with remote forcing. Correlation with the North Pacific forcing is clearly greater at 0 meters than at 200 meters (Table 1).

The first two vertical EOFs derived from the 4x33 matrix of interannual ocean temperature change in the upper 300 meters accounted for more than 92 percent of the variance. Column three of Table 1 shows that the first EOF (EOF1), which has nearly uniform loading over depth, is most closely correlated with Equatorial Pacific forcing. Column four shows that the second EOF (EOF2), which has greatest loading at 0 meters and sign reversal below 100 meters, is more closely correlated to regional atmospheric forcing.

The lag shown in the top row of Table 1 provides an additional distinction between regional and remote forcing. Positive lags in the top row suggest the signal related to equatorial forcing takes up to six months to reach the study region, which is consistent with the "remote" terminology and with the empirical studies of Enfield and Allen (1980) and Chelton and Davis (1982). The correlation of remote forcing at shorter lags (not resolved, or n.r., in Table 1) is consistent with observational and model studies of McCreary (1976), Huyer and Smith (1985), and Shriver *et al* (1991).

This study implied that interannual warming off the West Coast during fall-winter has two distinguishable geographical origins. The vertically-coherent signals related to the equatorial atmosphere-ocean system may result from propagating complex modal structures that combine to produce signals where vertical and horizontal propagation co-occur (Romea and Allen 1983).

## Additional Results

The time variation in seasonal oceanic response modes (DEOFs) of the coastal California Current region during 1954 to 1986 are shown in Figure 2. Each year has two DEOF series values, with the spring/summer value given first. Vertical bars (DEOF1) show remote forcing response, and dots (DEOF2) show response to regional atmospheric forcing. Together, EOF1 and EOF2 account for more than 92 percent of the variance in both spring/summer and fall-winter series. Note that the relative magnitude of variance explained by EOF1 (>74%) and EOF2 (>12%) is reflected in the magnitudes of the left and right scales, respectively. Part of the unequal importance of EOF1 and EOF2 may be due to the averaging and differencing procedures, which select strongly for biennial processes that produce maxima in years following or preceding years with minima (Norton and McLain 1993). This event type is clearly seen in the DEOF1 series (*ie*, 1965-1966, 1972-1973). In general, effects of the first mode will conceal effects of the second mode at biennial scales, but when there is little ocean change forced by the first mode, the second mode becomes more important (*ie*, 1969, 1978).

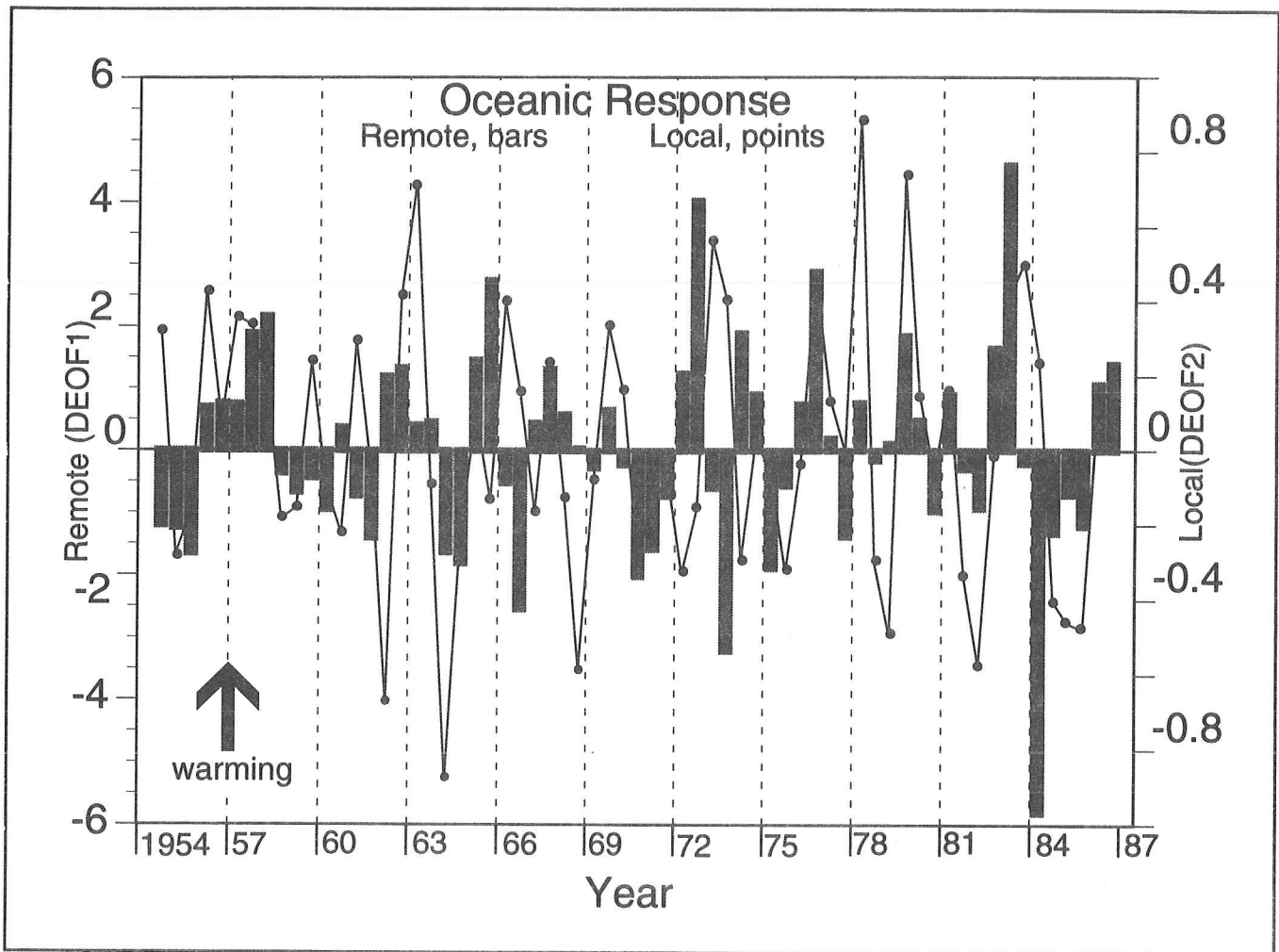


Figure 2. Northern coastal California Current response to remote (DEOF1) and local (DEOF2) atmospheric forcing from 1954 through 1986. The spring/summer value is plotted immediately to the right of the year tick at the bottom.

It is interesting to ask how well the DEOF series reflect environmental effects discussed by other researchers. Note that all moderate to strong El Niño events are represented by DEOF1 values exceeding 2.0 (1958, 1965, 1972, 1976, 1983) and that the largest warming signal in the series corresponds to the very extreme 1982-1983 event (Quinn *et al* 1987).

The most extensively documented California Current regional warming events of the series occurred in 1956-1958 and 1982-1983 (*eg*, Sette and Isaacs 1960; Wooster and Fluharty 1985). The 1956-1958 event was prolonged over three years when both EOF1 and EOF2 were in warming phase. Note that observation of anomalously warm ocean temperatures will lag the warming processes if warming begins during a cool ocean period, as in 1956 (Reid 1960). The timing of the 1982-1983 El Niño was quite different than the 1956-1958 event in that oceanic warming was intense for one year, followed by a cooling phase of similar magnitude and duration (Figure 2).

Selected references to California Current warm and cool events of inter-annual scale are shown in Table 2. Note that this report shows warming ( $\Delta W$ ) or cooling ( $\Delta C$ ) relative to the previous year. In contrast, references in Table 2 are most frequently to events that are warm or cool compared to an overall series mean. Nonetheless, the table suggests that most of the warming ( $\Delta W$ ) events identified by the DEOFs have been labeled as warm events by previous studies, and most of the cooling ( $\Delta C$ ) events have been labeled cool periods. The present material (Figure 2) may be used to compare the relative intensities of these events.

## **North Pacific Atmospheric Systems**

---

Previous work showed that large-scale temperature changes in the coastal California Current region appear related to SLP changes at  $45^{\circ}\text{N}\times 165^{\circ}\text{W}$  (Norton and McLain 1993). Oceanic changes related to this regional large-scale atmospheric forcing are represented by DEOF2 in Figure 2. Natural questions are:

- How are changes at  $45^{\circ}\text{N}\times 165^{\circ}\text{W}$  related to atmospheric changes over the entire North Pacific?
- How are coastal ocean temperature changes in the study region related to atmospheric events throughout the North Pacific?

To address these questions, the correlation between DEOF2 and the height of fall (September, October, November) 700mb atmospheric pressure surface was mapped (Figure 3).

From Figure 3 it is evident that the time variation in DEOF2 is related to large-scale atmospheric conditions that extend over the entire North Pacific and North American continent. The area of over  $5\times 10^7\text{ km}^2$  has three primary regions of correlation, arranged in a pattern arcing from southwest to northeast. Regions of alternating sign may represent atmospheric Rossby waves associated with winter cyclogenesis over the North Pacific, temperature change in the coastal study region, and other phenomena throughout the global atmosphere-hydrosphere system (Rasmusson and Wallace 1983).

In Figure 3, the area of negative correlation with maximum near  $50^{\circ}\text{N}\times 160^{\circ}\text{W}$  represents intensification or weakening of the Aleutian Low subsystem. Positive (negative) sea surface temperatures along the West Coast study area are correlated with negative (positive) height anomalies in the Aleutian Low. The pattern shown in Figure 3 is consistent with the relationship found for the single point ( $45^{\circ}\text{N}\times 165^{\circ}\text{W}$ ) used by Norton and McLain (1993), suggesting that the single point used in previous studies was adequate in representing Aleutian Low variation. Correlation of winter 700mb height with fall-winter DEOF2, spring 700mb height with spring/summer DEOF2, and summer 700mb height with spring/summer DEOF2 gave similar results, with the major differences in the

Warming and Cooling years in the California Current Region					
This Study Oceanic Response			Previous Studies		
Year	DEOF1	DEOF2	Source	Forcing	Ocean Observation
1955	ΔC	ΔC	Reid 1960	A	C
1956 - -57-58	ΔW	ΔW	Namias 1959, Stewart 1960, Reid 1960	A	ΔW, W
1962-63	-	ΔW	Namias 1963	A	W
1965	ΔW	-	Enfield & Allen 1980 Wyrтки 1975	O, A	W
1969	-	ΔW	Clark 1972	A	ΔW, W
1970-71	ΔC	ΔC	Norton et al. 1985 Emery & Hamilton 1985	O, A	C
1972	ΔW	-	Enfield & Allen 1980	O, A	W
1973	ΔC	ΔW	Emery & Hamilton 1985	A	C
1974	ΔW	-	Wyrтки 1977	O	-
1976	ΔW	ΔW	Norton et al. 1985	O, A	W
1977-78	-	ΔW	Chelton 1981	A	W
1979	-	ΔW	Norton et al. 1985	A	W
1983	ΔW	ΔW	Huyer & Smith 1985 Rienecker & Mooers 1986 Simpson 1992	O, A	ΔW, W
1985	ΔC	ΔC	Anon. 1986	-	ΔC, C
1986	ΔW	ΔW	Kousky 1987, Anon. 1987	O, A	W

ΔW - warming  
ΔC - cooling

A - atmospheric forcing  
O - oceanic forcing

C - ocean negative anomaly  
W - ocean warm anomaly

Table 2. Comparison of warming and cooling events and selected references, which apparently refer to the same events. DEOF1 and DEOF2 (columns 2 and 3) are series of time varying coefficients. Forcing designations in column 5 may be implied by the references and not specifically mentioned.

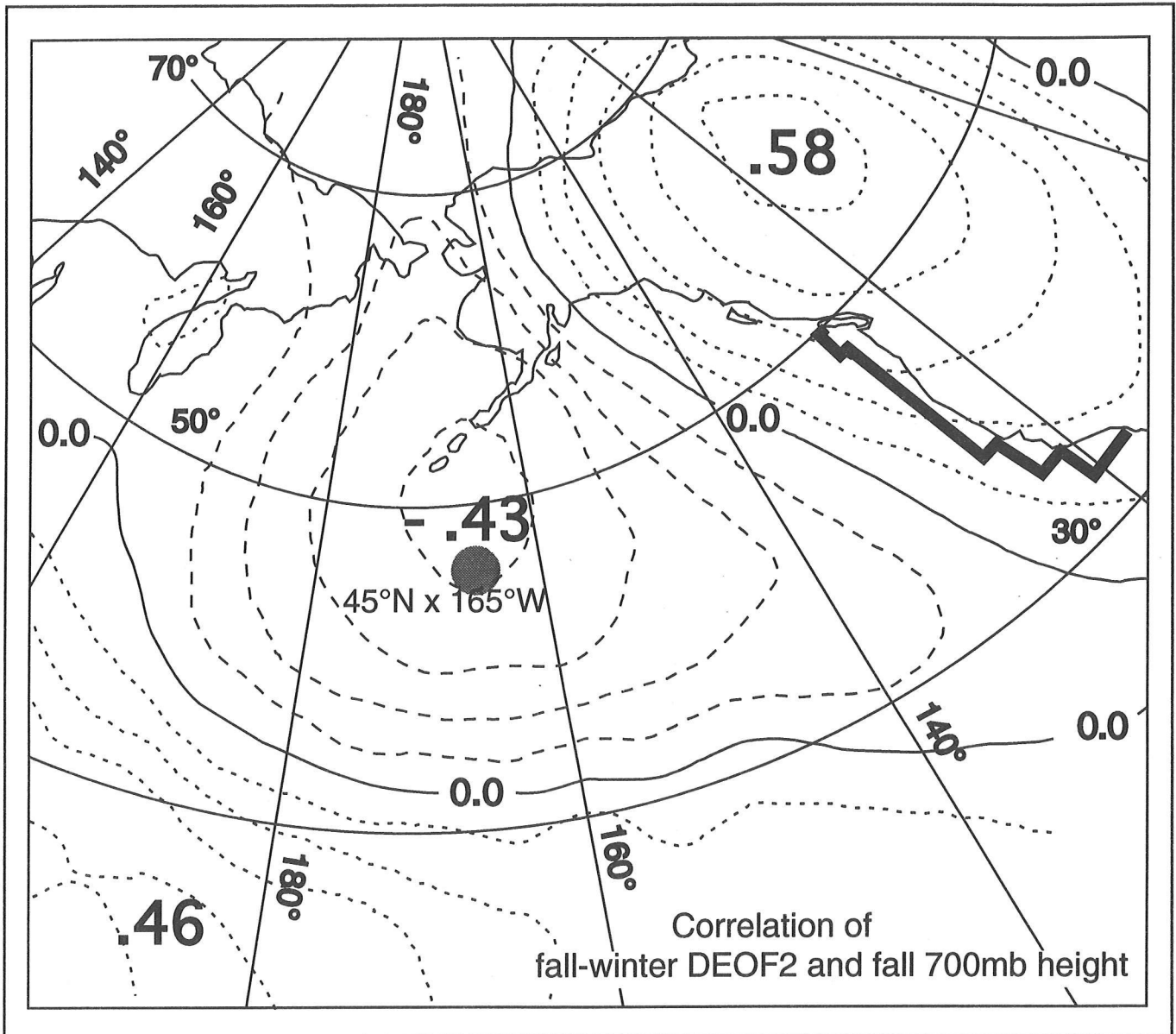


Figure 3. Correlation of the time-varying coefficients for the second EOF (DEOF2) for coastal ocean study area (heavy outline, right) with 700mb height field. Maximum correlations are shown in the largest bold numerals. Dotted and dashed contours show areas of positive and negative correlation, respectively.

magnitude of correlation maxima and minima. So, it appears that the spatial relationships shown in Figure 3 are consistent throughout the annual cycle. However, it is clear that other processes and forcing patterns are involved in changing the ocean temperature in the coastal study region, since upper ocean temperature change associated with EOF2 accounts for 18 percent of the total temperature change variance during spring/summer and 13 percent in fall-winter.

Correlation fields shown in Figure 3 indicate that anomalous west-to-east pressure gradients across the study area produce anomalous temperatures in the ocean surface layers. This is consistent with many previous studies (Table 2). Northward wind associated with such a gradient will lead to Ekman transport of generally warmer offshore water toward shore, creating an oceanic geopotential gradient favoring northward flow along the coast, which may lead to additional warming. Conversely, if the anomalous circulation pattern is reversed, southward wind would be more important in creating a cooler coastal ocean due to upwelling and increased influx of subarctic water from the north. However, wind-forced advection is not the only process creating regionally forced temperature anomalies in the coastal region. Anomalous strengthened (weakened) cyclonic atmospheric circulation may bring warmer (cooler), more (less) humid air into contact with the coastal ocean, which will lead to warming (cooling) in the ocean surface layers. Wind-forced mixing that penetrates the pycnocline leads to warming at depth and surface cooling. Curl effects associated with anomalous Aleutian Low development may be as important as Ekman transport in creating temperature anomalies in the coastal zone (Haney 1980, 1985; Rienecker and Ehert 1988)

In Figure 3, areas of positive correlation are found west of the date line south of 30°N and over the North American continent. These represent anti-nodes of the Aleutian Low, and overall this pattern strongly resembles the Pacific/North American (PNA) teleconnection (*eg*, Barnston and Livezey 1987). The greater correlation in the subtropical high and western Canada, as compared to the Aleutian Low, may be due to temporal mismatch in ocean DEOF2 (interannual difference) values and the atmospheric fields (single season).

For the single-point atmospheric indicator at 45°N×165°W, the association between coastal ocean temperature changes and the interannual difference of 6-month averages of sea level pressure corrected for the tropical to subarctic teleconnection had correlation coefficients exceeding 0.6 (Norton and McLain 1993). It should be noted that differencing reduces series autocorrelation so that the correlation coefficient values greater than 0.6 represent correlation of year-to-year events rather than longer climatic trends that tend to reduce degrees of freedom. Additional work will focus on comparing the ocean DEOFs with atmospheric fields that have been processed by procedures more similar to those used for the one-point indices.

## **Biological Interactions**

---

Uda (1962) noted that cyclic abundance of similar commercial fish species on either side of the temperate and subarctic Pacific Ocean correspond to variations in intensity of recurring atmospheric patterns. He also found that boom and bust of commercial fisheries had reverse phasing on either side of the North Pacific. If the area of negative correlation in Figure 3 is taken as approximating the mean dimensions of the Aleutian Low's cyclonic circulation, it can be seen that an increase in the Low's intensity and extent would bring cooling conditions to the western subarctic Pacific. These same atmospheric conditions would bring warming conditions to the eastern subarctic Pacific and the study area (Namias 1959). If the processes that change ocean temperature are associated with species reproductive success in a similar way on either side of the Pacific, then a weakening of the Low would contribute to the success of warm water species in the western Pacific as cooling conditions associated with southward winds inhibited the success of similar species in the eastern Pacific. If the second temperature change mode (DEOF2) gives a time series of atmospherically forced oceanic variation at the eastern Pacific margin, then it might be expected from the work of Namias (1959) and Uda (1962) that a similar atmospherically forced mode would be found in the western Pacific and that these modes might be important in forcing environmental conditions that allow the biological effects described by Uda (1962).

## **Conclusion**

---

Many studies (Table 2) have attempted to explain anomalous warming and cooling events along the West Coast of North America by considering either regional wind forcing or remote forcing through the ocean. The present work suggests that attempting to base interpretations on one forcing mechanism will fail because regional and remote ocean-atmosphere forces are both important and have characteristic oceanic responses.

Because of the tropical to mid-latitude atmospheric teleconnection (Wallace and Gutzler 1981; Rasmusson and Wallace 1983), negative or positive excursions by DEOF1 and DEOF2 frequently occur together (Figure 2). Note that the tropical El Niño teleconnection pattern in the North Pacific circulation (Rasmusson and Wallace 1983; Branston and Livezey 1987) is not unlike the correlation pattern with EOF2 shown in Figure 3. The existence of an intermittent atmospheric teleconnection makes it possible for statistically reasonable cases to be made for either forcing mechanism alone. However, considering only one forcing mode limits the possibility of a mechanistic description of warming and cooling events in the coastal California Current region. This, in turn, severely limits possibilities for establishing descriptions of biological and physical events with the precision needed to allow conservationally adequate exploitation of the marine environment.

## References

---

- Anon. 1986. *1983 Physical, chemical and biological data*. University of California. Scripps Institution of Oceanography Reference 86-3, 96 pp.
- \_\_\_\_\_. 1987. *Surface water temperatures at shore stations, United States West Coast, 1986*. University of California. Scripps Institution of Oceanography Reference 87-11, 39 pp.
- Branston, AG, and RE Livezey. 1987. Classification, Seasonality and Persistence of Low-Frequency Atmospheric Circulation Patterns. *Mon. Wea. Rev.* 115(1083-1126).
- Chelton, DB. 1981. *Interannual variability of the California current — physical factors*. Calif. Coop. Oceanic Fish. Invest. Rep. 22, pp. 34-48.
- Chelton, DB, and RE Davis. 1982. Monthly mean sea-level variability along the west coast of North America. *J. Phys. Oceanogr.* 12(757-784).
- Clark, NE. 1972. Specification of sea surface temperature anomaly patterns in the eastern north Pacific. *J. Phys. Oceanogr.* 2(391-404).
- Emery, WJ, and K Hamilton. 1984. Atmospheric forcing of interannual variability in the northeast Pacific Ocean. *J. Geophys. Res.* 90(857-868).
- Enfield, DB, and JS Allen. 1980. On the structure and dynamics of monthly mean sea level anomalies along the Pacific coast of North and South America. *J. Phys. Oceanogr.* 10(557-578).
- Haney, RL. 1980. A numerical case study of the development of large-scale thermal anomalies in the central north Pacific Ocean. *J. Phys. Oceanogr.* 10(541-556).
- \_\_\_\_\_. 1985. Midlatitude sea surface temperature anomalies: a numerical hindcast. *J. Phys. Oceanogr.* 15(787-799).
- Huyer, A, and RL Smith. 1985. The signature of El Niño off Oregon, 1982-1983. *J. Geophys. Res.* 90(7133-7142).
- Kousky, VE. 1987. The global climate for December 1986-February 1987: El Niño returns to the Tropical Pacific. *Mon. Wea. Rev.* 115(2822-2837).
- McCreary, JP. 1976. Eastern tropical response to changing wind systems: with application to El Niño. *J. Phys. Oceanogr.* 6(632-645).
- McLain, DR, RE Brainard, and JG Norton. 1985. Anomalous warm events in eastern boundary current systems. *Calif. Coop. Oceanic Fish. Invest. Rep.* 26(51-64).
- McGary, JW. 1960. Surface temperature anomalies in the Central North Pacific, January 1957-May 1958. *Calif. Coop. Oceanic Fish. Invest. Rep.* 7(47-51).
- Namias, J. 1959. Recent seasonal interactions between north Pacific waters and the overlying atmospheric circulation. *J. Geophys. Res.* 64(631-646).
- \_\_\_\_\_. 1963. Large-scale air-sea interactions over the north Pacific from summer 1962 through the subsequent winter. *J. Geophys. Res.* 68(6171-6186).
- Norton, JG, DR McLain, RE Brainard, DM Husby. 1985. El Niño event off Baja and Alta California and its ocean climate context. Pages 44-72 in *Niño effects in the eastern subarctic Pacific Ocean*. WS Wooster and DL Fluharty, editors. Washington Sea Grant Program, University of Washington, Seattle.
- Norton, JG, and DR McLain. 1993. Year-to-year changes of vertical temperature distribution in the California Current region: 1954 to 1986. Pages 45-54 in *Proceedings of the Ninth Annual Pacific Climate (PACLIM) Workshop*. KT Redmond and VL Tharp, Editors. California Department of Water Resources, Interagency Ecological Studies Program Technical Report 34. (A more detailed manuscript has been accepted for publication in *J. Geophys. Res.*, Oceans.

- Quinn, WH, VT Neal, SE Antunez de Mayolo. 1987. El Niño occurrences over the past four centuries. *J. Geophys. Res.* 92(14449-14461).
- Rasmusson, EM, and JM Wallace. 1983. Meteorological aspects of the El Niño/Southern Oscillation. *Science* 122(1195-1202).
- Reid, JL. 1960. Oceanography of the northeastern Pacific Ocean during the last ten years. *Calif. Coop. Oceanic Fish. Invest. Rep.* 7(77-90).
- Rienecker, MM, and CNK Mooers. 1986. The 1982-1983 El Niño signal off northern California. *J. Geophys. Res.* 91(6597-6608).
- Rienecker, MM, and LL Ehert. 1988. Wind stress curl variability over the north Pacific from the comprehensive ocean-atmosphere data set. *J. Geophys. Res.* 93(5069-5077).
- Romea, RD, and JS Allen. 1983. On vertically propagating coastal Kelvin waves at low latitudes. *J. Phys. Oceanogr.* 13(1241-1254).
- Sette, OE, and JD Isaacs, editors. 1960. The changing Pacific ocean in 1957 and 1958 (symposium). *Calif. Coop. Ocean Fish. Invest. Rep.* 7(14-217).
- Simpson, JJ. 1992. Response of the Southern California current system to the mid-latitude North Pacific coastal warming events of 1982-1983 and 1940-41. *Fisheries Oceanography* 1(57-79).
- Shriver, JF, MA Johnson, JJ O'Brien. 1991. Analysis of remotely forced oceanic Rossby waves off California. *J. Geophys. Res.* 96(749-757).
- Stewart, HB. 1960. Coastal water temperature and sea level-California to Alaska. *Calif. Coop. Oceanic Fish. Invest. Rep.* 7(97-102).
- Wallace, J, and D. Gutzler. 1981. Teleconnections in the geopotential height field during the northern hemisphere winter. *Mon. Wea. Rev.* 109(784-812).
- Uda, M. 1962. Cyclic correlated occurrence of world-wide anomalous oceanographic phenomena and fisheries condition, *J. Oceanogr. Soc. Japan.* 20th Anniv. pp. 368-375.
- Wyrtki, K. 1975. El Niño — The dynamic response of the equatorial Pacific ocean to atmospheric forcing. *J. Phys. Oceanogr.* 5(572-584).
- \_\_\_\_\_. 1977. Sea level during the 1972 El Niño, *J. Phys. Oceanogr.* 7(779-787).



# Modeling the Effect of Snow on Seasonal Runoff within the Truckee River Drainage Basin

Richard L. Orndorff and Rachael G. Craig

**ABSTRACT:** We estimate monthly runoff for a 2-dimensional solution domain containing those areas tributary to Pyramid Lake, Nevada (the Truckee River drainage basin) at a 1-kilometer grid cell spacing. Mean monthly temperature and precipitation values from a previously reported local climate model (Stamm and Craig 1992) are input to a snow model (Orndorff and Craig 1993), which calculates monthly snowfall, snowpack, and snowmelt. The parameterized runoff model computes monthly runoff at each grid point from rain and snowmelt information provided by the snow model. The runoff model assumes initial zero soil moisture at each grid point, then solves for interception, evapotranspiration, infiltration, saturated and Hortonian overland flow, baseflow, and soil moisture storage for each month in the year, iterating until steady state convergence criteria are met. Monthly runoff values from those grid cells contributing to the Truckee River are summed spatially to estimate mean monthly river flow.

To calculate the effect of snow on the hydrologic system, we perform two experiments. In the first we assume that all precipitation falls as rain; in the second we assume that some precipitation falls as snow, thus available water is a combination of rain and snowmelt. We find that considering the effect of snow results in a more accurate representation of mean monthly flow rates, in particular the peak flow during the melt season in the Sierra Nevada. These preliminary results indicate that a relatively simple snow model can improve the representation of Truckee River basin hydrology, significantly reducing errors in modeled seasonal runoff.

Simulation of runoff is an important part of a surface hydrology model of the southwestern United States. It provides the link between climate and hydrology, allowing the testing of climate estimates with observed streamflow data. We compute runoff using the method of Craig and Ingraham (in preparation), applied here to a 2-dimensional solution domain at a 1-kilometer grid cell spacing (Figure 1). We are prevented from using a finer resolution by the computational demands of the computer models and by the fact that the kilometer-spaced data are interpolated from averaged 30-second latitude and longitude data. We expect to lose extreme highs and lows in elevation and their corresponding extreme climatological values.

The model has been modified to make solutions in two dimensions using rain and snow information provided by the snow model. In addition, modules have been added to compute monthly percentage of daylight hours as a function of obliquity, longitude of the earth, and latitude to more accurately represent variations in potential evapotranspiration. The parameterized model estimates interception, Hortonian overland flow, saturated overland flow, potential and actual evapotranspiration, infiltration, soil moisture storage, and baseflow. Runoff, the sum of Hortonian overland flow, saturated overland flow, and baseflow, is summed spatially within a drainage basin for comparison to observed streamflow and other

applications. An experiment is performed to estimate the impact of seasonal snowpack on Truckee River streamflow.

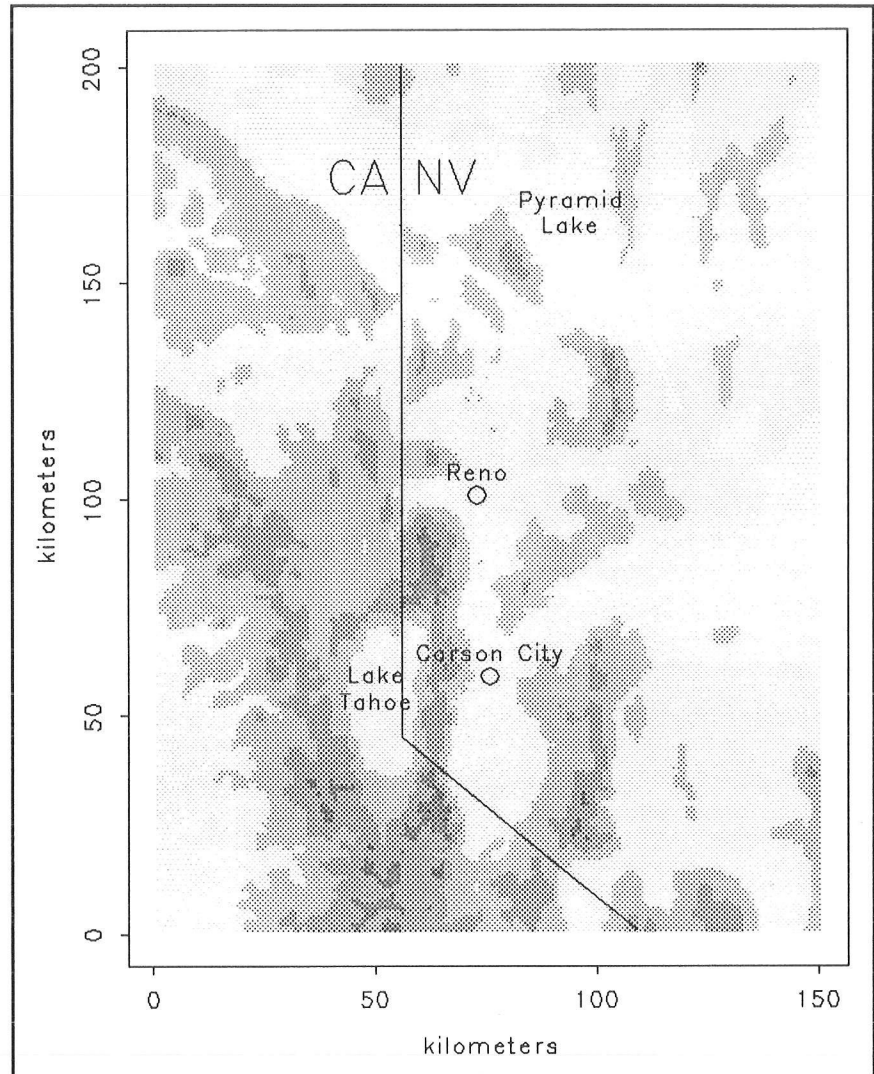
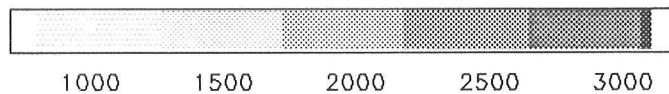


Figure 1. Digital Elevation Model of the Truckee River Drainage Basin at a 1-Kilometer Grid Cell Spacing  
Elevation



## Methodology

A previously reported local climate model (Stamm and Craig 1992; Stamm 1991) calculates monthly temperature and precipitation from a set of independent variables computed from spatial variations in boundary conditions that include elevation, insolation, CO<sub>2</sub> concentration, January and July winds, and January and July sea surface temperatures. Mean maximum monthly temperature and total monthly precipitation are determined for a gridded domain that includes the entire drainage basin tributary to Pyramid Lake, Nevada (the Truckee River drainage basin; Figure 2). A previously reported snow model (Orndorff and Craig 1993) then calculates monthly rain, snowfall, snowpack, and

snowmelt. We predict no perennial snowpack within the solution domain at a 1-kilometer spacing, so ice accumulation and glacier growth are not issues requiring attention here.

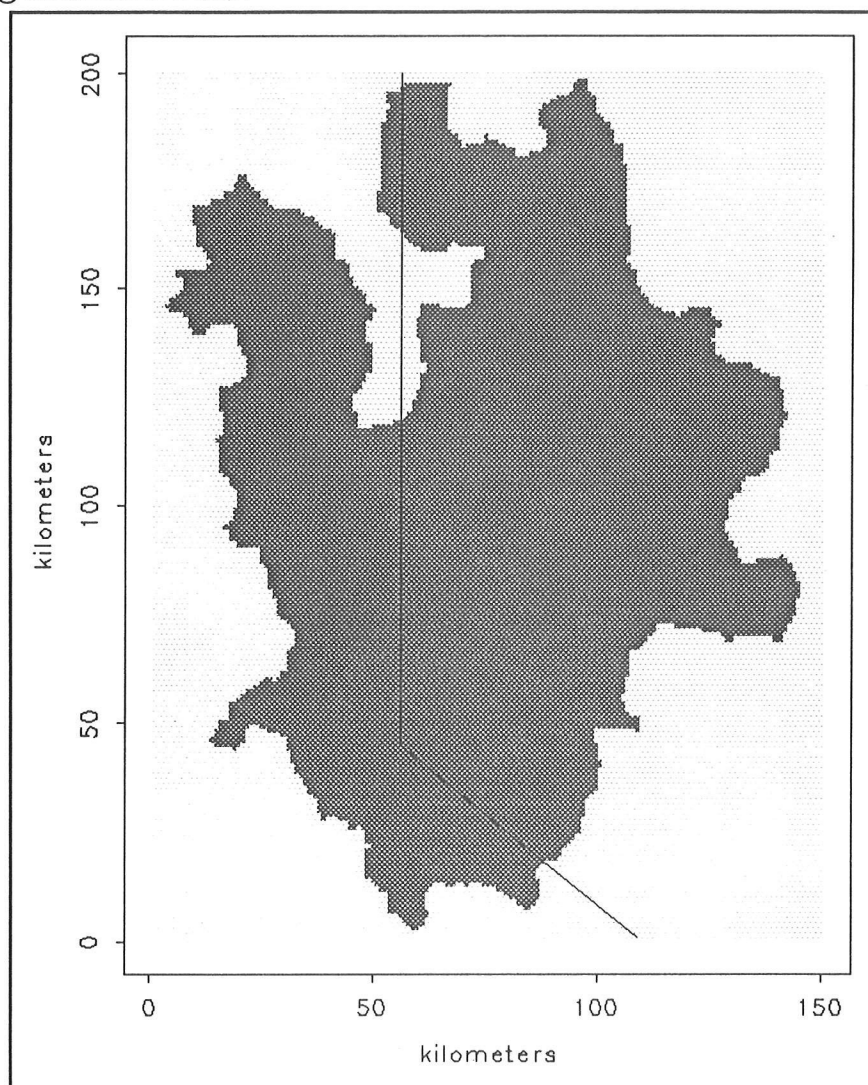


Figure 2. Internally Draining Basins (shaded) within the Truckee River Solution Domain

Mean monthly runoff is computed for each grid point within the solution domain for each month as a function of available surface water. Available surface water is defined here as surface water in liquid form and is made up of rainfall and snowmelt. Matrices containing rainfall and snowmelt values are passed to the runoff model by the snow model. The runoff model computes interception, Hortonian overland flow, saturated overland flow, evapotranspiration, soil moisture, and baseflow for each month, then calculates runoff as the sum of Hortonian overland flow, saturated overland flow, and baseflow (see flow chart, Figure 3).

Monthly interception loss,  $L$ , taken as a constant fraction,  $c_1$ , of precipitation that falls as rain, is subtracted from monthly rainfall,  $R$ , which is then added to monthly snowmelt,  $M$ , to estimate available surface water,  $W$ .

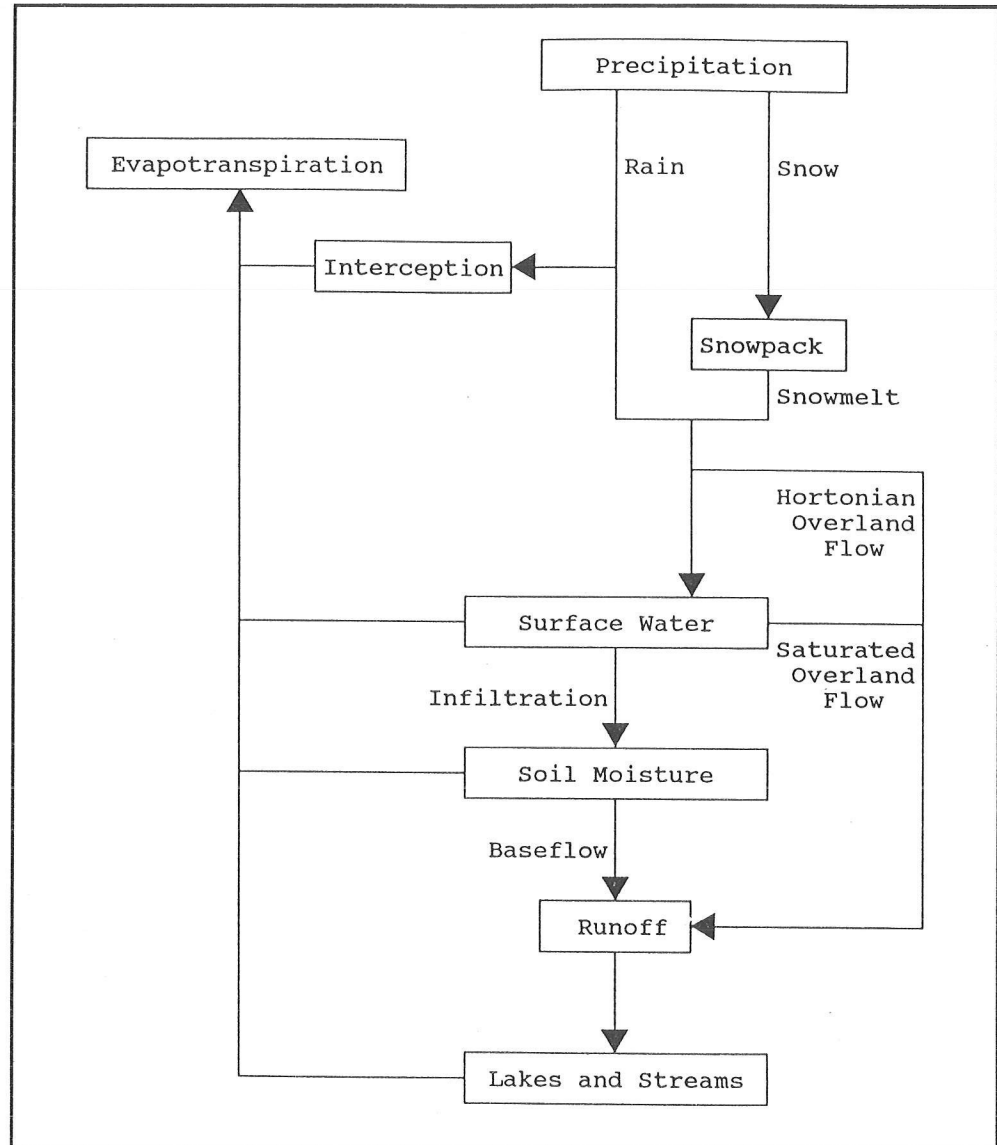


Figure 3. Flowchart of Hydrologic Variables Included in Runoff Calculations

$$L = c_1 R \quad (1)$$

$$W = (1 - c_1) R + M \quad (2)$$

A constant fraction,  $c_h$ , of the available surface water is allowed to run off directly (representing Hortonian overland flow,  $H$ ).

$$H = c_h W \quad (3)$$

Hortonian overland flow is subtracted from available surface water to calculate infiltration,  $I$ .

$$I = W - H = (1 - c_h) W \quad (4)$$

Monthly potential evapotranspiration,  $PET_t$ , is computed via the Blaney-Criddle equation (Blaney and Criddle 1962), which Eagleson (1970) reports represents conditions in the western United States (water use

limited by water supply). Singh (1989) presents a number of methods for estimating  $PET$ , a comparison of which demonstrates that the Blaney-Criddle method is the best of the temperature-based methods and, in addition, appears to be applicable to most of the United States.

$$PET_i = k_i T_i d_i / 100 \quad (5)$$

and annual  $PET$  is then,

$$PET = \sum (k_i T_i d_i / 100) \quad i = 1 \text{ to } 12 \quad (6)$$

where  $k_i$  is an empirical monthly consumptive use coefficient,  $d_i$  is mean monthly percentage of annual daylight hours, and  $T_i$  is mean monthly air temperature in degrees Fahrenheit.

Consumptive use coefficients are dependent upon extant vegetation. We use values recommended by Cruff and Thompson (1967) for group III sites in the western United States (0.75 for January through April, 0.90 for May through October, and 0.75 for November through December).

We compute  $d_i$  for each point within the solution domain as a function of latitude and obliquity. The absolute value of the hour angle,  $\alpha$ , is related to latitude,  $\phi$ , and declination,  $\delta$ , as follows (Berger, 1978):

$$\cos \alpha = -\tan \phi \tan \delta \quad (7)$$

Declination depends on obliquity,  $\epsilon$ , and the true longitude of the earth,  $\sigma$ ,

$$\sin \delta = \sin \epsilon \sin \sigma \quad (8)$$

The absolute value of the hour angle is transformed into total daylight hours,  $D$ , by the relation:

$$D = \alpha (24/2\pi) \quad (9)$$

Equation (9) is solved, and total daylight hours are summed over each month and the year to calculate  $d_i$  for the latitude of each grid cell, the longitude of the earth for each day of the year, and the modern obliquity value ( $23.439972^\circ$ ).

Adjusted potential evapotranspiration,  $PET_a$ , is computed as the product of  $PET$  and a storage coefficient,  $c_s$ .

$$PET_a = c_s PET \quad (10)$$

The storage coefficient is the ratio of actual soil moisture,  $S$ , to the field capacity of the soil,  $C$ , and represents increasing resistance to evaporation with decreasing soil moisture.

$$c_s = S/C \quad (11)$$

After computing  $PET_a$ , the runoff model discriminates between four distinct scenarios (Figure 4):

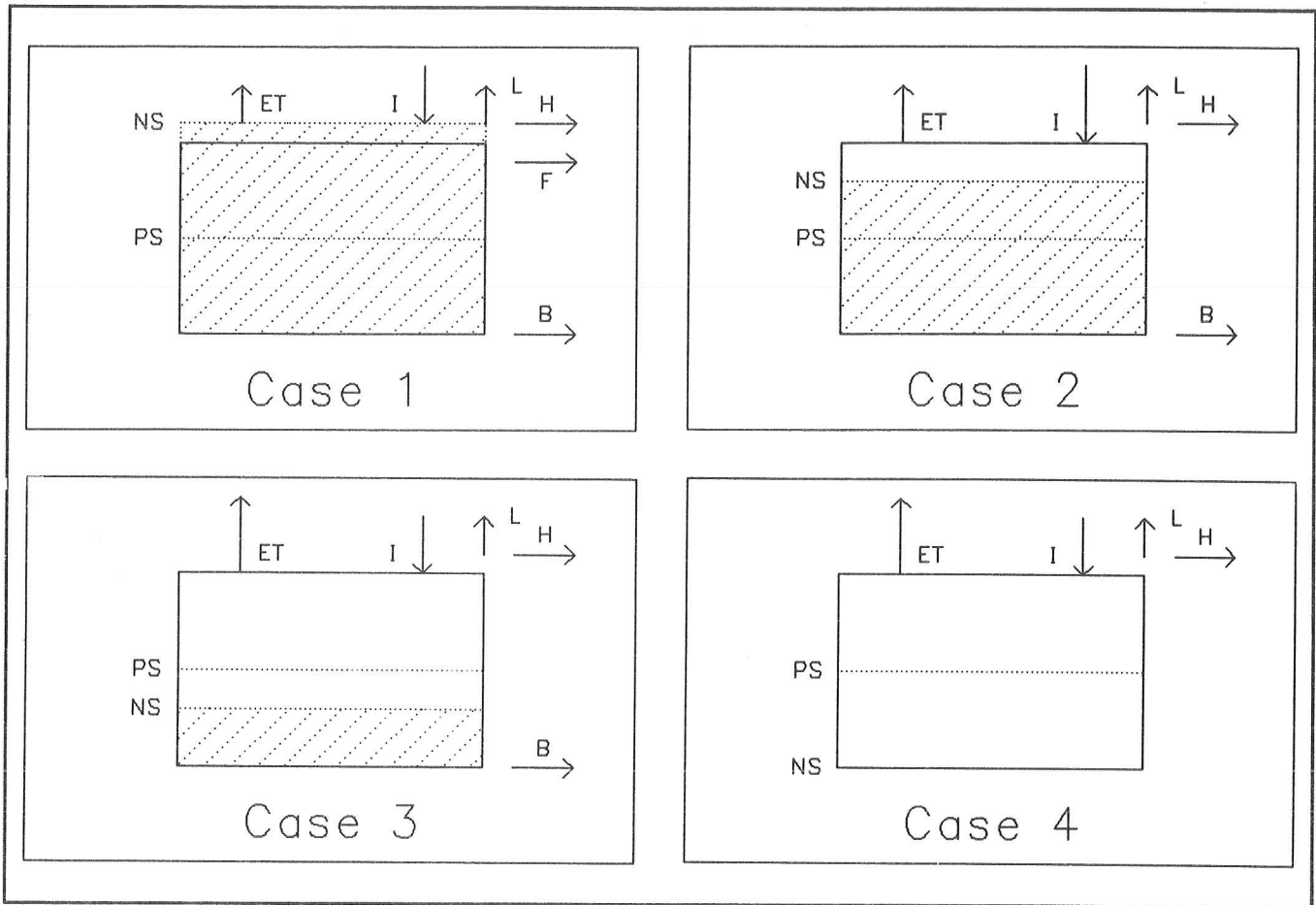


Figure 4. The Runoff Model Distinguishes between Four Distinct Scenarios: (1) infiltration exceeds AET with overflow, (2) infiltration exceeds AET with no overflow, (3) AET exceeds infiltration and soil moisture decreases, and (4) AET exceeds infiltration and soil desiccates completely. (Symbols are defined in text.)

1. If infiltration is greater than actual evapotranspiration,  $AET$ , and the soil moisture field capacity,  $C$ , is exceeded, then the excess is saturated overland flow,  $F$ ,

$$F = I - AET + PS - C \tag{12}$$

$$NS = C \tag{13}$$

where  $PS$  is antecedent soil moisture storage and  $NS$  is new soil moisture storage.  $PET_a$  is completely satisfied, so,

$$AET = PET_a \tag{14}$$

2. If infiltration is greater than  $AET$  but the soil moisture field capacity is not exceeded, then soil moisture increases with no saturated overland flow,

$$F = 0 \tag{15}$$

$$NS = PS + I - AET \tag{16}$$

Again,

$$AET = PET_a \quad (17)$$

3. If  $AET$  exceeds infiltration but does not exceed the sum of infiltration and soil moisture storage, soil moisture decreases. Once again,

$$F = 0 \quad (18)$$

$$NS = PS + I - AET \quad (19)$$

$$AET = PET_a \quad (20)$$

4. If  $AET$  exceeds or equals the sum of recharge and soil moisture storage, then the soil is totally desiccated.

$$F = 0 \quad (21)$$

$$NS = 0 \quad (22)$$

$$AET = PS + I \quad (23)$$

Case 4 does not occur, because the storage coefficient never allows evapotranspiration to exceed storage.

A fraction,  $c_b$ , of water contained within the soil (after accounting for evapotranspiration) is lost through baseflow,  $B$ .

$$B = c_b NS \quad (24)$$

Runoff,  $R$ , at each grid cell for each month is then computed as the sum of Hortonian overland flow, saturated overland flow, and baseflow.

$$R = H + F + B \quad (25)$$

Parameter values are listed below.

Parameter	Value
Soil Moisture Capacity ( $C$ )	300 mm
Interception Fraction ( $C_1$ )	12%
Hortonian Overland Flow Fraction ( $c_h$ )	5%
Baseflow Fraction ( $c_b$ )	5%

Solutions of the runoff model are iterative. At each grid cell, an initial condition imposed is that  $PS$  is zero for each month. The model moves forward year-by-year in 1-month timesteps until  $NS$  equilibrates, that is, for month  $i$  and year  $j$ ,

$$NS_{i,j} = NS_{i,j-1} \quad \text{for all } i \quad (26)$$

At this point, hydrologic variables are recorded and the model moves to the next grid cell, where the iterative process is repeated.

## Identifying Contributing Basins

Basin identification is based on a digital elevation model of the solution domain. A computer program (Singer 1985) calculates grid cell drainage directions from the model, then uses these values to identify individual basins and drainage divides. Basins draining internally within the solution domain are shown in Figure 2.

Runoff values for those grid cells contained within the internally draining basins are summed for each month to estimate mean monthly Truckee River streamflow. Actual flow rates, measured at Reno, Nevada, do not include runoff contributions from downstream basins, which are included in the runoff model, as contributions from all basins tributary to Pyramid Lake are summed. We expect the contributions from these low-elevation basins to be small compared to contributions from basins upstream of Reno and to be a constant bias in both experiments.

## Solutions

The presence of a seasonal snowpack and the resulting lag in snowmelt runoff are important factors in accurately predicting streamflow from climate estimates in mountainous areas such as the Sierra Nevada (Kattelmann 1991). To calculate the effect of snow on the hydrologic system, we perform two experiments. In the first, all precipitation is constrained to fall as rain, while in the second the snow code is used to compute the fraction of precipitation that falls as snow, as well as snowmelt and resulting snowpack.

Hydrographs in Figures 5 and 6 show mean monthly flow rates for the Truckee River for experiment I (no snow), experiment II (snow), and actual values measured at Reno.

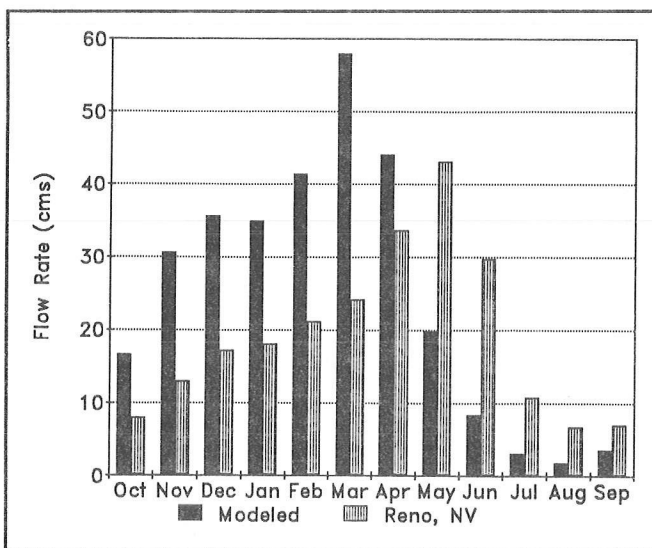


Figure 5. Modeled Mean Monthly Streamflow Assuming All Precipitation Falls as Rain for All Months

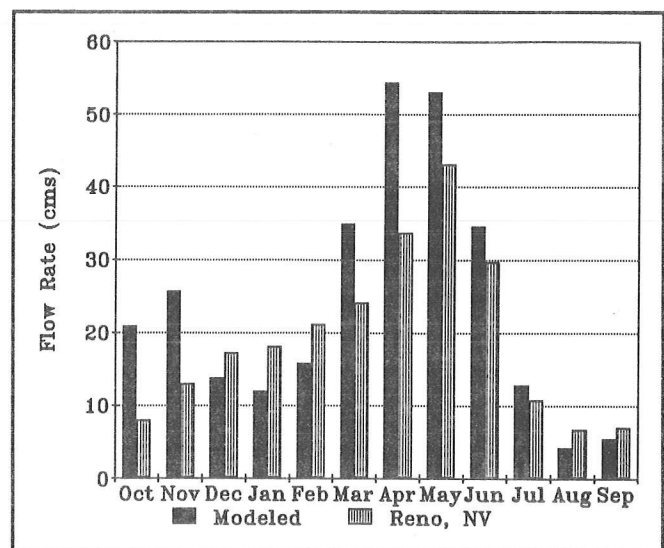


Figure 6. Modeled Mean Monthly Streamflow Considering the Effect of Seasonal Snow on Basin Hydrology

Figures 7 and 8 show deviations from observed mean monthly flow rates for experiment I and experiment II, and Figure 9 shows the deviation of experiment II from experiment I. The sum of the squares of the deviation of modeled and observed is 311 for experiment I and 60 for experiment II, a factor of five difference.

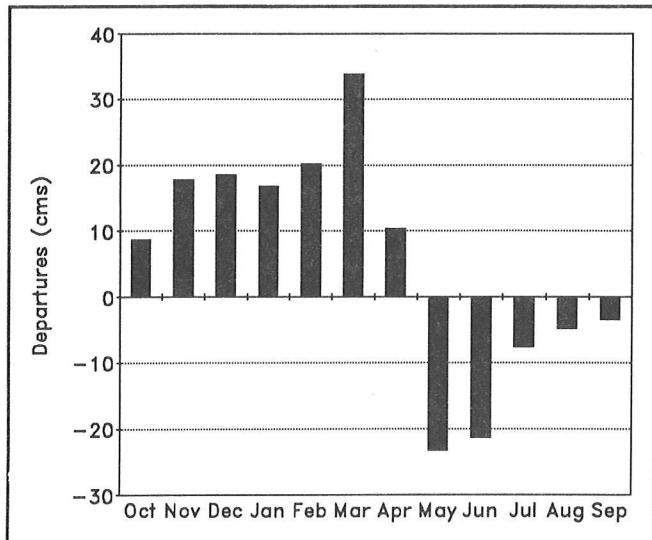


Figure 7. Departure of Modeled Monthly Streamflow from Observed, Assuming All Precipitation Falls as Rain

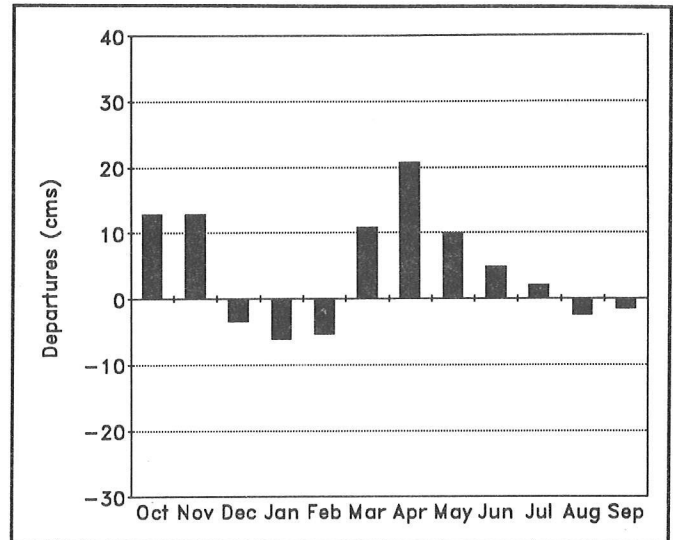


Figure 8. Departure of Modeled Monthly Streamflow from Observed Considering the Effect of Seasonal Snow

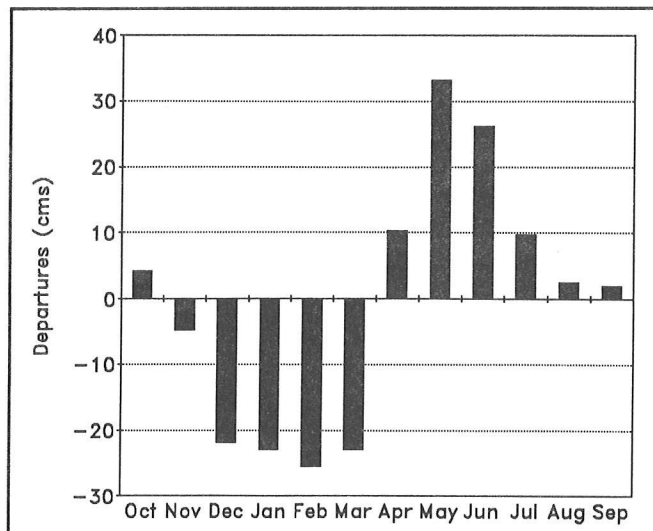


Figure 9. Departure of Modeled Monthly Streamflow Considering Snow Effects from Modeled Monthly Streamflow Assuming All Precipitation Falls as Rain

A chi-square test of the two modeled solutions with a predictor calculated as the mean of the two modeled solutions allows us to reject the null hypothesis that there is no significant difference between results of experiments I and II at the 95% confidence level. Experiment I leads to over-prediction of streamflow in winter and under-prediction of flow in summer. Experiment II results in slight under-prediction of winter and summer flow, but captures better the spring runoff peak that occurs from March through June.

Deviations of experiment II from observed may be the result of under-predicting fall and spring snowfall. More fall snow would lead to a lowering of the positive fall runoff

departure and, in addition, would provide more snowpack for winter snowmelt, which would increase winter runoff and correct to some degree the negative runoff departure we see there. Increased spring snowfall would lower the positive spring runoff departure and delay the peak runoff, which the model predicts one month too soon (in April compared to the observed peak in May).

In terms of absolute values, mean annual Truckee River flow measured at Reno is 19.34 m<sup>3</sup>/sec (with a standard deviation of 12.71 m<sup>3</sup>/sec), compared to 23.92 m<sup>3</sup>/sec for experiment I and 24.79 m<sup>3</sup>/sec for experiment II. It is interesting that the mean departure for experiment I is less than that of experiment II. This is the result of large positive and negative departures canceling one another out in experiment I.

## Conclusions

---

We conclude that even the simple methods for considering the effect of seasonal snow reported here result in a more accurate representation of mean monthly streamflow rates. These preliminary results indicate that considering the effect of snow improves the characterization of Truckee River basin hydrology, significantly reducing errors in the seasonal distribution of modeled runoff. We infer that use of such a model will be important in reconstruction of paleolake levels in the Great Basin.

## References

---

- Berger, AL. 1978. Long-Term Variations of Daily Insolation and Quaternary Climate Changes. *Journal of Atmospheric Science*. 35:2362-2367.
- Craig, RG, and N Ingraham. 1993. *An Isotope Constrained Analysis of a Regional Climate/Hydrology/Isotope System*. In preparation.
- Cruff, RW, and TH Thompson. 1967. *Comparison of Methods Estimating Potential Evapotranspiration from Climatological Data in Arid and Subhumid Environments*. U.S. Geological Survey Water Supply Paper 1839-M. 28 pp.
- Eagleson, PS. 1970. *Dynamic Hydrology*. McGraw-Hill Book Company, New York. 462 pp.
- Kattelmann, R. 1991. Peak Flows from Snowmelt Runoff in the Sierra Nevada, USA. Pages 203-211 in *Snow, Hydrology and Forests in High Alpine Areas*. H Bergmann, H Lang, W Frey, D Issler, and B Salm, editors. International Association of Hydrological Sciences Publication 205.
- Orndorff, RL, and RG Craig. 1993. A Stochastic Model of Temporal Variations in Monthly Temperature, Precipitation, Snowfall, and Resulting Snowpack. Pages 165-172 in *Proceedings of the Ninth Annual Pacific Climate (PACLIM) Workshop*. KT Redmond and VL Tharp, editors. California Department of Water Resources, Interagency Ecological Studies Program Technical Report 34.
- Singer, M. 1985. *A Computer Simulation of the Growth and Dessication of Pluvial Lakes in the Southwestern United States*. M.S. Thesis, Kent State University, Kent, Ohio, 436 pp.
- Singh, VP. 1989. *Hydrologic Systems: Watershed Modeling*. Prentice Hall, Englewood Cliffs, New Jersey. 320 pp.
- Stamm, JF. 1991. *Modeling Local Paleoclimates and Validation in the Southwest United States*. Ph.D. Dissertation, Kent State University, Kent, Ohio, 211 pp.
- Stamm, JF, and RG Craig. 1992. Validation of a Semi-Lagrangian, Canonical Regression Model of Climates in the Southwestern United States. Pages 163-171 in *Proceedings of the Eighth Annual Pacific Climate (PACLIM) Workshop*. KT Redmond, editor. California Department of Water Resources, Interagency Ecological Studies Program Technical Report 31.

# Climatological Aspects of the Large-Scale Hydrologic Cycle in the United States

John Roads, Shyh Chen, Alex Guetter, and Konstantine Georgakakos

**ABSTRACT:** We describe a 2.5-degree gridpoint atmospheric hydrology/climatology of precipitable water, precipitation, atmospheric moisture convergence, and a residual evaporation or evapotranspiration for the coterminous United States. We also describe a large-scale surface hydrology/climatology of a residual soil moisture, streamflow divergence, or runoff, as well as precipitation and evaporation. Annual and seasonal means and interrelationships among various components of the hydrologic cycles are discussed.

It is generally believed that we have only a rough qualitative understanding of the earth's hydrologic cycle. We do not measure well, or even measure at all in many places, many hydrologic processes. To increase our quantitative knowledge of the hydrologic cycle, the international GEWEX GCIP program was initiated. As we begin this international program, though, it is important to establish just how well we do understand the hydrologic cycle from past, imperfect observations. We will then know what improvements the program has brought. Also, we need to use past observations for understanding low-frequency variations in the hydrologic cycle.

We have been constructing a large-scale 2.5-degree atmospheric hydrologic climatology over the United States. This gridpoint climatology consists of precipitation (see Roads *et al* 1991a,b), atmospheric precipitable water, atmospheric moisture divergence or convergence, and a residual evaporation (see Roads *et al* 1992). We use these atmospheric data along with United States streamflow outflow (see Guetter *et al* 1991 and Guetter and Georgakakos 1993) to also construct a large basin-scale surface climatology of precipitation, evaporation, runoff, and surface water storage (see Roads *et al* 1993a,b).

The atmospheric hydrologic cycle is:

$$Q_t = C + E - P;$$

precipitable water is increased by convergence of moisture and evaporation, and decreased by precipitation. (Note that convergence is the opposite of divergence:  $C = -D$ .)

The surface hydrologic cycle is:

$$W_t = -S - E + P;$$

surface water is decreased by streamflow divergence and evaporation, and increased by precipitation.

## Annual Mean

Figures 1 through 4 show the annual mean of components involved in the atmospheric portion of the United States hydrologic cycle. The precipitable water (Figure 1) has large geographic variations, varying from 10 kg/m<sup>2</sup> over the West, where the orography is quite high and the surface is relatively dry, to 30 kg/m<sup>2</sup> over the Gulf Coast and Florida. At comparable latitudes, the West Coast is dryer than the East Coast, until the Pacific Northwest is reached.

Precipitation (Figure 2) is characterized by large amounts in the Pacific Northwest and Mississippi Gulf Coast. The Pacific Northwest precipitation mainly exists along the coast, whereas the Gulf Coast precipitation is spread more uniformly over the entire southeastern part of the U.S. The driest region is the Great (Salt Lake) Basin, where precipitation is less than 1 mm/day, increasing slightly in the region of the Grand Canyon.

Evaporation (Figure 3) is calculated as a residual sum of atmospheric precipitable water variations and mainly precipitation and atmospheric moisture divergence. The evaporation is fairly consistent with the precipitation. The largest amounts occur over the Gulf Coast and Northwest, although the evaporation maxima are not reached in the exact same

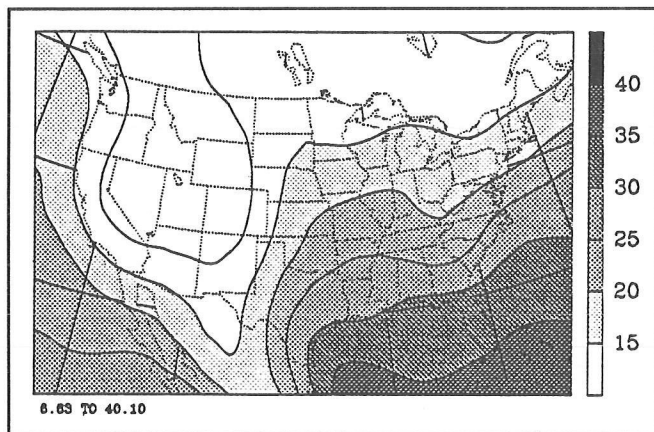


Figure 1. Annual mean atmospheric precipitable water (millimeters).

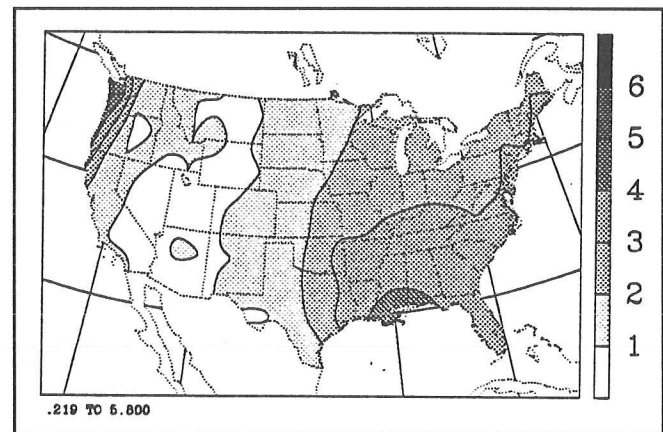


Figure 2. Annual mean precipitation (millimeters/day).

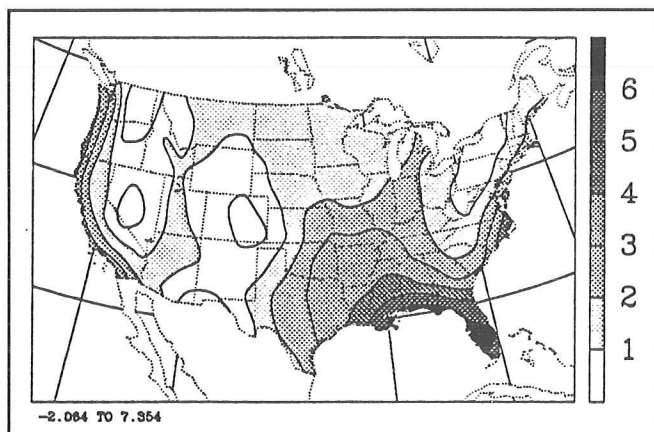


Figure 3. Annual mean residual evaporation (millimeters/day).

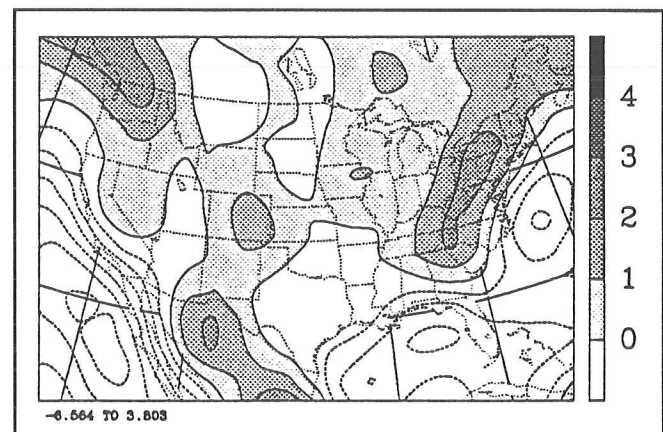


Figure 4. Annual mean atmospheric moisture convergence (millimeters/day). Negative convergence (divergence) is shown by dashed lines.

locations as the precipitation maxima. For example, the evaporation maximum over the Gulf Coast and Florida is to the east of the precipitation maximum; there is another maximum in the coastal regions of North Carolina. The evaporation maximum along the West Coast occurs over Oregon, rather than over Washington, where the precipitation is a maximum.

Precipitation and evaporation geographic differences are due to the vertically integrated atmospheric moisture convergence, shown in Figure 4. Note the predominant ocean divergence and predominant land convergence. At smaller scales, the West coast has the strongest divergence; the Gulf and East Coast have a smaller divergence. The divergence is strongest in low latitude regions where the precipitable water amounts are largest, but the convergence is strongest over the northern coastal areas, as well as the eastern edge of the Sierra Madres and Rocky Mountains.

### Seasonal Variations

Figures 5 through 8 show seasonal hydrologic budgets for the coterminous United States. Figure 5 shows the original data, including residual evaporation and streamflow divergence or runoff. Since annual runoff should be equal to annual mean convergence of atmospheric moisture, we modify the divergence to give the correct annual mean balance. This corrected divergence is then used to obtain a new residual estimate of evaporation, shown Figure 6. Comparisons of the new evaporation as well as the new moisture divergence curves in Figure 6 with the original moisture divergence and evaporation curves in Figure 5 show that the residual correction to the balance is small but important. The corrected residual evaporation is then used to deduce the variation in surface water

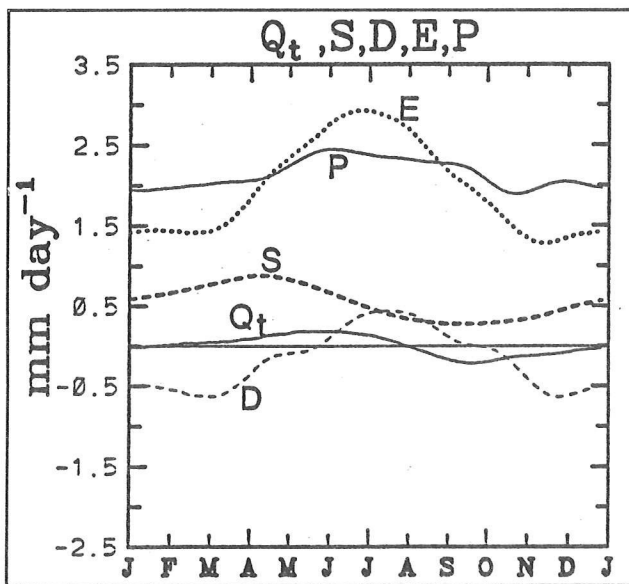


Figure 5. Original Hydrologic Data (millimeters/day). Preliminary residual evaporation, precipitation, runoff, atmospheric moisture divergence, and seasonal variation in atmospheric moisture storage are also shown.

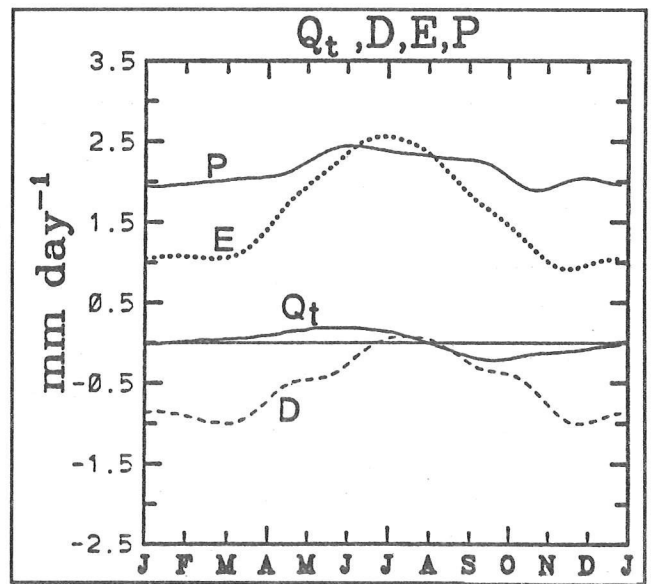


Figure 6. Terms in the Atmospheric Hydrologic Cycle (millimeters/day). All lines denote the same quantities shown in Figure 5. The residual correction to the moisture divergence is shown, as well as the final residual evaporation estimation.

storage, which is the difference between precipitation and evaporation and runoff.

Consider the atmospheric hydrologic cycle, shown in Figure 6. The dominant component is precipitation, which is slightly larger in summer than in winter. Evaporation is smallest in winter. During the summer, evaporation becomes slightly greater than precipitation. Convergence of moisture is smallest in summer; during the winter, the convergence is about the same order as evaporation. The smallest term in the atmospheric hydrologic cycle is atmospheric moisture storage, variations of which are not important for seasonal variations.

By contrast, the residual surface water storage term is important in the surface water budget, shown in Figure 7. Seasonal variations in water storage are just as important as streamflow divergence or runoff, but still smaller than precipitation and evaporation. As shown in Figure 8, the surface water increases on the order of 80 millimeters during the fall to spring months and decreases to zero (plus an arbitrary but unknown positive constant) during the summer months. Part of this surface water storage is presumably snow (see Marshall *et al* 1993). Interannual variations in surface water storage (not shown) are just as large as the seasonal variations.

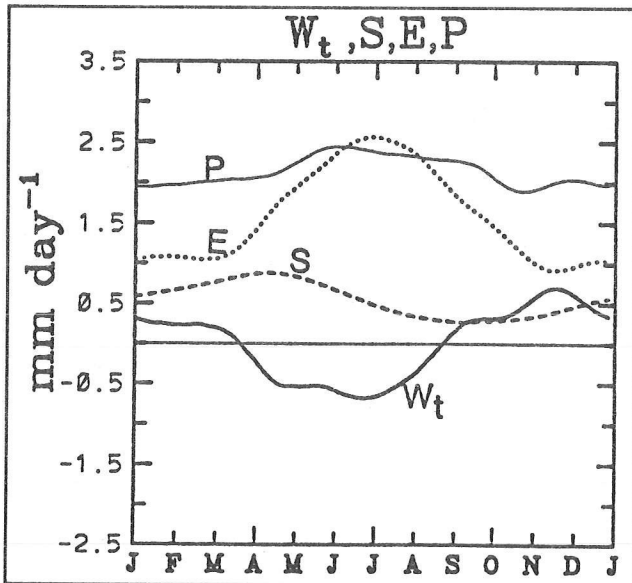


Figure 7. Terms in the Surface Hydrologic Cycle (millimeters/day)  
The new term shown here is the residual variation in the surface water storage.

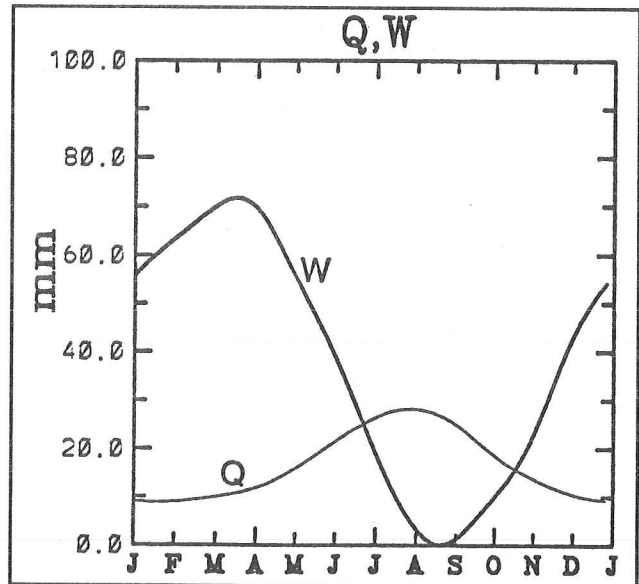


Figure 8. Seasonal Variation in Atmospheric Moisture and Residual Surface Water (millimeters)

## Summary

Various other details of the large-scale U.S. hydrologic cycle, deduced from present observations, are described in Roads *et al* (1993b). After the GCIP program, we will understand better just how accurate these deductions are.

## References

---

- Guetter, AK, J McCollum, KP Georgakakos. 1991. *The Line Integral of Net Outflow from the Continental U.S.* Abstract for the Fall AGU Meeting, San Francisco, December 9-13, 1991.
- Guetter, AK, and KP Georgakakos. 1993. U.S. Outflow Variability and Anomaly Patterns. Submitted to the Bulletin, AMS
- Marshall, S, JO Roads, G.Glatzmaier. 1993. Snow Hydrology in a GCM. Submitted to *Journal of Climatology*.
- Roads, JO, and TN Maisel. 1991a. Evaluation of the National Meteorological Center's Medium Range Forecast Model Precipitation Forecasts. *Weather and Forecasting*. 6(1):123-132.
- Roads, JO, TN Maisel, J Alpert. 1991b. Further Evaluation of the National Meteorological Center's Medium-Range Forecast Model Precipitation Forecasts. *Weather and Forecasting*. 6(4):483-497.
- Roads, JO, S-C Chen, J Kao, D Langley, G Glatzmaier. 1992. Global Aspects of the Los Alamos General Circulation Model Hydrologic Cycle. *Journal of Geophysical Research*. 97:10,051-10,068.
- Roads, JO, KP Georgakakos, AK Guetter. 1993a. Interannual Variations in the U.S. Hydrological Cycle. Proceedings of Conference on Hydroclimatology: Land-Surface/Atmosphere Interactions on Global and Regional Scales, January 17-22, 1993, Anaheim, CA.
- Roads, JO, S-C Chen, AK Guetter, KP Georgakakos. 1993b. Large-Scale Aspects of the U.S. Hydrologic Cycle. *Bulletin of the American Meteorological Society*, submitted.



# Is the California Drought Over?

Maurice Roos

For the 6-year period 1987 through 1992, most of California suffered the worst or near-worst drought in a recorded history of about 140 years. Based on tree ring reconstructions, it may have been the worst in more than 400 years.

The purpose of this paper is to review briefly the recent drought, then talk about the water supply situation this year, with some discussion of why the California drought is over hydrologically for most people; but for some, water supply problems continue.

## The Recent Drought

The recent 6-year drought is comparable to the 1929-1934 sequence of dry years. Statewide precipitation was about 75 percent of average. The deficit was amplified in streamflow, which was only about half average. This drought was not quite the worst on record for the Sacramento Basin of Northern California. Runoff during 1987 to 1992 averaged 54 percent of average, compared to 53 percent during 1929 to 1934.

Figure 1 shows Sacramento River Index runoff during the recent drought. Most years were about half average; only in 1989 was there a substantial change. Figure 2 shows the entire record of Sacramento River Index runoff since 1906.

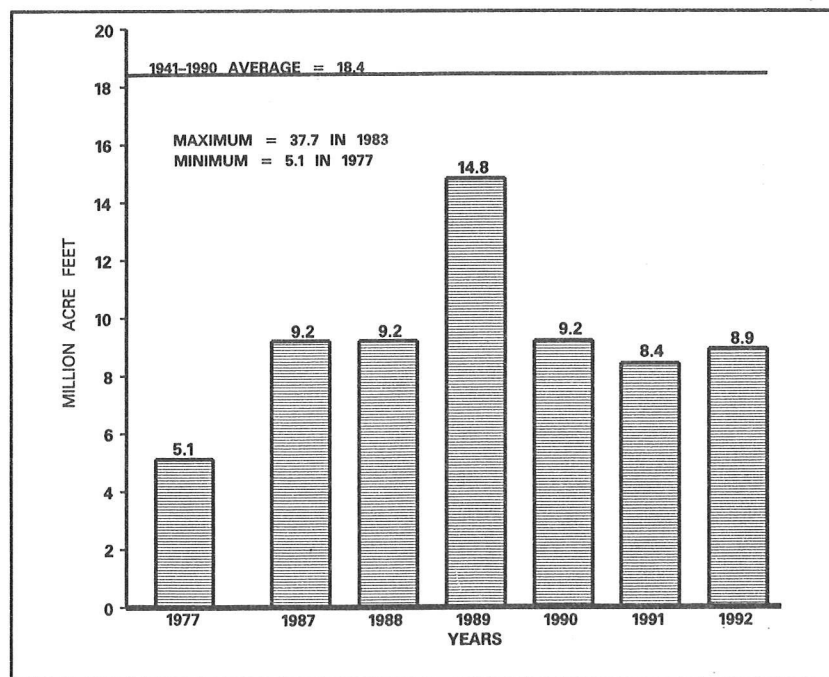


Figure 1. Sacramento River Index for Water Years 1977 and 1987 through 1992.

The water year is from October 1 through September 30.

The Sacramento River Index is the sum of unimpaired runoff from the Sacramento River at Bend Bridge, Feather River inflow to Lake Oroville, Yuba River at Smartville, and American River inflow to Folsom Lake.

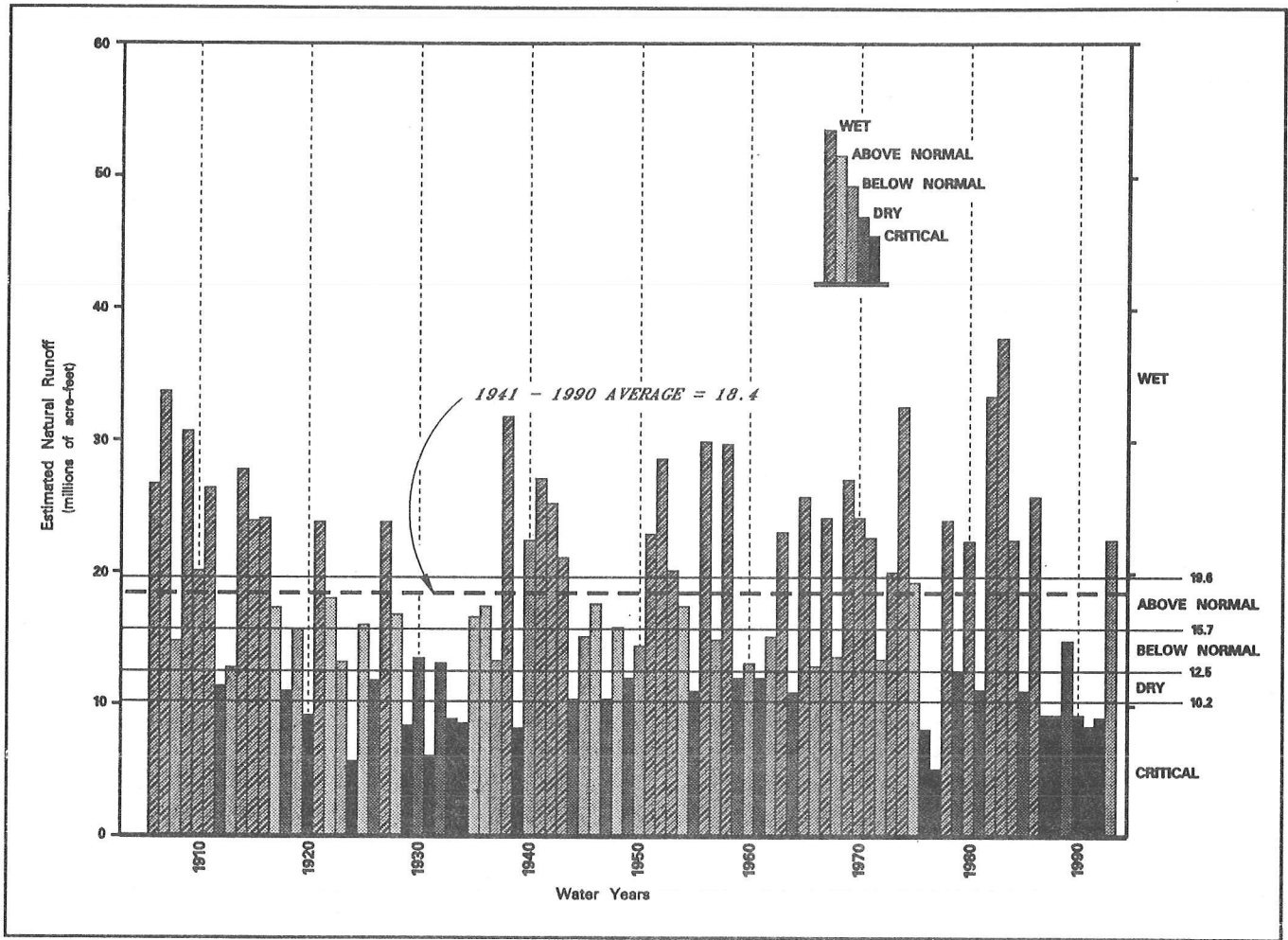


Figure 2. Sacramento River Index Since 1906  
 The Sacramento River Index is the sum of unimpaired runoff from the Sacramento River at Bend Bridge, Feather River inflow to Lake Oroville, Yuba River at Smartville, and American River inflow to Folsom Lake.

In the southern Sierra, the extended drought of the early 1930s was softened somewhat by an above-average water year in 1932. The recent drought, although varying somewhat from year to year, was an unrelieved string of six critical years in the southern Sierra Nevada. Figures 3 and 4 show how the recent drought compares with previous droughts for the Sacramento and San Joaquin river systems.

For the Sacramento River basin, a reconstruction of flow back to the year 1560 was made in 1986 for the Department of Water Resources by the Laboratory of Tree Ring Research at the University of Arizona in Tucson, using cores taken in the early 1980s from northern California into central Oregon. The reconstruction showed that the 1928 to 1934 dry period was the worst sustained drought since 1560. (Water year 1928 was near normal, but its dry season led into a set of six dry or critical water years; many water engineers refer to this period as the 7-year critical dry period, 1928-1934.) Using the median runoff of 15.7 million acre-feet as a threshold of dryness, there were fairly numerous 3- or 4-year droughts, one 5-year drought, and two 6-year droughts before 1900. The two 6-year periods were 1719-1724 and 1755-1760. None of the droughts lasted

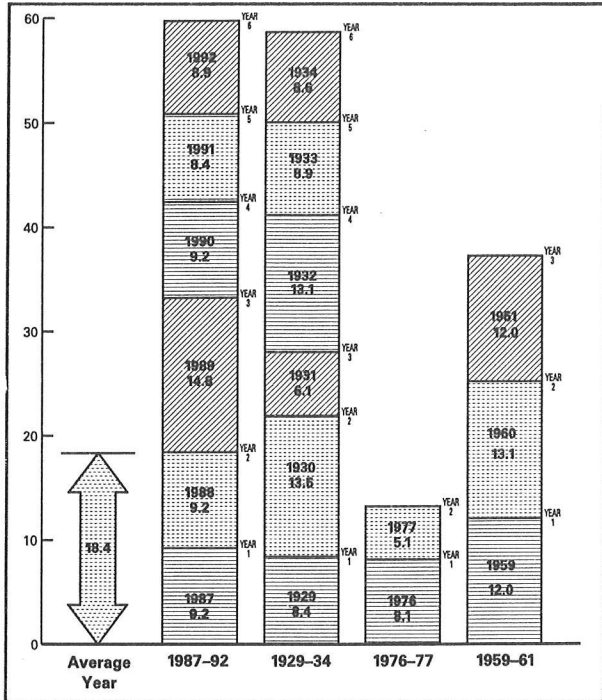


Figure 3. Comparison of Droughts, Sacramento River Index (Water Year Runoff in Million Acre Feet)

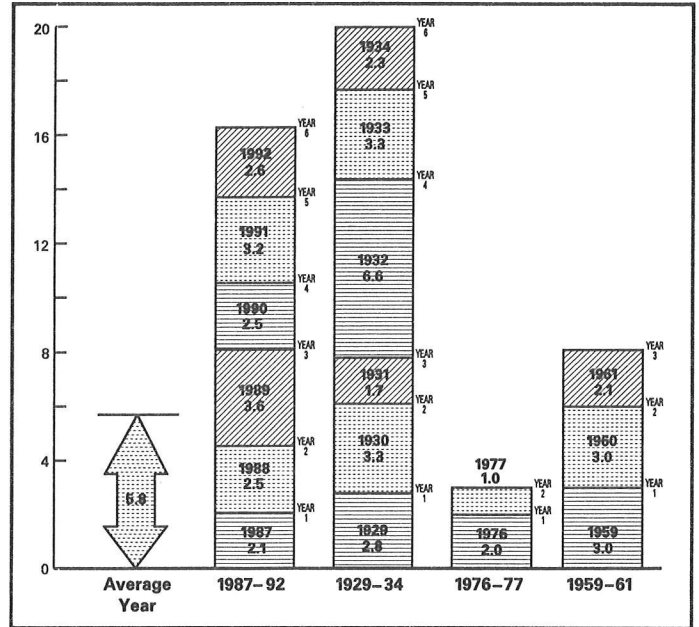


Figure 4. Comparison of Droughts, San Joaquin River Index (Water Year Runoff in Million Acre Feet)

over 6 years, although there was an 8-year period of less than average runoff from 1839 through 1846, with a break in 1842. John Bidwell, an early pioneer in Northern California, confirmed there was flooding in 1842 when he tried to ride from San Jose to Sacramento, but he later classified the year as moderate.

Table 1 is derived from the reconstruction. It shows dry periods with consecutive years of runoff less than 15.7 MAF (the historical median) lasting at least three years, prior to 1900, for the reconstructed Sacramento River Index. Also shown are the measured droughts since 1900.

The drought probably reached its nadir in 1991, even though reservoir storage was a little lower in the fall of 1992. The year 1991 was the year of the biggest State Water Project deficiencies and the most ambitious water bank program. California was saved from a desperate situation that year only by the "miracle March", with triple normal monthly precipitation.

Period	Length of Drought (years)	Estimated Average Runoff (MAF/year)
1579-1582	4	12.4
1593-1595	3	9.3
1618-1620	3	13.2
1651-1655	5	12.3
1719-1724	6	12.6
1735-1737	3	12.2
1755-1760	6	13.3
1776-1778	3	12.1
1793-1795	3	10.7
1839-1841	3	12.9
1843-1846	4	12.3
1918-1920 (actual)	3	12.0
1929-1934 (actual)	6	9.8
1959-1962 (actual)	4	13.0
1976-1977 (actual)	2	6.6
1987-1992 (actual)	6	10.0

\* Years with runoff less than 15.7 million acre-feet per year.

## Water Year 1993

But what about the current water year? What a contrast! The rainy season started poorly, with only about 20 percent of average November precipitation. But all three major winter months, December, January, and February, had far above average precipitation. March, too was good, with slightly over average rainfall. Seasonal precipitation statewide was about 150 percent of average on April 1 and was about 130 percent of average in the important water-producing areas of the northern Sierra. There was a pronounced south-to-north gradient, with southern California amounts more than 200 percent and northwestern California amounts near average. This pattern was also true in 1992, but in 1993 the wetness moved north almost to the Oregon border, 300 or 400 miles north of the 1992 location of this transition. This placed the Sierra Nevada in the wet zone, compared to quite dry conditions in the range during 1992.

The snowpack in 1993 is the heaviest since 1983. On April 1, snowpack water content was about 150 percent of average, and somewhat heavier in the southern Sierra where it is more useful. Reservoir storage had recovered to about 90 percent of average, the most on April 1 since 1987. The generous snowpack assured good snowmelt runoff and that most reservoirs would be at or above average later in the spring. The exceptions, which drag down the statewide average, are those those reservoirs that have large storage-to-average-runoff ratios, such as New Melones and Lake Berryessa. Even Lake Tahoe was still below its natural rim by about a foot.

Table 2 compares 1992 and 1993 water supply, and Figure 5 shows total storage in California's major reservoirs.

	1992	1993
Statewide Precipitation	90	150
Northern Sierra Precipitation	72	130
Snowpack Water Content	60	150
Reservoir Storage	70	90
Runoff, to date	45	110
April-June Runoff Forecast	55	135
Water Year Runoff Forecast	50	125

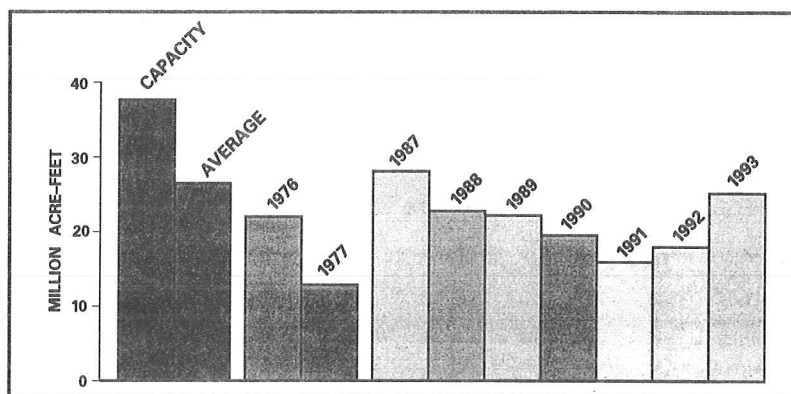


Figure 5. April 1 Storage in 155 Major California Reservoirs

Storage amounts from 1987 to 1993 include New Melones and Warm Springs reservoirs, which began operation after 1977. Storage amounts for 1989 to 1993 also include the new Spicer Meadows Reservoir, on the Stanislaus River.

## **Is the Drought Over?**

---

As soon as we began to see heavy rain and snow, and local flood scenes were shown on television, folks started asking, "Is the drought over?" and "How much more rain will it take?"

There is no single, neat "drought-end" formula that will apply statewide because of the large diversity in water systems, geography, and weather patterns. Each region will emerge from the drought at a different time, and economic effects will continue after water conditions return to normal. It will probably take years to restore some depleted ground water basins; others will continue to be overdrafted even after the drought.

In general, however, we devised a threefold scheme to assess when California could consider the drought over. The markers were:

- Storage in most major reservoirs is normal for the date (or we can reliably forecast enough runoff to fill to normal levels). Statewide, a 90 percent of average figure would be enough.
  - This threshold would probably show Sacramento Basin storage above average and the San Joaquin and North Coast (Trinity) basins below average. Neither is Lake Tahoe likely to recover.

or

- Runoff this water year is (or is reliably forecast to be) 110 percent of average.
  - This level of runoff was estimated to produce the storage recovery levels shown above. There is a lot of difference between basins. Recovery of normal storage at Lake Berryessa or on the Stanislaus River would take more than twice average runoff. Folsom Lake, on the American River, could reach flood control in a 75 percent runoff year.

or

- Reservoirs on the four major rivers of the Sacramento Basin reach flood control limits, or three of the four are making flood control releases.
  - This last item was included because we would look foolish claiming drought when the state's major water supply basin is in the flood control mode of operation.

We still were not sure in early February (which was dry for a couple of weeks) whether there would be enough rain to assure an end to the drought. At that point, reservoir storage was only 75 percent of average. During the third week of February, a new series of storms brought much rain and snow, assuring a good runoff year because of the heavy snowpack. On February 24, Governor Pete Wilson officially declared the drought over. Eventually, statewide reservoir storage climbed to 107 percent of average during the summer of 1993.

But water troubles were not over for everybody. Neither the federal Central Valley Project nor the State Water Project was able to make full water deliveries this year. The SWP moved up from a grim 10 percent allocation on December 1 to eventually provide all the water its contractors needed. This is a bit misleading; it appears that only about two-thirds of the original requests will be delivered. The big difference is a reduction in need for SWP water in southern California because local supplies are so good this year. Agricultural uses are probably reduced somewhat too, because of the lack of an assured supply early in the season when planting decisions were made. Because SWP agricultural customers had taken accumulated cutbacks exceeding a full 100 percent in 1990 and 1991, all SWP users, urban and agricultural, now share any shortages equally for the next five years.

The CVP eventually made full deliveries too, except on the west side of the San Joaquin Valley, where only 50 percent deliveries were made to project customers in areas served from the Sacramento-San Joaquin Delta.

The new twist in water supply is the rise of environmental needs, particularly for threatened or endangered fish. Near the end of March, when delta outflows were over 100,000 cubic feet per second, the SWP Banks Pumping Plant operated at only 3,000 cfs (3 out of 10 pumps) because of the endangered species act — primarily to protect winter run salmon and later the little delta smelt. This has led to a “regulatory” drought, which does not bode well for the future of the west side of the San Joaquin Valley. The federal Central Valley Project Improvement Act of last fall also reallocates at least 800,000 acre-feet of water basically away from agriculture to fish and wildlife.

Yes, the drought is over, but some water problems still remain in California.

# Long-Term and Seasonal Patterns in Coastal Temperature and Salinity along the North American West Coast

Franklin B. Schwing

Numerous integrated time series have been assembled that suggest global temperature has been increasing steadily over the last century. One example is the blended series of sea surface temperature (SST) anomalies for the Northern Hemisphere (Folland *et al* 1990). The systematic increase in temperature can be seen at individual locations as well, such as La Jolla, California (Figure 1). However, superimposed on the long-term warming trends of these series are decadal-scale fluctuations, periods of slightly increasing and even decreasing temperature followed by rapid increases in temperature. An alternative view is to interpret this pattern as a series of "regime shifts" (Figure 1), where the mean annual temperature over a short (few year) period makes a rapid shift in response to some environmental stimulus, following a decadal-scale period of relatively level temperature (MacCall and Prager 1988). This regime shift is followed by a long period of relatively level annual temperatures, then another sudden shift back near the previous level.

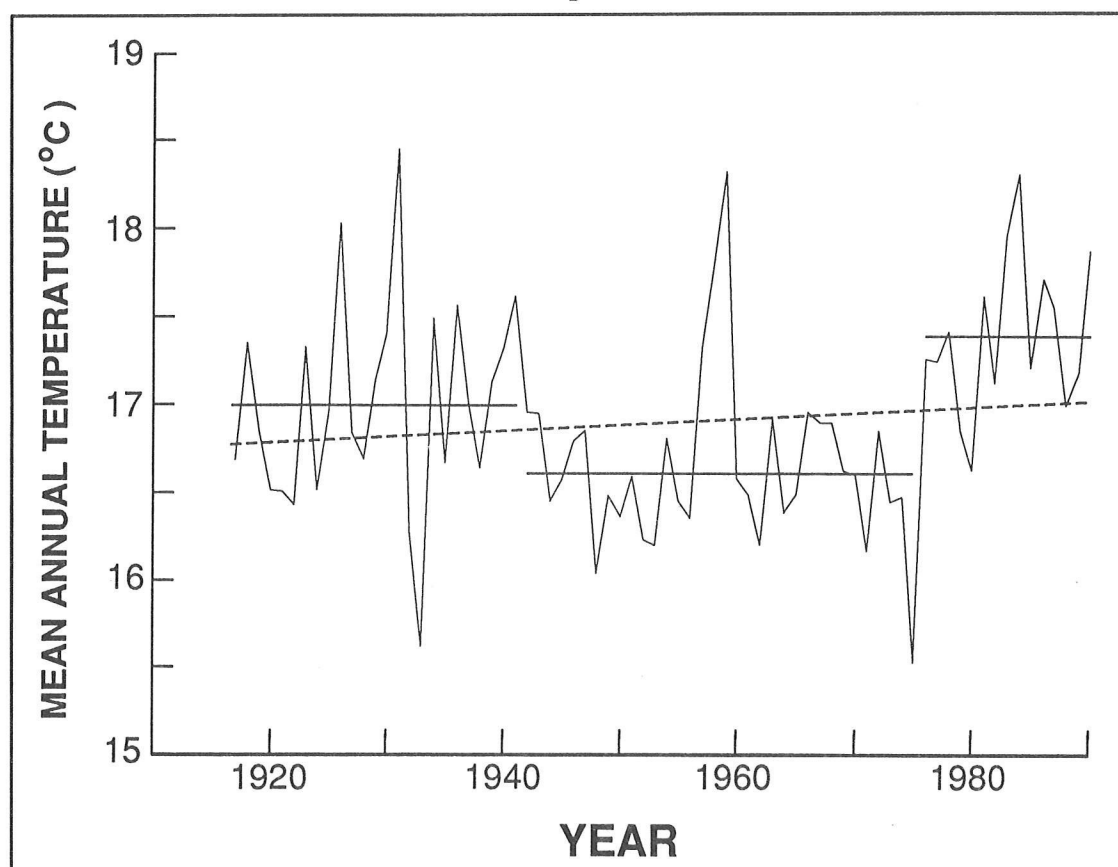


Figure 1. Mean Annual La Jolla Ocean Temperature Series, 1916-1990.

Broken line denotes linear fit to series ( $0.41^{\circ}\text{C}/100$  years,  $r=0.15$ ).

Solid horizontal lines denote long-term averages shown for three periods: 1916-1941, 1942-1975, 1976-1990.

With either interpretation, we must examine annual-to-decadal fluctuations in SST, define and understand the physical processes responsible for variability on these time scales, and predict the magnitude of temperature change if we are to find the true "climate change" embedded within these individual and composite series. We also must examine regional (sub-ocean basin) spatial scale patterns, because certain areas may be more susceptible to, hence better indicators of, climate change. Regional comparisons also focus more on the ecosystem, where climate change has a biological consequence. Since the physics of ocean regions are generally dominated by one or a few important processes, it is easier to separate out shorter-term patterns from climate effects.

Long monthly-averaged ocean temperature and salinity time series are available from about 40 sites along the North American west coast (Table 1, Figure 2).

Table 1  
STATIONS AND PERIODS OF TIME SERIES USED IN THE STATE-SPACE ANALYSIS

Station	Latitude	Longitude	Temperature	Salinity
Seward	60°06'	149°27'	1925-1982	1926-1939
Cape St. James	51°56'	131°01'	1934-1984	1934-1971
Neah Bay	48°22'	124°37'	1935-1986	1936-1979
Crescent City	41°45'	124°12'	1933-1947, 1950-1990	1934-1947, 1950-1979
Bodega Bay	38°19'	123°04'	1957-1990	1975-1990
Farallon Islands	37°25'	122°36'	1925-1942, 1955-1990	1925-1942, 1955-1990
Avila	35°10'	120°45'	1972-1990	
LaJolla	32°52'	117°15'	1916-1990	1916-1990
OS P	50°00'	145°00'	1950-1982	
OS N	30°00'	140°00'	1954-1974	

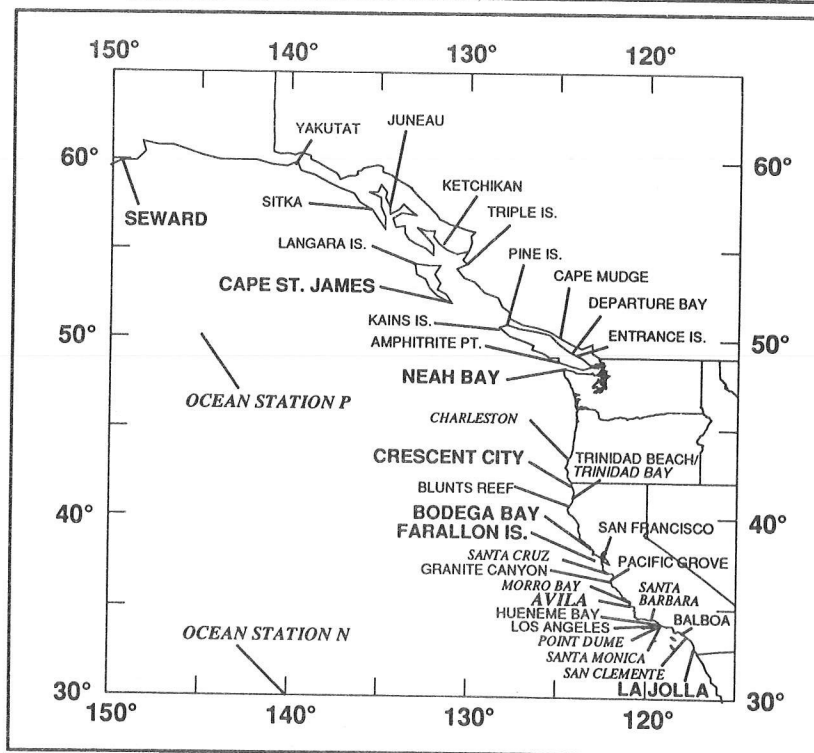


Figure 2. Location of Stations with Long-Term Monthly Temperature and Salinity Time Series. Sites analyzed in this paper shown in bold. Salinity data not available at italicized stations.

In this pilot study, data for 1931-1990 from eight coastal stations are examined to test the utility of a state-space statistical model (developed by Dr. Roy Mendelssohn, PFEG) in separating and describing seasonal patterns and long-term trends. The stations are: Seward (SE), AK; Cape St. James (CJ), BC; Neah Bay (NB), WA; Crescent City (CC), Bodega Bay (BB), Farallon Is. (FI), Avila (AV), and La Jolla (LJ), CA. These stations were selected based on their series length, their exposure to the ocean, and the extent to which they represent distinct physical regions. For NB, CC, FI, and LJ, long salinity time series are analyzed as well. In addition, temperature from two ocean stations, OSP and OSN, are included to contrast coastal and central ocean sites. For the full study to follow this analysis, all coastal stations will be used. Table 1 shows the location and length of series analyzed here.

## Methods

Numerous statistical methods are available to remove “noise” from time series and enhance the signal of interest (*eg*, averaging, spectral filters, spline fits). Normally in smoothing splines,

$$y(t) = T(t) + S(t) + I(t) + E(t) \quad (1)$$

where  $y(t)$  is the total signal,  $T(t)$  the trend,  $S(t)$  the seasonal signal,  $I(t)$  the irregular stationary term, and  $E(t)$  the error, all at time  $t$ . You minimize a term that trades off the goodness of fit to the data with a smoothness constraint, some order of the derivatives are usually zero. Equivalent to smoothing splines, we assume finite differences are constrained. For a smoothness prior, we assume that the series trend, which is made up of the level

$$u(t) - (u(t-1) + b(t-1)) = e_1, N(0, \sigma^2_1) \quad (2a)$$

and slope

$$b(t) - b(t-1) = e_2, N(0, \sigma^2_2), \quad (2b)$$

is equal to a normal random variable  $N$  with zero mean and variance  $\sigma$  determined from the constraint that the term be zero. The resulting trend is non-parametric and non-linear. For a first-order trend, on the other hand, Equation 2a,b might be set to zero, giving a linear fit ( $y = u + bx$ ).

Likewise, for the seasonal term

$$\sum_{\tau=0}^{11} S(t-\tau) = e_3, N(0, \sigma^2_3) \quad (3)$$

we would assume some variance about the zero mean in  $N$ . The constraint that Equation 3 equals zero is equivalent to having a stationary seasonal signal; *ie*, each year would be composed of an identical annual curve composed of the averages of the calendar months. Instead, the

seasonal series is non-stationary and non-deterministic. The amplitude, phase and shape of the series can vary over any 12-month period, the mean of which is approximately zero. The non-zero mean of the series is included in the trend. The whole model can be put into state-space form and solved by a combination of Kalman filtering and maximum likelihood, after estimating the variance values initially.

An example of the various series generated by the model is given in Figure 3. The left graph shows the raw monthly La Jolla temperature series, with the trend superimposed in bold. The right graph shows the seasonal and AR (bold) series, plotted on the same scale. It is clear that the trend includes interannual variability, such as ENSOs, and decadal and longer-scale trends. Also note that the trend includes some super-annual variability, which was excluded from the seasonal series due the maximum likelihood calculations.

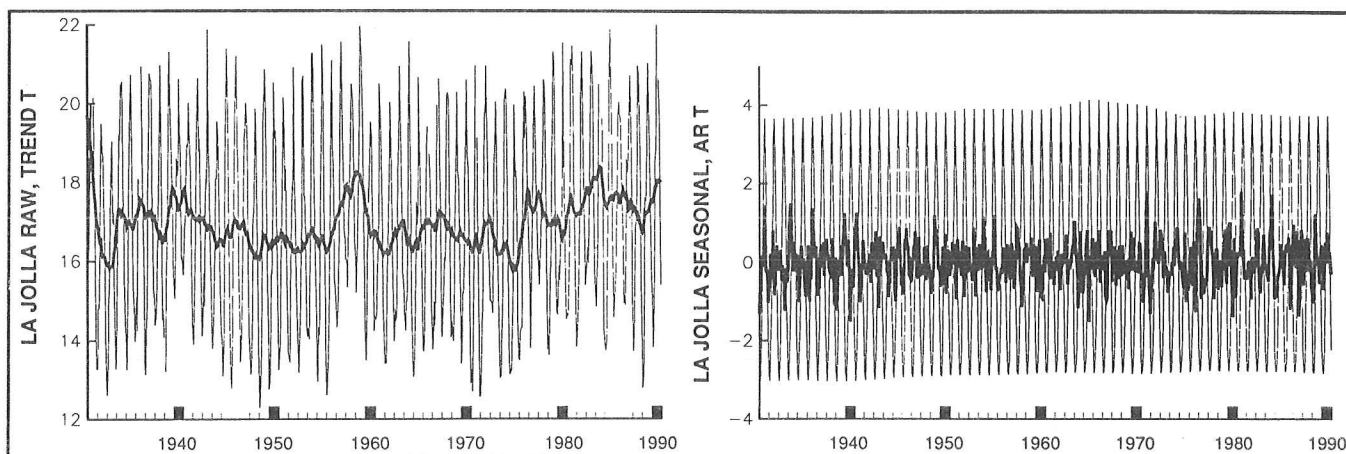


Figure 3. Example of Raw Monthly and State-Space Model Series for La Jolla Temperature, 1930-1990. Plot at left shows raw and trend model (bold) series; plot at right shows seasonal model and AR (bold) series. Units are in °C.

## Seasonal Patterns

I focus first on seasonal patterns, comparing seasonal series at LJ, FI, CC, and NB (Figure 4). Seasonal amplitude was smallest off central California, where coastal upwelling in spring and summer counters seasonal warming. This also resulted in an April temperature minimum and September temperature maximum off central California. Stations off southern California, northwestern United States, Vancouver Island, and Alaska had higher annual amplitudes, with a February minimum and September maximum. Phase shifts in months of temperature maxima and minima caused variations in annual amplitude throughout the series. The secondary maximum in February at FI also fluctuated over time.

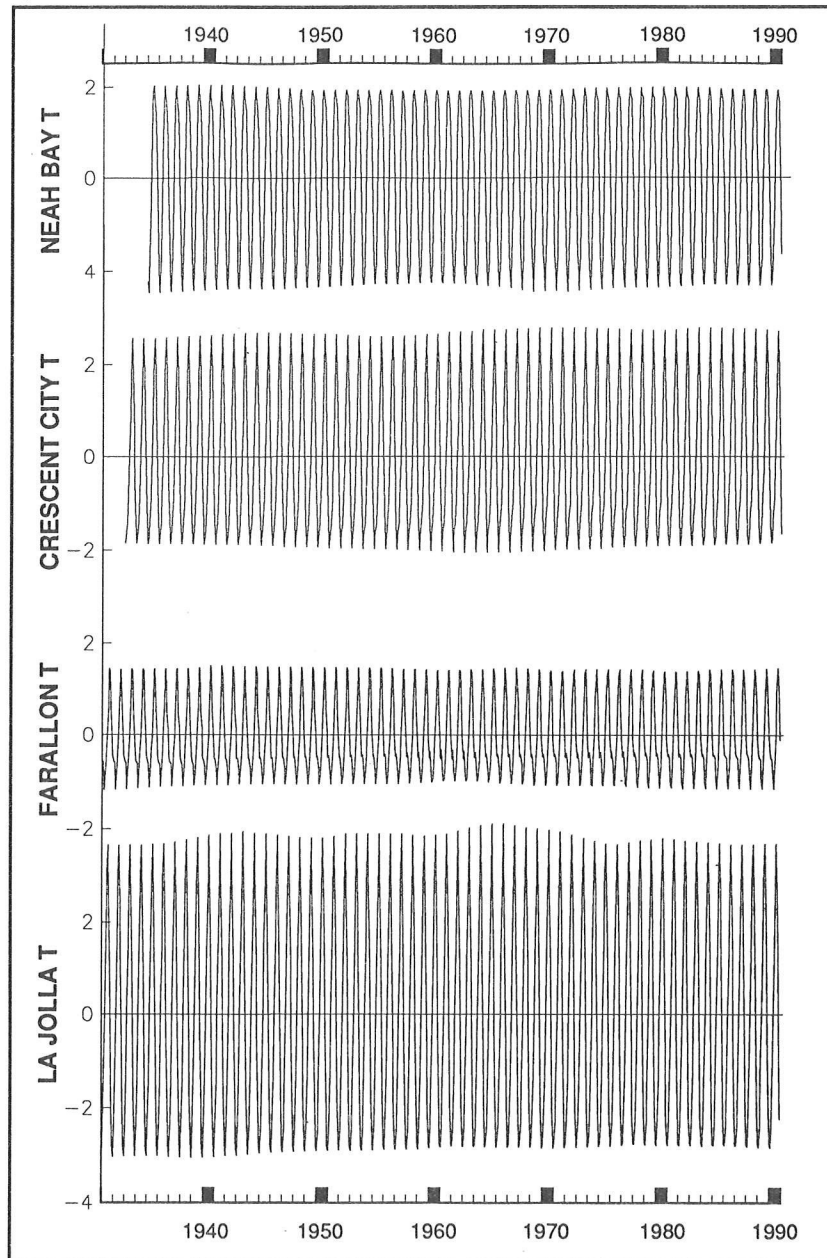


Figure 4. Seasonal Model Temperature Series at Neah Bay, Crescent City, Farallon Islands, and La Jolla, 1930-1990. Units are in °C.

In contrast, seasonal salinity had its largest amplitude off central California (Figure 5). Compare this to the very small amplitude at LJ (note the change in scale for LJ). At FI, the seasonal salinity minimum was in January/February; the maximum was in June/July. As with temperature, this is related to the importance of seasonal upwelling in this region. Other stations had January minima and August maxima (in phase with temperature). The minimum salinity displays more interannual variability at all sites, due to an upper limit on salinity set by the hydrographic characteristics of each region. Fluctuations in the salinity minimum were due mainly to precipitation and runoff variability.

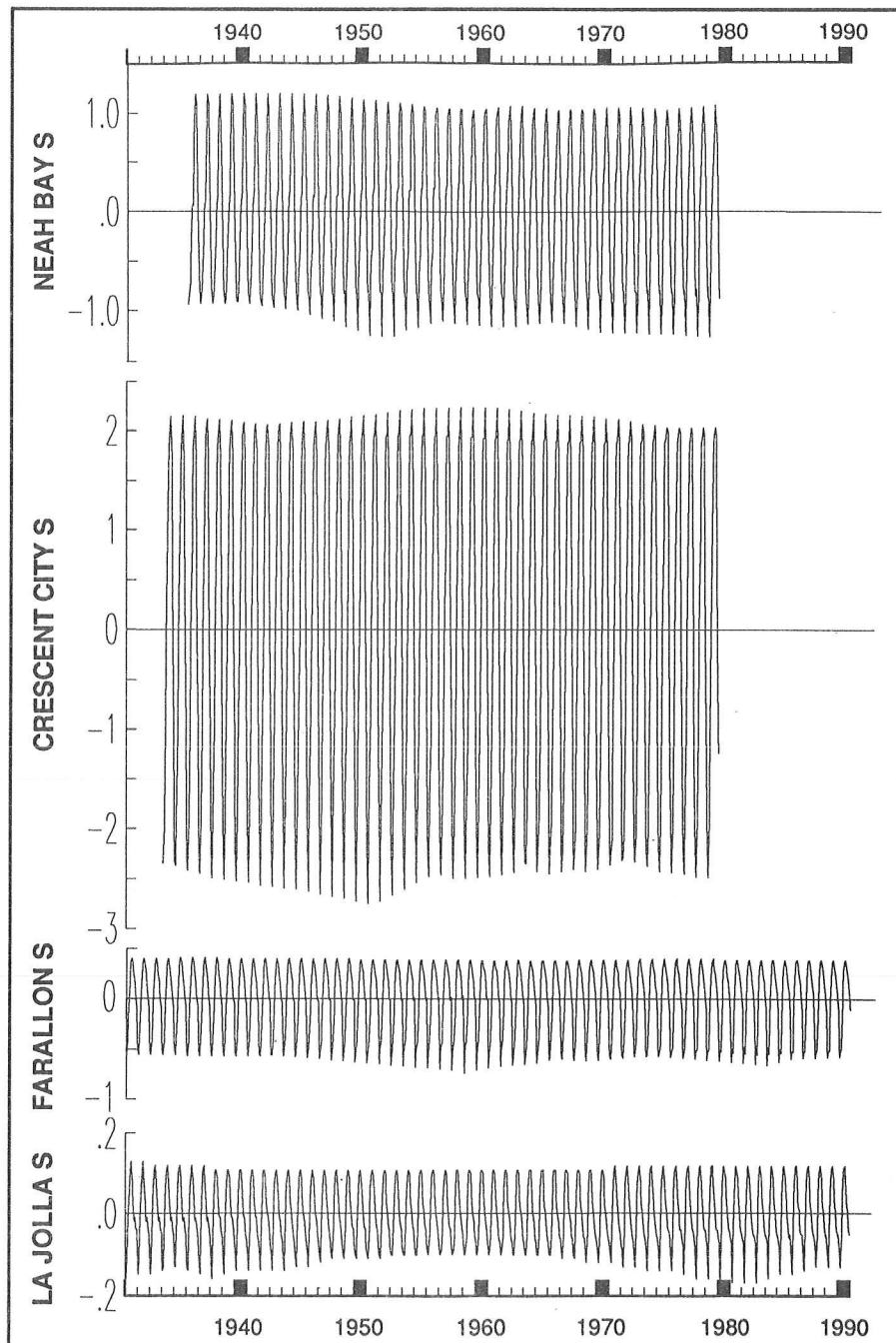


Figure 5. Seasonal Model Salinity Series at Neah Bay, Crescent City, Farallon Islands, and La Jolla, 1930-1990. Units are parts per thousand.

Again trends in salinity maxima and minima were associated with phase shifts, as well as changes in the magnitude of salinity in each month. At LJ, the lowest salinity minima (eg, 1938, 1982) were due to changes in March salinity, such that March values were much less than February at these times but greater than February when the salinity minimum was higher (eg, 1960). As with FI seasonal temperature, several stations show secondary salinity maxima and minima, which were due to phase shifts. Seasonal FI salinities in December were normally lower than in November, but December salinities were higher than in November in the late 1950s.

A close-up of FI seasonal temperature and salinity for 1960 to 1980 makes these patterns more apparent (Figure 6). The annual (January to December) signals are not sine curves, as they would be for a series-long annual average; temperature was negative 7 or 8 months each year (December to July). The spring minimum in temperature decreased uniformly from 1960 to 1980 due to a shift in the month of the minimum from April to May. There also was a shift in the maximum from September to October over this period. Generally, February temperatures were greater than January's, resulting in a secondary maximum. The difference in temperature between these months varied from 0.05 to 0.2°C. Near the start and end of the 60-year series (Figure 5), FI temperatures were lower in February than in January. Salinity was in quadrature with temperature at FI, but in phase off northwestern United States and southern California. At FI, salinities were lowest in January (occasionally in February), and greatest in July (occasionally in August). The salinity minimum decreased linearly from 1960 to 1980. Some phase shifting is seen in the winter salinity minimum.

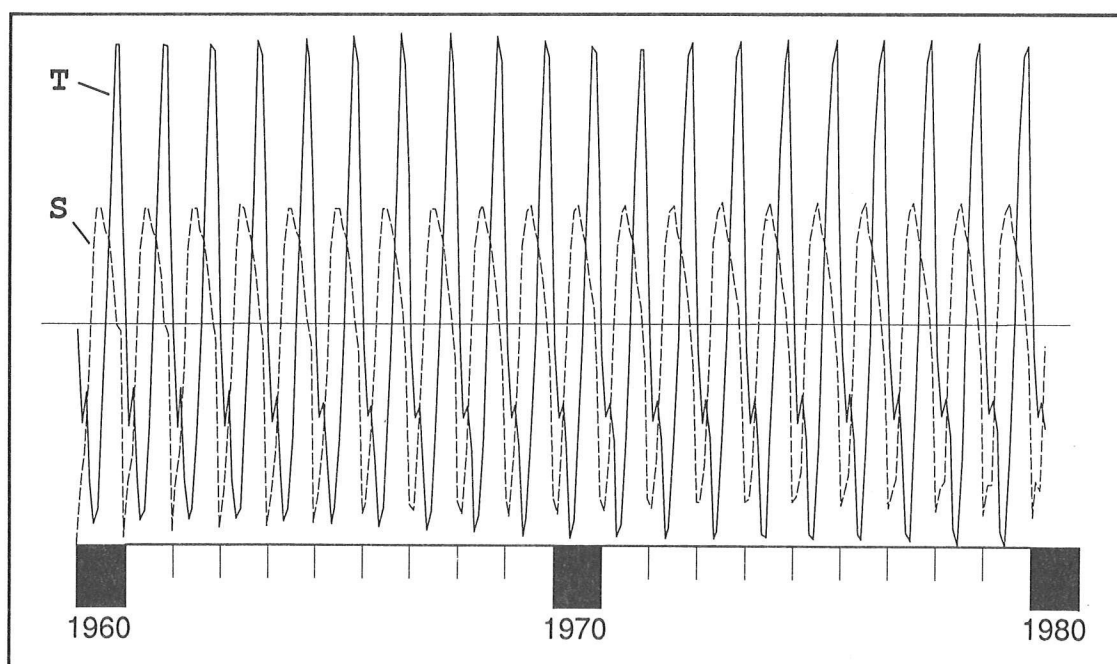


Figure 6. Detail of Farallon Islands Seasonal Model Series, 1960-1980.  
Temperature (T) is solid line; salinity (S) is broken line.

Mean temperature and salinity for April to July (the upwelling “season”) were calculated in each year from the seasonal model series for LJ, FI, CC, and NB (Figure 7). Except for LJ, all April-July seasonal temperature series decreased with time and all salinity series increased with time, implying increased upwelling. Magnitude of the changes was about 0.05-0.1°C and 0.1ppt over 60 years. Correlations versus time are highly significant. Changes in April-July temperature and salinity are not linear over time; certain years stand out as times of substantial change in slope (eg, 1943, 1963-1965). Regressions of temperature against salinity ( $T/S$ ) at NB, CC, and FI are highly significant and negative, consistent with the  $T/S$  upwelling relationship. The  $T/S$  LJ slope is positive and not statistically significant, implying multidecadal changes in upwelling are not a factor here. This is consistent with the fact that during these months, upwelling is a dominant process off northern and central California but not near LJ. A next step is to determine if variations in other environmental series (*ie*, wind, sea level) are linked to these fluctuations.

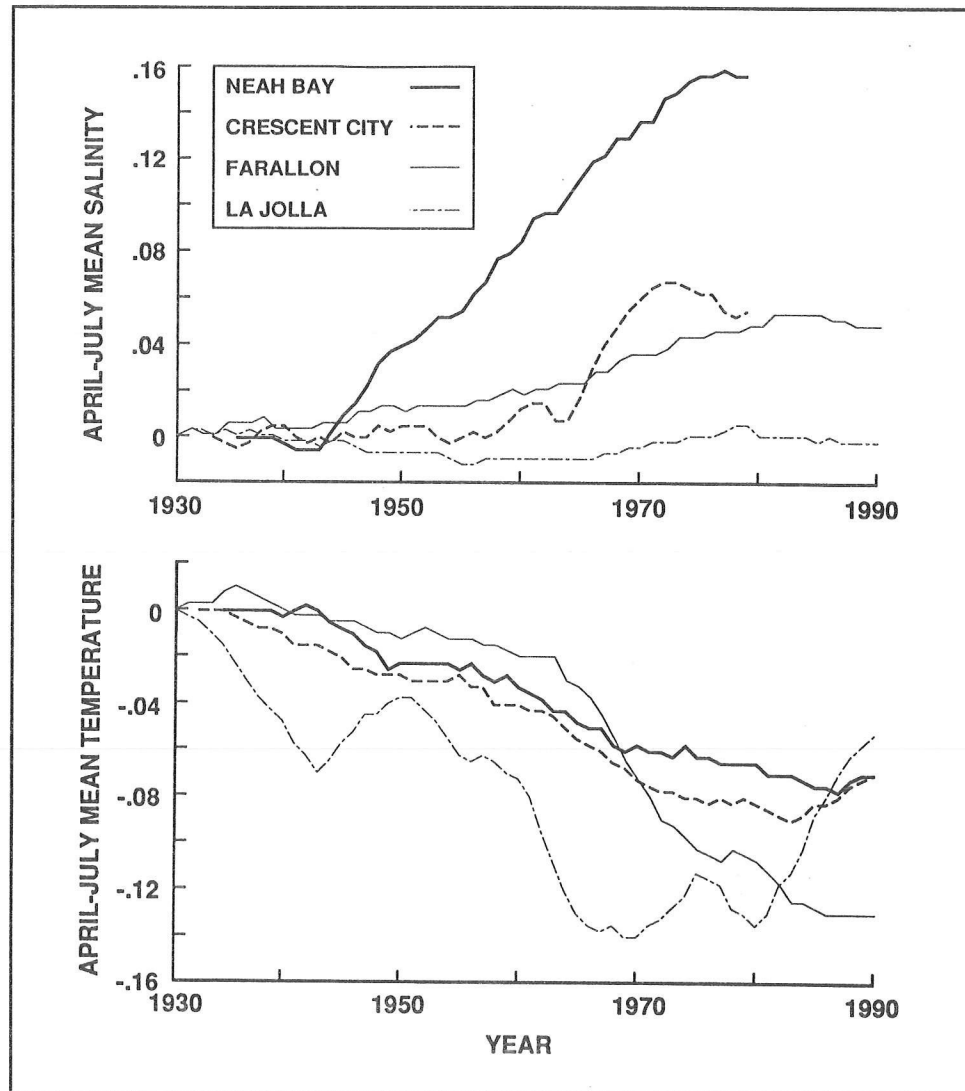


Figure 7. Time Series of Temperature and Salinity Averaged from April-July Monthly Values in Each Year, Derived from Seasonal Model Series, for Neah Bay, Crescent City, Farallon Islands, and La Jolla. Units are °C for temperature and parts per thousand for salinity.

Regression slopes of April-July temperature and salinity from the raw FI series against time are of the same signs as for the seasonal series (temperature negative, salinity positive) but not statistically significant (Table 2). Slopes in similar series derived from the model trend data are opposite (temperature positive, salinity negative) and less well correlated. Evidence for increased upwelling cannot be seen in the trend series, which are analogous to averaged, smoothed, or low-pass-filtered series. The FI April-July trend slopes and *r* values for temperature and salinity are virtually identical to those for the annual averages, implying that seasonal effects of upwelling do not occur in the trend series. The raw FI annual averages are the same sign as these, but opposite the sign of the April-July raw averages. Changes in temperature and salinity due to upwelling are an order of magnitude lower than the climate change variations in these series, and they are confined to spring and summer and, thus, are dwarfed by the trends of increasing temperature and decreasing salinity (at FI) in the raw observations.

Table 2  
SLOPE OF LINEAR FIT AND CORRELATION (*r*) BETWEEN  
AVERAGE FARALLON ISLANDS TEMPERATURE AND SALINITY VERSUS YEAR,  
DETERMINED FROM SEASONAL AND TREND MODEL SERIES AND FROM  
RAW MONTHLY-AVERAGE TIME SERIES

*NS denotes r is not significant at the 0.05 level.*  
*April-July refers to yearly averages for those months; 12 month refers to yearly averages for all months.*

		Temperature		Salinity	
		Slope (°C/year)	<i>r</i>	Slope (ppt/year)	<i>r</i>
Seasonal	(April-July)	-0.0027	-0.94	0.0010	0.97
Trend	(April-July)	0.0159	0.30	-0.0111	-0.28
	(12 month)	0.0179	0.33	-0.0127	-0.29
Raw	(April-July)	-0.0075	-0.15(NS)	0.0037	0.22(NS)
	(12 month)	0.0100	0.26(NS)	-0.0023	-0.24(NS)

Examination of other stations reveals similar patterns. AV, BB, and OSN all show a net decrease in April-July temperature over the length of the seasonal series, counter to the temperature increase in the trend series at these sites. In contrast, OSP temperature increased over this period. Stations north of 50°N show no steady pattern in April-July temperature.

Phase shifts in the coastal series may be related to temporal shifts in wind stress or large-scale current patterns (*eg*, California Undercurrent/ Davidson Current). A time series of yearly averages of monthly estimates of April-September alongshore wind stress off California (Bakun 1990) shows a statistically significant increase over time, corresponding to an increase in upwelling intensity. The series trend agrees with that at other latitudes along the western North American coast and other coastal upwelling regions. Thus, there may be a relationship between long-term increases in wind stress and coastal upwelling rates along the west coast, which would be most obvious during spring and summer. Further analysis of coastal wind, temperature, salinity, and sea level series is needed to clarify this relationship.

## Trend Series

Trend model series for the eight coastal sites examined, plus OSN and OSP, are presented in Figure 8. Temperature series are offset, relative to Seward, by the amount ( $^{\circ}\text{C}$ ) shown in parentheses. Note that the model fits a trend through missing observations. Some of these periods are apparent (eg, FI in 1943-1954). Major ENSO events (Quinn *et al* 1987) are shown with the darker shaded vertical lines; moderate ENSO years are shown with the lighter shaded vertical lines.

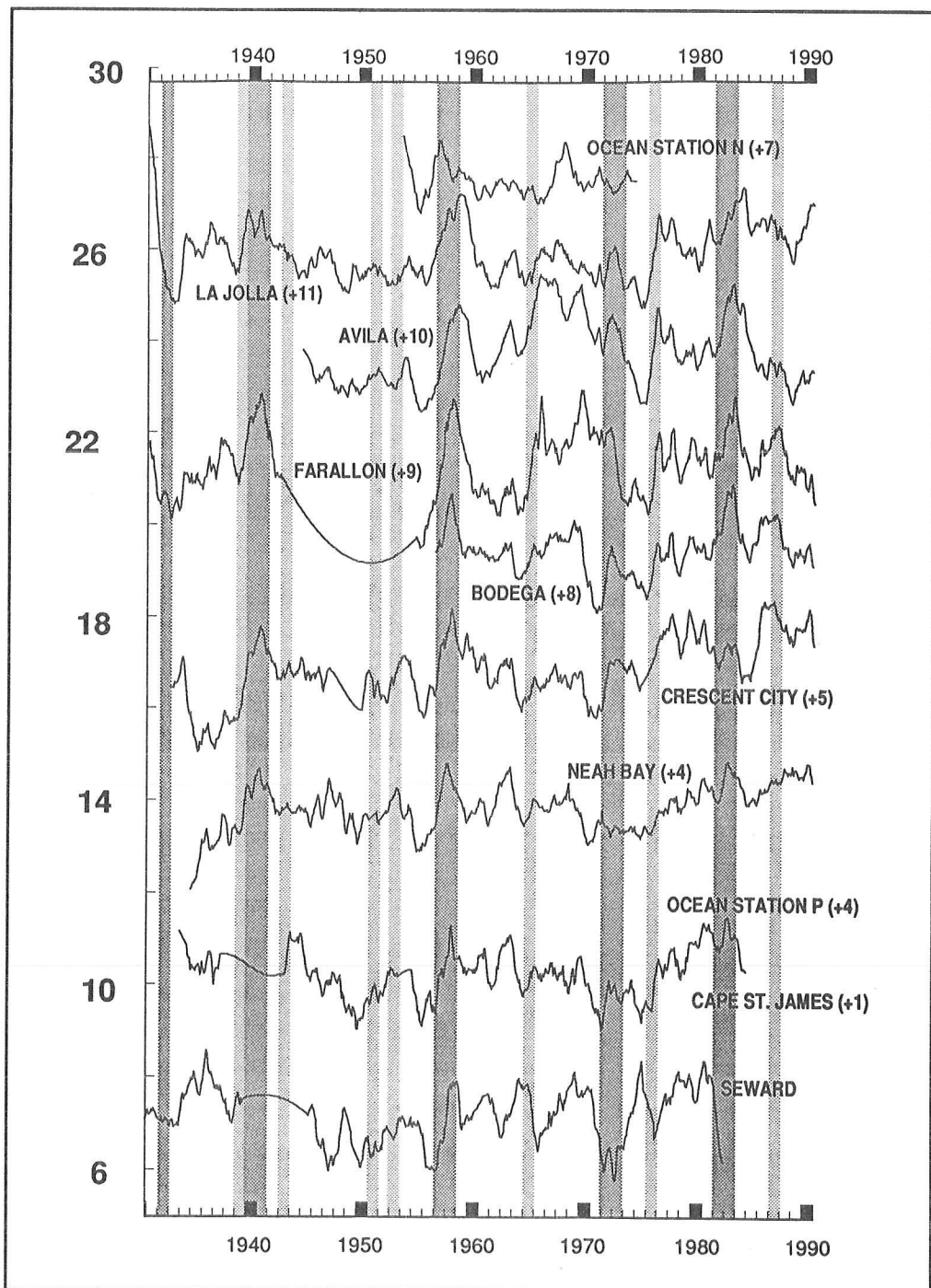


Figure 8. Trend Model Series for Temperature, 1930-1990.

Values in parentheses denotes vertical offset of series, in  $^{\circ}\text{C}$ , relative to Seward. Darker shaded vertical lines show major ENSO events; lighter shaded vertical lines show moderate ENSO events, based on Quinn *et al* (1987).

are noted by lighter shaded lines. Large-scale warming effects of ENSOs are seen. Some ENSO events (*eg*, 1973) appear to be constrained to southern stations.

Numerous other regional differences in the trends are evident. Most sites have series-length warming trends that are highly non-linear and display considerable variability on annual/decadal scales. Most series have 10- to 20-year periods of relatively level temperature, followed by 10- to 20-year periods of rapid temperature increase. Some series have multi-year periods of decreasing temperature. Interannual variation on a 2-year period is seen frequently at most sites, possibly the Quasi-Biennial Oscillation (CD Keeling, pers comm).

Finally consider the suggested shifts to a cool regime in 1941 and to a warm regime in 1975 (Figure 1). The 1975 shift occurs rapidly at LJ and AV. At sites farther north, shifts are less dramatic and occur over several years, appearing more as gradual transitions than sudden shifts. The cool shift in 1941 is more difficult to document and appears less dramatic at LJ relative to the 1975 shift. The regime shift concept may be valid for some regions (*eg*, southern California), but it has a considerable degree of inter-regional difference. Keep in mind that series presented here are model trends derived from the monthly values of temperature (12/year) with the seasonal patterns removed, very different from those in Figure 1, which are annual averages (1/year). Future studies should focus on what mechanisms may be responsible for such shifts (*eg*, ENSO), and how the effect spreads along the coast (*ie*, a sudden shift off southern California that "diffuses" northward).

The salinity trend series (LJ, FI, CC, NB) show even larger regional differences (Figure 9). Large fluctuations are correlated visually to the PACLIM freshwater runoff series (Cayan et al 1988); *ie*, NB to Puget Sound (about 1945), CC to Columbia River, FI to San Francisco Bay. Lack of significant freshwater input near LJ may be responsible for the relatively small variations there. ENSOs are evident as lower salinity, presumably due to greater runoff associated with higher rainfall. The most outstanding features in LJ salinity are the sudden drops in 1941 and 1976, coincident with the regime shifts. This suggests that large-scale changes in current patterns, which probably dominate water characteristics at LJ, may be linked to such shifts.

Bakun (1990) noted a significant increase in April-September alongshore wind stress off California. However, the pattern reversed in the mid-1970s toward decreasing wind stress, corresponding to the increase in the temperature trend series, especially that at LJ. Thus, there is a potential link between "regime shifts" in wind and temperature. It will be enlightening to apply the state-space model to the wind series analyzed by Bakun, and compare upwelling trend and seasonal model series for wind to patterns in the ocean temperature model series described here.

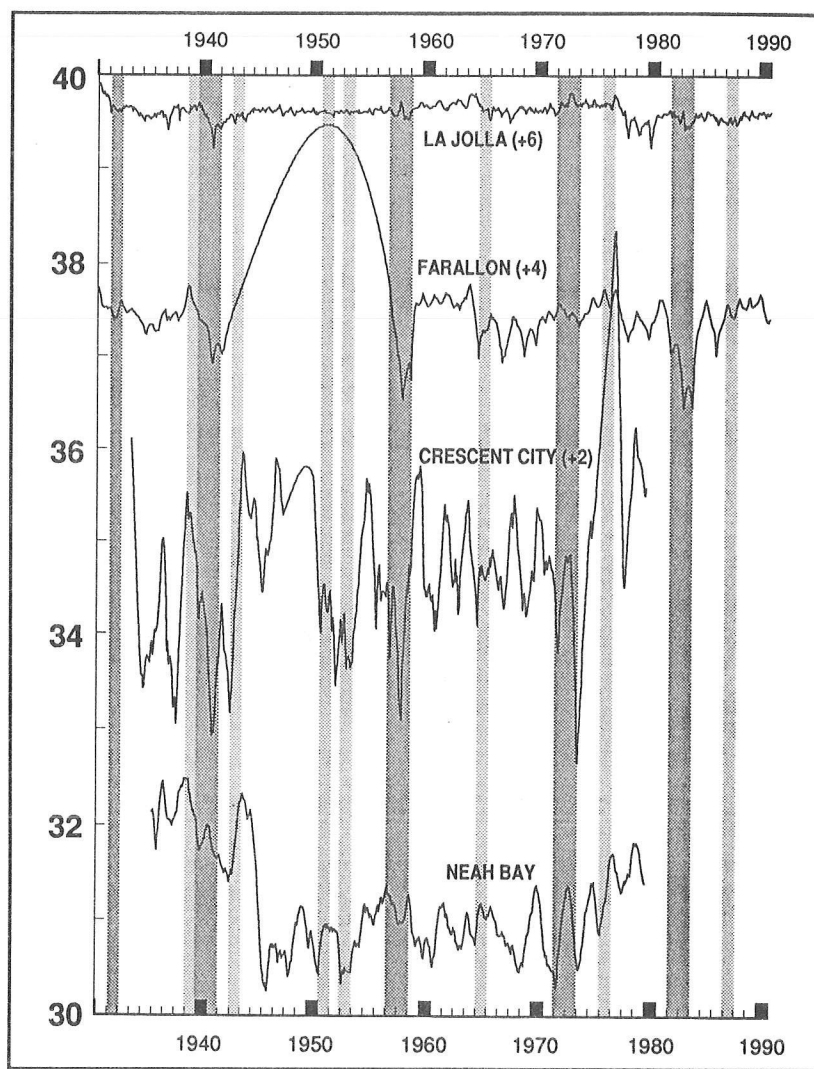


Figure 9. Trend Model Series for Salinity, 1930-1990.  
 Values in parentheses denotes vertical offset of series, in ppt, relative to Seward.  
 Darker shaded vertical lines show major ENSO events; lighter shaded vertical lines  
 show moderate ENSO events, based on Quinn *et al* (1987).

Table 3 shows correlations ( $r$ ) between various trend model series. Values in the upper-right half of the matrix are correlations between temperature for the ten stations. The sparse lower-left portion of the matrix shows  $r$  values representing salinity at four sites (LJ, FI, CC and NB). Underlined values on the diagonal are correlations between temperature and salinity at those four sites. Because the series have different lengths, the number of observations ( $n$ ) differs for various pairings ( $n=252(w/OSN)-720$ ). Correlations that are not statistically significant (0.05 level) are italicized. Correlations between temperature at most stations are significant, probably due to ENSOs and interannual events (large-scale processes); all are positive. LJ temperature is particularly well correlated with other sites. Seward and OSN temperatures are generally uncorrelated with other series. Correlations between temperature series are greater than between salinity series, and the sign for salinity is not consistent. A strong negative  $T/S$  correlation is seen at FI; the other three  $T/S$  correlations are smaller. Of the four sites examined, only CC has a positive  $T/S$  correlation.

Table 3  
CORRELATIONS BETWEEN COASTAL STATION TEMPERATURE AND SALINITY TREND SERIES

Upper-right diagonal shows *r* values between temperature series.  
Lower-left diagonal shows *r* between salinity series for Neah Bah, Crescent City, Farallon Islands, and La Jolla.  
Correlations between temperature and salinity at these four sites are underlined.  
Correlations not statistically significant (0.05 level) are italicized.

	Correlations Between Shore Stations								
	SE	CJ	NB	CC	BB	FI	AV	LJ	OSN
OS P	0.14	0.57	0.54	0.64	0.47	0.22	0.08	0.43	0.21
Seward	==	0.44	0.01	0.01	0.01	0.42	0.23	0.19	-0.08
Cape St. James		==	0.52	0.39	0.70	0.42	0.47	0.52	0.05
Neah Bay			<u>-0.17</u>	0.76	0.67	0.30	0.23	0.50	0.31
Crescent City			0.06	<u>0.17</u>	0.58	0.34	0.10	0.49	0.34
Bodega Bay					==	0.55	0.37	0.66	0.24
Farallon Islands			-0.35	0.17		<u>-0.86</u>	0.56	0.73	0.10
Avila							==	0.43	0.08
La Jolla			-0.34	0.22		0.14		<u>-0.16</u>	0.35

With the exception of OSP (Table 4), linear fits to all coastal temperature trend series versus time have positive slopes and, except for the two northernmost stations and OSN, are statistically significant (despite the considerable non-linear shape of the series). The greatest slopes are seen off northern and central California, despite the fact that the standard deviations

Table 4  
ESTIMATES OF LINEAR FITS TO TEMPERATURE AND SALINITY TREND SERIES AGAINST TIME

*r* denotes correlation between series and time.

Temperature				
	Series Mean (°C)	Linear Slope (°C/yr)	Standard Deviation of Slope (°C/yr)	<i>r</i>
Seward	7.22	0.0015	0.0015	0.04
Cape St. James	9.26	0.0024	0.0014	0.07
Neah Bay	9.84	0.0136***	0.0010	0.45***
Crescent City	11.84	0.0244***	0.0012	0.60***
Bodega Bay	11.45	0.0070**	0.0025	0.14**
Farallon Islands	11.97	0.0179***	0.0019	0.33***
Avila	13.75	0.0132***	0.0022	0.24***
La Jolla	16.94	0.0060***	0.0013	0.18***
OS P	8.25	0.0048*	0.0024	0.10*
OS N	20.53	-0.0060	0.0034	-0.11

Salinity				
	Series Mean (ppt)	Linear Slope (ppt/year)	Standard Deviation of Slope (ppt/year)	<i>r</i>
Neah Bay	31.17	-0.0174***	0.0017	-0.41***
Crescent City	30.81	0.0220***	0.0026	0.34***
Farallon Islands	33.72	-0.0117***	0.0014	-0.29***
La Jolla	33.60	-0.0005**	0.0002	-0.10**

\* P<0.05  
\*\* P<0.01  
\*\*\* P<0.0001

of slopes are similar in all regions. The FI temperature slope is three times that for the LJ series for the common 60-year period analyzed here, so differences in the series length do not necessarily account for the differences in slope. It is obvious, however, that because of the substantial decadal swings in temperature and salinity (Figures 8 and 9), analysis of different length series could provide very different linear fits. For salinity, the LJ slope and standard deviation is much smaller than the others. The slope for CC salinity versus time is positive; NB, FI, and LJ are negative.

## Summary

---

The state-space model appears to be a powerful tool in separating interannual-to-interdecadal fluctuations in environmental time series from seasonal patterns of variability. Further testing of the method on additional time series will provide a better indication of its applicability and, hopefully, a more thorough understanding of the linkages between long-term variations in atmospheric forcing and the coastal ocean's response to this variability, as well as the potential contribution of natural and anthropogenic signals, and regional differences in these effects. Results presented here demonstrate the importance of evaluating temporal and spatial variability over the entire spectrum, rather than simply at global climate scales, when examining long-term environmental fluctuations.

The results show a clear separation of the non-stationary seasonal signal from the non-linear trend for coastal ocean temperature and salinity. Overall, the temperature trend series are highly correlated with each other. Superimposed on a general, statistically significant pattern of increasing temperature are significant fluctuations on annual-decadal scales (*eg*, ENSO, "regime shifts"), as well as substantial regional differences in the rate of warming and in the degree to which interannual events affect the overall trend. Salinity trends are more ambiguous but appear to be linked to regional differences in freshwater runoff and possibly changes in ocean circulation.

Like the trend series, significant regional differences were found in the seasonal series. The utility of estimating non-stationary seasonal patterns is demonstrated with the finding of a systematic decrease in temperature and increase in salinity during spring and summer, evidence that coastal upwelling is increasing in intensity. This pattern cannot be discerned in the trend series and is not statistically significant in the raw observations. It also is most prevalent in areas where seasonal upwelling is a major process. Shifts in the phase and amplitude of the seasonal cycle over several decades are suggested with this technique as well.

In future studies, the entire set of coastal temperature and salinity data will be incorporated with series of wind and sea level observations to examine the relationship between atmospheric and oceanic variables. The model will be updated to derive separate estimates of trend and

seasonal series common to the entire set (*ie*, the “global” signal), in contrast to those unique to regions or even individual sites. This will provide a better contrast between truly global/climate changes and regional/ecosystem level environmental fluctuations. The addition of other model terms to estimate the role of phenomena such as ENSO and the QBO will be considered as well.

## Acknowledgments

---

The author greatly acknowledges Dr. Roy Mendelsohn, PFEG, Monterey, California, for his assistance and expertise in development and application of the state-space model. Data used in the analysis were supplied by Dr. John McGowan and Pat Walker, MLRG, Scripps Institution of Oceanography, La Jolla, California, and obtained from the PACLIM Time Series Data Base. I also thank Dr. Dave Keeling, SIO, for his provocative comments following the presentation of these results at the PACLIM '93 Workshop.

## References

---

- Bakun, A. 1990. Global Climate Change and Intensification of Coastal Ocean Upwelling. *Science*. 247:198-201.
- Bottomley, M, CK Folland, J Hsiung, RE Newell, DE Parker. 1990. *Global Ocean Surface Temperature Atlas (GOSTA)*. Joint Met. Office/Massachusetts Institute of Technology Project. 20+iv pp and 313 plates. HMSO, London.
- Cayan, DR, DR McLain, WD Nichols, JS DiLeo-Stevens. 1988. *Monthly Climatic Time Series Data from the Pacific Ocean and Western Americas*. USGS Open-File Report. 379 pp.
- Folland, CK, TR Karl, KY Vinnikov. 1990. Observed Climate Variations and Change. Pages 195-238 in *Climate Change, the IPCC Scientific Assessment*. JT Houghton, GJ Jenkins, JJ Ephraums (editors). WMO/UNEP/IPCC. Cambridge University Press.
- Jones, PD, TML Wigley, G Farmer. 1991. Marine and Land Temperature Sets: a Comparison and a Look at Recent Trends. Pages 153-172 in *Greenhouse-Gas-Induced Climatic Change: a Critical Appraisal of Simulations and Observations*. ME Schlesinger (editor) Elsevier, Amsterdam.
- MacCall, AD, and MH Prager. 1988. Historical Changes in Abundance of Six Fish Species Off Southern California, Based on CalCOFI Egg and Larva Samples. *CalCOFI Reports*. 29:91-101.
- Quinn, WH, VT.Neal, SE Antunez de Mayolo. 1987. El Niño Occurrences over the Past Four and a Half Centuries. *Journal of Geophysical Research*. 92:14,449-14,461.



# **Appendix A**

## **AGENDA**

---

Tenth Annual Pacific Climate (PACLIM) Workshop,  
April 4-7, 1993



# AGENDA

Tenth Annual Pacific Climate Workshop  
Asilomar Conference Center, Pacific Grove, California  
April 4-7, 1993

Meal Schedule  
Breakfast 7:30-9:00 am  
Lunch 12:00-1:00 pm  
Dinner 6:00-7:00 pm

## Sunday Evening, April 4, 1993

### **Recent Weather/Climate Variability**

Moderator: Walt Dean

- 7:00-7:20 Welcome and Announcements
- 7:20-7:40 *Recent Climate Anomalies in the Western United States, 1992/1993*  
Kelly Redmond, Western Regional Climate Center, Reno, NV
- 7:40-8:00 *Is the California Drought Over?*  
Maurice Roos, California Department of Water Resources, Sacramento, CA
- 8:00-8:20 *Operation of Real-Time Warning System for Debris Flow in San Francisco Bay Area*  
Gary Barbato, Raymond Wilson, and Robert Mark, National Weather Service, Redwood City, CA
- 8:20-8:40 *Satellite Views of North American Weather and Climate, 1991-1992*  
Tom Murphree, Mark Boothe, and Mike McCann, Naval Postgraduate School, Monterey, CA
- 8:45 — Social

## Monday Morning, April 5, 1993

### **Invited Talks, Remote Sensing and Climate**

Moderator: Dan Cayan

- 8:15-8:55 *Satellite Estimates of Surface Velocity, Chlorophyll Concentration, and Temperature in the California and Peru-Chile Current Systems*  
Ted Strub, Corinne James, and Andrew Thomas, Oregon State University
- 8:55-9:35 *An Experimental Land Cover Characteristics Data Base and Its Potential Use in Land-Atmosphere Interactions Modeling*  
Louis Steyaert, Thomas Loveland, James Merchant, Jesslyn Brown, and Bradley Reed, U.S. Geological Survey, Reston, VA
- 9:35-10:10 *Land Surface Characterization Using Multidate AVHRR Imagery*  
Frank Davis, University of California, Santa Barbara
- 10:10-10:25 Poster Introductions (One Minute Each)
- 10:25-10:55 Break

- 10:55-11:35 *Airborne and Satellite Snow Cover Mapping for the Coterminous United States, Alaska, and Canada*  
Tom Carroll, National Weather Service, NOAA, Minneapolis, MN
- 11:35-12:15 *Management of High Volume Remote Sensing Data (Sequoia 2000: Archiving, Processing, and Graphics for Massive Climate Data Sets)*  
Jim Frew, University of California, Berkeley

Monday Afternoon, April 5, 1993

**Invited Talks, Remote Sensing and Climate** (continued)

- 1:40-2:20 *Unmasking the Face of the Sea Floor: Advances and Challenges in Sonar Mapping*  
Mike Field, U.S. Geological Survey, Menlo Park, CA
- 2:20-3:00 *Remote Sensing of Climate-Related Geological Phenomena in Arid Regions*  
Carol Breed, U.S. Geological Survey, Flagstaff, AZ
- 3:00-3:30 Break
- 3:30-3:50 *Passive Microwave Remote Sensing of Snowpacks*  
Ed Josberger, Per Gloersen, Al Chang, and Al Rango, U.S. Geological Survey, Tacoma, WA
- 3:50-4:10 *Application of Satellite-Derived Products for Near Real-Time Climate Monitoring*  
Alan Basist and Norman Grody, NOAA, Climate Analysis Center, Camp Springs, MD

Monday Evening, April 5, 1993

**Invited Talk**

- 7:30-8:25 *Regional to Global Scale Temperature and Precipitation Inferred from the Microwave Sounders*  
John Christy, University of Alabama, Huntsville
- 8:30— Social

Tuesday Morning, April 6, 1993

**Regional Hydrological Variability**

Moderator: Roy Walters

- 8:30-8:50 *ENSO and Western United States Climate: An Upper Air Perspective*  
Kelly Redmond and Daniel Cayan, Western Regional Climate Center, Reno, NV
- 8:50-9:10 *Semiempirical Down-Scaling of Coarse-Resolution GCM Output for the Western United States to the Local Scale for Temperature, Precipitation, and Streamflow*  
Rick Freeman and John Dracup, University of California, Los Angeles
- 9:10-9:30 *California Precipitation Patterns During Warm ENSO Events*  
Joel Michaelsen, University of California, Santa Barbara
- 9:30-9:50 *Low-Frequency Climatic Variability and the Frequency of Winter Floods in the Southwestern United States*  
Robert Webb and Michael Dettinger, U.S. Geological Survey, Tucson, AZ
- 9:50-10:20 Break

- 10:20-10:40 *Winter Atmospheric Circulation and Drought in the Sierra Nevada*  
Michael Dettinger and Daniel Cayan, U.S. Geological Survey, San Diego, CA
- 10:40-11:00 *Meteorologic Influences on the Stable Isotope Signals of Rainfall in Central California*  
Eric Edlund, Leticia Menchaca, and B. Smith, University of California, Berkeley
- 11:00-11:20 *Development of an Isohyetal Analysis for Oregon Using the Prism Model*  
George Taylor, Chris Daly, and Wayne Gibson, Oregon State University
- 11:20-11:40 *Interannual Variations in the United States West Hydrologic Cycle*  
John Roads, Konstantine Georgakakos, Alex Guetter, and Shyh-Chin Chen,  
Scripps Institution of Oceanography, La Jolla, CA
- 11:40-12:00 *Validation of Cloud Fields Predicted by Regional Climate Modeling for  
Western United States*  
Melanie Wetzel, Desert Research Institute, Reno, NV

Tuesday Afternoon, April 6, 1993

**Regional Climate Variability**

Moderator: Kelly Remond

- 1:30-1:50 *Rapid Teleconnections Associated with Individual Tropical Cyclones*  
Ronald Gelaro, Tom Murphree, and James Goerss, Naval Research Laboratory,  
Monterey, CA
- 1:50-2:10 *The Climate of the H.J. Andrews Experimental Forest, Oregon, and Its Regional Context*  
David Greenland, University of Oregon, Eugene
- 2:10-2:30 *The Quasi-Biennial Oscillation as Seen in Global Marine Temperature Records  
Since 1860*  
Charles Keeling and Timothy Whorf, Scripps Institution of Oceanography, La Jolla, CA
- 2:30-2:50 *Seasonal Trends of Maximum and Minimum Temperatures in California*  
Lynda Klein and Jim Goodridge, California State University, Chico
- 2:50-3:20 Break
- 3:20-3:40 *Near and Distant Connection of Atmospheric Processes to Ocean Temperature Change  
in the Coastal California Current Region*  
Jerrold Norton, Daniel Cayan, and Douglas McLain, Pacific Fisheries, Monterey, CA
- 3:40-4:00 *Biases in Long-Term Environmental Data Series and Their  
Implications for Fisheries Oceanography*  
Claude Roy and Richard Parrish, Pacific Fisheries, Monterey, CA
- 4:00-4:20 *Long-Term Patterns in Coastal Temperature and Salinity Along the  
North American West Coast*  
Frank Schwing, Pacific Fisheries, Monterey, CA

Tuesday Evening, April 6, 1993

**Invited Talks**

- 7:30-8:25 *Archeological Reconstruction of the Early Holocene Environment in California*  
James West, U.S. Bureau of Reclamation, Sacramento, CA
- 8:25-8:30 *A Submersible View of Disaerobic and Cold Vent Fauna Along the Peru Margin*  
Walt Dean, U.S. Geological Survey, Denver, CO
- 8:30— Social

Wednesday Morning, April 7, 1993

**Paleoclimate Studies**

Moderator: Carolyn Isaacs

- 8:30-8:50 *Late Pleistocene and Holocene Moisture Sources in Mexico and the Caribbean*  
Platt Bradbury, U.S. Geological Survey, Denver, CO
- 8:50-9:10 *Spatial Variations of Precipitation Regimes in the Western United States:  
An Explanation for Regional Heterogeneity in the Paleoclimatic Record*  
Cathy Whitlock and Patrick Bartlein, University of Oregon, Eugene
- 9:10-9:30 *Century-Scale Pulsations in Delivery of Pacific Moisture to the  
Interior of North America*  
Roger Anderson and Bruce Allen, University of New Mexico, Albuquerque
- 9:30-9:40 *Age Distribution of Laminated Sediments on the Continental Slopes of North America*  
Eileen Hemphill-Haley, U.S. Geological Survey, Menlo Park, CA
- 9:40-10:10 Break
- 10:10-10:20 *Modern and Ancient Floods on the Narmada River, Central India*  
Lisa Ely, Pennsylvania State University
- 10:20-10:40 *CO<sub>2</sub>-Driven Changes in Limber Pine (*Pinus flexilis*) Morphology and Physiology  
During the Last 25,000 Years*  
Pete Van de Water, Steven Leavitt, and Julio Betancourt, University of Arizona,  
Tucson
- 10:40-11:00 *Understanding Coupled Climatic, Hydrological, and Ecosystem Response to GCC in  
the Colorado Rockies Biogeographical Area*  
Tom Stohlgren, Jill Baron, Timothy Kittel, National Park Service, Ft. Collins, CO

# **Appendix B**

## **POSTERS**

---

Tenth Annual Pacific Climate (PACCLIM) Workshop,  
April 4-7, 1993



## POSTER PRESENTATIONS

---

Tenth Annual Pacific Climate Workshop  
Asilomar Conference Center, Pacific Grove, California  
April 4-7, 1993

*A Long Mid-Pleistocene Pollen Record from Buck Lake, Klamath County, Oregon*

David Adam and Andrei M. Sarna-Wojcicki, U.S. Geological Survey, Menlo Park, CA

*Paleoclimate Interpretations of Montane Meadow Stratigraphies from the Sierra Nevada: Comparisons with Other Proxies*

Scott Anderson, Northern Arizona University, Flagstaff

*The Paleoclimatic Potential of Laminated Lake Sediments in West Central Mexico: Laguna de Juanacatlan, Jalisco, Mexico*

Roger Byrne and Leticia Menchaca, University of California, Berkeley

*Modeling Global Climate Change Impacts on Glacier National Park*

Daniel Fagre, National Park Service, West Glacier, MT

*Paleoclimate Reconstructions from Remote Sensing of Bajades, Western North America*

Alan Gillespie, University of Washington, Seattle

*Coastal Temperature-Salinity and the Bakun Upwelling Index*

John McGowan, Scripps Institution of Oceanography, La Jolla, CA

*Convective and Rotational Parameters Associated with Three Tornado Episodes in Northern and Central California*

John Monteverdi and John Quadros, San Francisco State University, San Francisco, CA

*California Rainfall Related to Type 1 ENSO Events*

Jan Null, National Weather Service, Redwood City, CA

*Modeling the Effect of Snow on Seasonal Runoff in the Truckee River Drainage Basin*

Richard Orndorff and Richard Craig, Kent State University, Kent, OH

*Performance of Seasonal Streamflow Models During Prolonged Drought Episodes?*

Larry Riddle, Scripps Institution of Oceanography, La Jolla, CA

*Seasonal Resolution, Santa Barbara Basin Paleoceanography*

Arndt Schimmelmann, C. Lange, G. Kuhn, W. Berger, and M. Tegner, Scripps Institution of Oceanography, La Jolla, CA

*A Numerical Study of the Effects of Sea Level Rise: Delaware Bay*

Roy Walters, U.S. Geological Survey, Tacoma, WA

*DMSP Data for Real-Time Access*

Warren Yogi, NOAA, Monterey, CA



**Appendix C**  
**ATTENDEES**

---

Tenth Annual Pacific Climate (PACLIM) Workshop,  
April 4-7, 1993



## ATTENDEES

Tenth Annual Pacific Climate Workshop Attendees  
Asilomar Conference Center, Pacific Grove, California  
April 4-7, 1993

David Adam  
US Geological Survey - MS 915  
345 Middlefield Road  
Menlo Park, CA 94025  
415/329-4970  
Fax FTS 459-4975

Diana Anderson  
University of California, Riverside  
Dept of Earth Sciences  
Riverside, CA 92521  
714/787-2194  
Fax 714/787-4324

R Scott Anderson  
ES&Q Studies Program  
Box 6013, North Arizona University  
Flagstaff, AZ 86011  
602/523-5821  
Fax 602/523-7290  
anderson@nauvax.ucc.nau.edu

Roger Y Anderson  
University of New Mexico  
Dept of Earth & Planetary Sciences  
Albuquerque, NM 87131  
505/277-1639  
Fax 505/277-8843  
ryand@triton.unm.edu

Lisa Ramirez Bader  
US Geological Survey  
Box 25046, MS 939, DFC  
Denver, CO 80225  
303/236-5547  
Fax 303/236-0459  
lbader@sedproc.cr.usgs.gov

Gary E Barbato  
NOAA/National Weather Service  
660 Price Avenue - Forecast Office  
Redwood City, CA 94063-1497  
415/364-4610  
Fax 415/364-2599

Alan Basist  
NOAA/Climate Analysis Center  
Room 605, WWB, 5200 Auth Road  
Camp Springs, MD 20746  
301/763-8227  
Fax 301/763-8395  
abasist@sun1.wwb.noaa.gov

Julio L Betancourt  
US Geological Survey  
1675 West Anklam Road  
Tucson, AZ 85745  
602/670-6821

J Platt Bradbury  
US Geological Survey  
Box 25046, DFC, MS 919  
Denver, CO 80225  
303/236-5666  
Fax 303/236-5690

Carol S Breed  
US Geological Survey  
2255 North Gemini Drive  
Flagstaff, AZ 86001  
602/556-7174  
Fax 602/556-7169

Roger Byrne  
University of California, Berkeley  
Dept of Geography  
501 Earth Science Bldg  
Berkeley, CA 94720  
510/643-8108  
Fax 510/642-3370  
arbyrne@ucbmsa.bitnet

Mike Carr  
US Geological Survey  
National Center, MS 104  
12201 Sunrise Valley Drive  
Reston, VA 22092  
703/648-4450

Tom Carroll  
National Weather Service  
Office of Hydrology, W/OH23  
6301 - 34th Avenue South  
Minneapolis, MN 55450  
612/725-3039  
Fax 612/725-3338  
Omnet: t.carroll

Daniel Cayan  
Scripps Institution of Oceanography  
0224, University of California, San Diego  
La Jolla, CA 92093-0224  
619/534-4507  
Fax 619/534-8561

John Christy  
University of Alabama, Huntsville  
Room A-11, Research Institute  
Huntsville, AL 35899  
205/895-6257  
Fax 205/895-6970  
christy@storm.msfc.nasa.gov

Kenneth Cole  
115 Green Hall, NPS/CPSU  
Dept of Forest Resources  
University of Minnesota  
St Paul, MN 55108  
612/624-4296  
Fax 612/625-5212  
kcole@mercury.forestry.umn.edu

Peter Comanor  
National Park Service, 490  
Wildlife & Vegetation Division  
PO Box 37127 (WASO 490)  
Washington, DC 20013-7127  
202/343-8126

Richard G Craig  
Kent State University  
Dept of Geology  
Kent, OH 44240  
216/672-7987  
Fax 216/672-7949  
rcraig@gilbert.kent.edu

Ernest P Dagher  
National Weather Service  
660 Price Avenue  
Redwood City, CA 94063  
415/876-9122  
Fax 415/364-2599

Peter Dartnell  
US Geological Survey  
345 Middlefield Road, MS 999  
Menlo Park, CA 94025  
415/354-3086  
Fax 415/354-3224  
pete@octopus.wr.usgs.gov

Frank Davis  
University of California, Santa Barbara  
Dept of Geography  
Ctr for Rem Sensing & Envir Optics  
Santa Barbara, CA 93106  
805/893-3438  
Fax 805/893-3146  
fd@geog.ucsb.edu

Walter E Dean  
US Geological Survey  
Box 25046, MS 939, DFC  
Denver, CO 80225  
303/236-5760  
Fax 303/236-0459  
dean@sedproc.cr.usgs.gov

Michael Dettinger  
US Geological Survey  
5735 Kearny Villa Road, Suite O  
San Diego, CA 92123-1135  
619/637-6845  
Fax 619/637-9201  
mddettin@s101pcasnd.wr.usgs.gov

Eric Edlund  
University of California, Berkeley  
Dept of Geography  
501 Earth Sciences Bldg  
Berkeley, CA 94720  
510/643-8108  
Fax 510/642-3370  
eric@pollen1.berkeley.edu

Lisa Ely  
Pennsylvania State University  
Earth System Science Center  
248 Deike Bldg  
University Park, PA 16802  
814/865-7042  
Fax 814/865-3191

Daniel B. Fagre  
National Park Service  
Glacier National Park  
West Glacier, MT 59936  
406/888-5441  
Fax 406/888-5581

Mike Field  
US Geological Survey  
345 Middlefield Road, MS 999  
Menlo Park, CA 94025  
415/354-3088  
Fax 415/354-3191

Dianne Fox  
US Geological Survey  
Box 25046, MS 939, DFC  
Denver, CO 80225  
303/236-1647  
Fax 303/236-3459  
dfox@sedproc.cr.usgs.gov

Frederick Wade Freeman  
University of California, Los Angeles  
3066 Engineering I  
Los Angeles, CA 90024-1593  
310/206-8612  
Fax 310/206-7245

Jim Frew  
University of California, Berkeley  
Computer Science Division  
571 Evans Hall  
Berkeley, CA 94707  
510/642-0267  
Fax 510/642-5615  
frew@cs.berkeley.edu

Ron Gelaro  
Naval Research Laboratory  
Monterey, CA 93943-5006  
408/656-4749  
Fax 408/878-4769

Alan Gillespie  
University of Washington  
Dept of Geological Sci, AJ-20  
Seattle, WA 98195  
206/685-8263  
Fax 206/685-2379  
alan@oz.geology.washington.edu

James Goodridge  
31 Rondo Court  
Chico, CA 95928  
916/345-3106  
Fax same (phone first)

Jim Gower  
Institute of Ocean Sciences  
PO Box 6000  
9860 West Saanich Road  
Sidney, BC, Canada V8L 4B2  
604/363-6558  
Fax 604/363-6479

David M Graber  
National Park Service  
Sequoia and Kings Canyon National Parks  
Three Rivers, CA 93271  
209/565-3171  
Fax 209/565-3497

David Greenland  
University of Oregon  
Dept of Geography  
Eugene, OR 97403-1251  
503/346-4541  
Fax 503/346-2067  
greelan@oregon.uoregon.edu

Bill Halvorson  
University of Arizona  
National Park Service, CPSU  
125 Biological Sciences East  
Tucson, AZ 85721  
602/670-6885  
Fax 602/670-5001

Eileen Hemphill-Haley  
US Geological Survey  
345 Middlefield Road, MS 999  
Menlo Park, CA 94025  
415/354-3085  
Fax 415/354-3191  
eileen@octopus.wr.usgs.gov

Linda Heusser  
Clinton Road  
Tuxedo, NY 10987  
914/351-5290  
heusser@refl.nyu.edu

Caroline Isaacs  
US Geological Survey  
345 Middlefield Road, MS 999  
Menlo Park, CA 94025  
415/354-3014  
Fax 415/354-3191

Anne Jeton  
US Geological Survey  
333 West Nye Lane  
Carson City, NV 89706  
702/887-7628  
Fax 702/887-7629

Ed Josberger  
US Geological Survey  
Ice & Climate Project  
University of Puget Sound  
Tacoma, WA 98416  
206/383-7945  
Fax 206/383-7967  
ice@ups.edu

Charles David Keeling  
Scripps Institution of Oceanography  
0220, University of California, San Diego  
La Jolla, CA 92093-0220  
619/534-4230  
Fax 619/534-0784  
cdkeeling@ucsd.edu

Lynda M Klein  
California State University, Chico  
1154 Sierra Vista Way  
Chico, CA 95926  
916/898-5262  
Home 916/893-4236

Joanie Kleypas  
Walsh and Associates  
2888 Pearl East Circle, Suite 108  
Boulder, CO 80301  
303/443-3282  
Fax 303/443-0367

John Laurmann  
Stanford University  
Dept of Civil Engineering  
c/o 3372 Martin Road  
Carmel, CA 93923-8230  
408/625-6696

Chin-I Lin  
Pacific Gas & Electric  
R&D Department  
3400 Crow Canyon Road  
San Ramon, CA 94583  
510/866-5396  
Fax 510/866-5318

Ana MacKay  
US Geological Survey  
1675 West Anklam Road  
Tucson, AZ 85745  
602/670-6821  
Fax 602/670-6806

John A McGowan  
Scripps Institution of Oceanography  
0228, University of California, San Diego  
La Jolla, CA 92093-0228  
619/534-2074  
Fax 619/534-6500

Christi McMichael  
6280 Acorn Street  
San Diego, CA 92115  
619/286-1592  
Fax 619/286-2014

Ted Melis  
4500 West Speedway Road  
Tucson, AZ 85745  
602/882-6154

Leticia Menchaca  
University of California, Berkeley  
Dept of Geography  
501 Earth Science Bldg  
Berkeley, CA 94720  
501/643-8108  
Fax 510/642-3370  
leticia@pollen1.berkeley.edu

Joel Michaelsen  
University of California, Santa Barbara  
Dept of Geography  
Santa Barbara, CA 93106-4060  
805/893-2296  
Fax 805/893-3146  
joel@elvis.geog.ucsb.edu

John P Monteverdi  
San Francisco State University  
Chair, Dept of Geosciences  
1600 Holloway Avenue  
San Francisco, CA 94132  
415/338-2061  
Fax 415/338-6136  
montever@sfsuvax1.sfsu.edu

Tom Murphree  
Dept of Meteorology, MR-Me  
Naval Postgraduate School  
Monterey, CA 93943-5000  
408/656-2723  
Fax 408/656-3061  
murphree@lady.met.nps.navy.mil

Jerry Norton  
Pacific Fisheries Environmental Group  
National Marine Fisheries Service  
PO Box 831  
Monterey, CA 93942  
408/656-3311  
Fax 408/656-3319  
Omnet: pfeg.monterey

Jan Null  
National Weather Service  
660 Price Avenue  
Redwood City, CA 94063  
415/364-4610  
Fax 415/364-2599

Richard Orndorff  
Kent State University  
Dept of Geology  
Kent, OH 44242  
216/672-7987

Kathy Pagan  
NASA Ames Research Center  
MS 245-5  
Moffett Field, CA 94035  
415/604-1096  
Fax 415/604-3625  
pagan@cloud1.arc.nasa.gov

Richard H Parrish  
Pacific Fisheries Environmental Group  
PO Box 831  
Monterey, CA 93942  
408/656-3311  
Fax 408/656-3319

David H Peterson  
US Geological Survey  
345 Middlefield Road, MS 496  
Menlo Park, CA 94025  
415/354-3366  
Fax 415/354-3363

Cynthia H Pilskein  
MBARI  
160 Central Avenue  
Pacific Grove, CA 93950  
408/647-3719  
Fax 408/649-8587  
pici@mbari.org

John Quadros  
National Weather Service  
660 Price Avenue  
Redwood City, CA 94063  
415/876-9382

Paula Quintero  
US Geological Survey  
345 Middlefield Road, MS 999  
Menlo Park, CA 94025  
415/354-3201  
Fax 415/354-3191

Kelly Redmond  
Western Regional Climate Center  
Desert Research Institute  
PO Box 60220  
Reno, NV 89506-0220  
702/677-3139  
Fax 702/677-3157  
krwrcc@nimbus.sage.unr.edu

Larry Riddle  
Scripps Institution of Oceanography  
0224, University of California, San Diego  
La Jolla, CA 92093-0224  
619/534-1869  
Fax 619/534-8561  
riddle@kidlat.ucsd.edu

John Roads  
Scripps Institution of Oceanography  
0224, University of California, San Diego  
La Jolla, CA 92093-0224  
619/534-2099  
Fax 619/534-8561  
jroads@climat.ucsd.edu

Maurice Roos  
CA Dept of Water Resources  
1416 Ninth Street  
PO Box 942836  
Sacramento, CA 94236-0001  
916/653-8366

Claude Roy  
Pacific Fisheries Environmental Group  
PO Box 831  
Monterey, CA 93942  
408/656-3311  
Fax 408/656-3319

Arndt Schimmelmann  
Scripps Institution of Oceanography  
A-015 University of California, San Diego  
La Jolla, CA 92093-0215  
619/534-4605  
Fax 619/534-0784

Frank Schwing  
Pacific Fisheries Environmental Group  
PO Box 831  
Monterey, CA 93942  
408/656-3311  
Fax 408/656-3319  
Omnet: f.schwing

Lisa Cirbus Sloan  
University of California, Santa Cruz  
Institute of Marine Sciences  
Santa Cruz, CA 95064  
408/459-3693  
Fax 408/459-4882  
lcsloan@rupture.ucsc.edu

Louis T Steyaert  
US Geological Survey  
521 National Center  
Reston, VA 22092  
703/648-4575  
Fax 703/648-5542  
lsteyaert@isdres.er.usgs.gov

Thomas J Stohlgren  
National Park Service  
Natural Resource Ecology Lab  
Colorado State University  
Fort Collins, CO 80523  
303/491-1980  
Fax 303/491-1965  
toms@nrel.colostate.edu

Ted Strub  
Oregon State University  
Ocean Admin Bldg 104  
Corvallis, OR 97331-5503  
503/737-3015  
Fax 503/737-2064  
pts@osuvax.oce.orst.edu / Omnet:t.strub

Robert N Swanson  
Pacific Gas & Electric  
Meteorology Services C8A  
PO Box 77,0000  
San Francisco, CA 94177  
415/973-1331  
Fax 415/973-1016

Sus Tabata  
Institute of Ocean Sciences  
PO Box 6000  
9860 West Saanich Road  
Sidney, BC, Canada V8L 4B2  
604/363-6573  
Fax 604/363-6746  
Telemail: IOS.BC

George H Taylor  
Oregon State University  
Strand Ag 326  
Corvallis, OR 97331-2209  
503/737-5705  
Fax 503/737-2540  
oregon@ats.orst.edu

Jan W van Wagtendonk  
National Park Service  
Yosemite National Park  
El Portal, CA 95318  
209/372-0465  
Fax 209/372-0569

Peter K Van de Water  
1051 North Warren  
Tucson, AZ 85719  
602/881-7418

Roy A Walters  
US Geological Survey  
1201 Pacific Avenue, Suite 901  
Tacoma, WA 98402  
206/593-6505  
Fax 206/593-6514  
roy@zapwatcm.wr.usgs.gov

Robert H Webb  
US Geological Survey  
1675 West Anklam Road  
Tucson, AZ 85745  
602/670-6821  
Fax 602/670-6806

Stephen G Wells  
University of California, Riverside  
Dept of Earth Sciences - 036  
Riverside, CA 92521-0423  
909/787-4367  
Fax 909/787-4324  
wells@ucrvms

G James West  
US Bureau of Reclamation  
3429 Oyster Bay  
Davis, CA 95616  
916/753-8901  
Fax 916/978-5284

Melanie Wetzel  
Desert Research Institute  
PO Box 60220  
Reno, NV 89506  
702/677-3137  
Fax 702/677-3157  
wetzel@nimbus.sage.unr.edu

Marie White  
Pangaea  
25870 Hatton Road  
Carmel, CA 93923  
408/624-5880  
Fax 408/624-5880

Cathy Whitlock  
University of Oregon  
Dept of Geography  
Eugene, OR 97403-1251  
503/346-4566  
Fax 503/346-2067

Gary Wilson  
National Park Service  
204 Gentry Hall  
University of Missouri  
Columbia, MO 65211  
314/882-8645  
Fax 314/884-5133  
muccgw.remozhi@ssgate.missouri.edu

Warren Yogi  
National Oceanographic & Atmospheric Admin  
2560 Garden Road, Suite 101  
Monterey, CA 93950  
408/647-4233  
Fax 408/647-4225  
Omnet: oag.monterey

James R Young  
Southern California Edison  
GO 1, Room 405  
2244 Walnut Grove Avenue  
Rosemead, CA 91770  
818/302-9191  
Fax 818/302-9730





